

**INVESTIGACIÓN SOBRE EL USO DE MUROS DE FÁBRICA
PARA EL REACONDICIONAMIENTO SÍSMICO MASIVO DE
ESTRUCTURAS PORTICADAS DE HORMIGÓN ARMADO DE
MEDIA ALTURA: APLICACIÓN A CONSTRUCCIONES
EXISTENTES EN PAÍSES EN VÍAS DE DESARROLLO
DAÑADAS POR TERREMOTOS RECIENTES**

Research on the use of masonry infill walls for the massive seismic retrofitting of medium-height reinforced concrete framed structures: application to existing buildings in developing countries recently damaged by earthquakes

Tesis Doctoral

Programa de doctorado: Ingeniería Civil y Arquitectura

Doctoranda: **ANA LUISA RAMÍREZ MÁRQUEZ**

Director: **AMADEO BENAVENT CLIMENT**



ugr

Universidad
de Granada

Granada, 2017

Editor: Universidad de Granada. Tesis Doctorales

Autora: Ana Luisa Ramírez Márquez

ISBN: 978-84-9163-560-4

URI: <http://hdl.handle.net/10481/48434>

El doctorando / The *doctoral candidate* [Ana Luisa Ramirez Márquez] y los directores de la tesis / and the thesis supervisor/s: [Amadeo Benavent Climent]

Garantizamos, al firmar esta tesis doctoral, que el trabajo ha sido realizado por el doctorando bajo la dirección de los directores de la tesis y hasta donde nuestro conocimiento alcanza, en la realización del trabajo, se han respetado los derechos de otros autores a ser citados, cuando se han utilizado sus resultados o publicaciones.

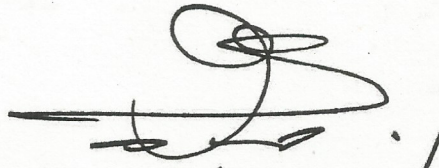
/

Guarantee, by signing this doctoral thesis, that the work has been done by the doctoral candidate under the direction of the thesis supervisor/s and, as far as our knowledge reaches, in the performance of the work, the rights of other authors to be cited (when their results or publications have been used) have been respected.

Lugar y fecha / Place and date: GRANADA 15 JUNIO 2017

Director/es de la Tesis / Thesis supervisor/s;

Doctorando / Doctoral candidate:



Amadeo Benavent
Climent

Firma / Signed



ANA LUISA RAMIREZ
MARQUEZ

Firma / Signed

Agradecimientos

Quisiera dedicar estas palabras de agradecimiento a todas las personas que han contribuido, con su tiempo, conocimiento y dedicación, a la elaboración de esta memoria. En primer lugar a mi director de tesis, Dr. Amadeo Benavent-Climent. Desde el principio entendí que tenía frente a mí una persona visionaria que manejaba de manera excelente los conocimientos más complejos de la ingeniería sísmica. A lo largo de estos años ha sido capaz de transmitirme su particular punto de vista de la ingeniería sísmica, enfocada desde un planteamiento basado en balances de energía, y su altruismo en la aplicación de esta materia. A él quiero agradecer su tiempo, sus enseñanzas, su perseverancia y paciencia conmigo, pero especialmente el haber sido el principal responsable de que pudiese alcanzar uno de mis sueños, poder orientar mi carrera académica a mejorar las condiciones de vida de las personas procedentes de países en vías de desarrollo.

Asimismo quiero expresar mi enorme gratitud al Prof. Santiago Pujol y al Prof. Mete Sozen. Me siento muy afortunada de haber tenido, en dos ocasiones, la oportunidad de hacer una estancia de tres meses en la Universidad de Purdue. Su extensa y particular experiencia en países en vías de desarrollo, su capacidad de encontrar lo simple y lo correcto en lo complejo y caótico, y su excepcional trato humano son un ejemplo inigualable que nunca podré agradecer suficientemente.

También quisiera agradecer a Maximiliano Pittore y al Prof. Stefano Parolai por acogerme en el GFZ en Potsdam durante el último año. Estoy teniendo la oportunidad de colaborar con un equipo enormemente multidisciplinar, que no se limita al buscar aplicar las más exquisitas innovaciones en investigación a servicios de alerta temprana de desastres naturales en países en vías de desarrollo. El nivel humano y académico de todas las personas con las que tengo la suerte de rodearme es, sin duda alguna, uno de los mejores regalos que me ha dado la carrera investigadora.

De un modo especial quisiera agradecer a todos los profesores, personal investigador y en especial estudiantes de doctorado de los últimos años del Departamento de Estructuras de la Universidad de Granada. A lo largo de estos años siempre me he sentido acompañada en todos los aspectos por un grupo de personas competentes, nombraros uno a uno eternizaría este apartado pero gracias de corazón por vuestras palabras de ánimo, vuestros comentarios y ante todo por vuestro ejemplo. También agradecer al Profesor José Rodríguez Montero del Departamento de Ingeniería de la Construcción y Proyectos de Ingeniería por dejarme utilizar todas las herramientas del Laboratorio de Materiales que dirige, por ayudarme a ser rigurosa en los ensayos experimentales, y sobretodo por su alegría y disponibilidad sin límites.

Quisiera dedicar unas palabras especiales a las personas más importantes para mí, a mi familia que es muy grande, y mis amigos, los de siempre y los nuevos que parece que estuvieron siempre. Todos y cada uno habéis compartido conmigo de una manera particular estos años de trabajo, ilusiones, retrocesos y avances, pero sobretodo de felicidad. A mi padre por haberme inculcado desde pequeña la necesidad de trabajar para un mundo mejor, donde las desigualdades económicas no impliquen diferencias en cuanto a seguridad ni oportunidades. A mi madre por su

ejemplo, por ayudarme a buscar el equilibrio entre desarrollo profesional y familiar, sin comprometer ni renunciar necesariamente a ninguno. A mis hermanos Victoria, Carmen y Antonio, y a sus respectivas familias, y muy en especial a mi querido sobrino Víctor, por todas las vivencias inigualables que hemos pasado juntos. A mis padrinos Ángel y Luisa, por su cariño, sus ánimos y su apoyo en todo momento.

Quisiera dedicar estas últimas palabras de agradecimiento a mi marido José Ángel y a nuestros hijos Ana Cristina, José Luis y el pequeño angelito. A José Ángel, porque no hay nadie como tú, por vivir con intensidad la vida a mi lado, por ser mi compañero, mi apoyo y mi cómplice en un proyecto de vida que parece no tener barreras y superarse cada día en retos y alegrías. A nuestros hijos, por vuestra compañía, vuestras sonrisas, vuestra confianza, vuestro cariño, vuestra exclusividad y por vuestro amor tan grande, inigualable e incondicional.

A lo largo de las últimas décadas, el nivel de daños y la frecuencia de colapso de estructuras y edificios debido a la acción sísmica se ha reducido en los países desarrollados gracias al avance en el conocimiento de la ingeniería sísmica y a la implementación de la misma en las normativas. Esta materia no ha surgido como una nueva ciencia desligada de todo lo demás, sino que por el contrario se apoya en el conocimiento previo que se tiene del comportamiento de las estructuras sometidas a distintos tipos de cargas. En general, el diseño estructural para cargas gravitatorias y para cargas sísmicas viene regulado por códigos y normativas nacionales y/o comunitarias como es el caso de la EHE, NCSE-02 (normativas españolas), y de los eurocódigos (normativa europea). Estas normativas, a su vez, se van actualizando periódicamente a través de comités de expertos a los que se les encarga valorar e incorporar los conocimientos suficientemente consolidados y validados. La obligatoriedad de aplicar una normativa o no es algo que corresponde al gobierno de cada país. En general los países desarrollados, no sólo obligan a aplicar códigos concretos, sino que también se esfuerzan por cooperar internacionalmente en la mejora de los mismos. La situación es bastante distinta en los países en vías de desarrollo. Los limitados recursos económicos de estos países hacen que deban destinarlos a tratar de asegurar bienes y servicios de primera necesidad. En estos países a menudo la seguridad estructural no se aborda desde un planteamiento basado en conocimientos científicos, sino como un oficio que transmite conocimientos heurísticos sencillos de maestro constructor a peón. Consecuentemente los daños producidos por terremotos presentan grandes diferencias entre un país desarrollado y un país en vías de desarrollo. El objetivo último de esta Tesis es servir de puente entre el conocimiento científico y los conocimientos heurísticos fácilmente aplicables y materializables en un contexto de medios económicos y técnicos limitados.

El primer aspecto que se ha afrontado en esta Tesis es la influencia que tienen los muros de mampostería en el comportamiento sísmico de los edificios. Los muros de mampostería son considerados como elementos no estructurales en muchas normativas como la normativa española, sin embargo hay evidencias de que su presencia puede elevar significativamente la resistencia y la rigidez lateral del edificio. Esta Tesis parte por ello de la cuantificación de la influencia de los muros en la vulnerabilidad de los edificios, investigando el escenario real y próximo que ofreció el terremoto de Lorca de 2011. El Capítulo 3 de esta tesis presenta la investigación numérica que realizada en la ciudad de Lorca tras el terremoto de Mayo de 2011. El estudio partió del dimensionamiento y modelado de dos edificios reales de la ciudad de Lorca. Cada uno de los edificios se dimensionó sin muros y con muros de mampostería para poder cuantificar

su influencia. A continuación se llevó a cabo el estudio de vulnerabilidad de cada uno de los edificios basado en un índice de daño energético. Finalmente los resultados obtenidos fueron contrastados con análisis dinámicos directos en los que se utilizó el acelerograma del terremoto de Lorca de mayo de 2011 obteniendo resultados coherentes con los daños observados mediante inspección visual. Las conclusiones de este estudio mostraron la elevada influencia de los muros de mampostería en el comportamiento sísmico del edificio y la necesidad de (i) considerarlos como elementos estructurales en la predicción del daño, y (ii) diseñar adecuadamente la distribución de estos elementos para poder beneficiarse de su influencia.

Tras los resultados de esta primera parte de la investigación se planteó la posibilidad de emplear los muros de mampostería como solución de refuerzo y de reacondicionamiento sísmico en países en vías de desarrollo. Los muros de mampostería concentran varias ventajas que los hacen propicios para ser aplicados como elementos de reacondicionamiento sísmico en países en vías de desarrollo, entre ellas: (1) su bajo coste económico, (2) son universales, en todos los lugares se construyen y tienen propiedades muy similares, (3) no es necesaria una formación técnica ni constructiva del operario que los implanta, (4) los propios muros se pueden aprovechar como elementos de partición interior o de cerramiento exterior, y (5) se pueden demoler y reconstruir fácilmente en caso de que hayan sido dañados por un terremoto.

La investigación sobre el empleo de muros de mampostería como solución de refuerzo y de reacondicionamiento sísmico partió de un amplio estudio experimental que incluyó ensayos estáticos y dinámicos con mesa sísmica. El Capítulo 4 explica en detalle la campaña experimental que se llevó a cabo en el Laboratorio de Estructuras de la Universidad de Granada para evaluar el comportamiento sísmico de los muros de mampostería utilizados como elementos de reacondicionamiento sísmico. En los ensayos dinámicos se utilizó una estructura porticada de hormigón armado que había sido sometida ya a dos campañas de ensayos dinámicos para el estudio de dos tipos de disipadores histeréticos. Estas campañas previas de ensayos habían provocado un cierto nivel de daño en la estructura porticada, que se manifestó principalmente en la formación de rotulas plásticas en los extremos de los pilares. Esta estructura porticada tenía además la ventaja de que había sido proyectada para soportar únicamente cargas gravitatorias, lo cual es un caso muy común en las estructuras existentes en países en vías de desarrollo. Al haber sido previamente sometida a simulaciones sísmicas, esta estructura era también adecuada para representar un edificio existente situado en países en vías de desarrollo que había sido dañado por un sismo y que se pretendía reacondicionar mediante la instalación de muros de mampostería. Por estos motivos, el siguiente paso consistió en reacondicionar el pórtico añadiendo dos muros de mampostería sin aperturas en ambos pórticos en la dirección del sismo. Las dimensiones de los ladrillos se ajustaron para que cumplieran el factor de escala para las longitudes de $2/5$ con el que se había diseñado y proyectado el pórtico, y se diseñaron y fabricaron conforme a las recomendaciones gubernamentales en Haití en cuanto a volumen de huecos y resistencia a compresión. El pórtico con muros de mampostería se sometió a varias simulaciones con la mesa sísmica que trataban de reproducir dos escenarios diferentes: (1) el de un terremoto frecuente seguido de una réplica con características similares al primer terremoto; (2) el de un terremoto raro para estudiar el comportamiento de la estructura cuando está sometida a grandes desplazamientos laterales. A partir de los resultados experimentales se propuso un modelo numérico para representar el comportamiento del muro bajo cargas laterales cíclicas arbitrarias. El modelo idealiza el muro como una barra diagonal equivalente que trabaja sólo a compresión. El modelo incluye (i) la definición de la envolvente de la curva desplazamiento-fuerza lateral del muro bajo carga laterales, y (ii) la propuesta de una combinación adecuada de parámetros para ajustar el comportamiento histerético bajo cargas cíclicas del muro mediante el algoritmo de Bouc-Wen.

El siguiente paso consistió en llevar a cabo una investigación numérica en la que se buscaba evaluar el efecto de la implantación de muros de mampostería como medida de reacondicionamiento sísmico en Haití. Dicho estudio constituye el Capítulo 5. Se partió para ello de los datos de campo recogidos por equipo de investigadores liderado por un profesor (Santiago Pujol, Purdue University) que formaba parte del equipo del proyecto de investigación en el marco del cual se realizó esta Tesis. Este equipo había recabado información de edificios en Haití dañados por el terremoto de 2010. Uno de los tipos de edificios que resultaron más dañados durante este sismo fueron los de uso educativo. Por ello y por la especial importancia que tienen este tipo de edificios se decidió centrar la investigación en edificios de uso escolar. A partir de información de campo obtenida en Haití se plantearon dos configuraciones de edificios en planta. El estudio de los datos reales evidencia que los edificios dedicados a escuelas presentan siempre entre 2 y 3 plantas, por tanto se establecieron dos prototipos para cada configuración, la primera con dos plantas y la segunda con tres plantas. Los cuatro edificios planteados se dimensionaron en Tricalc. Para suplir la ausencia de normativa constructiva en Haití se utilizó la normativa española solo para cargas gravitatorias. Los edificios se modelaron en Idarc. Para definir el comportamiento histerético de los elementos estructurales se utilizaron los parámetros calibrados en campañas experimentales previas, para el caso de las vigas y las columnas, y los obtenidos en la campaña experimental objeto de esta Tesis, para el caso de los muros. Uno de los aspectos en los que se ha centrado esta Tesis ha sido investigar la influencia del área de muro por área total de planta en el comportamiento del edificio frente a sismo. Para ello se estudiaron los cuatro edificios diseñados con distintas configuraciones y áreas de muro. En el estudio se varió tanto la cantidad de muros como la disposición de los mismos en planta. La metodología para evaluar la influencia de la cantidad de muros se basó en el estudio de curvas de fragilidad para cada edificio, para distintos escenarios y estados de daño. Para un determinado nivel de daño (Ocupación Inmediata, Daño Limitado, Daño Severo, Cercano al Colapso), una curva de fragilidad proporciona la probabilidad de que se rebase ese nivel de daño para un determinado nivel de intensidad sísmica caracterizado por el desplazamiento espectral \bar{S}_d . Las curvas de fragilidad siguen una distribución lognormal estándar definida por dos parámetros: (1) el desplazamiento espectral medio del edificio y (2) la desviación típica del logaritmo natural del desplazamiento espectral. El estudio paramétrico de estos valores para todos los edificios permitió proponer curvas de fragilidad en función de la configuración geométrica del edificio y del número de plantas. Otro índice de daño que se ha evaluado en este capítulo fue el definido por *Hassan y Sozen (1997)* a partir del estudio de múltiples escenarios post-terremoto y que permite determinar si un edificio es vulnerable o no frente a un terremoto, entendiéndose por vulnerable alta probabilidad de colapso o de daño severo irreparable ante un evento sísmico.

Este índice que se presenta en detalle en el Capítulo 5, y permite de manera rápida y sencilla estimar el área de muro necesaria para asegurar que el edificio no es vulnerable frente a un terremoto. De forma sintética, lo que se pretende con este estudio es: (i) determinar el área de muro necesaria para garantizar que el daño provocado por un terremoto no rebasa un determinado nivel y (ii) proponer curvas de fragilidad para el edificio reacondicionado sísmicamente con los cuales se puedan realizar estudios de riesgo sísmico.

Finalmente en el Capítulo 6 tiene un fuerte carácter aplicado y en él se proponen pautas de actuación y estrategias de reacondicionamiento sísmico sencillas susceptibles de ser implementadas en la normativa sísmica de países en vías de desarrollo. En primer lugar se expone una guía para la evaluación del daño de un edificio tras un terremoto. En la primera parte se describe cómo llevar a cabo la evaluación del daño en el edificio, esto es, las comprobaciones a realizar, los distintos tipos de daño que se pueden encontrar en los elementos estructurales y

la determinación de si son aceptables o no. Se plantean también medidas para reparar vigas y columnas en caso de que sea necesario elevar su capacidad sismorresistente a un nivel mínimo, antes de plantearse la estrategia de reacondicionamiento mediante muros de mampostería. La segunda parte de esta guía propone la estrategia de reacondicionamiento sísmico mediante muros de mampostería. Para ello basándose en la fórmula propuesta por Hassan y Sozen se determina el área mínima de muros de ladrillo necesarios para asegurar que el edificio sobreviva un evento sísmico. A continuación, y sobre la base de los resultados del Capítulo 5, se expone cómo obtener curvas de fragilidad aproximadas para el edificio reacondicionado que permitan realizar estudios de riesgo sísmico. Por último, todo ello se aplica al caso concreto de un colegio de Haití que sufrió daños severos y que se refuerza empleando la estrategia de reacondicionamiento desarrollada en esta Tesis.

Over the last few decades, the level of damage and the frequency of structural collapse incidents due to seismic action have been reduced in developed countries thanks to advance knowledge in earthquake engineering and the implementation of such in building codes. This subject has not emerged as a new, isolated science, but rather it is based on prior knowledge regarding the behavior of structures subjected to different types of loads. In general, the structural design for both gravitational seismic loads is regulated by national and/or community building regulations and codes such as EHE, NCSE-02 (Spanish building codes), and Eurocodes (European building codes). These codes, for their part, are regularly updated by committees of experts who are in charge of assessing and incorporating sufficiently detailed and well-founded knowledge. The obligation to implement or not legislation is at the behest of the government of each country. Generally speaking, not only do developed countries require specific codes of practice, but they also strive to cooperate internationally in improving these standards. The situation is quite different in developing countries. The limited economic resources of these countries means that they should be used to try to secure basic goods and services. Moreover, structural safety in these countries is not often addressed using scientific knowledge, but rather as a trade that transmits simple heuristic knowledge from master builder to labourer. Consequently, the damage caused by earthquakes in a developed country can be hugely different to that of a developing country. The ultimate goal of this Thesis is to bridge the gap between scientific and heuristic knowledge which is easily applicable and attainable in a context of limited economic and technical resources.

The first aspect addressed in this Thesis is the influence of masonry infill walls on the seismic behavior of buildings. Masonry infill walls are considered non-structural elements in many building codes such as the Spanish building codes. There is, however, evidence that their presence can significantly increase the strength and lateral rigidity of the building. This Thesis begins from the quantification of the influence of these walls on the vulnerability of the buildings, investigating the real and recent scenario brought about by the Lorca earthquake in 2011. Chapter 3 of this Thesis presents the numerical research carried out in the City of Lorca after the earthquake in May 2011. The study began by the sizing and modelling of two real buildings in the city of Lorca. Each of the buildings was measured with and without masonry infill walls in order to be able to quantify their influence. The vulnerability study of each of the buildings was then carried out based on an energy-based damage index. Finally, the obtained

results were compared with direct dynamic analysis in which the accelerogram of the 2011 Lorca earthquake was used obtaining results consistent with the damages observed through visual inspection. The conclusions of this study showed the great influence of masonry walls on the seismic behavior of the building and the need to (i) consider them as structural elements in the prediction of damage, and (ii) adequately design the distribution of these elements in order to benefit from their influence.

After obtaining the results from the first part of the research, the possibility of using masonry infill walls as a reinforcement and seismic retrofitting solution in developing countries was considered. Masonry infill walls have several advantages that make them suitable to be used as seismic retrofitting elements in developing countries, including: (1) their low economic cost, (2) they are universal; they are made everywhere and have very similar properties, (3) technical or structural training for the worker who erects them is not necessary, (4) the walls themselves can be used as internal partitions or external enclosures, (5) they can be demolished and rebuilt easily in the case of earthquake damage.

The research on the use of masonry infill walls as a seismic retrofitting and reinforcement solution was based on an extensive experimental study that included static and dynamic tests with a shake-table. Chapter 4 explains in detail the experimental campaign carried out in the Structures Laboratory of the University of Granada to evaluate the seismic behavior of masonry infill walls used as seismic retrofitting elements. In the dynamic tests, a reinforced concrete framed structure was used which had already been subjected to two dynamic test for the study of two types of hysteretic dampers. These previous test campaigns had caused a certain level of damage in the reinforced concrete frame structure, which appeared mainly in the formation of plastic hinges at the ends of the pillars. This reinforced concrete frame structure also had the advantage of being designed to only withstand gravitational loads, which is very common in existing structures in developing countries. Having previously been subjected to seismic simulations, this structure was also suitable to represent an existing building found in developing countries, which had been damaged by an earthquake and which was supposed to be retrofitted with the installation of masonry infill walls. For these reasons, the next step was to retrofit the frame by adding two masonry infill walls without openings on both frames in the direction of the earthquake. The dimensions of the bricks were adjusted to meet the scale factor for lengths of 2:5 with which the frame was planned and designed. Moreover, they were designed and made in accordance with the recommendations of the government of Haiti in terms of volume of voids and compressive strength. The frame with masonry walls underwent several simulations with the shake-table which tried to reproduce two different scenarios: (1) that of a frequent earthquake followed by a replica with similar characteristics to the first earthquake; (2) that of a rare earthquake to study the behavior of the structure when subjected to large lateral displacements. From the experimental results, a numerical model was proposed to represent the behavior of the wall under random cyclic lateral loads. The model conceptualizes the wall as an equivalent diagonal bar that only works when subjected to compression. The model includes (i) the definition of lateral force displacement enveloping curve of the wall under load, and (ii) the proposal of a suitable combination of parameters to adjust the hysteretic behavior under cyclic loads of the wall using the Bouc-Wen algorithm.

The following step was to carry out a numerical investigation in order to try and evaluate the effect of the construction of masonry infill walls as a measure of seismic retrofitting in Haiti. This study can be found in Chapter 5. We used field data collected by a team of researchers led by a professor (Santiago Pujol, Purdue University) who was part of the research project team within the framework in which this Thesis was carried out. This team had collected information from

buildings in Haiti damaged by the 2010 earthquake. Buildings used for educational purposes were some of the buildings that suffered more damage from this earthquake. As a result of this, and due to the great importance of these types of buildings, the decision that this research would focus on buildings for educational use was made. From the field information obtained in Haiti, two configurations of building floor plans were proposed. The study of the actual data shows that buildings used for schools have always had between 2 and 3 stories, therefore two prototypes were established for each configuration; the first with two stories and the second with three stories. The four buildings were measured using Tricalc. In the absence of building codes in Haiti, Spanish building codes were used for gravitational loads only. The buildings were modeled on Idarc. In order to define the hysteretic behavior of the structural elements, the parameters calibrated in previous experimental campaigns were used for of beams and columns, and those obtained in the experimental campaign of this Thesis were used for the walls. One of the aspects which this Thesis has focused on has been to investigate the influence of the wall area by total floor area on the behavior of the building in the face of an earthquake. Therefore, the four buildings designed with different configurations and wall areas were studied. The number of walls in the study varied as did the layout of such. The methodology used to evaluate the influence of the number of walls was based on the study of fragility curves for each building, for different scenarios and damage states. For a given level of damage (Immediate Occupation, Limited Damage, Severe Damage, On the Verge of Collapse), a fragility curve provides the probability that this level of damage is exceeded for a given seismic intensity level characterized by the spectral shift \bar{S}_d . The fragility curves follow a standard lognormal distribution defined by two parameters: (1) the average top spectral displacement of the building and (2) the standard deviation of the natural logarithm of the spectral shift. The parametric study of these values for all the buildings allowed us to propose fragility curves according to the geometric configuration of the building and the number of stories. Another damage index evaluated in this Chapter was the one defined by *Hassan and Sozen (1997)* based on the study of multiple post-earthquake scenarios and that allows us to determine whether or not a building is vulnerable in the face of an earthquake, on the understanding that it has a high probability of collapse or irreparable severe damage in the face of a seismic event.

This index, which is presented in detail in Chapter 5, and which allows us to quickly and easily estimate the wall area needed to ensure that the building is not vulnerable to an earthquake. In summary, the aim of this study is to: (i) determine the wall area needed to ensure that the damage caused by an earthquake does not exceed a certain level; and (ii) propose fragility curves for the seismically retrofitted building with which studies of seismic risk can be carried out.

Lastly, Chapter 6 is of great importance in that it offers guidelines of action as well as proposing simple seismic retrofitting strategies that can be implemented in the seismic codes of developing countries. Firstly, a guide is shown for the evaluation of the damage to a building after an earthquake. The first part describes how to carry out damage assessment in the building, that is the checks to be performed, the different types of damage that can be found in the structural elements and the determination of whether or not they are acceptable. Measurements are also proposed to repair beams and columns in case it is necessary to raise their earthquake-resistant capacity to a minimum level, before considering the strategy of retrofitting using masonry infill walls. The second part of this guide proposes the strategy of seismic retrofitting using masonry infill walls. To this end, and based on the formula proposed by Hassan and Sozen, the minimum area of brick walls necessary to ensure that the building survives a seismic event is determined. Following this, and based upon the results in Chapter 5, how to obtain approximate fragility curves for the retrofitted building which allow studies of seismic risk is shown. Finally, all of the

above applies to the specific case of a school in Haiti that suffered severe damage and has been reinforced using the retrofitting strategy developed in this Thesis.

Contents

Agradecimientos	v
Resumen	vii
<i>Extended Abstract</i>	xi
Contents	xv
List of figures	xix
List of tables	xxi
1 Introduction	1
1.1 Problematical situation in developing countries placed in earthquake prone areas with medium/high seismicity	1
1.2 Specific case: damage description in schools buildings after 2010 earthquake in Haití	2
1.3 State of the art	4
1.3.1 Seismic retrofitting systems in reinforced concrete frame structures	4
1.3.2 Masonry infilled reinforced concrete frames. Numerical Studies	6
1.3.3 Masonry infilled reinforced concrete frames. Experimental Studies	9
1.4 Masonry infill panels in design and seismic codes	10
1.5 Seismic retrofitting of RC frames using masonry infill panels in the normative . .	11
2 Motivation. Objectives. Methodology.	13
2.1 Motivation	13

2.2	Objectives	14
2.3	Methodology	16
3	Seismic assessment of RC frame structures in Lorca under the 2011 earthquake: influence of masonry infill panels	17
3.1	The 11 th May 2011 earthquake in Lorca	17
3.2	Typical buildings in Lorca and methodology to assess their vulnerability	18
3.3	Input energy of Lorca earthquake	19
3.4	Description of buildings under study	20
3.5	Damage prediction on the buildings according to an energy-based seismic index	23
3.6	Damage at story level	25
3.7	Conclusions	28
4	Experimental investigation, analysis of results and proposals	31
4.1	First experimental campaign: Static test to determine masonry panel properties	31
4.2	Second experimental campaign: dynamic shaking table tests	36
4.2.1	Design of the dynamic tests	36
4.2.1.1	Design of the prototype building and test structure without infill walls	36
4.2.1.2	Description of the test structure with infill panels, test set-up and instrumentation	37
4.2.1.3	Seismic simulations	39
4.2.2	Analysis of test results and comparison with predictions	44
4.2.2.1	Overall response. Frequency analysis. Damping	44
4.2.2.2	Capacity curve of the overall structure	51
4.2.2.3	Stiffness variation with maximum relative displacement	52
4.2.2.4	Estimation of equivalent strut parameters: Stiffness and Strength. Comparison with predictions	52
4.2.2.4.1	Estimation of the stiffness	52
4.2.2.4.2	Estimation of strength	53
4.2.3	Proposed models	58
4.2.3.1	Proposed model for predicting the force-displacement relationship of the infill under static monotonic loading	58
4.2.3.2	Proposed model for predicting the response of the RC frame with infills under cyclic loading	60
4.2.3.2.1	Constitutive laws adopted for concrete and steel	61

4.2.3.2.2	Model for beams and columns	61
4.2.3.2.3	Model for masonry infill panels	64
5	Numerical investigation	69
5.1	Definition of the prototype buildings without infills	69
5.2	Design of the prototype buildings without infills	70
5.3	Description of the prototype buildings with infills	72
5.4	Cases of study: 2D numerical models of the prototype buildings with infills	73
5.5	Retrofitted buildings with masonry walls	73
5.6	Seismic performance of the retrofitted buildings	73
5.7	Seismic vulnerability	76
5.8	Parametric analysis of the fragility curves	78
5.9	The priority index [<i>Hassan and Sozen, 1997</i>]	83
5.10	Proposed approach to evaluate the seismic risk of RC frames seismic upgraded with infill walls	86
6	Methodology for seismic retrofitting of reinforced concrete frames using masonry infill panels	89
6.1	General considerations and scope of application of the proposed solution	89
6.2	Assessment of the damaged structure and limits of the application of the masonry infill panel retrofitting strategy	90
6.2.1	Maximum level of damage of the existing structure	90
6.2.2	Minimum required dimensions of the columns of the existing RC frame	93
6.2.3	Consideration of existing masonry walls	96
6.3	Guidelines for seismic retrofitting of reinforced concrete frames with masonry infill walls. Criteria to follow and checks required	97
6.4	Determine the required ratio $\sum A_{MasonryWall}/\sum A_{floor}$ for different seismic scenarios	100
6.5	Comparison with field data	100
7	Conclusions	107
8	Bibliography	111
	Appendices	123
A	Definition of Prototypes	125
B	Pushover curves of prototypes	145

List of Figures

3.1	Input energy spectra of Lorca mainshock	20
3.2	Plan of Lorca prototypes	21
3.3	Frame elevation of prototype P1-W	22
3.4	Frame elevation of prototype P2-W	22
3.5	Vulnerability curves and expected damage for Lorca earthquake	25
3.6	Distribution inter-story drift	27
3.7	Distribution of η_i , $\eta_{i,frame}$ and $\eta_{i,wall}$	28
3.8	Index of damage of Park and Ang (I_{PA})	29
4.1	Mortar compression test	32
4.2	Static test set up and compression stress-strain curve	34
4.3	Static Masonery Test	35
4.4	Prototype structure	37
4.5	Detailing of the RC frames and slab of the test specimen	39
4.6	Test set up	40
4.7	Dynamic test set up and instrumentation	41
4.8	Location of strain	42
4.9	Time story of the acceleration	44
4.10	Normalized spectrum	45
4.11	Total base shear vs. drift for simulations	46
4.12	Seismic simulation	47
4.13	Total dissipated energy and sum of maximum strain energy	48

4.14	Crack pattern on wall 1 and wall 2	50
4.15	Capacity curve	51
4.16	Variation of effective stiffness	52
4.17	Model proposed by Fiorato	55
4.18	Macroelement and failure modes	56
4.19	roposed force-displacement relationship for infill wall	60
4.20	Materials stress-strain relationships	62
4.21	Proposed model and comparison with experimental results	67
4.22	Capacity curve comparison	68
5.1	Prototypes 4x2 and 4x4	71
5.2	Configurations of prototypes	74
5.3	Example of damages states for a masonry wall	76
5.4	Example of determining damage states	77
5.5	Fragility curves	79
5.6	Variation of S_d and β as R increases	80
5.7	Proposed fragility curves	82
5.8	2-Levels prototypes: Ratio of masonry infill walls vs Priority Index	86
5.9	3-Levels prototypes: Ratio of masonry infill walls vs Priority Index	86
6.1	Irregularities in the vertical dimension triggers soft story effect and captive columns	91
6.2	Types of damage in RC columns	92
6.3	Reparation of local damage in column	93
6.4	Reparation of global damage in column	94
6.5	Building under construction in Haiti	96
6.6	Types of damage in masonry infill walls	98
6.7	Sketch of the plant	101
6.8	Frames in D1. Windows in one span and openings in the other span	103
6.9	Buckling of rebars. Shear crack on the longitudinal axix of the column	103
6.10	Clay masonry walls configuration	104
6.11	3D representation of a retrofitting configuration (Prof. Pujol, The New York Times 2010)	104
6.12	Fragility curve for the retrofitted building	105

List of Tables

1.1	Comparison of losses produced by Haiti and Kobe earthquakes	2
1.2	Masonry infill walls in design and seismic codes	10
3.1	Design prescriptions	23
3.2	Plastic strain energy distribution vectors	26
4.1	Standard used to evaluate material properties	32
4.2	Default Lower Bound	34
4.3	Scale Factors	38
4.4	Elements properties	38
4.5	PGA in Port-au-Prince	43
4.6	Seismic scenario under study	43
4.7	Scaling factor for Calitri record	44
4.8	Natural frequency of the specimen during and after each seismic simulation	46
4.9	Estimation of damping for each simulation	48
4.10	Results of the seismic simulations	49
4.11	Lateral strength estimation for different failure modes	58
4.12	Bouc-Wen hysteretic parameters: fixed values	67
4.13	Bouc-Wen hysteretic parameters: variables values	67
5.1	Properties in plan of selected prototypes	70
5.2	Permanents and variable actions	72
5.3	Nomenclature of prototypes	72

5.4	Mean damage and probability of exceeding a given damage state	78
5.5	Proposed values for \bar{S}_{d,DS_i}	81
5.6	Proposed values for β_{DS}	81
5.7	Priority Index for 2-levels prototypes as a function of R	84
5.8	Priority Index for 3-levels prototypes as a function of R	85

1.1 Problematical situation in developing countries placed in earthquake prone areas with medium/high seismicity

Over the last few decades earthquakes of varying magnitudes have struck different countries around the world, causing damage to populations and infrastructure that vary greatly even when the seismic characteristics of the events are very similar.

Since approximately the 60's most countries have developed construction standards and codes which aim to increase human safety in seismic events. The good construction of a building needs a definition of structural elements and materials for each given state (i.e. load combination), and for the people that construct the building to interpret this definition correctly. In this type of cases, the level of exposure of the people in case of earthquake, or other natural events, can be limited through numerical simulations and vulnerability studies.

In most developing countries, construction codes are promoted but not enforced. Sometimes a standard or code is just a series of recommendations in order to guide workers during the construction process. The reasons for not enforcing a code are varied, and include (i) some of the steps of the code enforcement process (such as obtaining a construction license, or a land property deeds) are time-consuming and costly; (ii) municipalities or organisms in charge of supervising the process are normally understaffed. Self-construction is the most common practice in developing countries, and it is considered as the construction of a building by the dwellers themselves or masons, who have not been properly trained (*Johansson, Mayorca, Torres, Leon*). The practice of self-construction normally extends to public and civil constructions, such as schools, local hospitals and supermarkets. The number of buildings in a developing country that are erected by following a standard or by self-construction is unknown.

The likelihood of seismic events in a given area is related to multiple variables. Each of them is weighted depending on how it affects (i) the activation process of a fault and (ii) if it empowers or eases a specific type of rupture of the fault. These parameters mostly concern geophysical

properties of the soil, and their levels of accuracy are directly related to the level of training which scientists have, and the development of arrays of devices in the region, such as seismic stations, accelerometers in specific places, etc. Over the last few decades, evidence has also shown that the presence of human industrial activities, such as fracking, is changing soil behavior provoking changes in the equilibrium of the soil layers. In the case of developing countries, there is a lack of information on this field, and only study of an extensive set of possibilities can cover the knowledge gap.

Nevertheless, recent studies (*Bilham 2010*) have called for UN enforcement of building codes, stating that since 1900, the level of damage caused by serious earthquakes is not defined by their magnitude. Developing countries have more casualties, a higher number of affected people, and bigger losses than developed countries (*Noy 2009*). An example given by Hou (*Hou et al.*) compares (Table 1.1) how two similar events, Haiti 2010 and Kobe 1995, had very different consequences. In this comparison, Haiti's losses are higher in all areas except for economic losses. Nevertheless, this area is not easy to compare, as the economic development of each country is totally different: Economic losses in Japan were not related to basic needs, while in Haiti, they affected people's lives directly.

	Haiti 2010 Port-su-Prince	Japan 1995 Kobe
Date	12 January 2010	17 January 1995
Earthquake magnitude	7 ^a	7.3 ^g
Depth (km)	13 ^a	16 ^g
Epicenter distance to city (km)	25 ^a	20 ^g
Population of affected city (million inhabitants)	More than 2 (metropolitan area) ^b	About 1.5 ^h
Population density of affected city (inhabitants km ⁻²)	24,305 ^b	2,773 ^h
Deaths	223,000 ^c	6,434 ^g
Injured	300,000 ^d	40,000 ⁱ
Homeless people	1,300,000 ^c	300,000 ⁱ
Affected people	3,200,000 ^a	2,000,000 ^g
Direct economic losses (billion USD, adjusted to 2010 dollar values)	8-14 ^{c,f}	187.44 ^k

Sources:^aUSGS 2010; ^bIHSI 2009; ^cEM-DAT 2011; ^dDaniell 2011; ^eGovernment of the Republic of Haiti 2010a; ^fCavallo, Powell and Becerra 2010; ^gUSGS 1996; ^hKobe City Official Website 2011 (The number corresponds to the 2008 population. The page featuring 1995 figures is unavailable now; yet, the city population is almost the same as it was in 1995 just before the earthquake. The population slightly decreased after the disaster, but grew back to the 1995); ⁱEncyclopaedia Britannica Online 2011; ^jAsian Disaster Reduction Center 2002; ^kGuha-Sapir, Hargitt and Hoyois 2003.

Table 1.1: Comparison of losses produced by Haiti and Kobe earthquakes.

Focusing on developing countries, we are tempted to view the situation as confused and chaotic when starting to analyze the real scenario. This Thesis will look in depth at common variables and structural typologies found in countries with very limited economic resources, in order to find patterns and to establish a real and accurate procedure to assess vulnerability and retrofitting measures in developing countries.

1.2 Specific case: damage description in schools buildings after 2010 earthquake in Haiti

Haiti is known as the poorest country in the northern hemisphere. Some statistical parameters indicate how poor or rich a country is. In Haiti, the HDI (Human Development Index) in 2008 was 0.54. *Daniell (2011)* relates a low value of this parameter to a large number of deaths caused by an earthquake. He states that in a country with an HDI of 0.65 or lower, the number of

deaths on average since 1900 has been more than 500 per damaging earthquake. In contrast, for countries with a value of HDI higher than 0.8, the average number of deaths is 20. Some of the aspects that hinder the rapid recuperation of a country after a natural disaster are: population inequality and corrupt authorities. The level of inequality in Haiti is the seventh highest on the inequality index of 189 countries studied (*CIA 2011*). Moreover, the level of corruption in the country is one of the worst in the world (*Transparency International 2011*).

In January 12, 2010 Haiti was shaken by an earthquake of a magnitude of 7.3 on the Richter scale. The total damage, especially in terms of death and people injured, was difficult to discover. The official death toll was 316,000, but this value could have been overestimated by the government in order to get more aid from the international community. This hypothesis is supported by the fact that most studies estimate the number of deaths as between 200,000 - 210,000. Nevertheless, there is no evidence that this number was deliberately exaggerated (*Hou*). The number of injured people was more than 300,000 and it is assumed that the disaster displaced more than a million people [*DesRoches*]. This event also damaged half of the structures in the epicentral area. It is estimated that 60% of the nation's administrative and economic infrastructure was lost, and 80% of the schools and more than 50% of the hospitals were destroyed or damaged [*GOH 2010*].

As previously highlighted, the non-standardized manner of design and construction in Haiti obstructs seismic and vulnerability studies as only technical visual inspection can be considered as reliable. DesRoches (*DesRoches et al*) describes a low-rise reinforced concrete frame building that was in construction during the earthquake of January 12th 2010. The columns were slender with a depth in the range of 200-250, poor longitudinal reinforcement, of about 4 # 4. The steel was deformed and/or smooth, and columns and joint transverse reinforcement was minimal. There were also some reinforced concrete walls filling the space between two consecutive columns. From this description, the apparent weakness of the columns that, in addition, frame the wall with a very high lateral strength, that apparently defines a vulnerable scenario.

The previous significant earthquake event which took place in Haiti was in 1962, while other natural hazards, such as hurricanes, floods and droughts are extremely frequent. In the case of hurricanes, the measures taken to prevent damage, together with an absence of seismic detailing in building design, has increased the level of damage and amount of collapse especially in concrete buildings.

In June 2010, a group of seismic engineering students led by Professor Pujol from the University of Purdue went to Haiti and studied a total of 170 buildings, creating a complete database with information about (i) use and geometrical dimensions of buildings, (ii) number of stories, (iii) structural elements: type, dimension and location, and (iv) level of local and global damage (*Sim C, Song C, Skok N, Irfanoglu A, Pujol S, Sozen M*). In this Thesis, only the schools were studied in order to find similarities:

- Most of the buildings had two or three floors.
- The most frequent geometry in plan was two spans in one direction and from 4 to 6 in the orthogonal direction. It is necessary to highlight that they were a recurrent case, where there was one span in one direction and seven in the orthogonal direction. This geometrical disposition is not usually recommended by seismic standards.
- Reinforced concrete frames provided for lateral load bearing. The average dimensions for squared column depth was 300mm and for deep beam cross-sections was 300mmx500mm.

In some cases, there were concrete or masonry walls filling the gap between two consecutive columns.

- Walls with a height of half the story level normally supported the windows placed between two consecutive columns. This common disposition triggered damage concentration on columns and could be one of the reasons for the high percentage of schools buildings that collapsed.
- Local damage in schools buildings was mostly concentrated on the columns, and in some cases on the walls, with the loss of pieces and the separation of the frame.

A retrofitting system for schools buildings will be focused on increasing the lateral strength of the building without triggering shear failure on columns.

1.3 State of the art

1.3.1 Seismic retrofitting systems in reinforced concrete frame structures

The occurrence of an earthquake introduces an amount of energy into the building or structure that needs to be dissipated. This energy demand dissipation can be absorbed by the structural elements when yielding occurs using ductility. In this type of case, a suitable seismic design guarantees that the damage the structure experiences after the yielding of structural elements does not trigger the collapse of the structure during a catastrophic event. Research on energy dissipation has taken different paths, all of which have aimed to prevent the collapse of the structure.

Keeping the structure far enough away from collapse in the case of a severe earthquake can be approached from different angles. During the design of conventional reinforced concrete structures, reinforcement detailing can be studied in depth to ensure that plastic hinges develop in certain regions of the structural elements, and that they do not experience brittle failures in a seismic event. This can prevent collapse but does not avoid the damage to the structures. To control (reduce) the damage, innovative solutions need to be used. One of these solutions is to install special devices (dampers), which are able to dissipate the energy demand in the structure. The main goal of adding energy dissipation devices is to fix, a priori, the element where the hysteretic energy is dissipated, protecting the structural members from inelastic behavior (*Aiken et al. 1992*).

In the case of retrofitting, the principle is the same and the system used is determined by the special circumstances of a structure. During the last few decades, several seismic retrofitting systems have been developed for reinforced concrete structures. Depending on the operating mode used, and the level of damage control in the structure, we can differentiate between:

- Addition of Extra Structural Members
- Jacketing of structural elements
- Addition of Energy Dissipation Devices

Addition of Extra Structural Members is the most conventional measure and it refers mainly to including shear-resisting walls between two consecutive columns. These shear walls are normally made of reinforced or unreinforced concrete or masonry blocks. The addition of shear walls increases the stiffness and strength of the overall structure, delaying yielding on structural elements. By increasing the strength, the amount of energy that the building can store momentarily in form of elastic strain energy increases. This stored energy can be later dissipated by the inherent damping of the structure. The energy introduced into the system can also be dissipated using cycles of hysteresis of the structural elements in the frame structure and the walls.

Jacketing of Structural Elements in a reinforced concrete framed building aims to increase the seismic load bearing capacity of the total system. Moreover, in the design of the jacketing, not only can the retrofitting measures be considered, but also the concentration of inelastic deformations. Pravin (*Pravin 2011*) classifies the jacketing depending on the material and the constructive process as follows:

- i Adding steel plates (steel jacketing) around the columns, welding the extremes to ensure continuity in the plate and separating plates by a given distance along the column height increases the confinement of the column. In cases where longitudinal plates are anchored to the foundation and the roof, this system also increases the flexure capacity of the columns.
- ii Adding external longitudinal and transverse reinforcement to the column and concreting the vertical layer starting from the column, passing the new reinforcement bars and up to a given cover distance. The rebars are anchored to the roof and floor or foundation by drilling holes into the original structure, which are concreted after placing the rebars.
- iii Adding longitudinal and transverse fiber reinforcement polymer composite increases confinement of the column, and shear and flexure strength. Carbon is the most commonly used material for building the fibers, having many advantages, especially a high level of elasticity and strength.

Jacketing structural elements is an efficient retrofitting solution, that can be used only on damaged or selected elements, for which the economic cost is affordable, but (1) it needs a basic level of technical training to be implemented and (2) some materials, such as the steel plates and, especially, the carbon fibers need to be manufactured near the building. Both limitations are sufficient for the rejection of this retrofitting measure in developing countries.

Addition of Energy Dissipation Devices (EDD) is the most efficient and hi-tech measure for retrofitting RC framed structures. This methodology has been developed intensely during the last few decades. The EDD is in charge of dissipating, most of the energy input in the structure, while the rest of the structure remains basically elastic. The EDD's can be classified into two groups: displacement-dependent and velocity-dependent devices. The displacement-dependent devices are classified into friction devices and yielding devices (or metallic devices), depending on how they dissipate the energy. During severe earthquake excitations, the friction device slips and a large amount of the vibrational energy is dissipated mechanically in friction rather than the inelastic yielding of the main structural components (*Pall et al. 1982*). At the same time, while the yielding device yields and the dissipation of energy is achieved through the development of inelastic deformations. The number of EDD types has increased during the last few decades, covering different needs. In some cases these elements are very invasive, such as truss dampers, and in some other cases, they are just an element placed into a joint or between two other structural elements, depending on the needs of the retrofitting of the

building. In all cases, the properties of the frame need to be clear, and it is necessary to prevent shear failure in the structure caused by the induced forces from the EED. Most cases need manufacturing to develop the devices training during their construction, and especially during their implementation. Nevertheless, some efforts have been made recently to develop low-cost devices in order to use them on a massive scale (*Benavent-Climent, Morillas and Vico 2011*) and Slotted bolted connection (SBC) (*Grigorian et al. 1992*).

1.3.2 Masonry infilled reinforced concrete frames. Numerical Studies

Masonry infilled frames are normally used to define and separate different spaces inside an apartment or a building. Masonry is used to fill the frame after the construction of the columns and beams; consequently, the RC frame supports all the vertical loads, and the masonry wall is only submitted to its self-weight. In addition, modifications on the plant design of the building or apartment normally means the demolition and rebuilding of a wall in a different configuration. Although masonry infill walls are considered as non-structural elements, the damage inspection in post-earthquake scenarios together with the result of experimental campaigns show that the presence of masonry infill panels influences several dynamic properties of the building:(1) the fundamental period of the structure, that can be reduced by 1.5-2 in the cases where a building has been designed following European codes, “designed building”, as well as when the frame is not designed according to any code but imposing a cross section on the structural elements, “non-designed building” (*Asteris PG et al. 2015*). Some authors (*Chacker et al.*) have shown that this ratio could reach up to 2.4. The fundamental period is directly related to the stiffness of the structure. In seismic areas, ignoring the frame-infill panel interaction is not always safe, because, under lateral loads, the stiffness of the infill walls dramatically increases by acting as a diagonal strut, resulting in a possible change of the seismic demand due to a significant reduction in the natural period of the composite structural system (*El-Dakhakhni et al. 2003, 2006*). (2) The stiffness of a structure increases by as much 500% (*Pujol et al. 2008*) 440% (*Kappos et al. 2000*) for the stiffness of the bare frame; (3) the maximum lateral strength of an infilled frame is twice the maximum lateral strength of a bare frame (*Pujol et al. 2008*); (4) the ultimate interstory drift of masonry infill panels is conservatively considered as around 1.5% while some experiments have shown it can reach a value of 3%. The failure of masonry infill panels normally induces the catastrophic collapse of the story and the building.

Additional effects occur when the center of rigidity and the center of mass that can trigger torsional effects on a building do not coincide. These effects are considered even in some standards, as it is the case of Nepal. Also irregularities in stiffness, in plan and/or elevation, through a building can develop damage concentration in some regions of an RC building. Finally, when the infills do not cover the whole frame, captive columns appear, dramatically changing the behavior of the system.

It is extremely important to correctly weigh up all the advantages and risks associated with using masonry infill panels as a retrofitting measure in RC framed buildings. Although the presence of masonry infill panels can be very positive when seismic loads affect a building, if the previously defined parameters are not controlled in detail, a catastrophic failure in a building can occur.

The first recommendation for using masonry infill panels is to place the walls symmetrically on both main axes and continuous in the vertical direction. Some standards, as Eurocode 8, propose deeper analysis if this regularity is not achieved.

The numerical modelling of masonry infill panels is a complex issue due to the high non-linearity of the materials and the interaction between a frame and a wall. Micro-models aim to study the behavior of the structure through finite element models, while macro-models are based on an objectively similar representation of structural behavior.

Micro-models incorporate constitutive models that are assigned to at least three discretized elements: masonry walls and the surrounding interfaces. The mechanical properties and the linear and non-linear behavior of all the materials present in the structural elements need to be defined to obtain a reliable result. Masonry is studied by defining a spatial mesh with two different materials: brick elements and mortar joints. The complexity of the model can also be increased if linkage elements are added to simulate the interface connections and their influence. This approach produces an accurate simulation of masonry behavior. Nevertheless, it calls for a huge number of relatively small finite and contact elements, a step-by-step numerical integration algorithm, a system of equations that incorporates many variables, and the high probability of convergence problems at each step due to nonlinearities. Consequently, micromodels are computationally intensive and difficult to apply to the analysis of large structures. Page (*Page A, 1978, 1981, 1983*) proposed one of the first micromodels for masonry in which the material is presented as an assemblage of elastic brick continuum elements acting in conjunction with linkage elements which simulate the mortar joints. The joint elements are assumed to have high compressive strength (with nonlinear deformation characteristics), low tensile strength, and limited shear strength depending upon the bond strength and degree of compression present. *Sayed and Shrive (1996)* proposed a nonlinear elasto-plastic micromodel for face-shell-bedded hollow masonry using isoparametric shell elements. The micromodel also included the nonlinear effects caused by progressive cracking and geometric and material nonlinearities. Some other models have been proposed during these decades, varying in complexity (types of elements, presence of contact elements representing brick-mortar interaction, etc.) and precision (depending on material properties available and constitutive models): *Zhuge et al (1998)*, *Liu and Dawe (2003)*, *Zucchini and Lourenço (2002)*, the constitutive model for anisotropic quasi-brittle materials of *Gesualdo and Monaco (2015)*.

Asteris and his associates (*Asteris et al. 2011*) have studied the state of the art for macro-models in masonry infill panels in detail. The use of macromodels to represent the behavior of masonry infill panels under seismic loading aims to reduce the computational complexity of micromodels without compromising the result. After six decades of extensive experimental (*Smith 1966; Smith and Carter 1969; Page et al. 1985; Mehrabi et al. 1996; Buonopane and White 1999; Santhi et al. 2005a, b*) and numerical investigations (*Liauw and Kwan 1984; Dhanasekar and Page 1986; Saneinejad and Hobbs 1995; Asteris 2003, 2005, 2008; Moghaddam 2004*) we still cannot find a consensus that provides the definition of an unified approach for the design of infilled frame systems under lateral loads.

In the case of an infill wall without openings, it is accepted that the infill acts as a diagonal strut under compression, which connects the two loaded corners. It is necessary to provide geometrical and mechanical characteristics that represent the diagonal strut to represent the behavior of the wall.

The width, w of the equivalent strut measured in vertical, was related to the length of the strut, i.e., the diagonal of the masonry infill wall, d . Firstly, it was assumed that this relationship followed the one-third rule (*Polyakov 1960, Holmes 1961*):

$$\frac{w}{d} = \frac{1}{3} \quad (1.1)$$

Later, using experimental data, w was related to the relative stiffness between the frame and infill by Smith and his associates (*Smith 1966, 1967; Smith and Carter 1969*), using the parameter λ_h .

$$\lambda_h = h \sqrt[4]{\frac{E_w t_w \sin(2\theta)}{4EI h_w}} \quad (1.2)$$

where h is the column height between the centerlines of beams; E_w is the modulus of elasticity of masonry panel, t_w is the thickness of the masonry panel and the equivalent strut, EI is the flexural rigidity of the columns, h_w is the height of the infill panel, and θ is an angle, whose tangent is the infill height to length aspect ratio.

Different authors have established a relationship between w/d and λ_h (*Mainstone 1971, Mainstone and Weeks 1970, Mainstone 1974, Liauw and Kwan 1984, Decanini and Fantin 1987*), the most generally accepted formulation is that proposed by *Mainstone and Weeks 1970, Mainstone 1974*, which was included in FEMA-274 (*FEMA 1997*) for the analysis of rehabilitated buildings, and in FEMA 306 (*FEMA 1998*) and was accepted by several authors, such as *Klingner and Bertero 1978; Sobaih and Abdin 1988; Fardis and Calvi 1994; Negro and Colombo 1997; Fardis and Panagiotakos 1997; Kodur et al. 1995, 1998; Balendra and Huang 2003*, which is described as:

$$\frac{w}{d} = 0.175 \lambda_h^{-0.4} \quad (1.3)$$

Once the stiffness of the equivalent strut is defined, the maximum lateral strength is defined by studying different failure modes of the masonry infill panel, and the strength associated with it. After a number of experimental and numerical simulations, it is accepted that five masonry infill panel failure modes exist (*Wood 1978; El-Dakhakhni 2002; Ghosh and Amde 2002; El-Dakhakhni et al. 2003*).

1. The corner crushing mode (CC) is usually associated with weak masonry infill panels surrounded by a frame with weak joints and strong members. This is represented by crushing on the infill at, at least, one of the loaded corners (*Mehrabi and Shing 1997; El-Dakhakhni 2002; Ghosh and Amde 2002; El-Dakhakhni et al. 2003*)
2. The diagonal compression mode (DC) is associated with a very slender infill and the failure is caused by buckling in the out of plane of the infill. Crushing on the infill takes place on the central region.
3. The sliding shear failure mode (SS) is associated with an infill with weak joints and a strong frame. A part of the masonry wall slides horizontally over the joints.
4. The diagonal cracking failure mode (DK) is associated with a weak frame or a frame with weak joints and strong members infilled with a rather strong member. This failure mode often takes place at the same time as the SS failure mode, and can be detected by the formation of cracks across the loaded diagonal (*Mehrabi and Shing 1997; El-Dakhakhni*

2002). For strong brick units, the cracks are diagonally stepped along the bed joints. In this case, the infill slides along different-level bed-joints preserving its lateral load bearing capacity and energy dissipation. In the case of weak brick units, the pieces are broken, together with the bed joints. The crushing of the clay units produces faster degradation of the lateral strength and stiffness of the masonry infill wall.

5. The frame failure mode (FF) is associated with a weak frame or a frame with weak joints and strong members infilled with a rather strong infill. This failure mode can be observed after the development of plastic hinges in columns or at the beam column connection.

FEMA 356 states that walls are considered as slender, mainly dominated by flexure, when their aspect ratio is $r = h_w/L_w < 3.0$, while walls are considered as squat, mainly dominated by shear effects, when $r = h_w/L_w < 1.5 - 2$. CC and DC failure modes are associated with flexion behavior of the panel, while SS and DK failure modes are associated to shear behavior of the panel. Of the five modes, only CC and SS can be considered as mechanisms that will cause the failure of the system [Comité Euro-International du Béton (CEB) 1996]. DC is difficult to find as, normally, masonry infill panels are not slender (El-Dakhakhni et al. 2003). The fourth mode DK should not be considered as a failure mode because of the post-cracking capacity of the infill to carry additional loads. The FF mode is related to the frame not to the infill.

Several equations are proposed to identify the failure mode and will be studied in this Thesis in section 4.2.

1.3.3 Masonry infilled reinforced concrete frames. Experimental Studies

As mentioned in the previous section, the specific properties of the frame, infilled masonry, and joints determine the behavior of the system and the development of a given failure mode. Some experimental research has focused on the study of non-ductile reinforced concrete frames infilled with unreinforced masonry, (Fiorato et al. 1970; Al-Chaar et al. 2003; Mehrabi et al. 1994; Centeno et al. 2008) while some other efforts have been addressed to the study of reinforced concrete frames, designed according to current coding prescriptions (Fardis et al. 1999, Zarnic et al. 2001; Calvi et al. 2004; Hashemi and Mosalam 2006). Mehrabi (Mehrabi and Schuller, 1996) studied the influence of the strength of the surrounding frame: Strong and weak frames filled with the same type of masonry panel have been laterally loaded to its maximum shear and deformation capacity. They concluded that both configurations increase the lateral strength and energy dissipation capacity of the system, but in the case of weak frames, the strength capacity is lower and could influence the lateral load distribution along the structural elements of the building.

The highest drift values are also associated with diagonal cracking failure mode (DK). Nazir (Nazir, 2015) included the parameter of axial loading on the masonry wall for the development of SS or DK failures modes, he stated that if a masonry wall is subjected to pre-compression compression, σ_{pc} , on the wall $\sigma_{pc} \geq 0.15f'_m$, the dominant failure mode is DK. In case of multi level buildings with light roofs, the lower levels present DK while the top level can present SS failure mode.

1.4 Masonry infill panels in design and seismic codes

Masonry infill panels are frequently considered as non-structural elements in building design. The lack of conclusive experimental and analytical results to substantiate a reliable design procedure for this type of structure, together with the large number of parameters and possible failure modes involved, obstructs the achievement of a consensus for an unified approach for the design of infilled frame systems (*Asteris 2011*).

Table 1.2 provided by Kaushik (*Kaushik et al. 2006*) summarizes the aspects that different seismic codes consider regarding masonry infill panels in reinforced concrete frames. The next paragraph discusses different aspects related to each column in Table 1.2.

Country/Code	D ¹	T _a ²	Min. design force (%)		Irregularity		K ³	Drift	Infill			Out-of-Plane
			Frame	Infill	Plan	Elev.			σ_i^4	K_i^4	O ⁴	
Albania (1989)	Y	Y	x	x	x	x	1.2-1.5	x	x	x	x	x
Algeria (1988)	Y	Y	25	x	x	x	1.42-1.5	x	x	x	x	x
Bulgaria (1987)	Y	x	x	x	x	Y	1.5-3.0 ⁵	x	x	x	x	x
China (GBJ-11-89 1989)	Y	x	x	x	x	x	x	Y	x	x	x	x
Columbia (NSR-98 1998)	Y	Y	25	100	x	x	x	Y	x	x	x	x
Costa Rica (1986)	Y	Y	x	x	Y	Y	x	Y	x	x	x	x
Egypt (1988)	Y	Y	25	100	x	x	2.0	x	x	x	x	x
Ethiopia (ESCP-1-1983)	Y	Y	25	100	x	x	1.25	x	x	x	x	x
Eurocode 8 (2003)	Y	Y	50-65	x	Y	Y	1.2	Y	x	x	Y	Y
France (AFPS-90 1990)	Y	Y	x	x	x	x	x	x	x	x	x	x
USA (IBC 2003)	x	x	x	x	x	x	x	x	x	x	x	x
India (IS-1893 2002)	Y	Y	x	x	x	Y	x	x	x	x	x	x
Israel (SI-413 1995)	Y	Y	25	x	Y	Y	1.15	x	Y	x	x	x
Nepal (NBC-105,201 1995)	Y	Y	25	x	Y	Y	2.0	Y	Y	x	Y	Y
Philippines (NSCP 1992)	Y	Y	x	x	x	x	1.5	x	x	x	x	x
Venezuela (1988)	Y	Y	25	x	x	x	x	x	x	x	x	x
<i>FEMA – 306</i> ⁶	Y	x	x	x	x	x	x	Y	Y	Y	Y	Y

¹Dynamic analysis is required for *irregular* buildings, tall buildings, important buildings, and buildings located in high seismic regions. The specific requirements vary among different codes.

²T_a is the fundamental natural period of vibration for MI-RC frames.

³K is the ratio of seismic design forces for MI-RC frames to that for the RC frames without MI due to the difference in response reduction factor.

⁴ σ_i and K_i are the strength and stiffness of MI, respectively, and O is the openings in MI.

⁵Response coefficient for the soft-story buildings are required to be increased by two times the value for *regular* buildings with MI and three times the value for buildings without MI.

⁶*FEMA – 306* (ATC 1999) is not a code of standard practice of any country.

Table 1.2: Masonry infill walls in design and seismic codes.

The first column is related to irregular buildings. A building with masonry infill panels is regular when these panels are distributed in a pattern and symmetrically, relative to both principal axes and maintained in all the levels. As soon as any of these assumptions is not present, or the regularity of the building is not guaranteed after construction (addition of frames, stories, etc) the building is considered as irregular.

Most seismic codes use a new formulation for the calculation of the fundamental period as can be seen in column 2. Nevertheless, most codes define their own formulations so no agreement exists on this parameter.

The sharing of seismic forces between the frame and the infill presents some uncertainties. First of all, before cracking, the stiffness of the infill is much higher than that of the reinforced concrete frame. Consequently, masonry mainly supports the seismic loads in the building. Nevertheless, the weakness of the material in the infill and the abrupt loss of its lateral strength can, in some cases, trigger the failure of the building. For this reason, most of the codes state

1.5. Seismic retrofitting of RC frames using masonry infill panels in the normative

that the reinforced concrete frame must have a minimal lateral strength of 25% of the seismic lateral design forces. In the case of the Eurocode, this percentage increases up to 50-65%. Only Columbian, Egyptian and Ethiopian codes require the masonry infill to resist fully-designed lateral loads by structurally connecting the frame to the masonry infill panel.

The fifth column considers the codes that aim to balance the eccentricity effects produced by irregularity in plan of masonry infill panels.

The sixth column highlights the codes that penalize strength in columns and beams placed in stories where vertical irregularity exists, as the seismic forces at these levels will be higher.

The seventh column corresponds to the ratio of seismic design loads for masonry infill frames relative to the bare frame. It can be seen that the values cover a large range increasing from 20%-300%.

The ninth, tenth and eleventh columns refer to the influence of masonry in stiffness, strength and whether openings are considered or not. Eurocode 8 and Nepal code suggests modeling the masonry as a diagonal strut whose equivalent width is not specified. FEMA 306 is the only code that provides a detailed formulation for obtaining the equivalent mechanical and geometrical properties of a strut and identifies the four previously described failure modes described.

Including a better estimation of the effects of masonry infill panels in the seismic codes should be considered as a priority in seismic codes assuming that these elements have a major influence the seismic behavior of the building and cannot be simply considered as non-structural elements and defining a simple but accurate approach to model their influence.

1.5 Seismic retrofitting of RC frames using masonry infill panels in the normative

Scott and Deneff (1993) studied a case of seismic retrofitting of a building in western Kentucky. The main load bearing resisting system of the 5-story building was non-ductile concrete flat slab. Unreinforced masonry panels were used as retrofitting elements. The retrofitting measures aimed to ensure the operability of the building during and immediately after a designed earthquake, defined from a major New Madrid fault zone earthquake. This retrofitting scheme was repeated with another building with similar properties and construction, the Monte Cristo Hotel in Everett Washington, and the results were presented by *Lundeen and Perbix (1994)*.

Murray and Parker (1994) also studied unreinforced masonry infill panels as retrofitting elements. They studied the cases of some low-rise buildings located in western Tennessee, whose main load bearing systems were reinforced concrete frames with no ductility. As before, the performance criterion was to ensure the post-earthquake operability of the building.

Pincheira and Jirsa (1994) compared steel bracing and the addition of masonry infill walls as seismic retrofitting measures for non-ductile reinforced concrete frame buildings. *Miller and Gould (1996)* proposed different cases for retrofitting reinforced concrete frame buildings with masonry infill panels using (1) a base isolation system or (2) the incorporation of shear walls to a building.

Motivation. Objectives. Methodology.

2.1 Motivation

On May 11th 2011 a 4.5 M_W earthquake hit the city of Lorca in southern Spain. Two hours later, an aftershock, with a magnitude of 5.2, hit again the city. The relatively small earthquake caused a tragic toll of 9 deaths and 300 injured. Residential buildings were severely damaged or they collapsed, and historic heritage buildings were also severely damaged. The hypocenter of the earthquake was put at 2-4 km deep and at a distance of 3-7 km from the city center [(IGN, *www.ign.es*) and (IAG, *www.iag.es*)]. The maximum horizontal acceleration in Lorca reached a value of 0.36g. A post-earthquake depth study (*López-Comino et al. 2012*) showed that some characteristics of the event aggravated the consequences: (1) the existence of several slips, instead of a point source event, between the hypocenter and the city of Lorca, and (2) the rupture directivity oriented towards Lorca.

A seismic engineering group led by Professor Benavent-Climent in which the author of this Thesis participated, spent several days working in the city of Lorca in order to observe and assess the seismic damage caused by the earthquake. One of the main topics of this field study was to investigate the role played by the masonry infills in the response of the structures. It was observed that: (1) in some cases the over-strength and stiffness provided by the infills helped the buildings to survive the ground motion and prevented it from collapse; (2) in other cases, the interaction with the infills cause damage concentration in some stories –mainly in the base story– and this caused the structure to approach a state of near collapse. These observations triggered a deeper investigation on the influence of masonry infill panels in the overall behavior of the buildings. The results of this investigation are presented in Chapter 3 of this Thesis and were published in the Bulletin of Earthquake Engineering, 2014 (*Benavent-Climent A. et al. 2014*). The Lorca building stock has been described in detail by several authors after the May 2011 earthquake (*Alvarez Cabal et al. 2013*, *Ferliche et al 2012*, *Cabañas et al 2011*). Alvarez and his associates (*Alvarez Cabal et al. 2013*) concluded that (1) most of the building stock was constructed between the 1940s and the 1990s and (2) the most frequent typology in Lorca was 1st: reinforced concrete moment resisting frames with deep beams, 2nd:masonry structures and

3rd: reinforced concrete frames with wide beams. Two prototypes were proposed and modeled following the prescriptions of the two most probable seismic codes used in the design (first time-window: seismic code NCSE-94 and force code EH-91; second time-window: seismic code NCSE-02 and force code EH-98). Both prototypes were studied with and without masonry infill panels. It should be noted that masonry infill walls are considered as non-structural elements by the Spanish codes. As it will be explained in detail in Chapter 3 the results of this research conclude that the seismic response of the buildings changes drastically if we consider the presence of the infill walls or not.

One of the main conclusions of the study conducted for Lorca and explained in Chapter 3 is that, although the presence of masonry infill panels can trigger catastrophic effects when their distribution in plan and vertical is not controlled, it can also be profitable. Masonry infill panels are (1) extremely effective in increasing strength and stiffness, (2) cheap, (3) produced worldwide with similar properties, regardless of the technical level of the country and (4) easy to install. These conclusions and the deep concern of the author of this Thesis on the seismic vulnerability of developing countries located in seismic hazards regions are the main motivation of this Thesis.

The main idea that is developed and proved through experimental and numerical evidences along this Thesis is that infill walls can be implemented as a mass solution for seismic upgrading existing structures in developing countries. To develop this idea in a real scenario it was decided to apply it to the school buildings in Haiti. There are three several reasons for that: (1) a catastrophic earthquake hit the country recently and (2) there is a need for huge, low-cost mass-retrofitting measures; (3) information was available on the characteristics of structures in Haiti and the level of damage suffered because a member of the research project BIA 2011-26810 that funded this Thesis, Professor Santiago Pujol from Purdue University, conducted a deep field evaluation.

Chapter 5 develops the analysis carried out for buildings in Haiti. The field information was obtained from a database (*Chungwook Sim et al.*) provided by the NEES Project and coordinated by Professor Pujol from Purdue University. The most interesting structures were, due to their use, school buildings. The reported school buildings were composed of reinforced concrete frames with deep beams and unidirectional joists that coincided with the structural typology of the buildings in Lorca. The number of levels in Haiti was 2-3 while in Lorca it was 4.

2.2 Objectives

The general objective of this Thesis is to investigate the possibility for and effectiveness of using masonry infill walls as a massive seismic retrofitting strategy in developing countries. The idea is applied to Haiti for several reasons in addition to those explained above. First, the devastation suffered in January 2010 and the current need for rethinking methods which can increase building safety. Secondly, the huge number of schools that collapsed or were severely damaged. Third, similarities among constructions make it easy to implement a common seismic retrofit solution. School buildings in Haiti use a common structural typology. Normally the load bearing system is defined using reinforced concrete frames with unidirectional joists and a thin slab over them, slender and squared columns, and deep beams. In some cases, reinforced concrete walls are placed between consecutive columns, and the extremely high shear strength causes catastrophic effects when it triggers the shear failure of the surrounding columns. Another

consideration for assessing a retrofitting measure in Haiti is the economic factor. First, houses and public building construction and/or repair costs are the direct responsibility of the owner, which means that only a cheap solution would be attractive to and welcomed by the population. Second, every aspect of building construction is performed by owners or non-technically trained builders and masons. The easier and more familiar an aspect is, the higher the possibilities of success. For these reasons, masonry walls were considered the most effective measure to assess.

The particular objectives of this Thesis are summarized below:

1. To study the documentation concerning faults, locations and movements to determine realistic seismic hazard levels for Haiti in terms of peak ground acceleration, PGA, and return period, T_R . This particular objective is necessary due to the absence of acceleration records in Haiti for the last earthquake. These levels of seismic hazards have been used in the definition of the different earthquake scenarios under study: frequent earthquake scenario and maximum earthquake scenario.
2. To design and execute a test campaign consisting on static and dynamic shaking table tests, in which the effect of masonry infill panels is quantified and analyzed. The objective of the static tests is to characterize the properties of the masonry infills. The goal of the dynamic tests is to investigate the seismic behavior of the mixed system composed of the RC frame and the masonry infill walls. To represent a damaged frame, it was planned to use a RC frame already damaged in previous dynamics shaking test conducted on RC frames with dampers. The RC frame used had the damage concentrated on the extremes of the columns where plastic hinges developed.
3. To study the possibility of diagonal tension failure of the infill walls when the RC frame is subjected to large lateral displacements. In the presence of masonry infill panels, generally, higher values of lateral displacement are associated to the diagonal tension failure of the masonry infill panel. Several features have been identified to make the infill wall prone to this type of failure: (i) ratios height/length (h/l) of the infill wall lower than 1.5-2 and (ii) a weak frame or a frame with weak joints and strong members combined with a rather strong infill wall. These features can occur when typical existing RC frames in Haiti are retrofitted with new infill walls. Therefore, one of the main goals of the experimental campaign described in Chapter 4 is to investigate the possibility of diagonal tension failure of the infills under large forced lateral displacements.
4. To propose a simple diagonal strut equivalent model for the masonry infill walls, calibrated with the test results, that provides the envelope force-displacement curve of the infill under monotonic loadings.
5. To propose appropriate values for the parameters that control the Bouc-Wen model, so that the hysteretic behavior of the infill under dynamic seismic loads can be represented with this model.
6. To investigate quantitatively how the amount of masonry infill panels, installed in and existing RC frame, affects the vulnerability of retrofitted RC buildings. The vulnerability of the retrofitted buildings is intended to be described in terms of fragility curves that provide the probability of exceeding a given level of damage under a given level of the ground motion.

2.3 Methodology

This study starts by comparing in Chapter 3 the behavior of a RC building, (1) with and (2) without masonry infill panels, when it is subjected to lateral loads. Then, masonry infill panels are proposed as a retrofitting element in RC buildings in developing countries. The methodology used in this investigation comprises two approaches: an experimental approach that is described in Chapter 4 and a numerical approach described in Chapter 5. The experimental approach consists on performing static tests to characterize the properties of the infill walls, and dynamic shaking tests to investigate the seismic response of RC frames retrofitted with infill walls. The numerical approach consists on numerical analysis aimed mainly at modelling the force-displacement curves of the infills under lateral dynamic cyclic loads, and at obtaining fragility curves.

Seismic assessment of RC frame structures in Lorca under the 2011 earthquake: influence of masonry infill panels

*Part of the contents of this chapter has been published in
(Benavent-Climent et al., 2013)*

This Chapter assesses (1) the vulnerability of two specific buildings in the city of Lorca, and (2) the role played by the masonry infill panels used as partitions and exterior walls on their seismic behavior. In the absence of the detailed plan used for buildings the structure of the buildings, the program Tricalc has been used to design them using two different codes in Spain that cover the period in which they probably have been built. An energy-based vulnerability index, I_V Benavent-Climent (2011), that compares the energy input of the earthquake with the resistance of the building in terms of normalized energy input is used to quantify the expected level of damage. The predicted responses of the buildings, with and without masonry infill panels, are compared with the observed damage and with the results of the non linear dynamic analysis.

3.1 The 11th May 2011 earthquake in Lorca

Lorca is placed in the region of Murcia, in the southeast of Spain. With nearly 92000 inhabitants, this city suffered two earthquakes in May 2011 with catastrophic damage. The first hit was 4.6 M_w while the second one was 5.2 M_w . The effects of the earthquake motion were aggravated because of the directivity of the rupture fault towards Lorca, and the presence of multiple slips plans between the hypocenter and the city of Lorca [Lopez-Comino et al 2012]. The earthquake left a dramatic balance of 9 deaths and 324 injured. The consequences were also disproportionate concerning the historical buildings, administrative and residential edifices in the city: nearly 300 needed to be demolished and many others retrofitted. The economical loss due to the earthquake exceeded 1500 million euros.

3.2 Typical buildings in Lorca and methodology to assess their vulnerability

A very usual typology for residential constructions in the Mediterranean area consists on low- to mid-rise buildings with reinforced concrete frames and wide beams. In the city of Lorca, most of the buildings that experienced severe damage had this structural typology. Concerning the seismic design, the Spanish seismic code at the time these buildings were constructed prescribes a elastic response spectrum that was exceeded by the Lorca earthquake in a range of periods corresponding to many existing structures. These structures were designed by applying a strength-based seismic design approach that reduced the forces in case of an elastic response by a factor that is related to the ductility of the structure. The ductility is defined by $\mu = \frac{\delta_u}{\delta_y}$ as the ratio between the ultimate displacement of the structure, δ_u , and the yield displacement, δ_y .

In the case of Lorca, the referred low- to mid rise buildings should have been designed with an elastic response reduction factor of $\mu = 2$. Although this fact would justify the presence of plastic hinges on the structural elements, the experienced damage was, quantitatively, much more higher. Force-based methods are somehow questionable as it is not clear that the elastic response reduction factor μ and the supposed energy dissipation capacity of the structure are directly related [Decanini and Mollaloli 1998]. The energy-based approach is a preferable way that characterizes the demand of the earthquake and the capacity of the structure in terms of energy. Designing buildings in terms of energy demand and capacity will allow making a more realistic approach of the seismic problem.

The level of damage that a given structure will sustain after an earthquake can be predicted from an analytical or empirical methodology [Calvi et al. 2006]. The advantage of empirical methods is that they are based on experimental and post-earthquake data and thus, and are very reliable. Numerical methods are composed of complex numerical expressions that define material properties and relationships among materials, interfaces, and boundary conditions. These expressions are used in extensive non-linear dynamic analysis to produce the data that allow defining the analytical methodology. In the last two decades, a number of authors have proposed simplified inelastic procedures for seismic assessment [Fajfar and Gasparsic 1996, ATC-40 1996, Calvi 1999, Cosenza et al. 2005, Borzi et al. 2008] for which the response of the structure is approached by a pushover analysis and the demand of the earthquake by the response spectrum expressed in the terms of spectral displacement and acceleration. Within the recent past, Benavent-Climent (2011) proposed a simple analytical method to evaluate the vulnerability of a given building in terms of an energy-based index I_v that is summarized below:

- The seismic demand of the ground motion is characterized by means of a normalized input energy spectrum:
 - And a normalizing factor called the Seismic Hazard Energy Factor AE_I [Decanini et al. 1995, Sucuoglu and Nurtug 1995].
- The capacity of the structure to resist earthquake is characterized by means of two energy factors that define the change from elastic to inelastic state in the structure and the collapse state:
 - AE_{IS} represents, in terms of normalized input energy spectra, the maximum earthquake that the structure can support before developing inelastic behavior.

- AE_{IU} represents, in terms of normalized input energy spectra, the ultimate earthquake that causes the collapse of the structure.

Here, cumulative damage and damage concentration in a given story are specifically taken into account.

- Finally, the computation of I_V by means of AE_I , AE_{IS} , and AE_{IU} relates the specific dynamic properties of the building with the energy input spectral shape of the ground motion. I_V quantifies the level of damage on a building in a scale from 0 (no damage) to 1 (collapse).

3.3 Input energy of Lorca earthquake

The equation of motion of an inelastic single degree of freedom (SDOF) system subjected to a unidirectional horizontal ground motion is:

$$m\ddot{y}_t + c\dot{y} + Q(y) = 0 \quad (3.1)$$

where m is the mass, \ddot{y}_t is the absolute acceleration of the mass, c is the damping coefficient, \dot{y} is the relative velocity with respect to the ground and $Q(y)$ the restoring force.

Integrating eq. 3.1 with respect to y from the time that the ground motion starts yields:

$$\int m\ddot{y}_t dy + \int c\dot{y} dy + \int Q(y) dy = 0 \quad (3.2)$$

Considering that z_g the ground displacement, the relative displacement of the mass can be written as $y = y_t - z_g$ and noting that $dy = \dot{y}dt$ the energy equilibrium of a single degree of freedom system subjected to an unidirectional ground motion can be written as follows:

$$E_k + E_\xi + E_a = E \quad (3.3)$$

where,

$$E_k = \frac{m(\dot{y}_t)^2}{2}; \quad E_\xi = \int c\dot{y}^2 dt; \quad E_a = \int Q(y)\dot{y}dt; \quad E = \int m\ddot{y}_t dz_g \quad (3.4)$$

E_k is the absolute kinetic energy, E_ξ is the damping energy and E_a is the absorbed energy. E is the absolute energy input.

Also, E_a is compounded by two terms, $E_a = E_s + E_h$: the recoverable elastic strain energy E_s , and the irrecoverable hysteretic energy E_h . Thus, eq. 3.3 can be rewritten as:

$$E_k + E_\xi + E_s + E_h = E \quad (3.5)$$

The specific energy that contributes to damage, E_D , was defined by *Housner (1956)* as $E_D = E - E_\xi$. Also, the total energy input and the energy that contributes to damage can be expressed in terms of equivalent velocities as:

$$V_E = \sqrt{\frac{2E}{M}} \quad V_D = \sqrt{\frac{2E_D}{M}} \quad (3.6)$$

Finally, the energy input spectrum is obtained in terms of equivalent velocity by calculating V_E for SDOF systems with different periods.

The seismic stations are always oriented to record the two horizontal NS and EW component of the ground motion and, in some cases, the vertical component. The rupture directivity of the fault is of high interest as it defines the contribution of energy from each horizontal component to the total energy input. In the case of the Lorca earthquake, the rupture propagation was very pronounced from the epicenter towards Lorca, with a direction of N190°E (*Lopez-Comino et al. 2012*). To compute a total acceleration record in a given direction, each one of the horizontal components needs to be projected over the directional vector and the sum of both projections is the total record in that direction. *Benavent-Climent et al. (2011)* showed that the most harmful fault rupture direction for the Lorca 2011 earthquake in terms of energy input was N23°W (Fig. 3.1). Fig 3.1 shows the energy input spectrum for the main shock of the Lorca earthquake, obtained for different directions. Also presented in Fig 3.1 is the design energy spectrum proposed by *Benavent-Climent (2002)* for moderate seismicity regions and medium soil conditions considering a value of PGA equal to 0.12g (prescribed by NCSE-02 for Lorca).

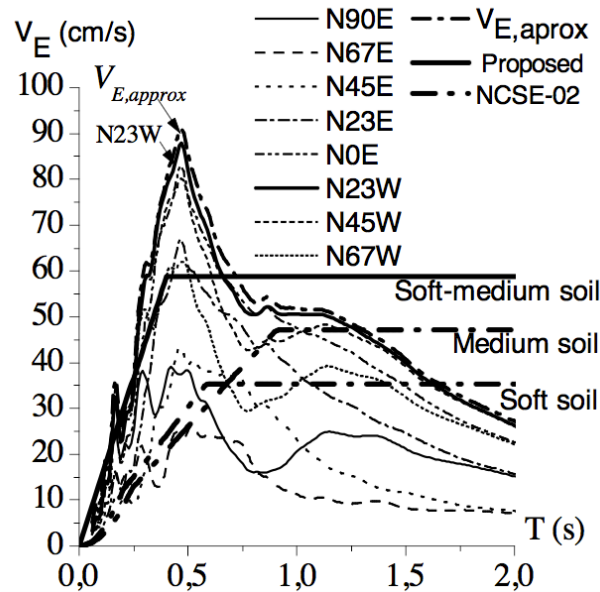


Figure 3.1: Input energy spectra of Lorca mainshock.

3.4 Description of buildings under study

A large number of damaged buildings had four to five stories and the same structural typology: RC frames with wide beams and unidirectional joists. Nowadays this system is not recommended by some international codes as ACI (*ACI Committee 318-08 2018*) and it was even banned by the seismic code published in Spain in 1995 NCSE-94 (*Ministerio de Obras Públicas 1995*) for seismic areas whose design PGA is larger than 0.16g. The actual code allows

the use of this structural typology but enforces the use of an elastic reduction factor of 2 and prescribes some requirements related to the beams. These buildings are normally used as residence structures and always account with masonry infill panels with regular distribution along the height from the first level to the top, normally used as separation elements. The ground floor is mostly used for small-medium commerce and accounts with wide openings and scarce presence of masonry infill panels. This difference on strength and stiffness between the ground floor and the rest of the building has been widely identified as a potential risk of soft story failure on the building.

This Chapter evaluates the expected damage and the behavior under seismic loads in 4-stories, RC frame structures with wide beams. The dimensions in plan of the building correspond to a real structure in the city of Lorca (Fig 3.2). To consider all the possibilities in the design in the years 1994-2008, two prototypes were defined:

- P1 symbolizes the building as constructed between 1994-2002, following the codes of reinforced concrete code EH-91 (*Ministerio de Obras Públicas y Transporte, 1991*) and the seismic code NCSE-94 (*Ministerio de Obras Públicas y Transporte 1995*).
- P2 symbolizes the building as constructed between 2003-2008, following the codes of reinforced concrete code EH-98 (*Ministerio de Fomento 1998*) and the seismic code NCSE-02 (*Ministerio de Fomento 2003*).

The buildings were designed using the platform Tricalc (*Artec S.A. 2010*) considering the masonry infill walls as non-structural elements. Figure 3.3 and 3.4 shows the final different sizes for both prototypes and Table 3.2 the prescriptions used in the design.

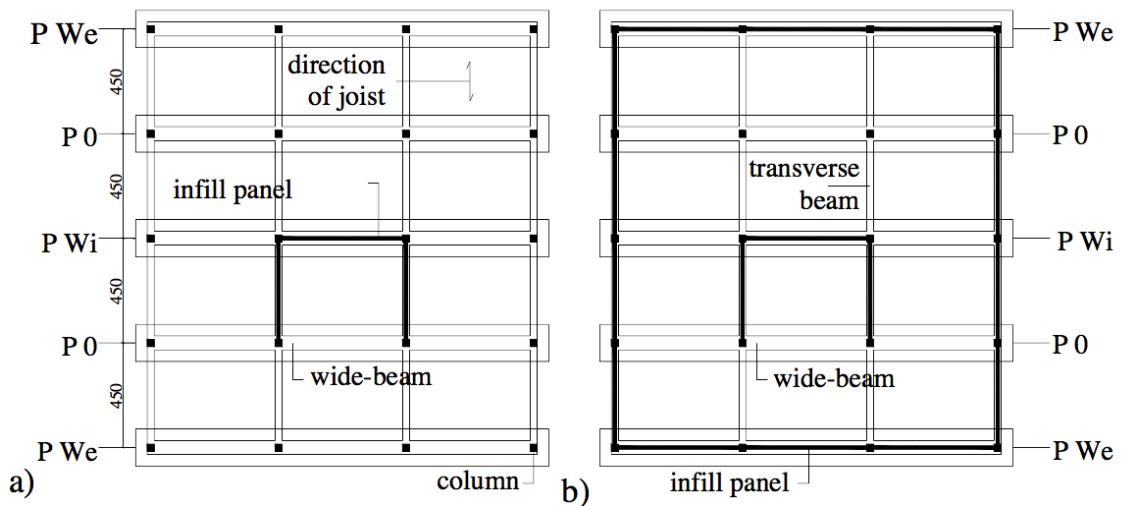


Figure 3.2: Plan of both prototypes: a) ground floor b) rest of the stories.

The nonlinear behavior of the buildings is assessed by means of the platform Idarc 6.1. The building is represented by means of macro-elements. For the reinforced concrete frame, beams and columns are assumed to behave as elastic elements with plastic hinges at the ends. Masonry infill panels are assumed to behave as diagonal truss effective only in compression.

The behavior of the beams and the columns is represented by means of the moment curvature diagram and the hysteretic rules that characterize the cyclic behavior: strength degradation, stiff-

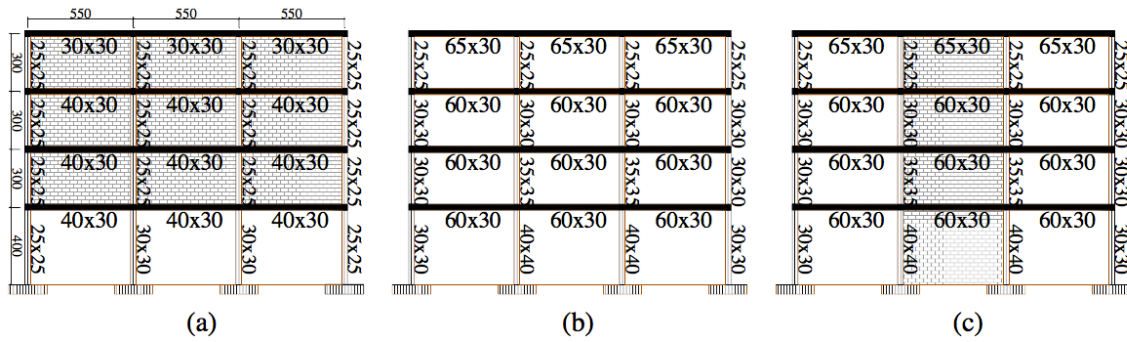


Figure 3.3: Frame elevation of prototype P1-W: a) exterior PWe, b) interior P0, c) central frame PWi.

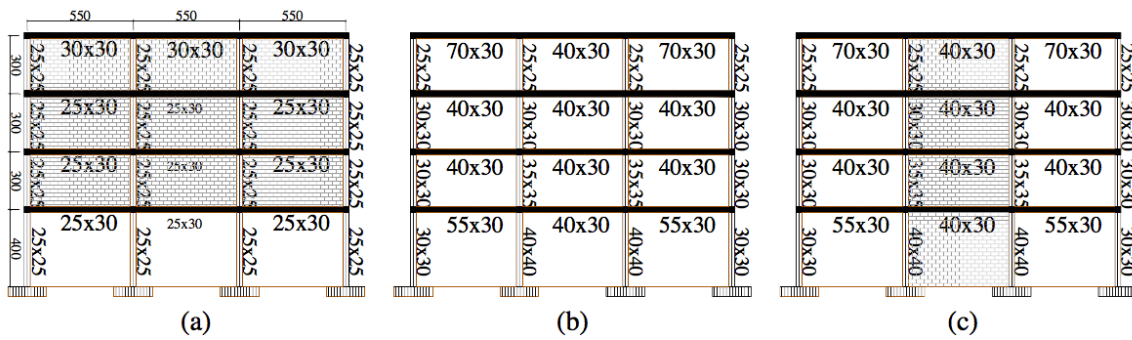


Figure 3.4: Frame elevation of prototype P2-W: a) exterior PWe, b) interior P0, c) central frame PWi.

ness degradation and pinching effect. For the bilinear moment curvature diagram of the beams, the yielding moment and the ultimate moment were also defined from these tests. The hysteretic values were obtained from previous static and dynamic experimental tests [Benavent-Climent 2007; Benavent-Climent et al. (2009a; 2010)]. For the columns, the trilinear moment curvature diagram was idealized using the platform Response-2000 including the effects of axial loads in the moment capacity of the columns (Bentz and Collins 2000). The hysteretic parameters were obtained by calibrating experiments conducted by Sezen and Moehle (2006).

The envelope that defines the behavior of masonry infill panels is given by means of the initial stiffness and the lateral yield strength. The hysteretic behavior is defined by means of the Bouc-Wen model implemented in Idarc that will be presented in detail in Chapter 4. All the values were calibrated from a previous seismic campaign conducted at Purdue University (Pujol et al. 2008).

Two cases of study are proposed for each building to determine the role of the masonry infill panels in the seismic behavior of the buildings during the Lorca earthquake:

1. Considering the presence of the masonry infill panels on the building. These prototypes will be denoted as P1-W and P2-W. Their fundamental period is 0.74s for both of them and
2. Without considering the masonry infill panels. These prototypes will be denoted as P1 and P2. Their fundamental periods are 1.3s and 1.4s respectively.

	Property	P1	P2
	Concrete strength	17.5 Mpa	25 MPa
	Steel yield strength	400 Mpa	400 MPa
Gravity loads	Self weight + dead loads intermediate floors		4.25 kN/m ²
	Self weight + dead loads of the roof		3 kN/m ²
	Live loads		3 kN/m ²
	Elastic response reduction factor		2
	Design PGA	0.11g	0.12g
	Soil condition		Type II medium-stiff soil
	Collapse mechanism	Not forced strong column-weak beam failure mechanism	

Table 3.1: Design prescriptions.

3.5 Damage prediction on the buildings according to an energy-based seismic index

The vulnerability of a building is defined by means of a curve that displays the variation in a given vulnerability index as the parameter that characterizes the earthquake motion changes. In this study, an energy-based seismic index, I_V , is used to assess the vulnerability of the prototypes, with and without masonry infill panels, as the normalized energy input of the earthquake increases (Fig. 3.5).

The damage potential of the ground motion is quantified by means of:

- $AE_I = \int_{T=0.05}^{T=4} \frac{E}{M} dT = 2611 \text{cm/s}^2$. AE_I is known as the Seismic Hazard Energy Factor, AE_I , (Decanini and Mollaioli 1998), defined as the area under the energy input spectrum per unit mass between 0.05s and 4s, where E is the total input energy and M is the mass of the building.

The resistance of the building to be damaged by the action of the earthquake is quantified by means of two energy factors that are determined by means of nonlinear dynamic analysis:

- AE_{IS} : Quantifies the level of the maximum earthquake that the building can bear without exceeding the elastic range.
- AE_{IU} : Associated to the ultimate earthquake that the structure can support before collapse

The energy-based seismic index that defines the vulnerability curve is computed as:

$$\begin{aligned}
 &\text{if } AE_I \leq AE_{IS} && I_V = 0 \\
 &\text{if } AE_{IS} \leq AE_I \leq AE_{IU} && I_V = \frac{(AE_I - AE_{IS})}{(AE_{IU} - AE_{IS})} \\
 &\text{if } AE_I \geq AE_{IU} && I_V = 1
 \end{aligned} \tag{3.7}$$

The values of AE_{IS} and AE_{IU} are determined from nonlinear dynamic analysis through an Incremental Dynamic Analysis (IDA) procedure (Vamvatsikos and Cornell 2002). The numerical model for each prototype is subjected to the recorded ground motion in Lorca scaled to a small value of PGA. This value of PGA is increased 0.005g until two levels:

- 1st When the prototype develops the first plastic hinge, at this point $PGA = PGA_S$.
- 2nd When the prototype reaches the verge of collapse, at this point $PGA = PGA_U$. The collapse of the model is assumed when the base shear falls more than 20% of the maximum value attained in the base-shear versus lateral displacement curve.

In an elastic system, the energy input is proportional to the square of the PGA . For this reason, and taking into account that the PGA of the earthquake in Lorca was $0.36g$, AE_{IS} and AE_{IU} of each prototype can be determined as:

$$\begin{aligned} AE_{IS} &= AE_I \left(\frac{PGA_S}{0.36g} \right)^2 = 2611 \left(\frac{PGA_S}{0.36g} \right)^2 \\ AE_{IU} &= AE_I \left(\frac{PGA_U}{0.36g} \right)^2 = 2611 \left(\frac{PGA_U}{0.36g} \right)^2 \end{aligned} \quad (3.8)$$

The expected damage in the buildings caused by the Lorca earthquake is obtained by the intersection of the vulnerability curve and the vertical line that define the normalized energy demand of the earthquake (Fig. 3.5). The left ordinate of the intersection point out the level of damage in the building under the Lorca earthquake in terms of I_V that ranges from $I_V=0$ (no damage) to $I_V = 1$. The right ordinate shows the damage degree L_d determined by the European macroseismic scale (*W.G.M. Scales 1998*). Past investigations (*Benavent-Climent 2011*) showed a good correlation between I_V and L_d .

Comparing the vulnerability curves in Fig. 3.5 we can conclude that:

- Prototypes buildings with infill walls, P1-W and P2-W, designed in agreement to codes in force in the two time windows 1994-2002 and 2003-2008, are clearly expected to collapse under Lorca earthquake, as $I_V > 1$.
- Prototype P1 without infill walls constructed according to the codes in force in the time window 1994-2002 is expected to undergoing moderate to severe damage as $I_V=0.7$ and $L_d \approx 4$. Similar analysis that based the computation of the vulnerability curves in the modal analysis and the pushover curve of the building (*Benavent et al. 2012*) yielded a value of $I_V=0.5$ and $L_d=3$.
- Prototype P2 without infill walls constructed according to the codes in force in the time window 2003-2008 is expected to be driven to the brim of collapse as $I_V=0.95$ and $L_d=4.8$. Similar analysis that based the computation of the vulnerability curves in the modal analysis and the pushover curve of the building (*Benavent et al. 2012*) yielded a value of $I_V=1$ and $L_d=5$.
- P1 and P2 do not represent real buildings in Lorca as all the structures had masonry infill panels. Nevertheless, the comparative study leads appreciating the negative effect of masonry infill panels in the seismic behavior of the prototypes. This adverse influence is aggravated by an irregular distribution of the walls along the stories which imperils the distribution of the plastic strain energy among the stories, and induces the damage to be localized mostly on the first story.

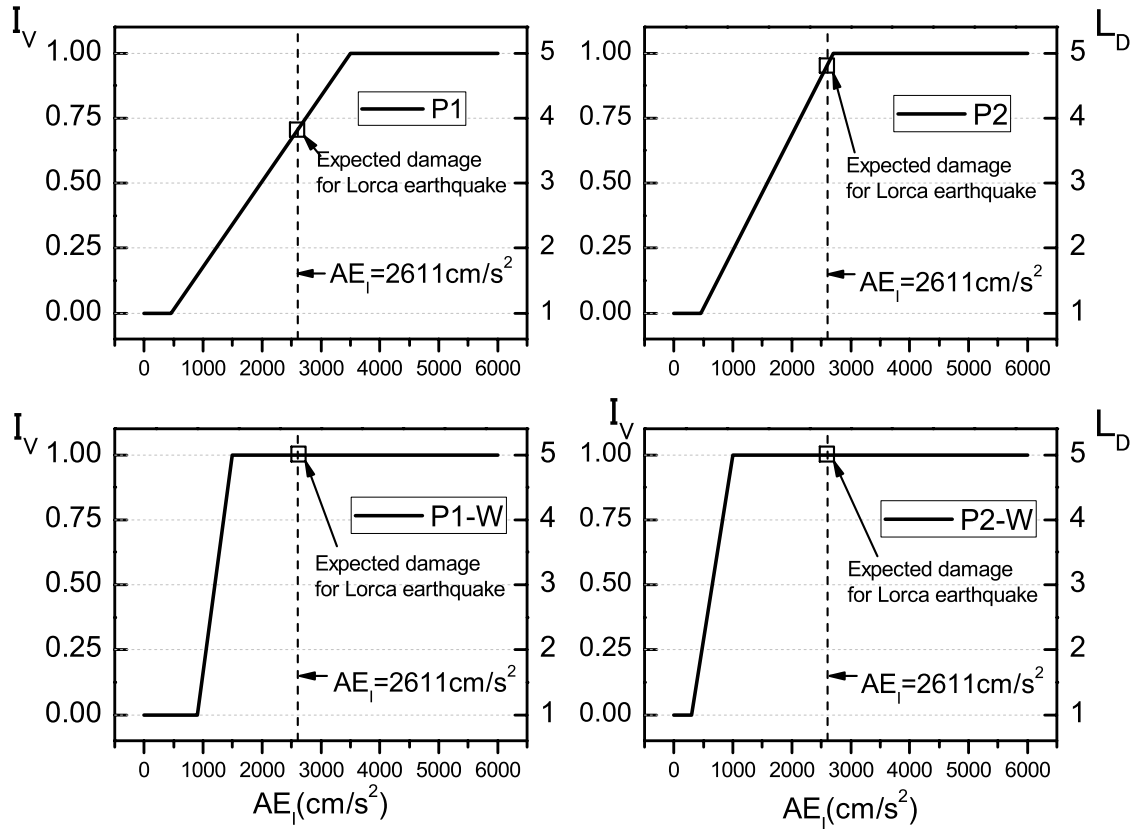


Figure 3.5: Vulnerability curves and expected damage for Lorca earthquake for models.

The distribution of damage along the different stories in the verge of collapse is also studied in this Chapter. Damage concentration in a given story can trigger the abrupt collapse of the building while the rest of the stories remain elastic. On the other hand, a homogeneous distribution optimizes the earthquake resistance of the building to lateral loads, allowing all the structural elements contribute to the dissipation of energy.

The distribution of plastic strain per stories, ψ_i (eq. 3.9), is calculated by dividing the plastic strain energy dissipated at any i th story when any j th story reaches its ultimate lateral displacement capacity, $E_{hmn,i}$ by the total energy dissipated in the building, $\sum_{K=1}^N E_{hmn}$. The results of all prototypes are presented in Table 3.2. The prototypes P1-W and P2-W concentrates almost all the plastic strain on the ground floor (96 and 97%). P1 and P2 present a more equilibrated distribution of plastic strain along the stories despite most of it (around 50%) concentrates in the ground floor.

$$\psi_i = \frac{E_{hmn,i}}{\sum_{K=1}^N E_{hmn}} \quad (3.9)$$

3.6 Damage at story level

The energy input spectrum of both earthquakes was similar in shape but with very different intensities: the first shock is much lower than the second one. The nonlinear dynamic analyses

Story	P1	P2	P1-W	P2-W
4	0.14	0.08	0.00	0.00
3	0.21	0.21	0.00	0.00
2	0.21	0.19	0.04	0.03
1	0.44	0.52	0.96	0.97

Table 3.2: Plastic strain energy distribution vectors.

were used to examine the damage at story level. The numerical models were subjected to two record motions:

- 1st First shock of the Lorca earthquake. The response of the buildings gave information of the level of damage on each building on the starting of the main shock which resulted in minor damage: the structural members experienced cracking at the first floor level, lateral inter-story drifts rested below the limit of the beginning of yielding, and the infill panels experienced no damage.
- 2nd An accelerogram that merged the first and the second (main) shock in Lorca. The response of the buildings gave reliable information of the real level of damage at the end of the main shock. As the level of damage caused by the first shock is almost despicable, the second shock is the responsible of the damage caused in the structures that is described below.

Three indicators of damage are presented in this section to assess the level of damage on the prototypes:

1. The maximum interstory drift normalized by the height of the building $\delta_{max,i}/h_i$ (Fig. 3.6). This parameter gives information about the “apparent damage” but neglects the accumulated damage caused by the plastic strain reversals.
2. The energy dissipated by means of plastic strains in the structural elements of each story, $E_{h,i}$, normalized by the product of the yielding forces and yielding displacements, Q_i, δ_i (Figure 3.7), this parameter is commonly known as η_i . η_i is specially recommended for existing buildings designed in agreement with older codes, as normally they have not been designed for maintaining strength in cyclical response in the inelastic range (*Fajfar and Gaspersic 1996*). Also, *Akiyama (1985)* states that the energy dissipated by means of plastic strains is a good estimator of the damage at each story level, and also that a similar value of η_i along the building imply that the plastic strain energy has been dissipated in an optimal way. $E_{h,i}$ is obtained by integrating the force-displacement curve in the i-story. For the prototypes P1-W and P2-W the structural elements, (i) RC frame and (ii) masonry infill walls, work in parallel, and $E_{h,i}$ is determined separately from the curve that defines the force displacement of the RC frame and the one that defines the force displacement curve in the masonry infill walls. The normalized $E_{h,i}$ parameter is commonly known as η_i and is given by:

- a) for prototypes without masonry infill walls P1 and P2:

$$\eta_i = \frac{E_h}{Q_{yi}\delta_{yi}} \quad (3.10)$$

b) for prototypes with masonry infill walls P1-W and P2-W:

$$\begin{aligned} \eta_i &= \eta_{i,frame} + \eta_{i,wall} \\ \eta_{i,frame} &= \frac{E_{h,frame}}{Q_{yi,frame}\delta_{yi,frame}} \\ \eta_{i,wall} &= \frac{E_{h,wall}}{Q_{yi,wall}\delta_{yi,wall}} \end{aligned} \quad (3.11)$$

It can be observed from Fig. 3.7 that η_i remains close to constant in all the stories in P1, but it is twice as large in the ground floor than in the rest of the stories for P2. The damage concentration is intensified in the prototypes P1-W and P2-W for which the presence of masonry infill walls is also accounted: The infill walls collapsed in the first story and the plastic hinges achieved the brim of their ultimate capacity.

3. The Park and Ang index (*Park and Ang 1985*) I_{PA} , which takes into account the damage associated with the maximum deformation and the cumulative damage and ranges from $I_{PA}=0$ (no damage) to $I_{PA}=1$ (collapse of the structure). In this study, I_{PA} is calculated separately for beams and columns (Fig 3.8) showing that damage concentration occurs in columns. In P2, the number of plastic hinges that develop at the ends of columns was three times higher than in P1. For the cases that the masonry infill panels were considered in the analysis, P1-W and P2-W, the elevated concentration of damage in the first story motivated the failure of the plastic hinges at the bottom of all columns on the first story, while the rest of structural elements only experience minor damage.

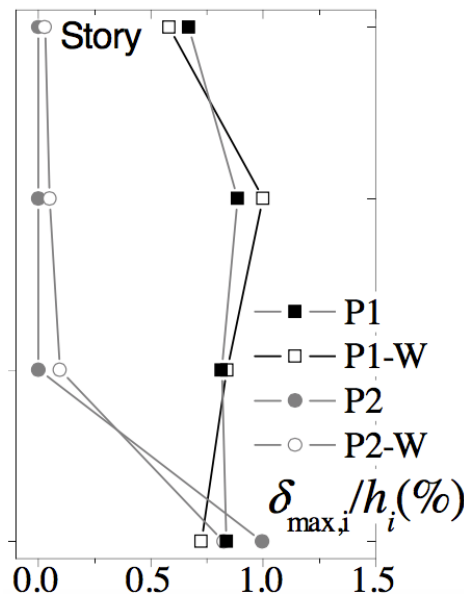


Figure 3.6: Distribution inter-story drift.

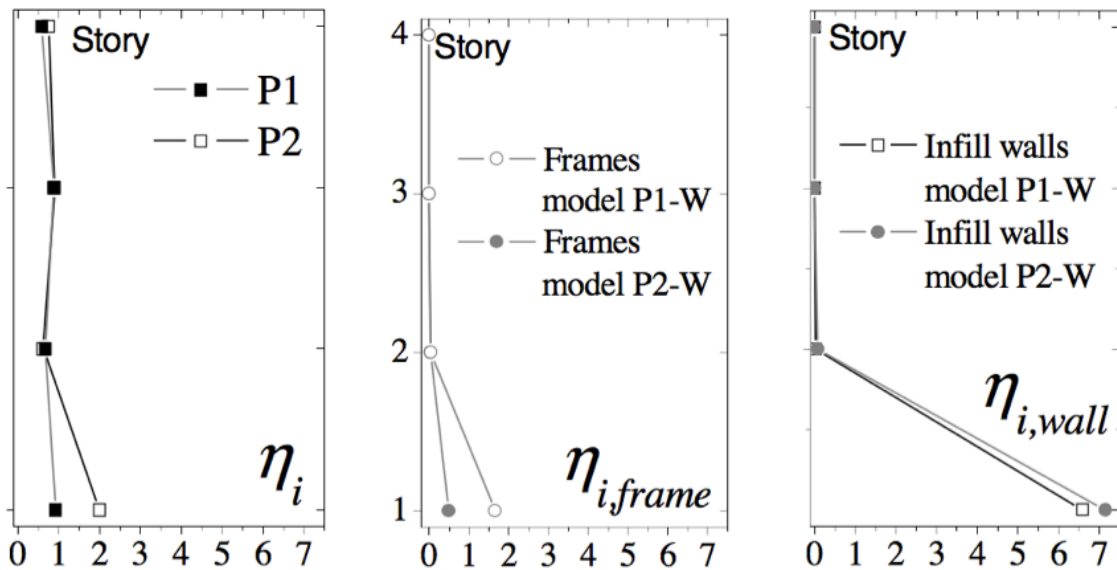


Figure 3.7: Distribution of η_i in bare frames P1, P2 (left); in the frames of the prototypes with infill walls P1-W, P2-W (center); and in the infill walls of the prototypes with infill walls P1-W, P2-W (right).

3.7 Conclusions

Considering or not the presence of masonry infill walls changes significantly the response of the building when subjected to lateral loads. The fundamental period, that is directly related with the inverse of the squared root of initial stiffness of the building, is reduced a half when including the effect of the masonry infill walls on the analysis.

This study has shown the very important influence of masonry infill walls in the seismic behavior of buildings subjected to an earthquake. The vulnerability analysis showed that the prototypes with masonry infill walls were expected to collapse under the Lorca earthquake ($I_V > 1$) while the prototypes without masonry infill panels were lightly “safer” $I_V = 0.75$ and $I_V = 0.95$. The reason for this performance is the adverse influence of the masonry infill panels in the seismic behavior of the building because of the irregular distribution along the height of the building that causes damage concentration, as it will be discussed below. The difference of stiffness provoked that more than the 90% of the total energy input by the earthquake to produce damage concentration on the first level. This problem could have been solved with an improvement in the design codes by considering one of the three options: (1) Use special gaps between the walls and the frame so that the infill walls do not contribute to the overall response; (2) Include special devices that participate in dissipating energy and (3) Ensure the regularity in plan and height of the masonry infill panels along the building.

For prototypes with masonry infill panels, the irregular presence of the walls risks the stability of the building in the stories with wide openings, as when the first levels are used for commerce. Different damage index based on (1) lateral displacement, (2) dissipated energy on the stories, (3) a combination of both lateral displacement and dissipated energy have shown that, for buildings with masonry infill panels, the damage concentrate at the “weakest level”, i.e. the one that does account with a significant lower amount of masonry infill panels. In contrast, the distribution of damage is almost homogeneous along the height of the building for prototypes without masonry infill panels. The damage concentration could have been controlled among sto-

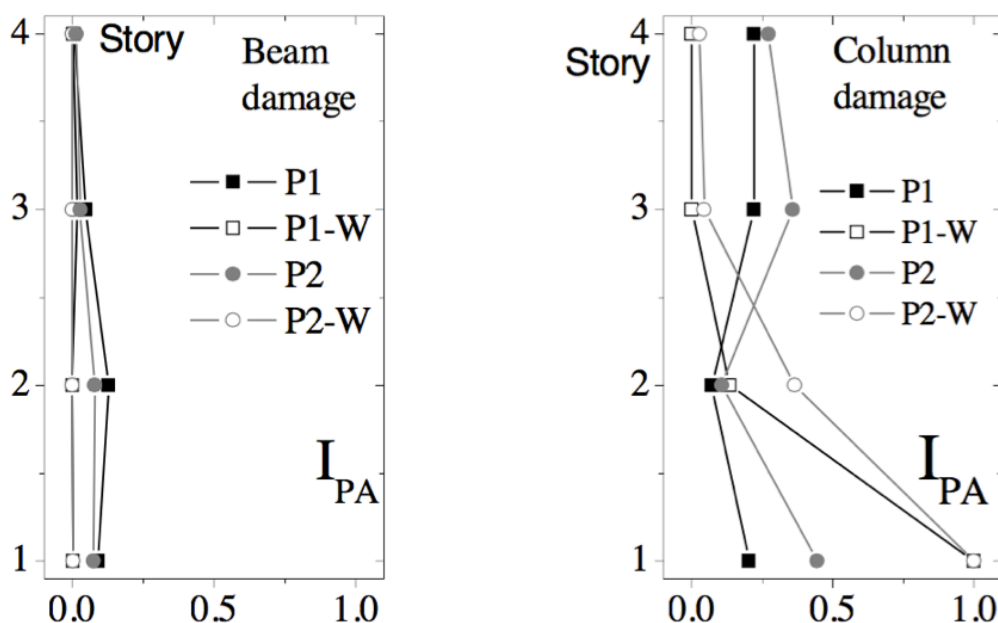


Figure 3.8: Index of damage of Park and Ang (I_{PA}) in: beams (left) and columns (right).

ries with a suitable scale of strength among columns and beams at a local plastic hinge level. If the interaction between the masonry wall and the RC frame would have been controlled or avoided the damage triggered by the Lorca earthquake in this typology of buildings, RC frames with wide beams, would have been much lesser and collapse could have been avoided.

The high value of the lateral strength and stiffness for the masonry infill panels in comparison to the RC frame elements defines a dual system, RC frame plus masonry infill panels, where the walls control the response. We might think then that, if a RC framed building is filled with masonry infill panels in a regular path, the diagonal struts that are formed on the masonry when it experiences lateral loads, control the response. Also, that the distribution of shear along the stories will symbolize the distribution of shear at different levels of a homogeneous wall. In this case, it would be needed to check that the shear strength of the surrounded columns is enough to bear the framing of the masonry and the convenient behavior of the building will be ensured. Based on this discussion, this Thesis will aim to assess the seismic behavior of a retrofitted building with masonry infill panels. First condition imposed is to maintain the regularity of the walls along the height so that damage concentration does not occurs and the forces are distributed linearly along the height. Secondly it will be useful to determine the conditions that make the walls withstand large drifts without abrupt lost of lateral strength, and to check if these conditions are realistic and can be easily achieved. These two aspects, together with the advantages of using masonry infill panels as a retrofitting element presented in Chapter 2, will definitely make the masonry infill walls a convenient retrofitting system for developing countries.

Experimental investigation, analysis of results and proposals

First, this Chapter presents the two campaigns of tests conducted for this Thesis. The objective of the first campaign was to determine the mechanical properties of the masonry infill walls proposed in this Thesis to seismic upgrade existing RC frames in developing countries. It consisted on static tests conducted on relatively small real-scale specimens that represented portions of masonry walls made with clay bricks. The second and more intense campaign of tests was aimed at investigating the dynamic behavior of the mixed system composed of the main RC frame and the infills walls. It consisted on several shaking table tests conducted on large test models ($3 \times 3 \text{m}^2$) that represented real structures scaled at $2/5$. Next, the results of the dynamic shaking table tests are analyzed and then compared with predictions. Finally, based on the results of the dynamic shaking table tests two proposals are made: (1) an equivalent diagonal single-strut model to characterize the infill wall in terms of force-displacement under monotonic loading; and (2) the appropriate values of the parameters that govern the Bouc-Wen model so that it can be used to obtain numerically the response of the infill walls under dynamic loadings.

4.1 First experimental campaign: Static test to determine masonry panel properties

An extensive test campaign was conducted to determine the mechanical properties of mortar, solid bricks and masonry (maximum bending, shear and compressive strength, and Young's modulus).

Mortar and masonry mechanical proprieties were evaluated following the standards in Table 4.1.

The construction of brick units was contracted out to Innovarcilla S.L. due to the need for suitable machinery for producing the scaled bricks. This was to ensure humidity control during drying, and to avoid the formation of micro cracks around the holes of the units and the scale of physical and mechanical properties. Innovarcilla S.L. provided the compressive strength value

Property	Code
Mortar compressive strength	UNE-EN 1015-11
Mortar bending strength	UNE-EN 1015-11
Brick unit compressive strength	UNE-EN 772-1
Masonry compression strength	FEMA 274 C 7.3.2.1
Young's module E_w	FEMA 274 C 7.3.2.1
Masonry shear strength	UNE-EN 1052

Table 4.1: Standard used to evaluate material properties.

for the brick units by following *UNE-EN 772-1 code*. This value did not present any substantial variations in three ten-day spaced static campaigns and was considered as a constant for all units.

- Mortar properties

The compressive and bending strengths of mortar were obtained following *UNE-EN 1015-11 code* in the Materials Laboratory of the University of Granada. Three sets of mortar specimens from each wall were tested daily from the construction of each wall (the second wall was completely built four days after the end of the construction of the first wall). When the values of compressive strength remained stable and similar for the mortar of both walls, the shake-table test campaign discussed in the next sections was conducted in the Structure Laboratory of the University of Granada. Figure 4.1(a) shows the evolution in time of the Compressive Strength of Mortar. This occurred on eleventh day after the end of the construction of the first wall. The mortar specimens tested under bending were 160mm x 40mm x 40mm. Each specimen was divided into two 80mm x 40mm x 40mm sub-specimens after the bending test and tested under compression (Figure 4.1(b)).

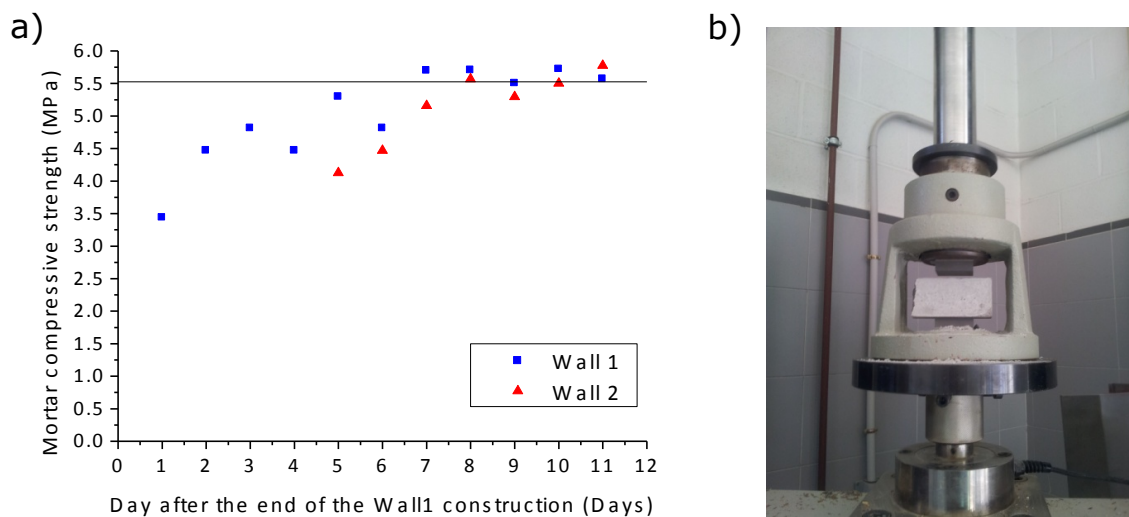


Figure 4.1: a) Evolution in time of the Compressive Strength of Mortar. b) Mortar compression test.

- Masonry properties

Several months later, an extensive campaign of static tests was conducted in the University of Granada, in the Materials Laboratory, following *FEMA 274*, *UNE-EN 1052-3* and *UNE-EN 1052-3:2003/A1* recommendations to determine masonry properties. In order to replicate the same conditions on the masonry as on the day of the shake-table tests, mortar was produced with the same proportions of water, cement and lime. Bending and compression strength were checked to ensure the same values as the wall had during the dynamic tests.

FEMA 356 (Table 7-1) states gives a set of values which classify masonry compression strength, Young's modulus and bed-slide shear strength depending on the quality of the mortar in the wall. The values proposed are considered to be conservative lower guidelines of the real ones, which could be expected to be up to 30% higher. The classifications of "Good condition", "Fair condition" and "Poor condition" aim to take into account the influence of mortar deterioration on the lateral behavior of the masonry wall. The proposed values are compared in (Table 4.2) with the values obtained in the static tests and they decreased by 30%. The masonry walls proposed in this Thesis as seismic upgrading solution are new elements to be installed in the structure and they should be ranked as being in "Good condition". Values from the static tests were 20% higher than the ones given in *FEMA 356*, which is considered as a good approximation, given the difference in the production processes between mortar from the laboratory and from normal construction conditions. This similitude justifies the use of values *FEMA 356* in further numerical analysis when there are no static tests available.

Three tests were performed to obtain masonry compressive strength and modulus of elasticity in compression and ten tests were performed to obtain bed joint shear strength at three different high levels in the wall.

- Masonry compressive strength

Three masonry prisms were constructed with the appropriate mortar and tested at the same age as the unreinforced masonry infill wall was when it was subjected to the dynamic tests. The prisms were capped by two steel plates on the top and bottom using a neoprene band that allowed homogeneous load distribution during the test, and they were tested under uniaxial compression 11 days after their construction. This was done to replicate the exact wall conditions that we had during the shake-table tests. Both the axial load and the axial displacement (measured with a grey scale video-extensometer between the top and bottom bricks) were recorded during these axial compression tests. Figure 4.2(a) shows the configuration of the test and Figure 4.2(b) the stress-strain curve. The typical failure mode consisted of vertical splitting and crushing.

- Bed-slide shear strength

Ten masonry prisms were constructed to evaluate bed-sliding shear strength at three levels in the height of the wall. *UNE-EN 1052-3* and *UNE-EN 1052-3:2003/A1* codes were used for the test set up and evaluation.

The triplet specimens were assemblies of three brick units connected with mortar joints. A constant normal stress was applied to the mortar joints to simulate the weight of the wall at three different height levels. The spring stiffness was chosen so as to transfer the required normal compressive force and to limit its fluctuation to 7% of the specific value and was subjected to a calibration process to ensure its accuracy. After the application of normal force, the middle unit was loaded to slide relative to the other two units.

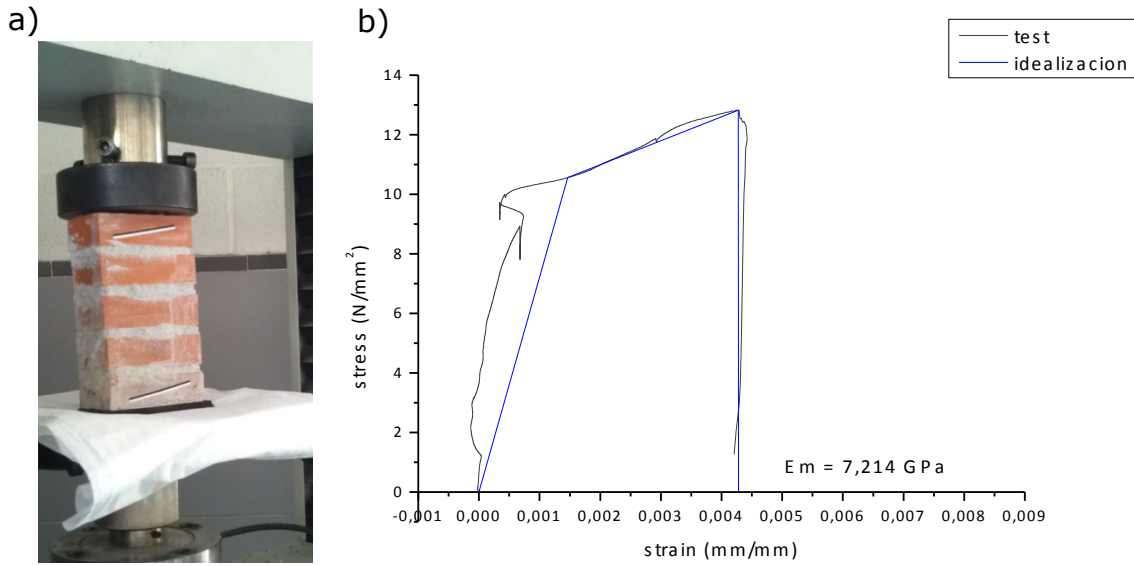
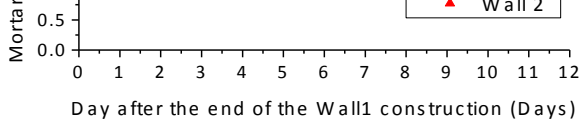


Figure 4.2: a) Static test set up. b) Compression stress-strain curve.

Figure 4.3 show the triplet scheme, spring calibration, test set up and typical mortar failure. Despite the bed-sliding shear strength test having been performed following the UNE code, the analysis of results was calculated following *FEMA 274*, which is allowed if the test set up based on a standard.

The values are summarized below, compared with *FEMA 356* recommendations for a good condition of masonry.

Property	FEMA 356		STATIC TESTS	
	Lower Bound	Expected	Lower Bound	Measured
Compressive strength f'_{cm} (MPa)	6.20	8.06 (6.20x1.3)	10.2/1.3=7.84	10.20
Elastic Modulus in Compression (GPa)	550 f'_{cm} =3.41	4.43 (3.41x1.3)	550·7.84=4.31	6.59
Bed-slide shear strength (MPa)	0.186	0.2418 (x1.3)	0.25/1.3=0.19	0.25

Table 4.2: Default Lower Bound Masonry Properties (good condition).

Infill walls were built one after the other. The construction of each wall took four days. The process started with the north wall and once this was built, the construction of the south wall was started. The dynamic shaking table tests test took place eleven days after the end of the construction of the south wall, when the mortar properties achieved stability and were similar in both walls (Figure 4.1(a)).

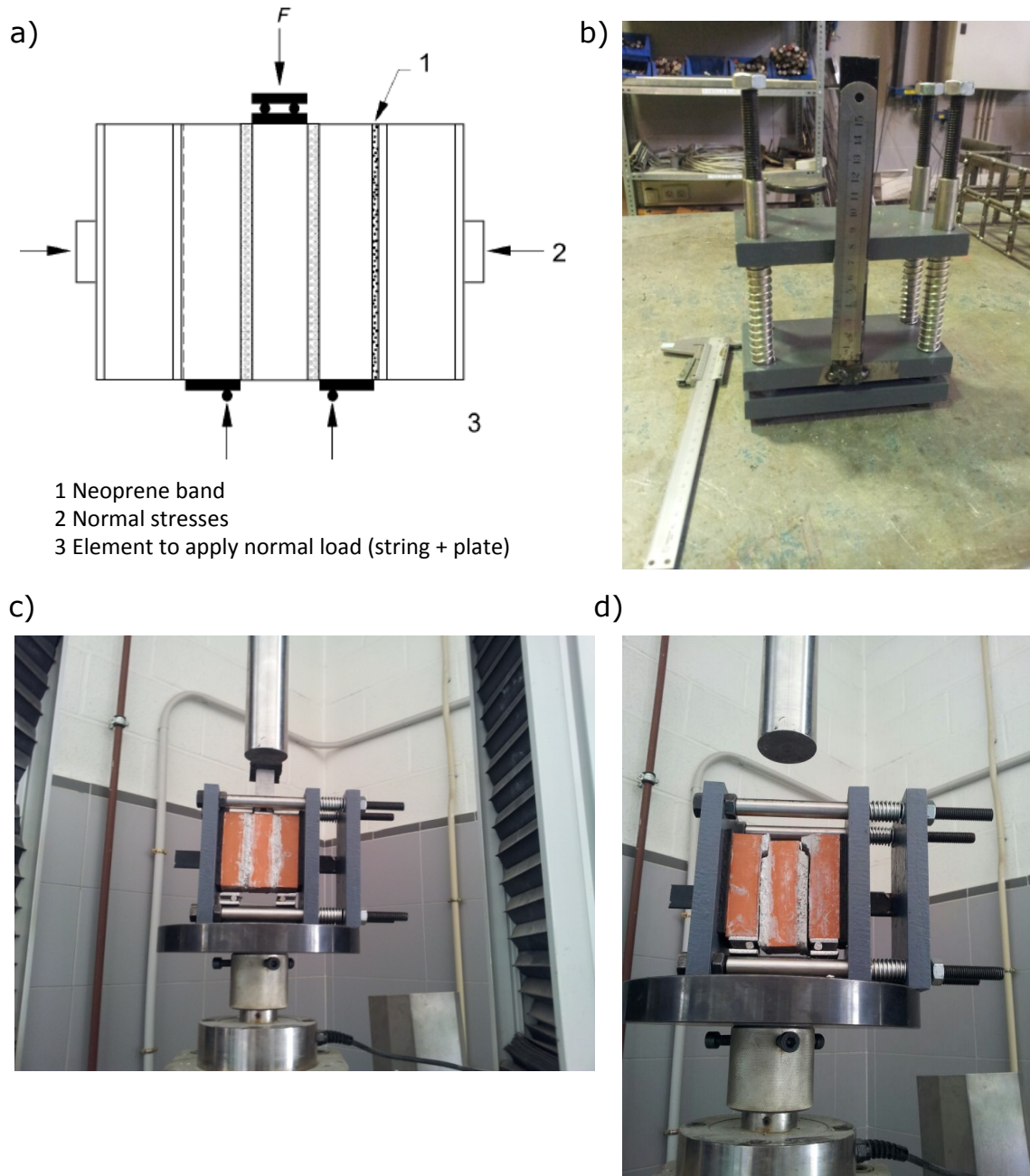


Figure 4.3: a) Triplette scheme. b) Spring calibration. c) Test set up. d) Typical mortar shear failure.

4.2 Second experimental campaign: dynamic shaking table tests

4.2.1 Design of the dynamic tests

The experimental campaign was designed in order to assess the behavior of the mixed system composed of the RC frame and the masonry infill walls. These walls are intended to be used as a retrofitting measure in reinforced concrete framed buildings that have previously been damaged by an earthquake event.

The experimental campaign could not replicate the real scenario in Haiti, as there is no information about technical detailing in buildings due to a lack of construction codes and standards. Moreover, the 2010 earthquake was not recorded in Haiti or nearby, so an acceleration record highlighting information about the properties of the does not exist. At this point, only field information and damage observed in the field can be considered as reliable.

For the sake of coherence with a possible post-earthquake scenario in Haiti, a prototype designed only for gravity loads that already presented some level of damage due to previous earthquakes was used to design the experimental campaign. Any damage on the model could only be caused by subjecting the structure to previous shake-table movement. The model was used to conduct two experimental campaigns, which aimed to assess two different brace-type dampers, which triggered the development of plastic hinges at both ends of columns. The details of the initial shaking table tests conducted on the RC frame test model without infill walls can be found in [Benavent-Climent *et al*, 2014 and Benavent-Climent *et al*, 2015]. In this context, the building of new masonry walls to fill the two parallel damaged frames in the loading direction was considered as the best way to reproduce the required scenario. In the absence of acceleration records for Haiti, the records from the Calitri earthquake recorded at Campano Luciano station were used. It was scaled to different PGAs, as it is explained throughout the study, in order to assess the behavior of the retrofitted structure during a new earthquake, an aftershock, and the final displacement capacity of the structure.

4.2.1.1 Design of the prototype building and test structure without infill walls

A 3 story prototype whose main load bearing system consisting of reinforced concrete frame structure and 3x3 bay was designed to support only gravity loads, as shown in Figure 4.4(a) The prototype was based on an existing structure which was not designed for seismic loads, and as a result, lacked ductile reinforcement details and the strength hierarchy between beams and columns which is given by modern seismic codes. The floor system was made up of one-way joists which were spaced 800mm apart. The main beams supported these joists and a concrete slab with a thickness of 60 mm was supported by these joists. One square meter of this floor system weighed 2.1 kN/m². The self-weight of a light plaster ceiling (0.12 kN/m²) and the self-weight of ceramic flooring (1 kN/m²) were added to this original weight to compute the total dead load of the floor, which was 3.22 kN/m². Regarding the roof, the self-weight of the coating used was 0.85 kN/m², resulting a total dead load of 2.95 kN/m². The dead load corresponding to the partitions were 1 kN/m². To compute and include the self-weight proceeding from beams and columns the specific weight for reinforced concrete was fixed to 25 kN/m³. These loads were multiplied by a factor of 1.5 for live loads and by 1.35 for dead loads. The concrete compressive strength considered in calculations f_{ck} was 25 MPa, and the yield strength for reinforcing steel f_{sy} was 500 MPa.

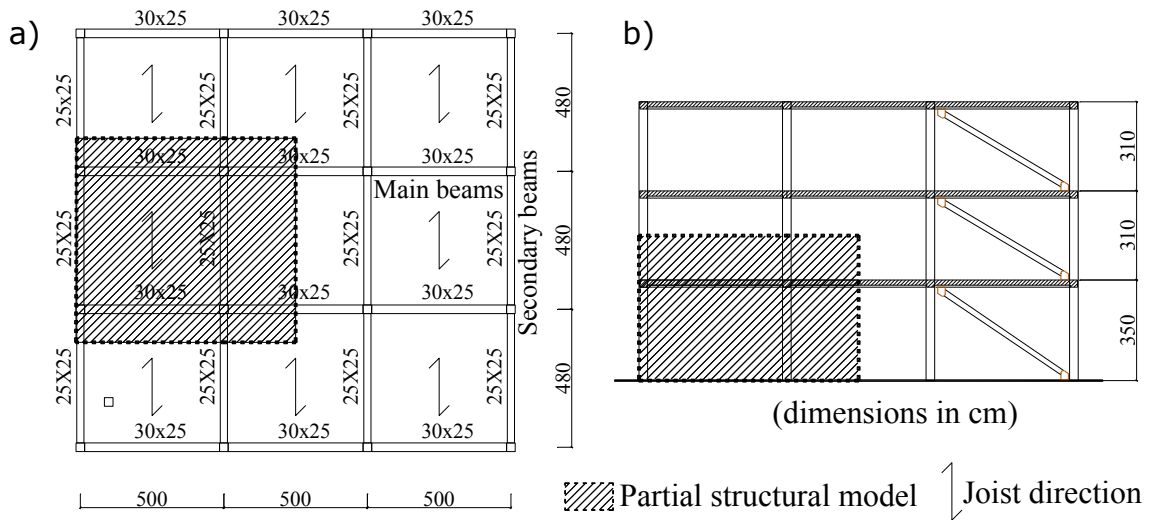


Figure 4.4: Prototype structure: a) plan; b) elevation.

A partial structural model was separated from the prototype structure (the shaded area in Figure 4.4(b)). The partial structural model, measured in the direction of the main beams, was one bay and a half. It was made up of two frames connected by the joists, the thin slab reinforced with a steel mesh, and perpendicular secondary beams. Special attention was needed to satisfy the similitude criterion between the partial structural model and prototype. Since both retrofitted slabs were equal in stiffness and differences caused by the two first campaigns were negligible, this point, gravity mass was considered as equal to seismic mass. The scale factor for length was fixed at 2/5 to accurately accommodate the partial structural model to the dimensions of the shaking table. The bond stresses developed between concrete and reinforcing steel in the model had to be the same as those developed in the prototype for true models (Zia *et al.* 1970), which was only possible if the scale factor for the stress-strain characteristic of the material was set to $S_E = 1$. Finally, the scale factor for response acceleration was set to $S_a = 1$ in order to obtain the same scale factors for force and mass without altering the gravity force. Hence the ground acceleration time histories had to be scaled in time and amplitude to provide consistently scaled seismic forces. The scaling law and resulting scale factors are presented in Table 4.3.

The test structure was built in the Structural Dynamics Laboratory of the University of Granada (Figure 4.5). The total mass, computed as the sum of the (i) mass of the floor diaphragm plus (ii) the actual weight of the floor diaphragm plus (iii) the added weight put on the top of the columns, was $m = 11295 \text{ kg}$.

Table 4.4 shows reinforcement ratios for beams, slab and columns. The concrete compressive strength as well as the reinforcement yield strength (for longitudinal and transverse reinforcement) is shown in Table 4.4. The longitudinal bars had lap splices at the base columns

4.2.1.2 Description of the test structure with infill panels, test set-up and instrumentation

- Description of the test structure with infill panels

The test structure consisted of filling the two RC bare frames in the loading direction with

Quantity	Scaling law	Scale factor
Length	S_L	2/5
Stress	S_σ	1.00
Gravitational acceleration	S_a	1.00
Force	$S_F = S_L^2 \cdot S_\sigma$	4/25
Gravity mass	$S_m^g = S_F \cdot (S_a^g)^{-1}$	4/25
Seismic mass	$S_m^s = S_m^g \cdot \lambda_m^{-1}$	4/25
Seismic acceleration	$S_a^s = S_F \cdot (S_m^s)^{-1}$	1.00
Time	$S_t = (S_L)^{0.5} (S_a^s)^{-0.5}$	0.63
Frequency	$S_f = (S_t)^{-1}$	1.59
Strain	S_ϵ	1.00

Table 4.3: Scale Factors.

Property	Beams / Dir. Of Motion	Beams / Transverse Dir.	Slab	Columns
Cross-Sec. Depth [mm]	100	100	25	120
Cross-Sec. Width[mm]	120	100	-	120
Longitudinal Reinf. Ratio	As/(bxd) = 0.9 to 2.7%	As/(bxd) = 0.7%	As/(sxd) = 0.15%	As/Ag = 0.8%
Transverse Reinf. Ratio Aw/(bxs)	0.35 to 0.84%	0.46%	0	0.36 to 0.6%
Long. Reinf. Yield Stress [MPa]	551	551	551	551
Tran. Reinf. Yield Stress [MPa]	636	636	0	636
Concrete Cylinder Comp. Strength [MPa]	38	38	38	38

Table 4.4: Elements properties.

solid clay bricks, preserving the 2/5 length scale.

The bricks were designed according to Haitian recommendations [MTPTC and MICT, 2010] for masonry walls, for which the dimensional proportions (length, height and width) were 20x5.7x10, the minimal uniaxial compression strength was 10MPa and it allowed the flow and continuity of the mortar of the vertical dimension through two arrays of five vertical cylinders. The diameter of each vertical cylinder was estimated using *CTE*, for solid clay bricks (total hole volume being relative to the total rough volume 15.7% < 25%; individual hole volume being relative to the total rough volume 1.57% < 12.5%). The manufacturing process of the bricks took place at “Innovarcilla Centro Tecnológico” (Jaén, Spain) where all the machines and their modules were updated to replicate the size and design of the bricks, and also to achieve optimal conditions in extrusion flow velocity and in rugosity. Humidity and temperature conditions were controlled during drying time.

The mortar had the verified properties required by *UNE EN 998-2* and *UNE EN 998-1* specifications for “ordinary outer constructions and protection against fire” and had a minimal compression strength of 7.5 MPa. The thickness of the mortar joint in the specimen was also to scale, resulting in a thickness of 4-6mm.

- Set up

The test setup can be seen in Figure 4.6. The mass required to simulate the upper floors was provided by steel plates leaning on the shake direction beams for the first floor. For the axial forces on columns, eight steel plates were held by the columns of the second floor. Figure 4.7 shows the test set up.

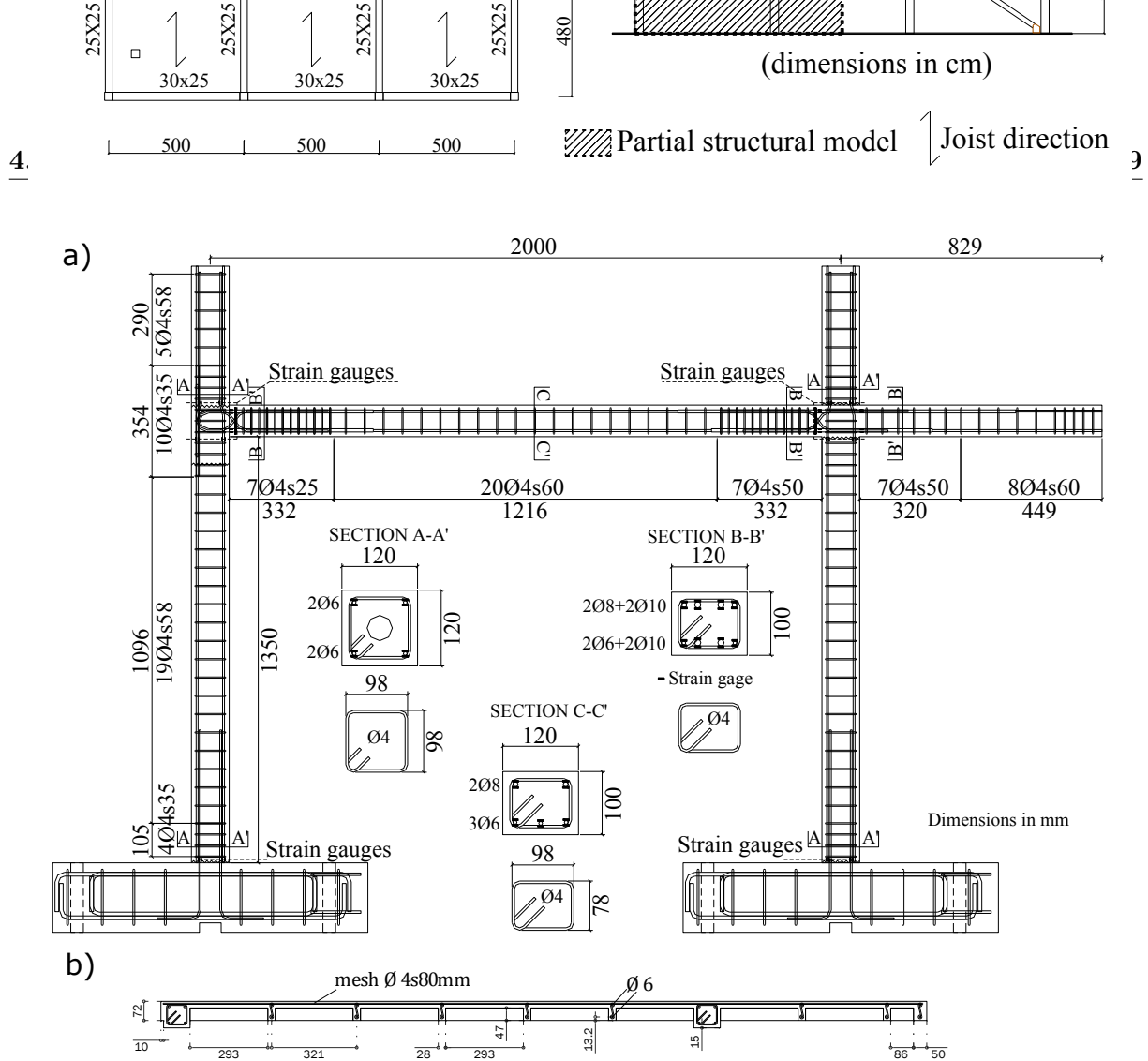


Figure 4.5: Detailing of the RC frames (a) and slab (b) of the test specimen.

- Instrumentation

The instrumentation array used in these tests included 216 strain gauges placed on the reinforcing bars, 5 accelerometers (piezoelectric type) and 15 LVDTs. Five video cameras were used to record and monitor the structural response at global and critical points, such as the base and the relative displacement between frames.

Relative displacement between the first story and the shake-table was measured by 2 LVDTs in the motion direction. There was a third LVDT that measured the displacement perpendicular to the loading direction and allowed torsion effects to be measured. Given that the upper part of the structure was stiffened by diagonal bars, displacements on the upper part of the columns were found to be basically the same as on the first floor. A positive story drift means that the upper floor moved westwards with respect to the shake table.

Strain gages were attached on the longitudinal and transverse reinforcing bars. Those data are used to calculate the axial strains and curvatures in the columns and beams.

4.2.1.3 Seismic simulations

Before retrofitting with infill walls, the RC frame structure was subjected to two consecutive campaigns of shake-table tests that are described in [Benavent-Climent *et al*, 2014 and Benavent-Climent *et al*, 2015]. Each campaign included several seismic simulations. In the first



Figure 4.6: Test set up.

campaign, the RC frame structure was tested with brace-type hysteretic dampers installed on both stories. In the second campaign, the second story was stiffened with very rigid steel cross braces and brace-type hysteretic dampers were only installed at the first story. These two campaigns damaged the RC frame structure, which triggered the development of plastic hinges at both ends of the columns of the first story (labeled 10, 20, 30, 40, 11, 21, 31 and 41 in Figure 4.8). In these hinges, the maximum strains ε_{max} in the longitudinal reinforcement exceeded the yield strain ε_y by up to 5 times, the maximum chord rotation θ_m exceeded the yield rotation θ_y ($=9.45 \times 10^{-3}$) by about 1.8 times and reached 40% of the ultimate rotation capacity θ_u ($=43.05 \times 10^{-3}$) of the section. Here, θ_y and θ_u were calculated using the equations proposed by *Fardis (2009)*. The Park and Ang index [*Park and Ang 1985*] of these hinges ranged between 0.48 and 1.29 at the lower end of the columns and between 0.23 and 0.24 at the upper ends. The width of the concrete cracks ranged between 0.08 and 0.2 mm. The structure reached maximum inter-story drifts of 1.5% and the residual inter-story drift was 0.12%. According to *ATC-40* and *FEMA-356* this corresponds to a seismic performance level of “life safety” and a moderate level of damage. The capacity curve of the bare RC frame was approximated by using a bilinear curve characterized by a yield inter-story drift of 0.27% and a yield base shear force normalized by the total weight of 0.10.

Next, the RC frame was retrofitted with two masonry infill walls (see Figure 4.6) and subjected to a third campaign of shake-table tests that included four seismic simulations. These simulations are referred to as C100, C100B, C200 and C250 hereafter.

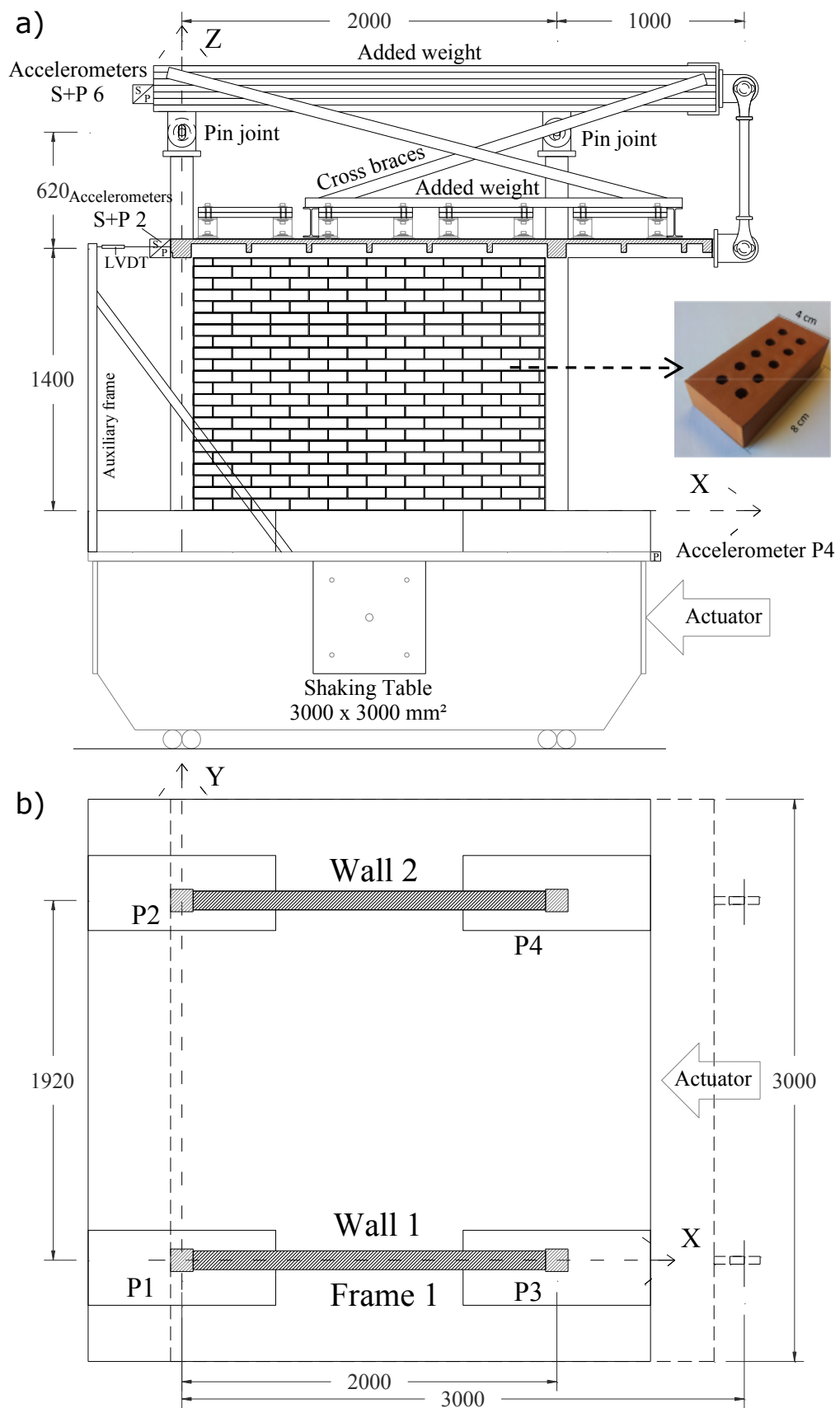


Figure 4.7: Dynamic test set up and instrumentation (dimensions in millimeters)

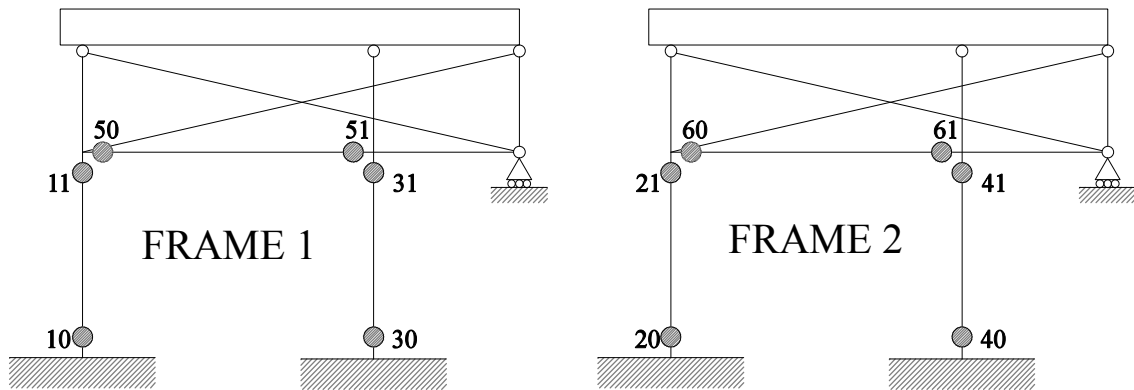


Figure 4.8: Location of strain gauges at the end of RC members

In all seismic simulations the NS component of the Campano-Lucano ground motion recorded at Calitri (Italy) was applied in a single horizontal direction (see actuator in Figure 4.7). This motion was recorded at a distance of 16km from the epicenter in stiff soil. The record corresponds to an earthquake of a moment magnitude of 6.9 and intensity VII on the MSK scale. The maximum acceleration was $0.15g$. To fulfill the similarity laws, the Calitri record was scaled in time by factor $S_t = 1/2$.

The dynamic-test campaign aimed to assess two different aspects of a reinforced concrete frame structure retrofitted with infill panels (RCIW), when subjected to four seismic hazard levels (SHLs):

- One aspect was to evaluate the seismic response of a damaged RCIW for a frequent earthquake scenario that implies a return period, T_R , of 200 years, where a main shock (seismic simulation C100) was also followed by a frequent earthquake aftershock, but which was lower in intensity with a T_R of 100 years (seismic simulation C100B) without sufficient time to evaluate and repair the original RCIW.
- The second aspect was to evaluate the ultimate capacity of the RCIW in terms of maximum displacement and maximum shear strength. This aspect was evaluated through two more new seismic simulations, C200 and C250, corresponding to a maximum earthquake scenario with T_R equal to 1500 years, and 5000 years.

The city of Port-au-Prince, in Haiti, was used as a reference to determine the amplitude scaling factor of the accelerogram. Port-au-Prince is surrounded by the Enriquillo-Plantain Garden and the Matheux-Neiba faults so it was also one of the cities that had the highest number of most damaged low-rise buildings in the earthquake on the 12th January 2010. A number of these buildings have been technically observed by Professor Pujol, from Purdue University, providing a powerful database where the plan and dimensions of the structures and the level of damage in each structural element typology are summarized [Chungwook Sim et al. <https://datacenterhub.org/resources/123>]. Also, an intense array of GPS devices provided information from the slip motions in the country, previous to and during this earthquake, which was used by Frankel [Frankel et al. 2011] to define probabilistic seismic hazard maps for the country, considering peak ground acceleration in stiff soil. The influence of the soil typology that amplifies the PGA can be measured through the shear wave velocity between 0 and 30 meters,

V_{S30} . Frankel [Frankel et al. 2011] also took into account the effect of soil amplification using the methodology proposed by Wald and Allen (2007) that empirically relates the value of V_{S30} (shear wave velocity between 0 and 30 meters) and topographic slope. The probabilistic seismic hazard map of Port-au-Prince which considers PGA is summarized in Table 4.5:

Type of soil	T_R (years)	V_{S30} (m/sec)	PGA (g)
Stiff soil	245		0.30
Stiff soil + soil amplification	245	300-360	0.36
Stiff soil	2475		0.60
Stiff soil + soil amplification	2475		0.70

Table 4.5: PGA in Port-au-Prince.

The PGA and the T_R are related using the following expression:

$$PGA_{TR} = PGA_Y \left(\frac{T_R}{Y} \right)^{0.4} \quad (4.1)$$

where Y is a given period of return and PGA_Y the value of PGA associated to Y . This expression is based on its similitude with $PGA_{TR} = PGA_{500} \left(\frac{T_R}{500} \right)^{0.4}$ from the Spanish Seismic Code *NCSE-02 (2002)*. The value of PGA associated with a return period of 245 years was used to estimate the PGA for a frequent earthquake scenario (seismic simulation C100 and seismic simulation C100B) while the value of PGA associated with a return period of 2475 years was used to estimate the PGA for a maximum earthquake scenario (seismic simulation C200 and seismic simulation C250).

The amplitude of the accelerogram records of Calitri was scaled by multiplying by a factor obtained after the expression:

$$S_{amplitude} = \frac{PGA(g)}{0.16g} \quad (4.2)$$

The values of PGA for the SHLs defined above, together with the scaling factor needed to be applied to the Calitri records, are summarized in Table 4.6:

Seismic scenario	SHL 1	SHL 2	SHL 3	SHL 4
Experimental simulation	C100	C100B	C200	C250
T_R (years)	200	100	1500	5000
PGA Port-au-Prince (g)	0.25	0.18	0.57	0.93
$S_{amplitude}$	1.56	1.13	3.56	5.81

Table 4.6: Seismic scenario under study.

Figure 4.9 shows the time history of the acceleration and Figure 4.10 shows the normalized spectrum of the original (unscaled) motion for 5% damping, together with the initial period of the RCIW structure and the period of the RC damaged frame.

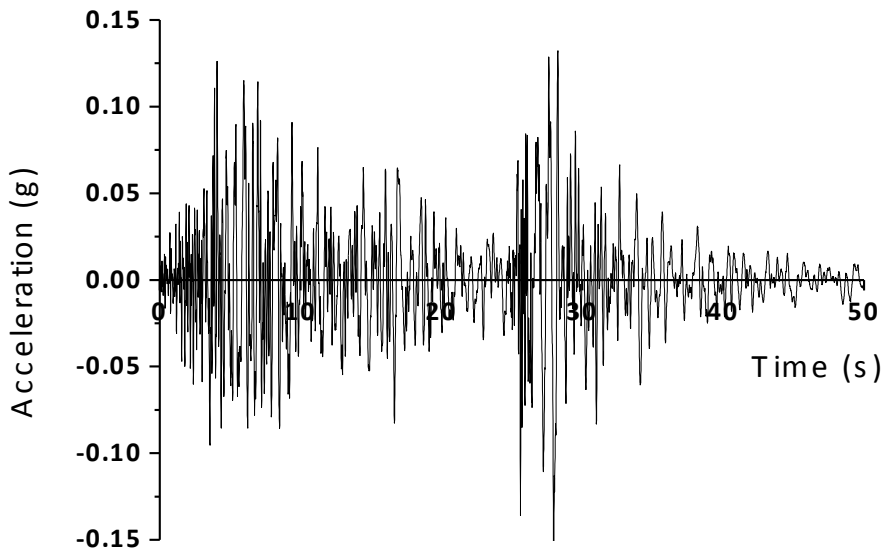


Figure 4.9: Time story of the acceleration.

A consequence of the sequence of the seismic simulations was that it guaranteed the increase of damage in the RCIW. This implied that any analysis of the test results after cracking in the RCIW should account for the repercussions of the loading history and the pre-existing damage to the RCIW. Also, cracking and damage in the structure was directly related to the change in the fundamental frequency of the structure, which required a re-evaluation of the scaling factor of the accelerograms so that the PGA of the motion introduced to the RCIW could be related to the PGA of the original earthquake. To measure this possible difference, the spectral acceleration was calculated as the mean of a range in the last two simulations that encompass all the frequencies between the fundamental frequency at the end of the previous tests with the fundamental frequency at the end of the given test, obtained by free vibration analysis. The new scaling factor $R_{S-amplitude}$ is the ratio between this spectral acceleration and the spectral acceleration for the same range of frequencies of the original earthquake record. Table 4.7 shows the differences between the amplitude factor estimated a priori and its comparison with the real one.

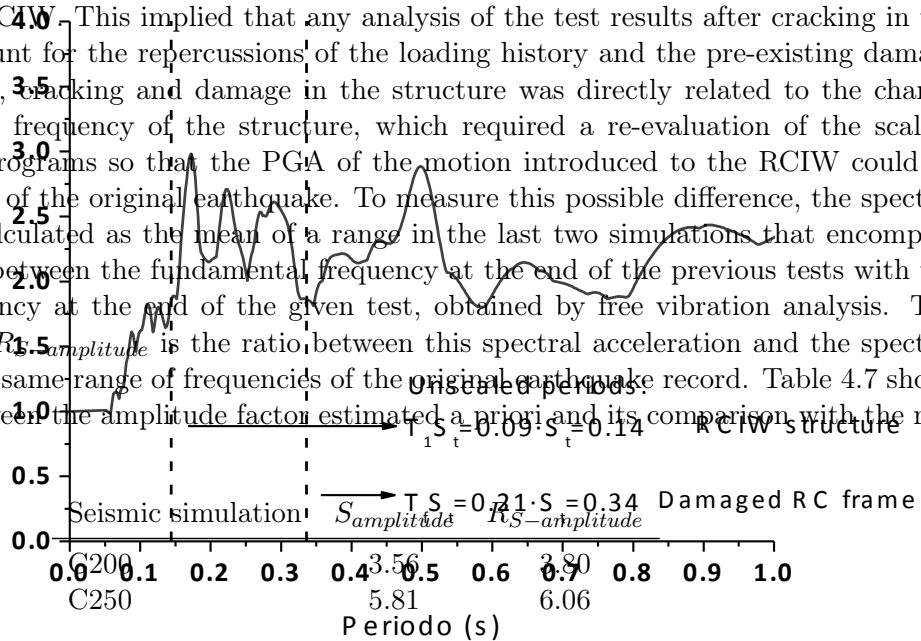


Table 4.7: Scaling factor for Calitri record.

4.2.2 Analysis of test results and comparison with predictions

4.2.2.1 Overall response. Frequency analysis. Damping

The test structure is idealized with a single degree of freedom system, of mass m , whose dynamic equilibrium is governed by:

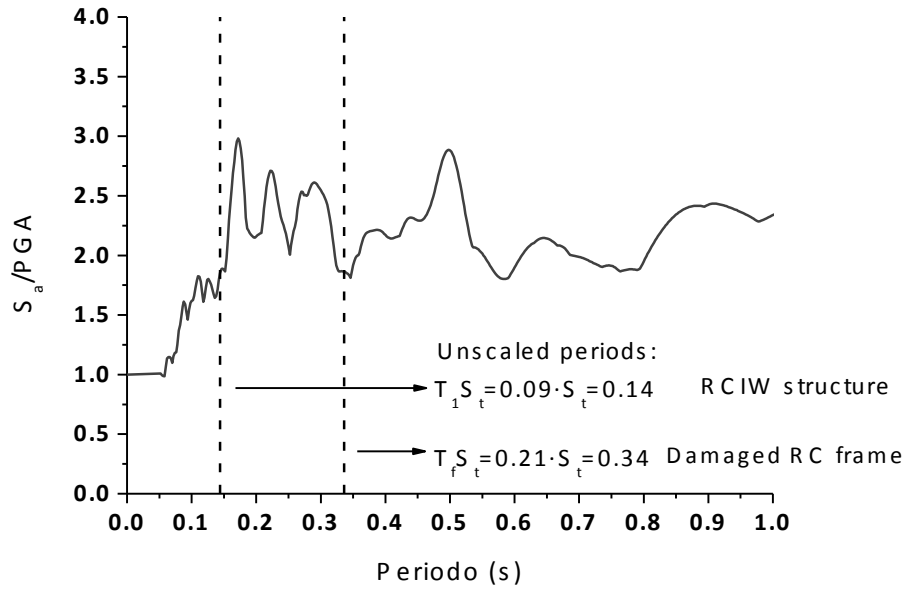


Figure 4.10: TNormalized spectrum.

$$m\ddot{u}' + c\dot{u} + Q_B = 0 \quad (4.3)$$

Here \ddot{u}' is absolute acceleration, c is the damping coefficient, \dot{u} is relative velocity and Q_B is the restoring force exerted by the structure. Since m was known and \ddot{u}' was measured with the accelerometers, the inertial force $F_{I,B}$, sum of the shear forces carried by the structure Q_B and the damping forces $F_{I,B} = m\ddot{u}' = (c\dot{u} + Q_B)$, can be readily calculated. For convenience, the shear force $F_{I,B}$ can be normalized by the total weight W ($=122$ kN), and the lateral displacement u by the clear story height h ($=1360$ mm), obtaining the inter-story drift. The normalized $F_{I,B}/W - ID$ curves are shown in Figure 4.11 for each seismic simulation.

- Frequency analysis.

As infill cracks separated from the surrounding frame quite early in the response, the frequency content of the non-linear response was controlled by the frame, despite the very high stiffness of the uncracked infills [Fardis *et al.* 1997].

An extensive analysis of both signals (input: shake table acceleration, output: first floor diaphragm acceleration) is shown in Figure 4.12. The complete signal of each motion was divided into a set of windows, with a 2^n number of elements, and whose extremes achieved zero. The Fourier response spectra was calculated for each window and the average of the values of the spectrum at each frequency is represented on the plotted figure, Figure 4.12 in blue, by using the Pwelch function. The results are displayed together with the global Fourier response spectrum for each signal (in red). This process aimed to extend the analysis and eliminate one-off peaks by the softening of the response spectrum and to increase its accuracy. Also, the Transfer function (TF) calculated as the Fourier transform of the diaphragm acceleration (A_{floor}) to the Fourier transform of the base acceleration (A_{base}) defines the natural frequency of the test structure. It is worth emphasizing the apparition of high frequencies directly related to the presence of the infill. The frequency associated with the presence of the infill did not necessarily decrease during the tests as different

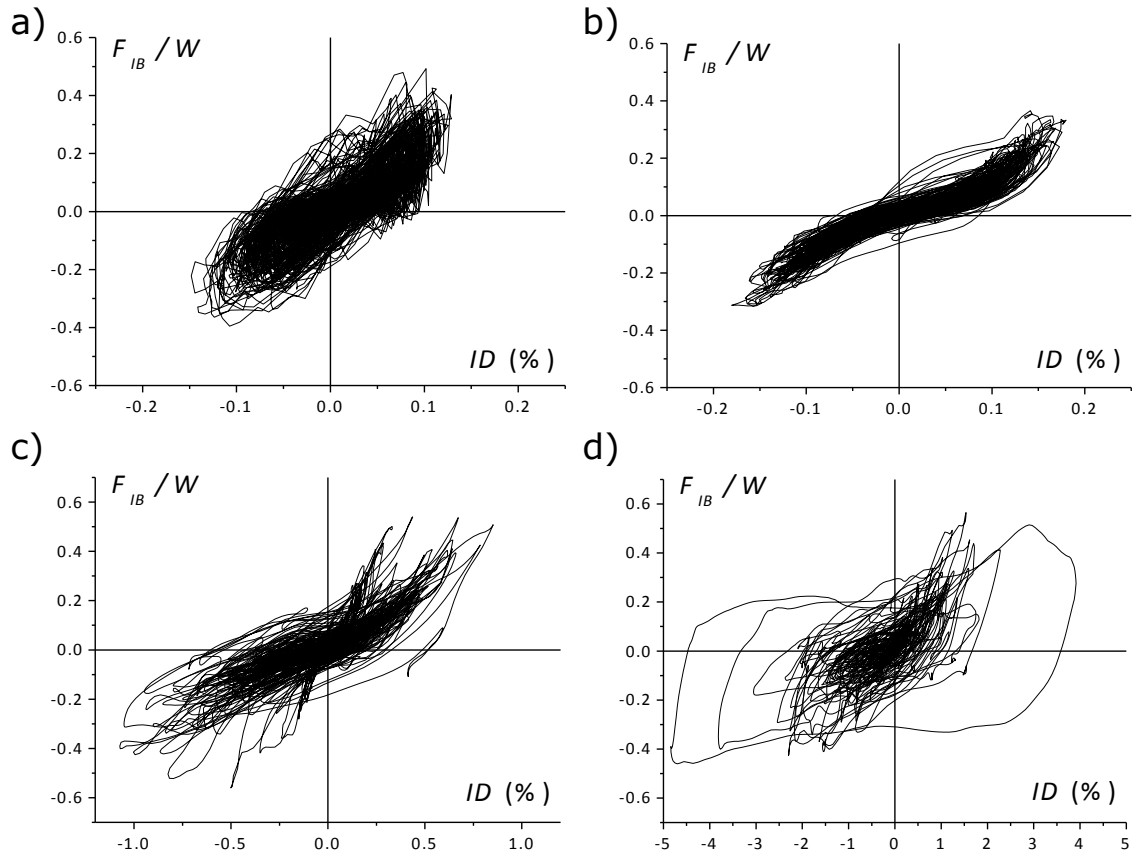


Figure 4.11: Total base shear vs. drift for simulations: a) C100, b) C100B, c) C200, d) C250.)

mechanisms of energy dissipation can develop during dynamic excitation. Nevertheless, the presence of high frequencies during C250 proved that the infill still works despite the large lateral displacement demand. Moreover, the value of this frequency in C100B (11.66 s^{-1} , i.e. fundamental period $T_1=0.086$) gives an accurate estimation of the initial stiffness of the whole structure. This is supported by the fact that the infill panels completely separated during C100B (Figures 4.14 (c) and (d)) and it is reasonable to consider that during this motion the maximum stiffness of the whole structure was attained. Table 4.8 summarizes the natural frequencies obtained by both methods for each run. It is worth noting that the frequency obtained in free vibration closely matches that obtained from the output acceleration of the Fourier Spectra, but the analysis of the transfer function was needed to understand the role of the infill panels during dynamic excitation.

Natural frequency	C100	C100B	C200	C250
$w \text{ (s}^{-1}\text{)}$ Transfer Function	5.53	3.74	2.99	2.01
$w \text{ (s}^{-1}\text{)}$ Free vibration	5.00	4.76	1.85	1.02

Table 4.8: Natural frequency of the specimen during and after each seismic simulation.

- Damping.

A marker of the variation in the dynamic properties of the RCIW caused by induced damage

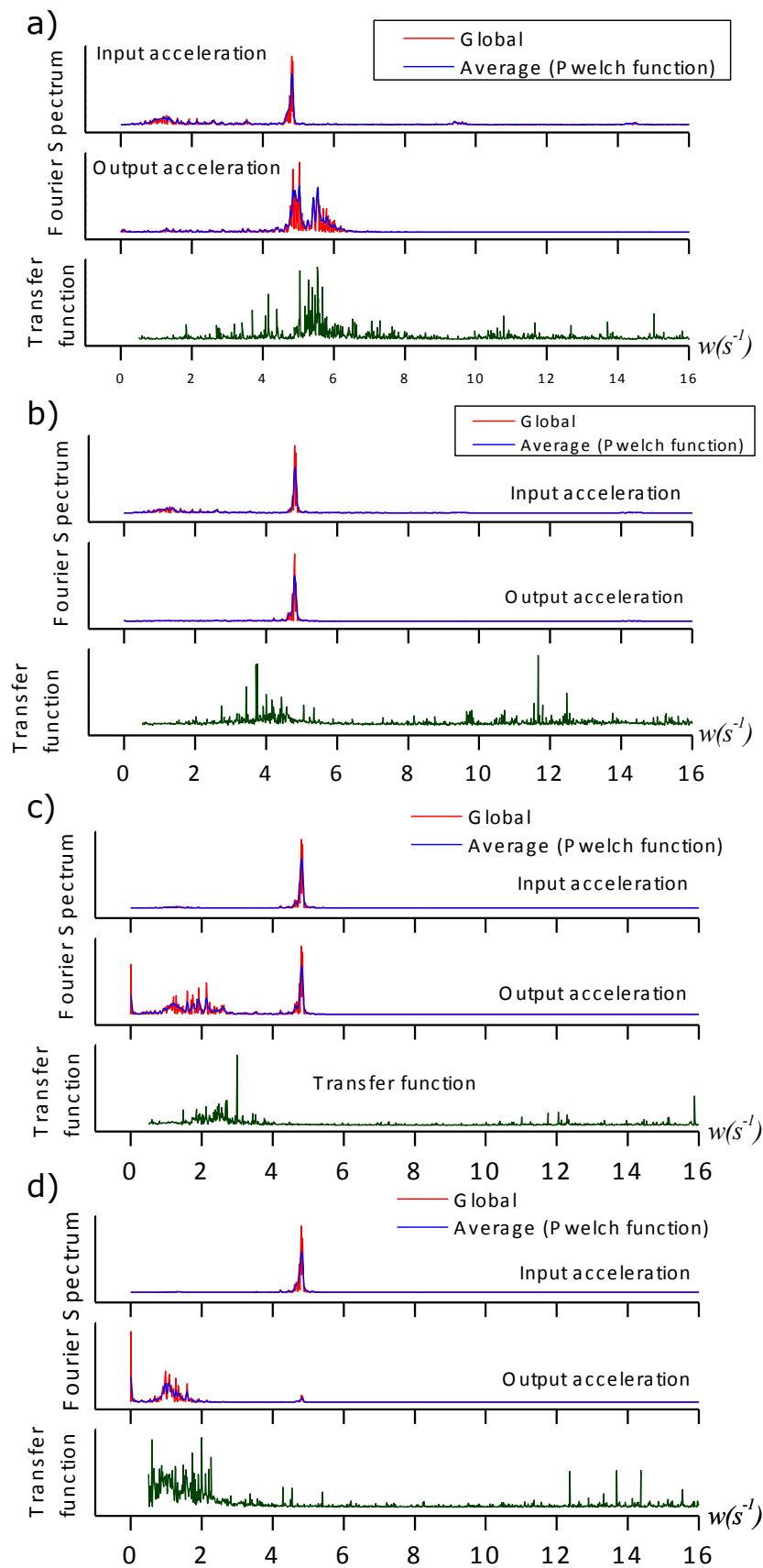


Figure 4.12: Seismic simulation: Frequency analysis, Fourier Spectra (red) versus Pwelch: input acceleration spectra and specimen acceleration spectra. Transfer function (green). a) C100, b) C100B, c) C200 and d) C250.

during each seismic simulation was the change in the damping ratio. The viscous damping ratio can be described as $\xi = \hat{c}/c_{cr}$ where $c_{cr} = 2mw_n = 4\pi\frac{m}{T_n}$ the critical damping of the test structure, m is the total mass, w_n is the natural frequency of the test structure and T_n is the natural period of the test structure.

The viscous damping ratio could be estimated at the end of each test, when the input of acceleration on the base of the structure was null but the structure was still moving in free vibration. This result is presented in Table 4.9.

A value of hysteretic and viscous damping (Table 4.9) was obtained using the energy equivalent method, which estimated the equivalent damping ratio as:

$$\xi = \frac{E_d}{4\pi E_{s0}} \quad (4.4)$$

where E_d is the dissipated energy and E_{s0} is the maximum strain energy in each cycle [Chopra, 2001].

Hashemi and Mosalan (PEER 2007/100) found that these damping values, when there is significant hysteretic energy dissipation in the test structure, are higher than those obtained using linear regression of function $F = -(\hat{c}\dot{u} + \hat{k}u)$ in the (u, \dot{u}) space. Nevertheless, the error is similar to the real one in both methods, as the equivalent energy method includes both the viscous damping and the inelastic deformations as sources of dissipating energy, and the regression method underestimated \hat{k} within each run leading to an overestimation of \hat{c} . Figure 4.13 shows the values of the total dissipated energy and the sum of the maximum strain energy over all cycles. It is worth noting that the difference between the values obtained from free vibration and the energy equivalent method can be also explained by the presence of different modes of vibration during the dynamic excitation and the free vibration.

	C100	C100B	C200	C250
ξ (%) Free Vibration (hysteretic)	3.4	4.0	2.7	1.9
ξ (%) Energy equivalent (viscous + hysteretic)	1.3	7.62	7.8	17.7

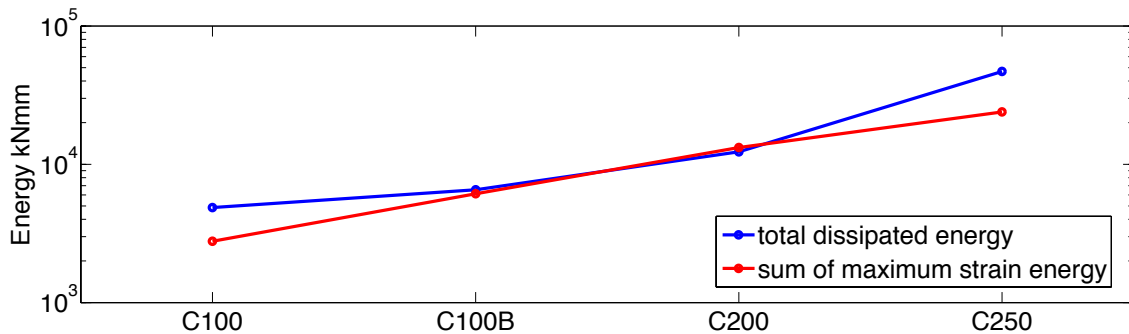


Figure 4.13: Total dissipated energy and sum of maximum strain energy.

- Overall response.

The overall response is summarized in Table 4.10 using the maximum absolute response acceleration, \ddot{u}_{max}^t , the maximum inter-story drift ID_{max} and the residual inter-story drift ID_r . This table also shows the peak acceleration applied to the shake-table, PGA , the fundamental period T_1 calculated at the end of each simulation, the fraction of critical damping ξ calculated at the end of each seismic simulation from the free vibration tests, the damage level, and the need for repair estimated according to *ATC-40* and *FEMA-356*. Figure 4.14 shows the mortar-brick crushing and cracking pattern visible to the naked eye at the end of each seismic simulation. Based on Figure 4.14, Table 4.10 and observations, the overall response can be summarized as follows:

		PGA (g)	T_1	ξ (%)	\ddot{u}_{max}^t (g)	ID_{max} (%)	ID_r (%)	Damage level	Need of repair
Prior to test		-	0.09	-		1.50	0.12		
Seismic simulations	C100	0.25	0.21	3.4	0.49	0.15	0.00	Minor	None
	C100B	0.18	0.21	4.0	0.37	0.18	0.01	Mild	Minor
	C200	0.57	0.54	2.7	0.56	1.07	0.06	Severe	Extensive
	C250	0.91	0.98	1.9	0.56	4.84	0.38	Severe	Beyond repair

Table 4.10: Results of the seismic simulations.

The inspection at the end of the C100 and C100B seismic simulations did not reveal any extra visible damage to the RC frame (i.e. in comparison to the damage state before strengthening with infill walls). The maximum ε_{max} strains recorded in the longitudinal rebars remained far below the yield strain ε_y (more precisely, $\varepsilon_{max} < 0.57\varepsilon_y$). Nevertheless, openings in the infill joints initiated in the seismic simulation C100 and extended and became clearly visible during the C100B simulation (see Figures 4.14 (c) and (d)). The infills started to separate from the central region of the enclosing beam and columns during the C100 simulation (Figures 4.14 (a) and (b)). This separation affected between 1/3 and 1/5 of the column height. During the seismic simulation C100B, this separation increased and diagonal and horizontal cracks were clearly visible in the infills, accompanied by some crushing on the mortar at the corners (see Figures 4.14 (c) and (d)). The maximum inter-story drifts experienced by the test specimen in the C100 and C100B simulations (0.15% and 0.18%) were too small to damage the RC frame, but large enough to cause noticeable cracking in the infill walls. This cracking in the infill walls caused the elongation of the fundamental period T_1 from 0.09s (before tests) to 0.21s at the end of seismic simulation C100. T_1 remained unchanged at the end of the C100B simulation. The effects of cracking and the possible sliding of the infill can also be observed in the $F_{IB}/W - ID$ curves, whose loops tend to be more pinched in the C100B seismic simulation (Figure 4.11 (b)) than in the C100 simulation (Figure 4.11 (a)).

During the C200 seismic simulation the test specimen reached an inter-story drift of 1%, and a large number of new cracks appeared in the columns. The maximum strains ε_{max} recorded in the longitudinal rebars of the columns reached up to 8.4 times the yield strain ε_y , while remaining below ε_y in the beams. The widths of the diagonal and horizontal cracks which had opened in the infills during previous simulations increased notably (see Figures 4.14 (e) and (f)). During C250 the specimen reached a maximum inter-story drift of 4.7%. The maximum strains ε_{max} recorded in the longitudinal rebars of the columns attained values of up to 10 times the yield strain ε_y , while remaining below ε_y in most beams. The columns bent and ended with a residual horizontal deflection at mid-point equal to 1.1% of the column height (see Figures 4.14 (g) and (h)). Some portions of the masonry units dropped/fell off. New large diagonal cracks developed in the infill walls.

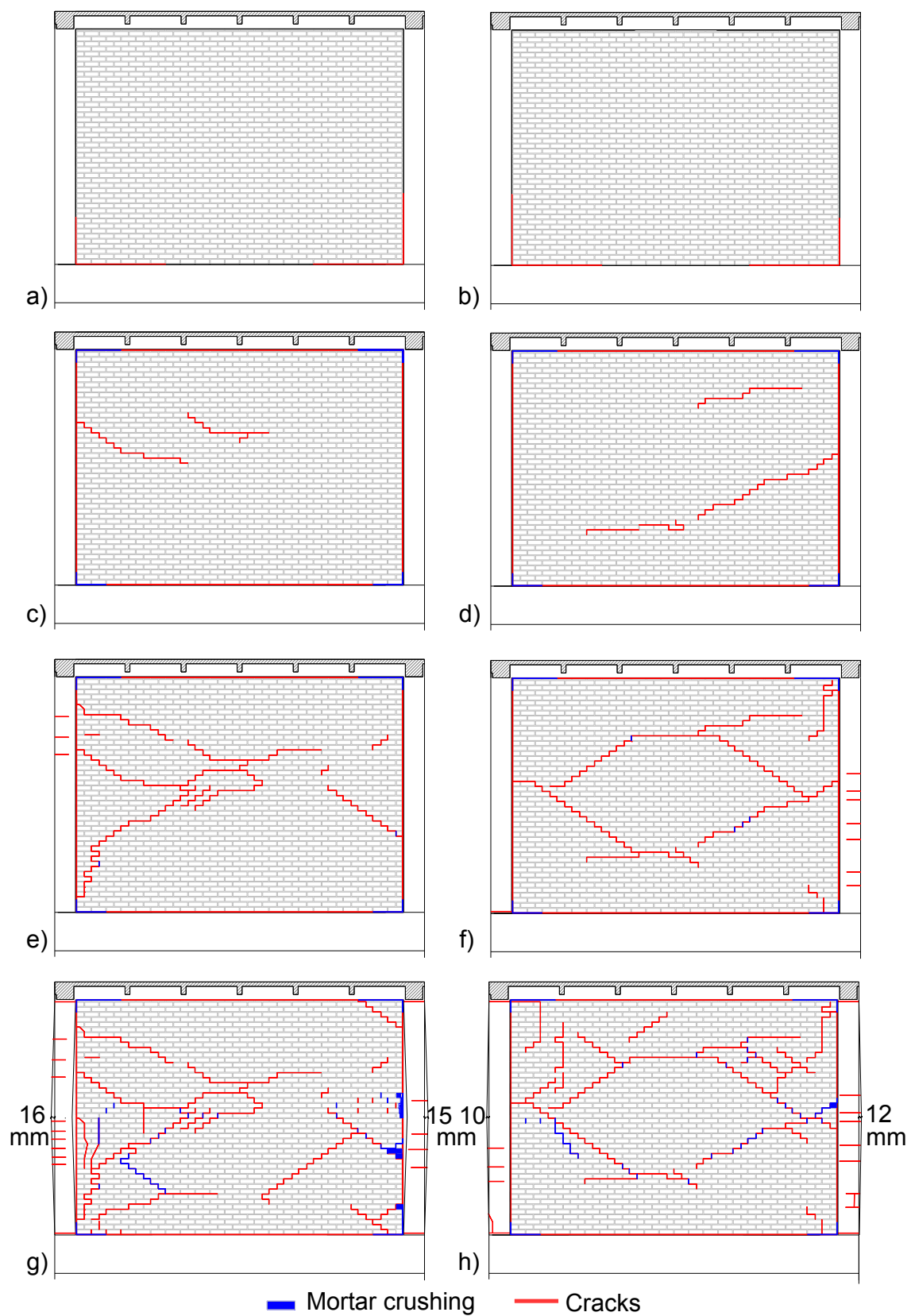


Figure 4.14: Crack pattern on wall 1 (left column) and wall 2 (right column) at the end of each seismic simulation: (a, b) C100; (c, d) C100B; (e, f) C200; (g, h) C250.

At this point, the test specimen was considered to have collapsed. The severe damage seen in the test specimen during the C200 and C250 simulations is consistent with the noticeable enlargement of the fundamental period T_1 , that increased by about 250% and 200%, respectively. This T_1 enlargement corresponds to a lateral stiffness reduction of up to 15% and 5% of the initial value. Nevertheless, it is worth noting the reasonable “full” loop of the $F_{IB} - ID$ relationship at about 5% drift in Figure 4.11 (d). This indicates that despite the severe level of damage endured by the test specimen in the last seismic simulation, this specimen was able to keep a sizeable portion of its maximum lateral capacity and dissipate a large amount of energy. It is also worth noting that, contrary to the common belief that RC frames with infill walls are relatively brittle, the test structure reached drift ratios of up to 5% without signs of catastrophic failure. This result opens a door to a new realm of possibilities for infill walls as a seismic retrofit solution for existing RC frames.

4.2.2.2 Capacity curve of the overall structure

When velocity is zero (i.e. instances of maximum lateral displacement), damping forces are null and inertia force $F_{I,B}$ equals the shear force resisted by the overall structure (frames+walls) Q_B . Points of null damping force are shown in Figure 4.15, where Q_B was normalized relative to weight W . From this point cloud, those points with drift ratios larger than drifts attained in previous cycles were selected and approximated with a four-segment polygonal curve that is shown with a dash-dot-dot line in the figure (experimental envelope). This curve can be interpreted as the experimental "capacity curve" of the overall structure. The initial segment of this curve ended at a drift of about 0.07%, that is, the structure remained linear up to approximately 0.07%.

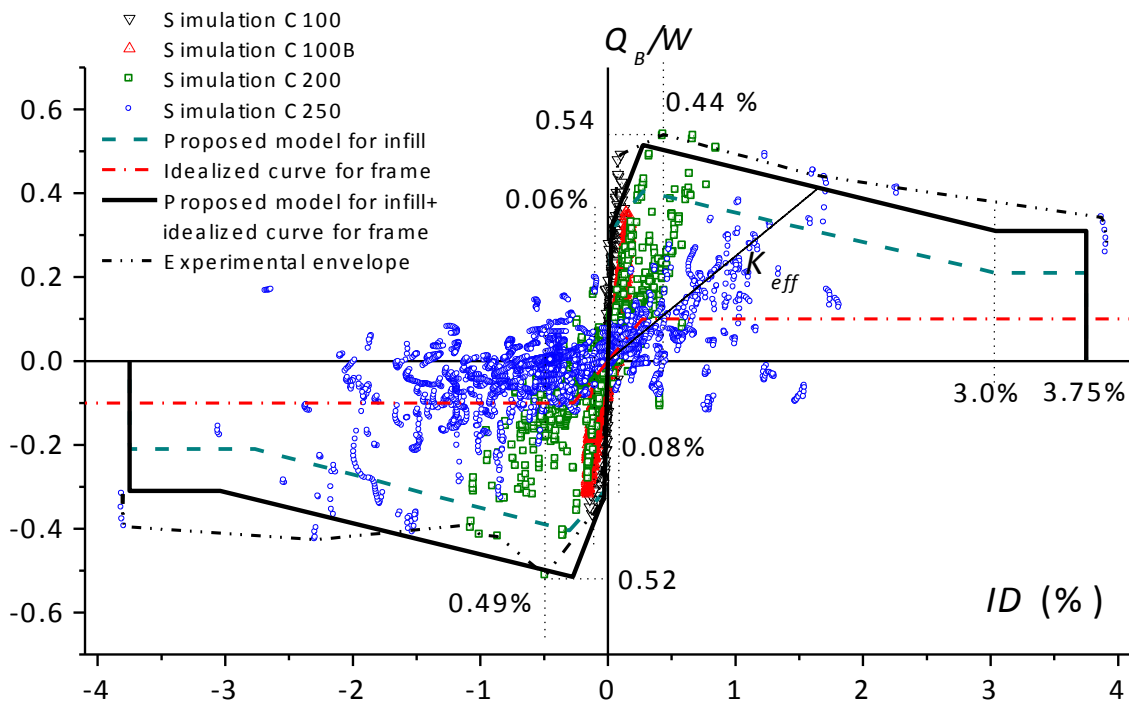
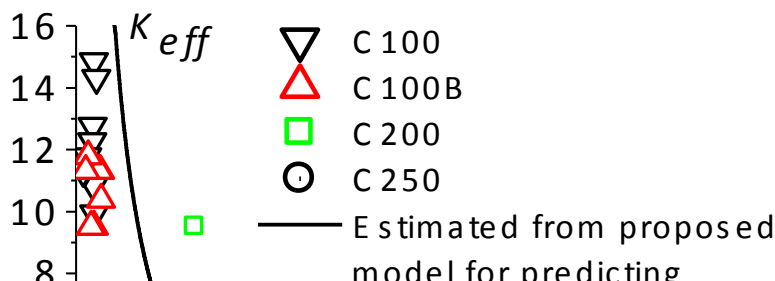
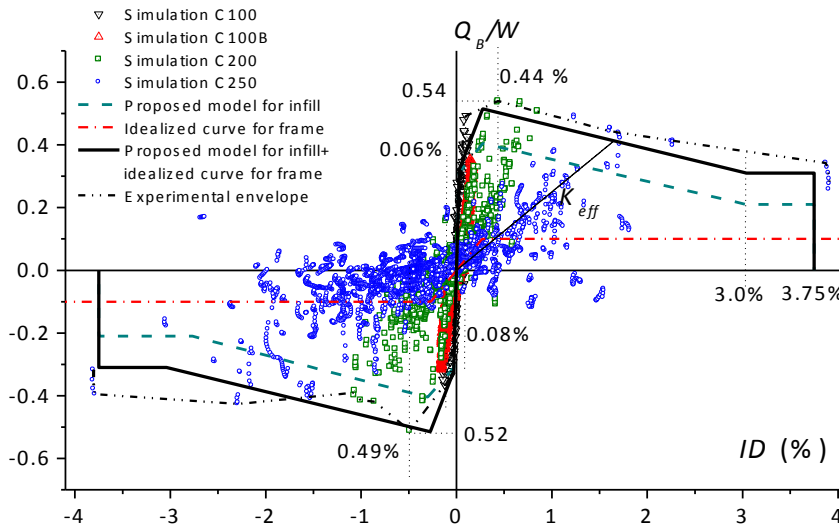


Figure 4.15: Points of null velocity, capacity curve and four-segment polygonal approximation.



4.2.2.3 Sti

To invest displacement $4\pi^2 M/T_{mean}^2$, the history of intervals. (ii) interval T_{mean} resulting value ratio ID reach 4.16 shows that decayed gradient Section 4.2.2. is, infill walls used for retro



s the relative used: $K_{eff} =$ us follows: (i) into 5 second period in each crossings. The maximum drift data, Figure (b), the stiffness changes made in cement. That they could be

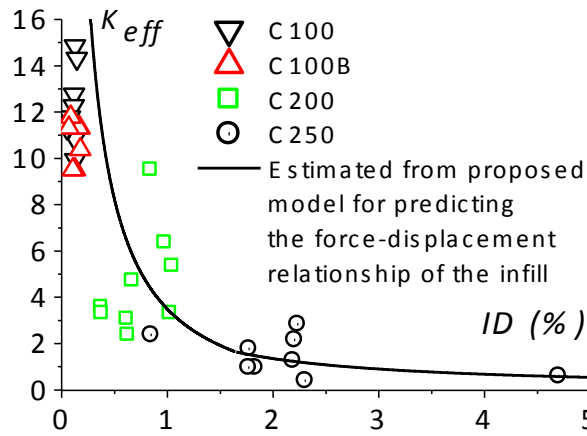


Figure 4.16: Variation of effective stiffness with maximum interstory drift ratio.

4.2.2.4 Estimation of equivalent strut parameters: Stiffness and Strength. Comparison with predictions

Different authors have proposed formulations for stiffness and maximum strength in masonry infill walls. Some of these approaches are compared below in order to find the best approximation to the values observed.

4.2.2.4.1 Estimation of the stiffness

Two stiffness values are of interest in masonry infill walls for understanding the behavior of the system: The initial stiffness and the secant stiffness. The initial stiffness can be computed through basic principles of mechanics. The system, at this point, behaves like two walls in parallel:

$$K_{w,el} = \frac{G_w A_w}{h_w} \tag{4.5}$$

The numerical value obtained was 63.6 kN/mm, which is 15% higher than the experimental value, 54.9 kN/mm.

In the force-displacement diagram, a segment linking the origin with the point of maximum strength defines the secant stiffness. The formulation proposed by *Mainstone (1971)* is commonly incorporated into different codes. It considers that the lateral behavior of a masonry wall after cracking can be represented by means of a diagonal strut, effective only in compression. The axial stiffness of the strut is obtained after defining an equivalent width that depends on the material properties of the RC frame and its mechanical properties:

$$b_w = 0.175 (\lambda_h h_w)^{-0.4} d_w \quad (4.6)$$

where d_w is the clear diagonal length of the infill panel, and λ_h is a coefficient defined by:

$$\lambda_h = \left(\frac{E_w t_w \sin(2\theta)}{4E_c I_c h_w} \right)^{0.25} \quad (4.7)$$

where I_c is the moment of inertia of the RC column. θ is the inclination of the diagonal of the masonry panel over the horizontal.

Using Eqs. (4.6) and (4.7), $K_{w,sec}$ can be calculated as follows:

$$K_{w,sec} = \frac{E_w b_w t_w}{L^2 + H^2} \cos^2 \theta \quad (4.8)$$

where L and H are bay length and the story height of the frame, respectively.

The numerical value for secant stiffness was 12.73 kN/mm, which is 15% higher than the experimental one, 11.05 kN/mm.

4.2.2.4.2 Estimation of strength

The total lateral strength of the system was compared by using different formulations and expressions below. An initial analysis considered the maximum lateral strength for the whole system using two approaches, while the second analysis studied the different failure modes on the infill to determine the maximum lateral strength supported by the panels.

Liaw and Kwan [*Liaw et al. 1984*] have proposed a formulation to obtain the maximum shear strength of the system based on the plastic collapse theory in conjunction with the penalty factor γ_p suggested by Wood [*Wood 1978*] to account for the non-ideal plasticity of masonry. To account for the failure element in the frame, the internal work for each element (beam, column and joint) was equalized by the external work on the frame. The maximum shear strength of the infill was given by:

$$V_c^T = \gamma_p \cdot f'_{me} \cdot t_{inf} \cdot h_{inf} \cdot \min \left\{ \sqrt{\frac{2(M_{pj} + M_{pc})}{\gamma_p \cdot f'_{me} \cdot t_{in} \cdot h_{in}^2}}; \frac{1}{tg\theta} \sqrt{\frac{2(M_{pj} + M_{pb})}{\gamma_p \cdot f'_{me} \cdot t_{in} \cdot h_{in}^2}}; \frac{4M_{pj}}{f'_{me} \cdot t_{in} \cdot h_{in}^2} + \frac{1}{6max(1; \tan^2 \theta)} \right\} = 2.09 \cdot 10^5 \min \{2.26 \cdot 10^{-4}; 2.93 \cdot 10^{-4}; 1.86 \cdot 10^{-4}\} = 38.8kN \quad (4.9)$$

with

$$\gamma_p = 2.663 \left(\frac{8M_{pj}}{f'_{me} \cdot t_{in} \cdot L_{in}^2} \right)^2 - 1.37 \left(\frac{8M_{pj}}{f'_{me} \cdot t_{in} \cdot L_{in}^2} \right) + 0.406 \leq 0.45 \quad (4.10)$$

In the above equations L_{in} is the length of the infill, M_{pc} (=3600 kNmm) is the plastic moment capacity of the column, M_{pb} (=8560 kNmm) is the plastic moment capacity of the beam, and M_{pj} (=3600 kNmm) is the plastic moment capacity of the joint (smaller of M_{pc} and M_{pb}). Since the test specimen has two identical frames with infills, the predicted total lateral strength normalized by total weight W is: $(2 \cdot 38.8)/122 = 0.63$. This value is slightly above (19%) than the experimental one (0.53).

The second approach was proposed by Fiorato [*Fiorato 1970*] and it is valid when the lateral strength of the system is not limited by the shearing capacity of the infill, but by the geometric and mechanical properties of the frame. This is the most likely situation expected in systems formed by old RC frames designed only for gravity loads (i.e. with relatively low resistance), and which have been retrofitted with new infill walls build with materials of relatively high strength. The total lateral strength of the system can be estimated by adding two contributions. One is the lateral capacity of the frame interacting with the infill V_{knee} , the other contribution is the friction force $V_{friction}$. As for the first contribution, V_{knee} can be estimated considering the “knee braced system” model shown in Figure 4.17. This model maintains that after shearing cracks form in the infill, the bottom segment of the infill braces the lower portion of the tension column, and the upper segment of the infill haunches at the intersection of the compression column with the beam. Under increased lateral loads, the unbraced portions of the columns tend to bend over the wall segments mobilizing a reduced effective height h_{eff} . Applying basic plastic collapse theory to this model yields the following equation for estimating V_{knee} :

$$V_{knee} = \sum_i^{N_{col}} \frac{2M_{u,i}}{h_{eff}} \quad (4.11)$$

where N_{col} is the number of columns and $M_{u,i}$ the yield capacity of column i . The second contribution $V_{friction}$ represents the lateral force transmitted through the wall segments by friction and can be estimated by:

$$V_{friction} = 0.45N \quad (4.12)$$

where N is the total vertical load acting on the infill wall, and 0.45 is an empirical coefficient. For one-bay structures with solid infills (i.e. without openings) Fiorato [*Fiorato 1970*] has proposed taking h_{eff} equal to half the height of the walls. Applying equations (4.11) and (4.12), the overall tested structure consisting of four columns and two infill walls, and normalizing by the total weight W , gives: $(V_{knee}/W) + (V_{friction}/W) = [(8 \cdot 3600)/(0.5 \cdot 1360)]/122 + (2 \cdot 12.74)/122 = 0.35 + 0.21 = 0.56$. This value is very close to that obtained experimentally (0.53). In addition, it is worth noting that the value of the lateral capacity maintained by the system under large drifts (see Figure 4.11 (d)) is close to $V_{friction}/W = 0.21$. This suggests that the friction mechanism explained above is responsible for the lateral strength reserve and energy dissipation capacity exhibited by the frame+infill system under very large imposed cyclic displacement.

Moreover, the total strength of the system could be estimated as the sum of the curve force-displacement for the frame [*Benavent-Climent et al. 2015*] and for the infill walls. In the

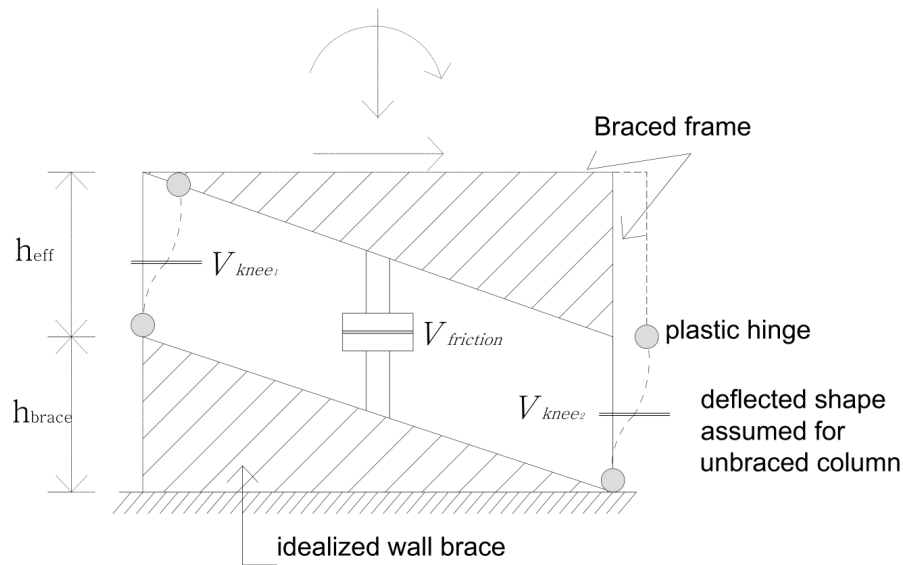


Figure 4.17: Model proposed by Fiorato to estimate lateral strength.

next paragraph, the estimation of the maximum capacity strength of the infill walls is made considering different authors and failure modes.

The external lateral load applied to the infill during a seismic action can be understood through the use of macroelements. By considering the masonry panel as a large-scale heterogeneous material, the lateral forces acting on it modified the equilibrium forces, and the wall behaved as a truss element. The principal stresses were inclined at θ degrees over the horizontal, coinciding with the direction of the diagonal Figure 4.18(Top). Based on this, the internal forces in the wall could be represented as a compressed diagonal strut that links the two loaded corners. Due to the internal compression forces, crushing could appear at the corners and/or the center of the loaded diagonal, (Compression failure mode Figure 4.18(c). At the same time, shear internal forces could open stepped mortar joints along the loaded diagonal (General shear failure) mode Figure 4.18(a). Tension forces developed in the diagonal that linked the “not-loaded” corners, these internal forces could also open the stepped diagonal crack along the loaded corners (Diagonal tension failure), or at least, make the occurrence easier by the decrease of the shear strength mode Figure 4.18(a). Finally, an entire partition of the wall could be moved horizontally with lateral loading, (Sliding-shear failure Figure 4.18(b).

Next, the strength associated with each failure mode was estimated using the different equations proposed in the relevant literature.

(a) Sliding-shear failure mode

The lateral strength limited by sliding-shear failure V_{slide} can be estimated using the equation given by *FEMA 273* and *FEMA 356*:

$$V_{slide} = A_n \cdot v_{me} = (40 \cdot 1880)mm^2 \cdot 0.25 \frac{N}{mm^2} = 18.8kN \quad (4.13)$$

where A_n is the area of net mortared section and v_{me} the bed-slide shear strength.

(b) Compression failure mode

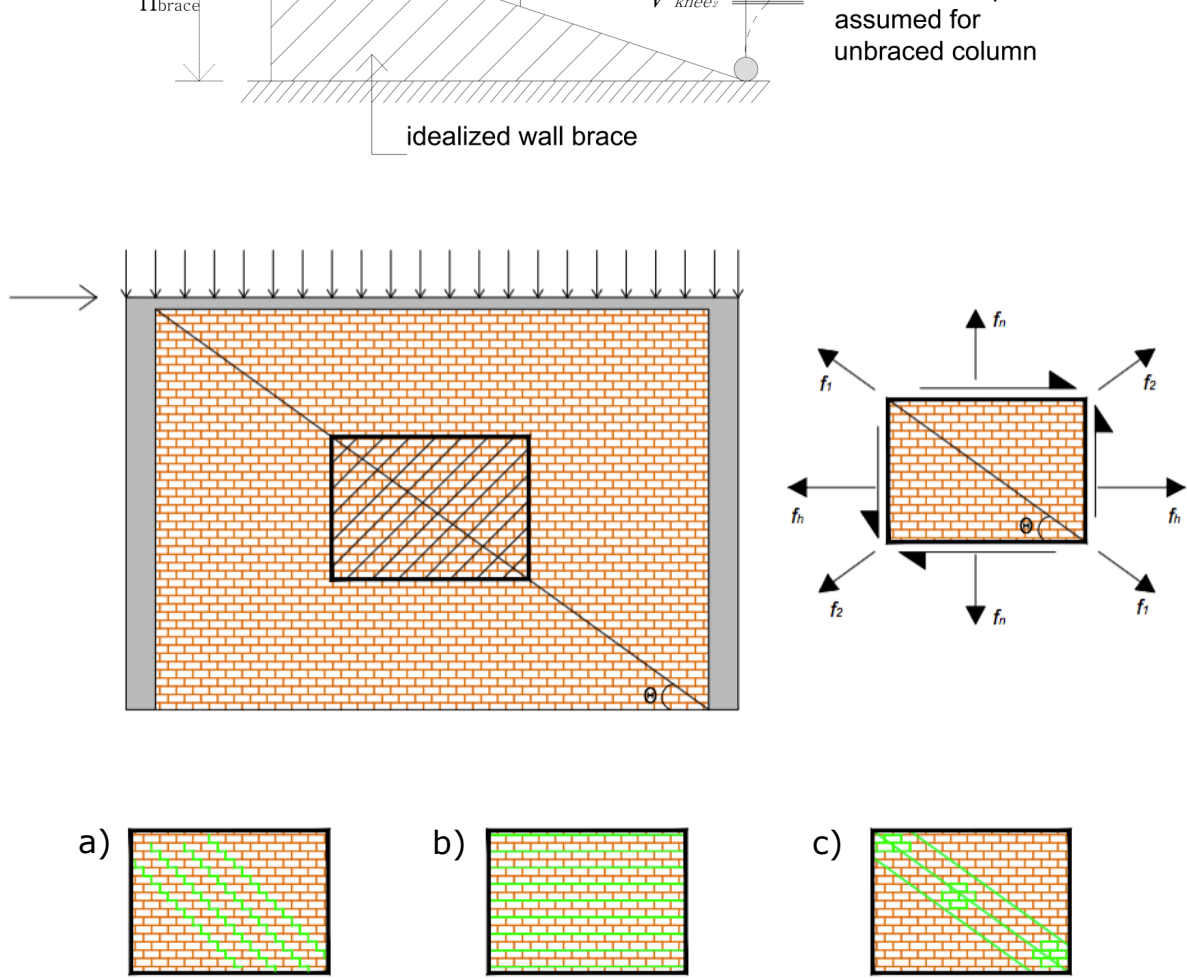


Figure 4.18: Top: Macroelement. Principal Stresses Bottom: Failure modes (a) Diagonal tension/ General Shear, (b) Sliding shear, (c) Compression

FEMA 306 uses a modified version of the method suggested by Stafford and his associates [Stafford et al. 1969] to estimate the lateral strength of infill V_c limited by compression failure of equivalent strut:

$$V_c = a \cdot t_{inf} \cdot f'_{me90} \cdot \cos \theta = 198 \cdot 40 \cdot \frac{50}{100} \cdot 10.20 \cdot \cos(0.6297) = 40.3kN \quad (4.14)$$

where f'_{me90} is the expected masonry strength in the horizontal direction, which may be set at 50% of the expected stacked prism strength f_{me} .

Mainstone (1971) has suggested calculating the infill strength as follows:

$$V_c = 0.56 \cdot (\lambda_I \cdot h_{inf})^{-0.875} \cdot f'_{me} \cdot h_{inf} \cdot t_{inf} \cdot \cot(\theta) = 82.59kN \quad (4.15)$$

(c) Diagonal tension failure mode

Based on the work by Saneinejad [Saneinejad et al. 1995], FEMA 306 gives the following equation to determine the lateral strength of an infill limited by diagonal tension failure mode (i.e. cracking shear of infill):

$$V_{cr} = \frac{2\sqrt{2} \cdot L_{in} \cdot t_{in} \cdot \sigma_{cr}}{\left(\frac{L_{in}}{h_{in}} + \frac{h_{in}}{L_{in}}\right)} \quad (4.16)$$

where the cracking stress σ_{cr} , which is to some degree dependent on the orientation of the principal stresses regarding the bed joints, can be taken as:

$$\sigma_{cr} = \frac{f'_{me}}{20} = 0.51 \quad \text{or} \quad \sigma_{cr} = v_{me} = 0.25 \quad (4.17)$$

Equation (4.16) predicts $V_{cr}=52$ kN for $\sigma_{cr}=0.51$ MPa and $V_{cr}=25.5$ kN for $\sigma_{cr}=0.25$ MPa. Flanagan [Flanagan *et al.* 1999] have suggested an alternative expression for predicting V_{cr} that uses the empirical constant k_{cr} determined empirically ($k_{cr}=0.066$) giving:

$$V_{cr} = k_{cr} \cdot L \cdot t_{in} \cdot \sqrt{f'_{me}} = 15.8kN \quad (4.18)$$

Finally, Zarnic [Zarnic *et al.* 2001] have proposed the following formulation for calculating the maximum lateral strength

$$Q_{w,max} = 0.818 \frac{L_w t_w f_{tp}}{1.925 L_w / h_w} \left(1 + \sqrt{(1.925 L_w / h_w)^2 + 1} \right) \quad (4.19)$$

where f_{tp} is the cracking strength of the infill equal to 0.25 MPa. This yields a value of 24.7 kN.

(d) General shear failure of the panel

Based on the works by Paulay [Paulay *et al.* 1992], *FEMA 273* gives the following equations to estimate the maximum V_{mi} and the final (residual) V_{mf} shear force carried by the infill panel. Axial loads on the wall are due to self-weight and represent a maximum of 0.8% of the shear strength (at the base of the wall where the maximum axial load is), for this reason *FEMA 273* makes little of its influence:

$$V_{mi} = A_{vh} \cdot \left[0.17 \cdot \sqrt{f'_{me}} + 0.3 \frac{P_w}{A_{vh}} \right] = 1880 \cdot 40 \cdot [0.17 \cdot \sqrt{10.2} + 0] = 40.9kN, \quad \text{top of the wall} \\ + \left\{ \begin{array}{l} 0 \\ 0.3 \frac{0.110(\frac{kg}{unit}) \cdot 22 \frac{units}{line} \cdot 51(lines) \cdot 9.8(\frac{m}{s^2})}{1880 \cdot 40} \end{array} \right\} = 41.26kN, \quad \text{base of the wall} \quad (4.20)$$

$$V_{mf} = 0.3 \cdot V_{mi} = \left\{ \begin{array}{l} 12.3kN \quad \text{top of the wall} \\ 12.37kN, \quad \text{base of the wall} \end{array} \right. \quad (4.21)$$

Shear failure causes stepped opening on the joints along the loaded diagonal. This is worth noting that for masonry panels with low aspect ratio h_w/l_w (i.e. $h_w/l_w < 1$) the diagonal crack normally includes a horizontal part in the center region of the crack.

Table 4.11 summarizes the lateral strength predicted for each failure mode recommended by the different codes and authors. It must be noted that the strengths calculated above are for a single wall: this must be multiplied by 2 to give the strength of the infills in the test specimen. In Table 4.11, it can be seen that the predicted capacity is very different depending on the failure mode considered. The capacity also varies significantly depending on the code or author considered within a given failure mode.

The study of the crack patterns (Figure 4.14) and the analysis of failure modes trigger the following conclusions: The presence of crushing on the corners of the infills and at different

Mode of failure	Prediction		Tests
	One wall V	2V/W	
Sliding shear failure		18.8	0.31
Compression failure	FEMA 306	40.3	0.66
	Mainstone	82.6	1.36
Diagonal tension	FEMA 306 $\sigma_{cr} = f'_{me}/20$	52.0	0.85
	$\sigma_{cr} = v_{me}$	25.5	0.42
	Zarnic et al.	24.7	0.41
	Flanagan and Bennett	15.8	0.26
General shear failure	FEMA 273	40.9	0.67

Table 4.11: Lateral strength estimation for different failure modes.

points, the possible sliding of the panel on its base in the first simulations, and the final crack pattern for each wall suggest that the panels developed a combination of “partial-failure” modes, as none of them caused the final failure of the panel. However, the combination of these factors resulted in peak lateral strength at a given ductility. Moreover, the two panels did not follow the same prevalent degradation pattern during shaking: wall 1 developed degradation mainly in a diagonal tension failure mode pattern, while wall 2 did so in a compression failure pattern. This peculiarity could be a consequence of the previous damage on the frame, or human effect during the construction of the panels themselves. In this study, the maximum strength was achieved by the most restrictive failure mode, diagonal tension. The high level of ductility attained can be interpreted as a result of the twist effect developed after wall 1 attained its maximum lateral strength. After that point, wall 1 strength started to decrease while wall 2 strength continued increasing (as the maximum compression strength was not achieved). In fact, it is worth noting that the residual eccentricity of the columns at mid height is 5mm higher in the columns surrounding wall 1 than in the columns surrounding wall 2.

4.2.3 Proposed models

4.2.3.1 Proposed model for predicting the force-displacement relationship of the infill under static monotonic loading

Modelling the masonry infills using diagonal struts is a widely used approach due to its computational efficiency. Many different models have previously been proposed for predicting the force-displacement relationship of the diagonal strut that represents the infill under monotonic loading [Dolšek 2008; Klingner 1976; Crisafulli 1997; Fardis 2006]. Most of these models are based on the results of static tests in which the maximum lateral drift (about 2.5%) applied to the infill did not exhaust its deformation capacity. Moreover, there is a lack of experimental data regarding the estimation of some parameters that govern these models [Celarec 2012]. This section proposes a model for characterizing the force-displacement relationship of masonry infill walls that is based on the results of dynamic shake-table tests that took the structure up to intolerable drifts. The loading conditions replicated on a shake-table through dynamic tests are believed to be much more realistic and closer to the actual condition of the infill during an

earthquake than that obtained from static tests. The proposed model consists of four branches, as shown in Figure 4.19. The first branch represents the initial elastic behaviour up to the first cracking event of the infill and its stiffness $K_{w,el}$ is obtained by applying basic principles of mechanics as follows:

$$K_{w,el} = \frac{G_w A_w}{h_w} \quad (4.22)$$

where G_w is the elastic shear modulus of the infill material and A_w is the cross sectional area of the infill panel. The maximum lateral strength $Q_{w,max}$ is determined with the simplified expression proposed by *Zarnic (2001)* as follows:

$$Q_{w,max} = 0.818 \frac{L_w t_w f_{tp}}{1.925 L_w / h_w} \left(1 + \sqrt{(1.925 L_w / h_w)^2 + 1} \right) \quad (4.23)$$

Past studies [*Celarec 2012; Panagiotakos 1996; Fardis 1996*] showed that the shear cracking strength $Q_{w,cr}$ is related to $Q_{w,max}$ by:

$$Q_{w,cr} = \frac{Q_{w,max}}{1.3} \quad (4.24)$$

The lateral displacement corresponding to the ordinate point $Q_{w,max}$ is determined from the secant stiffness up to the maximum strength, $K_{w,sec}$, given by Mainstone's formula [*Mainstone 1974b*], i.e. considering an equivalent strut width b_w equal to:

$$b_w = 0.175 (\lambda_h h_w)^{-0.4} d_w \quad (4.25)$$

where d_w is the clear diagonal length of the infill panel, and λ_h is a coefficient defined by:

$$\lambda_h = \left(\frac{E_w t_w \sin(2\theta)}{4 E_c I_c h_w} \right)^{0.25} \quad (4.26)$$

where I_c is the moment of inertia of the RC column and $\theta = \tan^{-1}(h_w/L_w)$. Using Eqs. (4.25) and (4.26), $K_{w,sec}$ can be calculated as follows:

$$K_{w,sec} = \frac{E_w b_w t_w}{\sqrt{L^2 + H^2}} \cos^2 \theta \quad (4.27)$$

where L and H are bay length and the story height of the frame, respectively. The third branch of the lateral force-displacement relationship of the infill is the post-capping degrading branch. Based on the data obtained from the tests conducted for this study the estimation of the stiffness $K_{w,deg}$ of this branch is proposed as follows:

$$K_{w,deg} = -0.1 K_{w,sec} \left[1 - \left(\frac{Q_{w,friction}}{Q_{w,max}} \right) \right] \quad (4.28)$$

The fourth branch is horizontal and corresponds to residual strength. In this study the friction component used in Fiorato's model and given by Eq. (4.12) is adopted. The adoption of 3.75% of the story height is given for ultimate displacement.

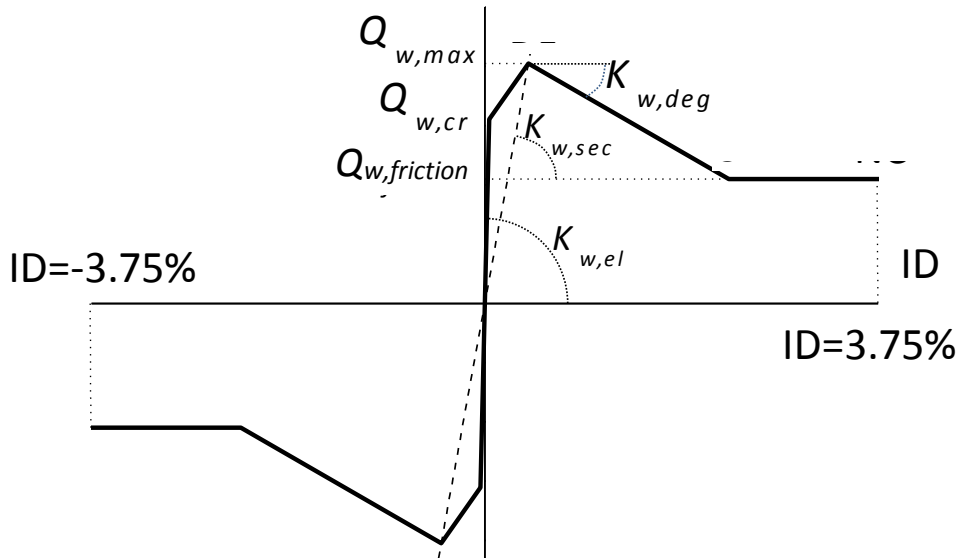


Figure 4.19: Proposed force-displacement relationship for infill wall.

Equation (4.28) is obtained considering that the displacement corresponding to the intersection point of the third and fourth branches is eleven times larger than that corresponding to the intersection point of the second and third branches. The force-displacement relationship of the infills predicted with the proposed model is drawn with dash lines in Figure 4.15. The bilinear approximation of the force-displacement relationship of the bare frame obtained experimentally by the authors in previous studies is also shown in this figure with dash-dot lines [Benavent-Climent *et al.* 2015]. The sum of both force-displacement curves is shown with solid bold lines in Figure 4.15 and it represents the behavior of the whole structure (infills+frame). Comparing this solid bold line with the experimental envelope shown with dash-dot-dot lines, it can be seen that the proposed model is reasonably close, yet conservative.

4.2.3.2 Proposed model for predicting the response of the RC frame with infills under cyclic loading

It is of great interest to replicate the behavior of the global system computationally, in order to obtain conclusions that are applicable to more extended scenarios and buildings. To this end the Idarc v.7 code [Reinhorn *et al.* 2009] is used. Idarc 7.0 implements the complex stress-strain relationships for concrete and steel materials by dividing the cross-section in fiber elements and integrating the stress-strain relationships. This allows the computation of the moment-rotation diagrams for reinforced concrete elements. The use of macromodels in the program for all the structural elements is an advantage of this software since it reduces the time required for computing the numerical analysis. Idarc 7.0 code includes the Bouc-Wen model and allows adjusting the parameters that control its behavior under both monotonic and cyclic loading. The Bouc-Wen model is adopted in this investigation for modeling the cyclic behavior of masonry infill panels, and it is calibrated with the experimental results in a two tier process: (1) first the parameters with a clear physic meaning that can be measured by the analysis of the experimental results are fixed, and (2) a parametric study is conducted with the rest of parameters. The response obtained for each combination of parameters through a non-linear

dynamic response analysis is compared in terms of maximum lateral displacement, maximum base shear and total energy dissipated with the values obtained in from the shaking table tests.

4.2.3.2.1 Constitutive laws adopted for concrete and steel

Idarc permits the introduction of the material properties to compute the element force-displacement (or moment-rotation) diagrams. Moreover, it also allows the force-displacement diagram to be directly introduced, from which the material properties are discovered.

The concrete uniaxial stress-strain behavior is defined in this study as parabolic until the maximum stress reaches f_c , and its corresponding deformation ε_0 (that is defined by the user) following the function $\frac{\sigma}{f_c} = 2 \left(\frac{\varepsilon}{\varepsilon_0} \right) - \left(\frac{\varepsilon}{\varepsilon_0} \right)^2$. This parabola is tangent in origin to the Young modulus of the concrete, E_C . When the maximum strength f_c is reached, the strength decreases as the strain increases with a slope $E_{CN} = f_c \cdot Z_f$, [the parameter Z_f , *Kent (1971)* includes the confinement effect of the cross section]. Concrete failure is defined by the ultimate deformation ε_u (Figure 4.20 (a)).

In the case of steel, three lineal branches define the stress-strain relationship. The first branch defines the elastic behavior of the rebar, from zero stress-strain to the yielding point; the slope is constant and corresponds to the Young response Modulus E_S . The slope of the stress-strain graph is reduced to zero after yielding of the material and maintains this value until the deformation corresponding to hardening is reached. Finally, the third slope is characterized by the strain hardening modulus until ultimate strength is reached (Figure 4.20 (b)).

The stress-strain relationship for compression in masonry is defined as parabolic until the compression strength reaches the maximum value, f'_m , and it then drops linearly until it reaches a fraction of f'_m , after that point the stress remains constant as the strain increases (Figure 4.20 (c)).

4.2.3.2.2 Model for beams and columns

Columns and beams are defined in the platform through lumped-plasticity models. The moment rotation diagram of each section is computed based on the size of the cross section, the longitudinal and transverse reinforcement, and the type of concrete and steel material defined.

Kunnath [*Kunnath et al 1992a*] explains in detail the computation of the moment rotation diagram in columns and beams, which is summarized below. The flexibility factor $1/EI$ is considered to vary linearly along the member length between each extreme section and the point of contraflexure. The flexural rigidity, EI , at the ends of the members is monitored throughout the analysis. The incremental moment-rotation relationship is established from the integration of the M/EI diagram. Finally, the flexibility matrix is expressed in the following incremental form:

$$\begin{pmatrix} \Delta\theta'_A \\ \Delta\theta'_B \end{pmatrix} = [f_s] \begin{pmatrix} \Delta M'_A \\ \Delta M'_B \end{pmatrix} \quad (4.29)$$

where $\Delta\theta'_A$, $\Delta\theta'_B$ are the incremental rotations corresponding to the moment increments $\Delta M'_A$ and $\Delta M'_B$, and $[f_s]$ is the flexibility matrix defined by the combination of shear and internal beam forces. In the case of the columns, the analysis accounts for the axial load in each column to compute the axial-moment interaction diagram.

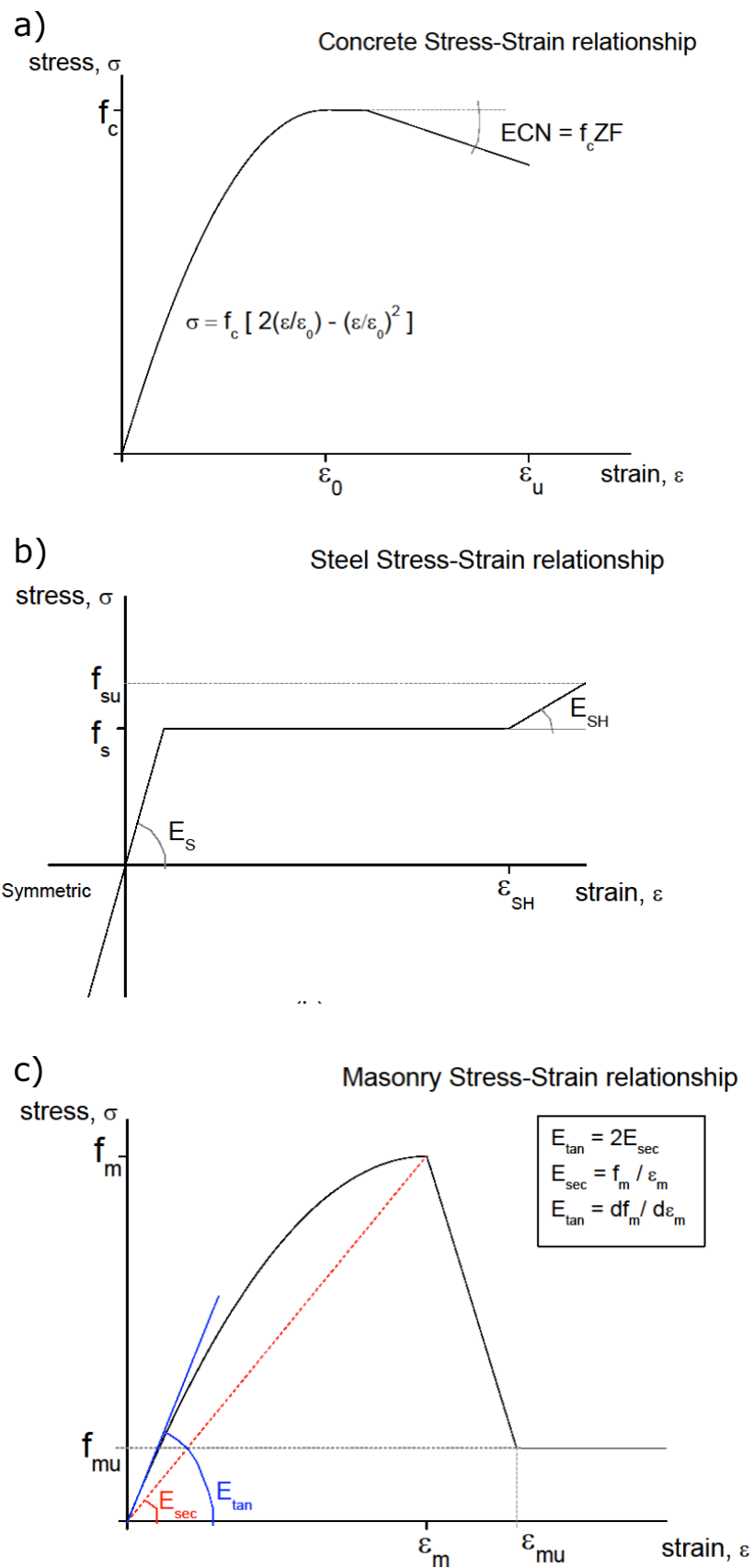


Figure 4.20: Materials stress-strain relationships. a) Concrete material, b) Steel material and c) Masonry material.

A transformation matrix $[C]$ that accounts for the rigidity length in the extreme of the element, either beam or column, is required to compute the stiffness matrix:

$$[C] = \frac{1}{1 - \lambda_A - \lambda_B} \begin{pmatrix} 1 - \lambda_B & \lambda_A \\ \lambda_B & 1 - \lambda_A \end{pmatrix} \quad (4.30)$$

the moments and rotations across the rigid panel zones are computed as:

$$\begin{pmatrix} \Delta M'_A \\ \Delta M'_B \end{pmatrix} = [C] \begin{pmatrix} \Delta M'_A \\ \Delta M'_B \end{pmatrix} \quad (4.31)$$

$$\begin{pmatrix} \Delta \theta'_A \\ \Delta \theta'_B \end{pmatrix} = [C]^T \begin{pmatrix} \Delta \theta'_A \\ \Delta \theta'_B \end{pmatrix} \quad (4.32)$$

and the moment rotation relationship can be defined in terms of the stiffness matrix as:

$$\begin{pmatrix} \Delta M'_A \\ \Delta M'_B \end{pmatrix} = [k_s] \begin{pmatrix} \Delta \theta'_A \\ \Delta \theta'_B \end{pmatrix} \quad (4.33)$$

where

$$[k_s] = [C] [f'_s] [C]^T \quad (4.34)$$

in which $[f'_s]$ is the inverted flexibility matrix.

The equilibrium of forces yields in:

$$\begin{Bmatrix} y_a \\ v_a \\ y_b \\ v_b \end{Bmatrix} = R_{B/C} \begin{Bmatrix} M_a \\ M_b \end{Bmatrix} \quad (4.35)$$

where

$$R_{B/C} = \begin{bmatrix} -1/L & -1/L \\ 1 & 0 \\ 1/L & 1/L \\ 0 & 1 \end{bmatrix} \quad (4.36)$$

Finally, the stiffness equation for the beam (B) or column (C) element is:

$$[k_{B/C}] = [R_{B/C}] [k_s] [R_{B/C}]^T \quad (4.37)$$

The moment rotation diagram with Idarc for beams and columns was obtained by the integration of the stress strain diagrams by the procedure outlined by *Kunnath et al (1992a)*. The strain at any section is given by:

$$\varepsilon(z) = \varepsilon_0 + z\varphi \quad (4.38)$$

where ε_0 is the strain at the centroid, z is the distance from given fiber to the neutral axis and φ is the curvature of the cross section. The aftermath axial load and moment in the cross section is given by:

$$N = \int E\varepsilon dA \quad (4.39)$$

$$M = \int Ez\varepsilon dA \quad (4.40)$$

The ultimate deformation is defined when (i) the specified ultimate compressive strain in the concrete is reached ($\varepsilon \geq \varepsilon_{cu}$) or (ii) the specified ultimate strength of one of the rebars reached ($f \geq f_{su}$). As mentioned previously, the confinement in the concrete has been considered to compute the ultimate deformation through the parameter ZF of the concrete stress-strain relationship. Hysteretic behavior is defined by three independent parameters in columns and beams: (1) Stiffness decay, the degradation of the stiffness is achieved by reducing the unloading stiffness as a function of ductility, (2) strength deterioration as a function of the dissipated hysteretic energy and (3) pinching/crack-closing by lowering the target point of the force-deformation curve upon crossing the force-axis. For both columns and beams, the parameters that define the level of degradation in the hysteretic rules were obtained from an experimental calibration campaign with static and dynamic tests [Benavent-Climent (2007) and Benavent-Climent et al. (2009a; 2009b)].

4.2.3.2.3 Model for masonry infill panels

The infill walls are modeled as diagonal struts, only effective under compression (macro-model). Idarc computes the effect of the infill walls at each step in the equilibrium formulation as an external lateral force on the beam-column joints of the corresponding compressed diagonal. There are several models for computing the force-deformation curve of infill panels in the bibliography and some of them are compared in this section using material properties and the geometry of the panel. In all cases, it can be noted in previous research that the values obtained for lateral strength and stiffness are highly dependent on the material properties of the surrounding frame [Chrysostomou].

(a) Stiffness

The formulation used in section 4.2.2.4.1 for secant stiffness [Mainstone 1971] was used to estimate the value of lateral stiffness.

This expression yields a value for lateral stiffness of 12.73 kN/mm for each masonry infill wall.

(b) Lateral strength

As explained in section 4.2.2.4.2, the formulation proposed by Zarnic was used to estimate the maximum lateral strength of the infills.

The hysteretic behavior of the infill panel is represented by two springs working in parallel: *Spring_{postyielding}* + *Spring_{hysteretic}*. Each one of the springs is defined by its stiffness. The two springs undergo the same deformation under a generalized force or moment M , and they share the force proportionally to their instantaneous stiffness [Mettupalayam 2000].

The first spring represents the post-yielding stiffness, and consists of linear elastic spring defined by the parameter $alphIW$:

$$k_{postyielding-spring} = alphIW \cdot k_0 \quad (4.41)$$

This parameter is defined as the ratio between post-yielding stiffness and initial stiffness. In all cases, and based on the experimental campaign, this value is considered as near to zero, $10e^{-5}$.

The second spring defines the envelope of the force-deformation diagram for masonry infill panels. The model implemented with Idarc was a modification of the model proposed by *Bouc (1967)* to include the contributions of *Wen (1976)*, *Baber and Noori (1985)*, *Casciati (1989)* and *Reinhorn (1995)*. The equation that defines the shape of the moment curvature diagram is:

$$k_{hysteretic-spring} = (1 - alphIW)k_0 \left\{ 1 - \left| \frac{M^*}{M_y^*} \right|^\eta \left[\beta sgn(M^* \dot{\phi}) + \gamma \right] \right\} \quad (4.42)$$

where ϕ is the curvature, M^* is the portion of the applied moment shared by the hysteretic spring and M_y^* is the yield moment of the hysteretic spring. The control parameters for Idarc are A , β , γ and η . Parameter A (not included in eq. 4.42) controls the scale of the response in the force-deformation diagram [*Song et al. 2006*]. *Ma et al (2004)* demonstrated that multiple parameter combinations exist that reproduce the same response for a given system subjected to a given excitation. This redundancy decreases when $A=1$. To reduce the model to a formulation with well-defined properties and, consequently, to ensure plasticity conditions [*Mettupalayam et al. 2000*], *Constantinou and Adnane (1987)* suggested imposing $A = \beta + \gamma$. Finally, the smoothness of the transition from elastic behavior to inelastic behavior is defined by η [*Mettupalayam et al. 2000*, *Song et al. 2006*].

The hysteretic spring works in series with the slip-lock spring, which aims to reflect the effect of pinching in hysteretic loops caused by close-closure, bolt slip, etc. The equation that governs this effect is given by:

$$k_{slip-lock} = \left\{ \sqrt{\frac{2}{\pi}} \frac{s}{M_\sigma^*} \exp \left[-\frac{1}{2} \left(\frac{M^* - \bar{M}^*}{M_\sigma^*} \right)^2 \right] \right\}^{-1} \quad (4.43)$$

where s is the slip length defined as $R_s (\phi_{max}^+ - \phi_{max}^-)$; $M_\sigma^* = \sigma M_y^*$ measures the range of the moment in which slip occurs and $\bar{M}^* = \lambda M_y^*$ is the mean moment level on either side around which the slip occurs. In conclusion, there are three control parameters R_s , σ , and λ . R_s and σ which have been estimated based on the experimental campaign, as they can be measured on the force-displacement diagram, and λ was chosen as equal to zero, i.e. the slip length is centered in the origin of the force-displacement or moment-curvature diagram.

The strength and stiffness degradation effects are included in the backbone curve. As they are a consequence of the degradation of the system caused by plastification of the masonry panels, they only affect the hysteretic spring behavior and not the post-yielding spring.

The stiffness decrease is represented as a function of the attained ductility, and is included as a coefficient that divides $k_{hysteretic-spring}$.

$$k_{hysteretic-spring} = \frac{k_{hysteretic-spring}}{\eta_i} \quad (4.44)$$

$$\eta_i = 1.0 + s_k \left(\frac{u_{max}^p + u_i}{2} \right) \quad (4.45)$$

s_k is the control parameter with Idarc to change the rate of stiffness as a function of i-step ductility u_i and the maximum attained ductility u_{max}^p . $s_k=0.31$

The strength capacity deterioration is expressed as a function of attained ductility and dissipated energy, in terms of shear force V_y at k-step: $V_y^k = s_\beta V_y^0$. s_β is related to the fatigue based damage index [Reinhorn and Valles, 1995] as $s_\beta = 1 - DI$; where

$$DI = \frac{\mu_{max}^p - 1}{\mu_c - 1} \frac{1}{\left(1 - \frac{s_{p1} \int dE_h}{4E_{hy}} \right)^{s_{p2}}} \quad (4.46)$$

where μ_{max}^p is the maximum attained ductility and $\mu_c = 15$ the defined ductility for the infill panel. $\int dE_h$ represents the cyclic energy dissipated before the start of the current reloading cycle, and E_{hy} is monotonic energy capacity. The control parameters for stiffness degradation are defined as $s_{p1} = 0.2$ and $s_{p2} = 0.1$.

The parameters γ , β , η , s_k , s_{p1} and s_{p2} cannot be measured directly during the shaking table tests. In order to determine a combination of parameters that best approaches the numerical solution to the experimental results, the following numerical campaign was developed: The numerical model of the frame was defined; beam and column moment diagram curvature was obtained after the integration of the stress strain diagram in the extreme sections. Steel and concrete properties (strength, strain at maximum compression) were defined based on static tests. The hysteretic rules proposed by Benavent et al [Benavent-Climent 2007; Benavent-Climent 2009a; Benavent Climent 2009b] were used to define beams and columns hysteretic rules. The masonry infill panel stiffness and strength were computed following the formulation of Mainstone and Zarnic et al, respectively [Mainstone 1971; Zarnic et al. 2001]. The parameters that define the infill panel hysteretic rules were classified as “fixed” and “variable”. Fixed parameters could be directly measured or estimated. Variable parameters were defined in the range given in Table 4.12, and varied with a given increment shown in the same table. The accelerations recorded at the base of the shake table (accelerometer 4) during the seismic simulations were concatenated to produce the C100/C200 (C100-C100B-C200) and C100/C250 (C100-C100B-C200-C250) recorders used in the numerical simulation. For each numerical simulation, all the parameters except one were fixed. The non-fixed parameter is varied in an appropriate range of values. The final response of the system in terms of maximum lateral displacement, maximum base shear and dissipated energy was compared with the experimental results to determine the combination that best fitted the experimental data. The calibration process for the variable parameters was developed in two tiers, first the parameters that defined the envelope of the force-deformation diagram were studied (Wen Bouc models parameters, γ , β , and η), while the rest of the variable parameters were fixed by the default value proposed with Idarc; second the parameters related to strength and stiffness degradation were modified one by one. Table 4.13 shows the combination of parameters that best fitted the response for C100/C200 and C100/C250.

Finally, Figure 4.22 shows the comparison between the four-segment polygonal model proposed in section 4.2.3.1 and the pushover curve obtained with Idarc.

Fixed

$$A = 1, \text{AlphaIW} = 10^{-5}$$

$$IS = 1, AS = 0.15, ZS = 0.1, ZBS = 0$$

Table 4.12: Bouc-Wen hysteretic parameters: fixed values.

Variable	Interval (increment)	Best approximation
γ	{0.05, 0.95} (inc. 0.05)	0.7
β	{0.05, 0.95} (inc. 0.05)	0.3
η	{1.0, 15.0} (inc. 0.5)	5.0
s_k	{0.1, 0.4} (inc. 0.01)	0.31
s_{p1}	{0.0, 1.0} (inc. 0.1)	0.2
s_{p2}	{0.0, 1.0} (inc. 0.1)	0.1

Table 4.13: Bouc-Wen hysteretic parameters: variables values.

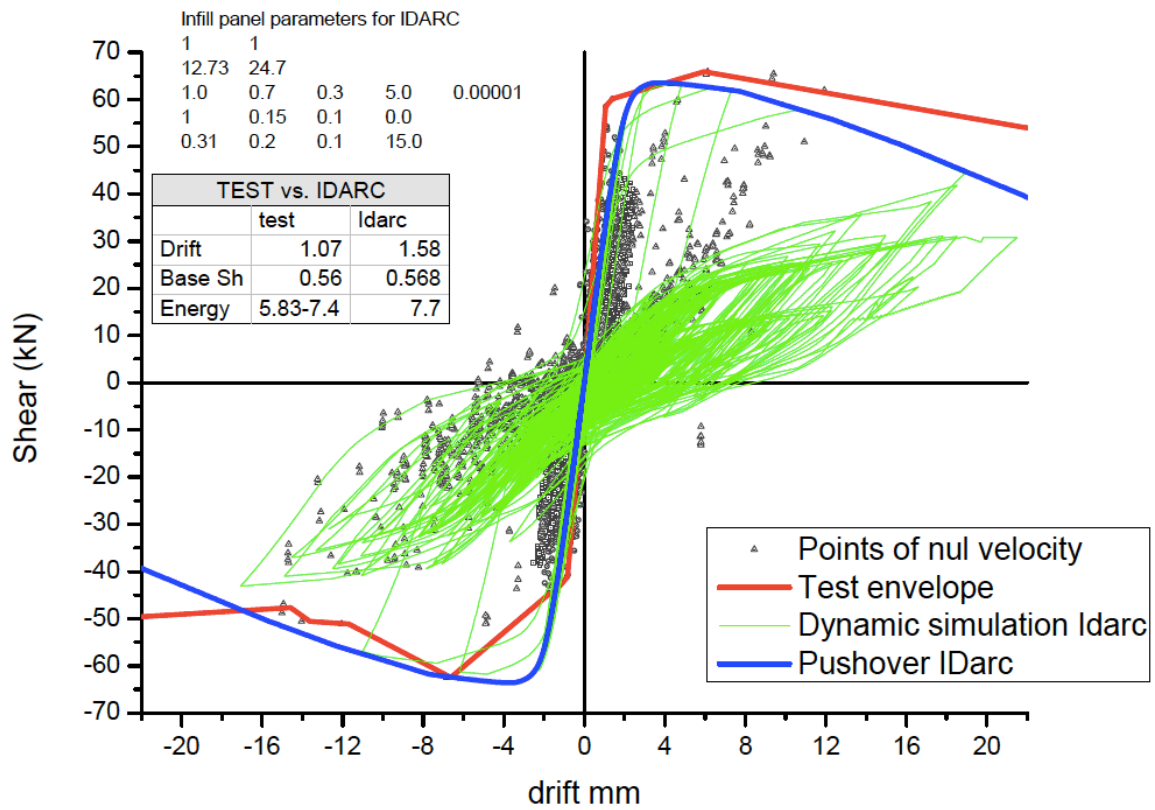


Figure 4.21: Proposed model and comparison with experimental results.

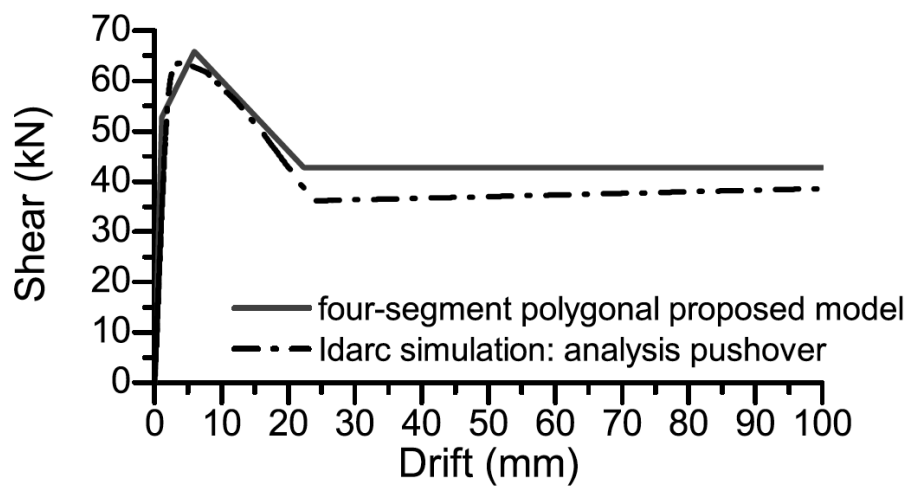


Figure 4.22: Capacity curve comparison: Proposed model versus Idarc Pushover analysis.

Numerical investigation

This Chapter investigates numerically the use of masonry infill panels as a retrofitting measure in developing countries. To this end, four prototypes of schools buildings in Haiti are analyzed. The buildings are modeled in Idarc and different combinations of masonry infill panels are proposed and modeled. The masonry infill walls are implemented following the formulation for lateral and stiffness strength, and hysteretic parameters, calibrated in section 4.2.2 and 4.2.3. The four-segment polygonal capacity curve proposed in section 4.2 is used to define damage states in the masonry panels, to compute a fragility analysis in order to determine the influence of the amount of masonry infill walls in the probability of exceedance of a given damage state.

5.1 Definition of the prototype buildings without infills

This study aims to evaluate the possibility of seismic retrofitting reinforced concrete frame buildings by means of masonry infill panels. This analysis focuses and applies to buildings that have been damaged by an earthquake, such that occurred at Haiti in February 2010. One month after this earthquake, a group of engineers from Purdue University led by Professor Santiago Pujol moved to Haiti to obtain information about the state of buildings after the earthquake. They decided to group the information in four classes: (1) sketch of the plant, (2) number of stories, (3) structural elements: type and dimensions, and (4) use of the building. All this information was used to concrete the objectives of this and to define the final prototypes.

The schools are considered of most interest, especially in developing countries, as the education represents the base of any society. Guaranty the education also includes accounting for safe buildings. The main interesting points in these buildings are: (1) the use (educational) of these buildings is priority in the society; (2) the dimensions and structural typologies are very similar in all the schools, so they are inclusive in one typology; (3) the number of stories is two or three in all the cases. The use of masonry infill panels to retrofit low-rise buildings is, beforehand, more viable than in the case of slender buildings.

There were a total of 21 school buildings whose structural system was composed by reinforced

concrete frames (RCF hereafter) with similar element dimensions: deep beams (30x50 cm) with unidirectional joists and squared columns (30x30 cm). The story height is 3.05m. Different span lengths in one direction are not usual and will not be considered.

Two plan distributions were of interest for this study:

1. Most of the schools have two spans in one direction and four-six in the other direction. This configuration will be studied in detail because of its frequency. In these buildings, access to the classroom normally takes place from the outside face of it. The lengths of the spans in both direction are the same in most cases.
2. Another configuration of interests is composed of buildings with same number of spans in both directions, whose lengths l_x , l_y (x is perpendicular to the direction of the unidirectional joists) have a ratio $\frac{l_x}{l_y}$ of $\frac{2.3}{1}$, with maximum l_x 7 meters.

Table 5.1 resumes the dimensions in plan of the two prototypes that will be presented in this study. Each of these buildings will be studied for the case of having two stories and three stories.

Label	N ^o of spans X	Length of spans X	N ^o of spans Y	Length of spans Y	Number of stories
2S4x2	4	5	2	5	2
3S4x2	4	5	2	5	3
2S4x4	4	7	4	3	2
3S4x4	4	7	4	3	3

Table 5.1: Properties in plan of selected prototypes

Figures 5.1(a) and 5.1(b) show the dimensions of the buildings. The plan XY of the building is placed at the center of the figure. On the right and top sides the three stories prototype is represented by means of the elevation in plan for both orthogonal directions, YZ plan and XZ plan respectively. On the left and bottom side the two stories building is represented by means of the elevation in plan for both orthogonal directions, YZ plan and XZ plan respectively.

5.2 Design of the prototype buildings without infills

The four prototypes were designed to represent the school buildings in Haiti. Each prototype counts with RC frames in both orthogonal directions, where the dimensions of columns and beams remain constant in the building, i.e. squared columns with cross section 30x30cm, and deep beams with cross section 30x50cm. The joists that form the one-way slab rest on the beams in the principal direction and transfer the superficial gravity loads to the RC frame.

The frames that represent the principal direction of the frames are denoted as F+Number while the orthogonal frames are denoted as f+number (Figures 5.1(a) and 5.1(b)). The estimated material properties were the strength of concrete, $f_c=25\text{MPa}$, diminished by a security coefficient of $\gamma_c=1.5$ and the strength of steel, $f_s=400\text{MPa}$ diminished by a security coefficient of $\gamma_s=1.15$.

The prototypes design did not account for any seismic detailing and ductility, and no lateral load or action was considered.

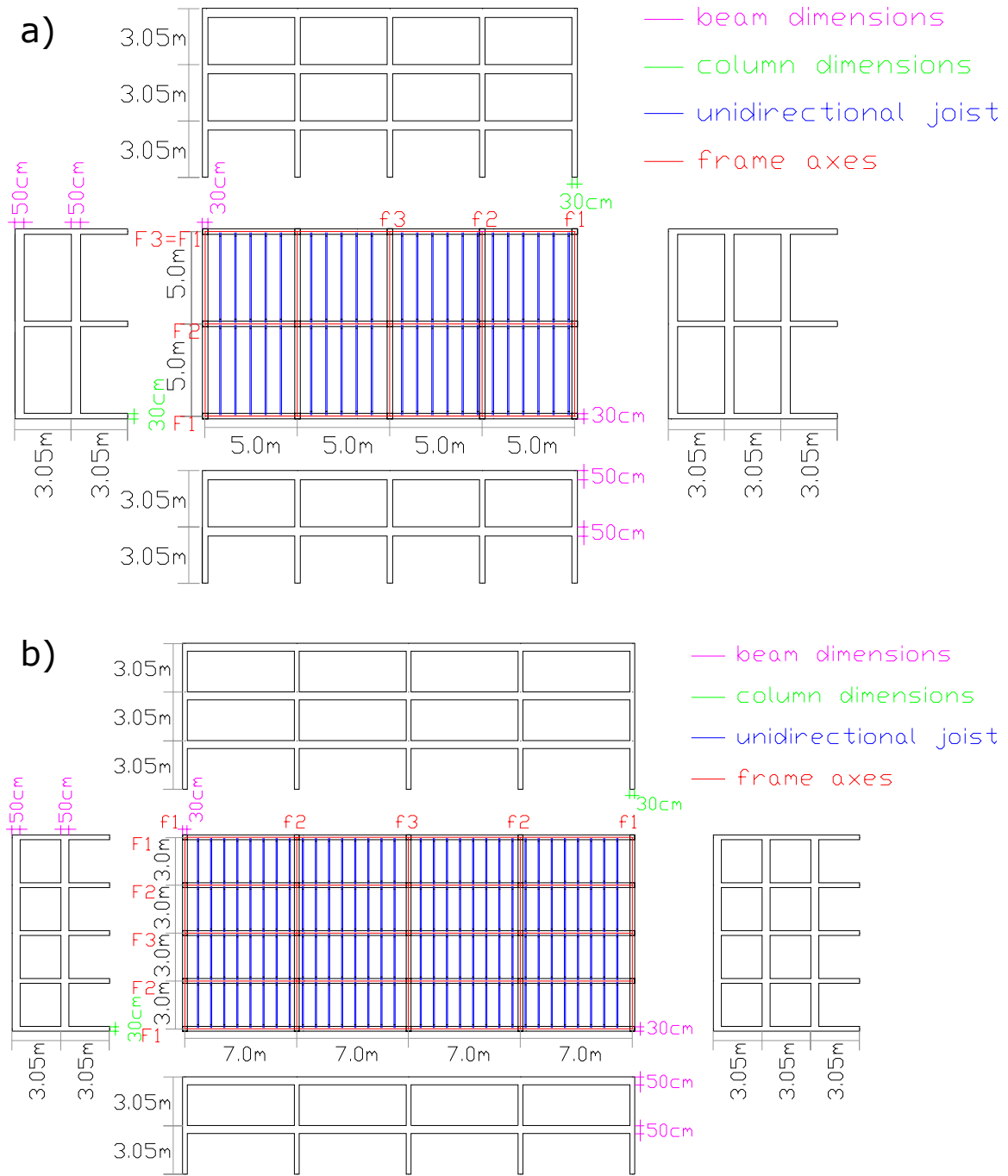


Figure 5.1: a) Prototype 4x2. b) Prototype 4x4

Gravity loads were combined and increased following the CTE prescriptions for permanent situations, eq. 5.1. The values corresponding to the different loads and coefficients are presented in Table 5.2.

$$\sum \gamma_{G,j} \cdot G_{k,j} + \gamma_{Q,1} \cdot Q_{k,1} \quad (5.1)$$

The load combination uses two hypotheses for each load: That the effect that the load produces on the building is favorable or unfavorable. The coefficients that regulate this effect are $\gamma_{G,j}$ and $\gamma_{Q,1}$ and the values used are $\gamma_{G,j} = 1.35$ (favorable) and 0.8 (unfavorable); and $\gamma_{Q,1} = 1.5$ (favorable) and 0.8 (unfavorable).

Permanent actions			Variable actions		
$\gamma_{G,j}$			$\gamma_{Q,1}$		
Favorable		Unfavorable	Favorable		Unfavorable
1.35		0.8	1.5		0.8
$G_{k,j}$			$Q_{k,1}$		
Structural elements' weight	Included in the analysis		Intermediate floors		Upper floor
Flooring and roof		$2kN/m^2$	C1, chairs and tables	$3kN/m^2$	Top deck $1kN/m^2$

Table 5.2: Permanents and variable actions.

5.3 Description of the prototype buildings with infills

For the sake of clarity, each of the four building prototypes is presented separately on its two orthogonal directions hereafter. The global behavior of the building will be presented to consider the adequate emplacement of masonry infill walls in both directions after the fragility and risk analysis.

Two cases of study result from each building defined in Table 5.1, each one in one of the orthogonal direction: parallel (suffix pAra in building name) and perpendicular (suffix pErp in building names) to the direction of the unidirectional joists of the slab. The resulting cases are named as follows:

$$\begin{array}{c|c|c|c} 2S4x2(+) & 3S4x2(+) & 2S4x4(+) & 3S4x4(+) \\ pAra & pErp & pAra & pErp \end{array}$$

Table 5.3: Nomenclature of prototypes.

Appendix A resumes the resulting details of beams and columns of the prototypes. Each building is presented separately in its two orthogonal directions and all the information is summarized on three tables. First table resumes the loading state of the building: loads on the beams and axial loads. Second table resumes the reinforcement on the beams and the third table resumes the reinforcement on the columns and the axial loads.

5.4 Cases of study: 2D numerical models of the prototype buildings with infills

Due to the absence of eccentricities between the center of mass and rigidity, the buildings are not expected to exhibit torsional effects. Furthermore, the hypothesis of rigid diaphragm leads to two independent cases of study for each prototype building with infills: one on the principal direction (direction of the beams that support the gravity loads transferred by the one-way joists slab) and one in the transverse direction. This gives a total of eight cases of study, each one is represented by a two dimensional (2D) numerical model. The support conditions of the structure were considered as fixed base.

The building seismic performance is analyzed in *Idarc v7 code*. The process of analyzing the building is divided in five main steps: Defining material properties; component modeling; define the structure as an aggregation of components; define the hysteretic rules for each element; conduct the non-linear analysis. The details of the numerical modeling have been previously presented in section 4.2.3. Loads, mass and reinforcement details have been presented in section 5.3. For both columns and beams, the parameters that define the level of degradation in the hysteretic rules were obtained from an experimental calibration campaign with static and dynamic tests [*Benavent-Climent (2007) and Benavent-Climent et al. (2009a; 20010)*]. For masonry infill panels, the parameters used were these calibrated with the experimental campaign (section 4.2.3 Tables 4.12 and 4.13), while for the case of the deep beams, theoretical values for mild degradation in the three different aspects (strength degradation, stiffness decay and pinching/crack closing) were used in the absence of test results.

Appendix B presents the pushover curves for each building.

5.5 Retrofitted buildings with masonry walls

Different configurations of walls are proposed hereafter in order to study the influence of masonry wall area on plan. The goal of this analysis is to quantify the variation of the expected damage level of the structure as the area of masonry infill wall in plant, in the direction of seismic loading, changes. The ratio parameter $R_{IW} = \frac{A_{IW}}{A_{floor}}$ quantifies the area of masonry infill walls for each combination.

Figures 5.2(a) and 5.2(b) resumes all the configurations proposed: Appendix A resumes the resulting details of beams and columns of the prototypes. Each building is presented separately in its two orthogonal directions and all the information is summarized on three tables. First table resumes the loading state of the building: loads on the beams and axial loads. Second table resumes the reinforcement on the beams and the third table resumes the reinforcement on the columns and the axial loads. Appendix B presents the pushover curve for each configuration.

5.6 Seismic performance of the retrofitted buildings

The seismic performance of each building is studied through the definition of different damage states. A damage state is reached when the lateral displacement on the infill walls achieve a given value, causing an irreversible change on its lateral load bearing capacity (strength or stiffness). These damage states are associated with a value of lateral top displacement of the

a)

Prototype 4x2 spans						
Ratio	0.04	0.03	0.02	0.01	X	
Wall configuration Perpendicular to joists					I	
					II	
					III	
Ratio	0.05	0.04	0.03	0.02	0.01	Y
Wall configuration Parallel to joists						I
						II

b)

Prototype 4x4 spans						
Ratio	0.05	0.033	0.025	0.017	0.0083	X
Wall configuration Perpendicular to joists						I
						II
						III
Ratio	0.035	0.021	0.014	0.007	0.0035	Y
Wall configuration Parallel to joists						I
						II
						III
						IV
						V

Figure 5.2: a) Configurations under study prototype 4x2. b) Configurations under study prototype 4x4.

building, which is used as a reference of the damage state of the building. This means that the building is considered to achieve a limit state, when any structural element (in this case we consider only infill walls as this is the main lateral load bearing system, in terms of strength and stiffness, of the building) at any story of the building achieves that limit state.

The four-segment polygonal capacity curve of the masonry infill panels (figure 4.19) is used to define four damage states on the masonry infill walls: The initial-elastic branch is associated with the well-known damage state “immediate occupancy” IO [*FEMA 273*]. According to a classification system that has been used by other [*Celarec, Ricci, Dolsek, EE 2012*] the point of the curve associated with a damage called “damage limitation (DL) limit” is located in the second segment of the polygonal curve, when the masonry panel reaches its maximum shear capacity. The point corresponding to a limit called “significant damage” (SD) is the point where the third and fourth segments meet [*Celarec, Ricci, Dolsek, EE 2012*]. The label SD can be assigned to the point at which the capacity curve becomes horizontal after a negative-slope branch. The last point of the four-segment polygonal curve was assumed to correspond to the label “near collapse (NC) limit” and its *ID* is 3.75% (according to the values of the experimental campaign).

The spectral top displacement is obtained by performing a modal analysis of the building and dividing the lateral top displacement by the modal participation factor Γ . The subroutines implemented in Idarc do not allow performing pushover analysis or modal analysis when the model includes elements modelled with the Bouc-Wen method. For these reasons, an external code is used to compute the modal analysis using a mass concentrated model, and the pushover is computed by means of a dynamic analysis with a synthetic record. The values of the accelerations in the synthetic record are increased linearly (0.1, 0.2, 0.3, . . . , 10) and the record is scaled to a PGA that ensures the collapse of the building. To sum up, the steps to relate each damage state (*DS*) with its corresponding value of spectral displacement $\bar{S}_{d_{DS}}$ are as follows:

- Obtain the pushover curve of the building. The pushover analysis is computed by performing a dynamic analysis with an artificial record in which acceleration increases monotonically.
- From the results of the pushover analysis the capacity curve (CC) for each masonry wall in the building is obtained. Then, the four segment polygonal curve proposed in this Thesis is determined for each wall to determine the damage states for the wall as follows: *IO* is defined for a strength value of $Q_{max}/1.3$ (Q_{max} is the maximum lateral strength of the infill); *DL* is defined when the masonry infill reaches its maximum strength Q_{max} . *SD* is assigned to the point at which the capacity curve becomes horizontal after a negative-slope branch and *NC* is defined for an interstorey drift of 3.75%. Finally, the damage states for the walls are plotted over the capacity curve of the masonry infill wall (Fig 5.3).
 - Conduct a modal analysis of the building and obtain the following parameters for the first vibration mode, (i) modal participation factor Γ , given by $\Gamma = \frac{\phi_1^T [M] r}{\phi_1^T [M] \phi_1}$, and (ii) the effective mass M_e , given by $M_e = \Gamma^2 \cdot [\phi_1^T [M] \phi_1]$.
- For each damage state of the masonry infill wall, find the step k at which a wall first achieves the displacement related to the damage state, and obtain the spectral displacement of the building by dividing the top displacement at step k (Figure 5.4) by the modal participation factor Γ .

At the end of the analysis, we have four pairs of values: damage states DS_i , spectral displacement \bar{S}_{d,ED_i} .

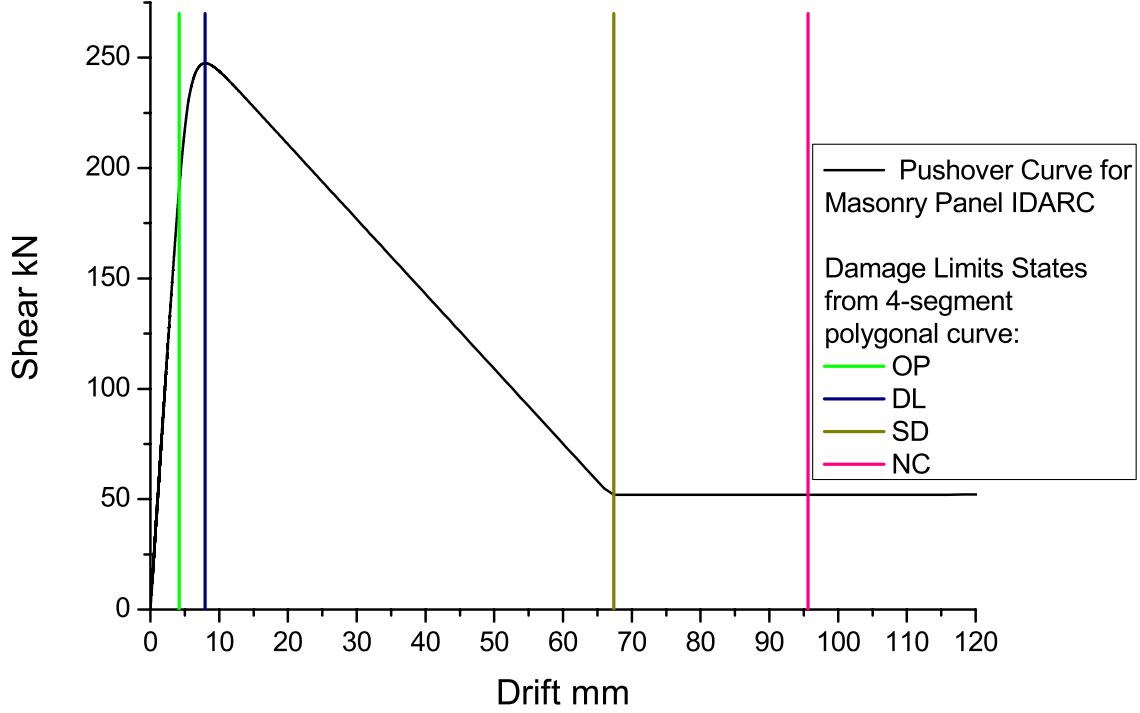


Figure 5.3: Example of damages states for a masonry wall.

5.7 Seismic vulnerability

Seismic vulnerability of each retrofitted building is characterized by the fragility curve associated with each damage state. A fragility curve represents the probability of achieving a given damage state when the building is subjected to an earthquake of a given severity. In this case, the severity of the earthquake is characterized by the spectral displacement \bar{S}_d . The method proposed in the Risk-UE project [Milutinovic and Trendafiloski 2003] is used hereafter to obtain four fragility curves from the capacity spectrum. This procedure is based on the following assumptions [Pujades et al]:

1. For each damage state, (DS_i), the corresponding fragility curve follows a lognormal cumulative distribution defined by: (i), the mean value at which the building reaches the damage threshold DS_i that is referred to as \bar{S}_{d,DS_i} , hereafter; and (ii), the standard deviation of the natural logarithm of this spectral displacement that will be called β_{DS} in this text. The value of the fragility curve at \bar{S}_{d,DS_i} is 0.5 and the probability of the damage level DS being larger or equal to DS_i , for a fixed value of \bar{S}_d is given by the following expression:

$$P [DS \geq DS_i | \bar{S}_d] = \phi \left[\frac{1}{\beta_{ED_i}} \text{Ln} \left(\frac{\bar{S}_d}{(\bar{S}_{d,DS_i})} \right) \right] \quad (5.2)$$

where \bar{S}_{d,DS_i} and β_{DS_i} have been defined previously, and ϕ is the normal cumulative

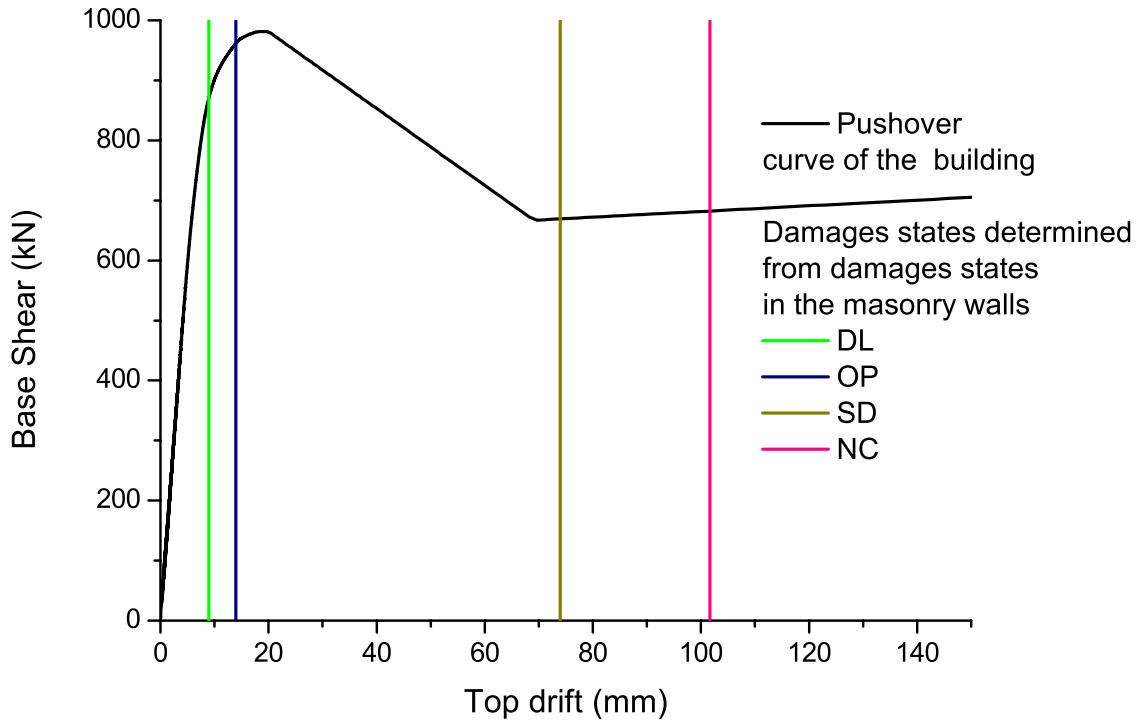


Figure 5.4: Example of determining damage states on the building from damage states on the masonry walls

distribution function; DS_i represents the discrete damage states: $DS_1 \equiv IO$; $DS_2 \equiv DL$; $DS_3 \equiv SD$ and $DS_4 \equiv NC$.

2. The damage is distributed according to a binomial probability distribution [EMS-98]. This assumption is based on previous studies of post-earthquake scenarios.

The computation of a fragility curve for each damage state is implemented by fitting eq. 5.2 to a set of “spectral displacement” - “probability of exceedance” values. Using the algorithm “non linear least squares” implemented in Matlab we can determine the value of β_{ED_i} that perform the best fit of eq. 5.2 to the data.

The procedure to obtain the four pairs of values “spectral displacement” - “probability of exceedance” for each DS_i is supported on the two assumptions mentioned above and the statistic definition of probability of exceedance. These pairs of values are obtained as follows:

- (I) The binomial probability distribution function is a function of the level of the mean damage, μ_D , defined as:

$$\mu_D = 2.5 \left[1 + \tanh \left(\frac{I + 6.25V_I - 13.1}{2.3} \right) \right] \quad (5.3)$$

where I is the intensity defined at the EMS-98 and V_I is the vulnerability index of the building that varies between 0 and 1. μ_D varies between 0 and 4.

- (II) The level of damage, $x(DS_i)$, for each damage state, DS_i , is defined as: $x(IO) = 1$; $x(DL) = 2$; $x(SD) = 3$; and $x(NC) = 4$.

(III) The binomial probability distribution (in assumption 2) can be approximated by the continuous beta distribution function defined by:

$$P_{\beta}(x) = \frac{\Gamma(t)}{\Gamma(r) \cdot \Gamma(t-r)} \frac{(x-a)^{r-1} (b-x)^{t-r-1}}{(b-a)^{t-1}} \quad a \leq x < b \quad (5.4)$$

if $t=8$.

Γ is the Gamma function, $a = 0$; $b = 5$. r is a function of t and μ_D defined as:

$$r = t \cdot (0.007\mu_D^3 - 0.0525\mu_D^2 + 0.2875\mu_D) \quad (5.5)$$

μ_D is fix for a given DS_i and can be obtained by integrating $P_{\beta}(x)$ between 0 and the corresponding value for $x(DS_i)$ and imposing that the probability of exceedance for that given damage state (IO ; DL ; SD and NC) is 0.5

$$1 - \int_0^{x(DS_i)} P_{\beta}(x) dx = 0.5 \rightarrow \mu_D \quad (5.6)$$

(IV) Once μ_D is fixed for DS_i , the probability of exceedance for the other three values of $x = DS_j, j \neq i$, is obtained as:

$$P [DS \geq DS_j | \bar{S}_d] = 1 - \int_0^{x(DS_j)} P_{\beta}(x) dx \quad (5.7)$$

Table 5.4 presents the values of μ_D and $P [DS \geq DS_i | \bar{S}_d]$ for $DS_i \equiv IO; DL; SD; NC$ for building 2S4x4pAr $R=0.017$ and Figure 5.5 the fragility curves obtained by fitting Eq. 5.2 to the data in Table 5.4.

DS_j	μ_D	$P [DS \geq DS_j \bar{S}_d]$			
		$\bar{S}_d = \bar{S}_{dIO}$	$\bar{S}_d = \bar{S}_{dDL}$	$\bar{S}_d = \bar{S}_{dSD}$	$\bar{S}_d = \bar{S}_{dNC}$
$DS_j = IO$	0.911	0.5	0.881	0.988	1
$DS_j = DL$	1.919	0.104	0.5	0.865	0.992
$DS_j = SD$	3.081	0.008	0.134	0.5	0.896
$DS_j = NC$	4.001	0	0.012	0.119	0.5

Table 5.4: Mean damage and probability of exceeding a given damage state.

5.8 Parametric analysis of the fragility curves

The uncertainties of studying the influence of masonry infill panels in seismic performance comprise a wide spectrum of possibilities including material properties, building design, geometry of the building, expected earthquake (intensity, frequency content). None of these parameters can be defined accurately, and the number of cases of study if we could combine all possibilities would trigger a huge and unrealistic scenario. For the sake of coherence, and in order to know

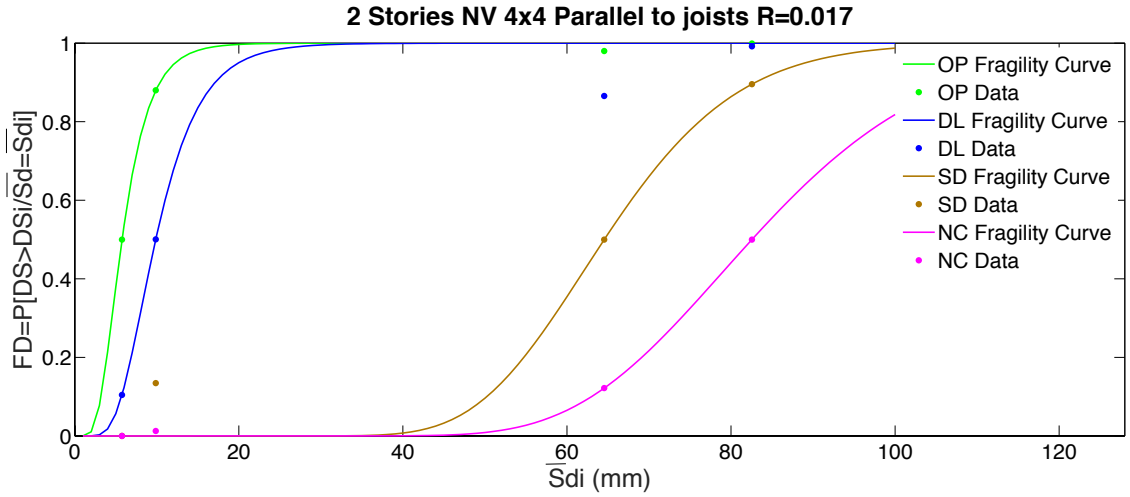


Figure 5.5: Example of fragility obtained curves.

the real influence of the ratio of infill panels $R_{IW} = \frac{A_{IW}}{A_{floor}}$, only the amount and configuration in plant of masonry infill wall has been modified at each building or case of study.

After the analysis that has been described through section 5.3, the statistic parameters \bar{S}_{d,DS_i} , β_{ED_i} (defined at section 5.7 assumption 1) are used in Figure 5.6 to evaluate the effects of changes in R in the seismic performance of schools buildings in Haiti.

The parametric analysis based on the value of the mean top lateral displacement at which the damage level state is reached, \bar{S}_{d,DS_i} and the standard deviation of the natural logarithm of this spectral displacement, β_{DS} , throws the next conclusions:

1. As the level of damage in the building increases, the value of \bar{S}_{d,DS_i} increases and the value of β_{DS} decreases.
2. For a given level of damage, the number of stories is inversely related to the value of \bar{S}_{d,DS_i} . As the number of stories increases, the value of \bar{S}_{d,DS_i} associated with a given level of damage decreases.
3. The number of spans of the building does not affect the parameter \bar{S}_{d,DS_i} while it has some influence on the parameter β_{DS} . This influence is more noticeable for damage states SD and NC . β_{DS} is, in most cases, higher for configuration 2x4 than for configuration 4x4.
4. The value of R slightly affects \bar{S}_{d,DS_i} and β_{DS} . This implies that for the purposes of risk assessment, the fragility curve a RC frames seismic retrofitted with infill walls of the type investigated in this Thesis can be established irrespective of R .

Based on the results plot in Figure 5.6 and the observation that \bar{S}_{d,DS_i} and β_{DS} can be considered as independent of the value of R , the following values are proposed for \bar{S}_{d,DS_i} and β_{DS} in Tables 5.5 and 5.6.

The values of \bar{S}_{d,DS_i} and β_{DS} proposed in Tables 5.5 and 5.6 give the proposed fragility curves plot in Figures 5.6 (a-d)

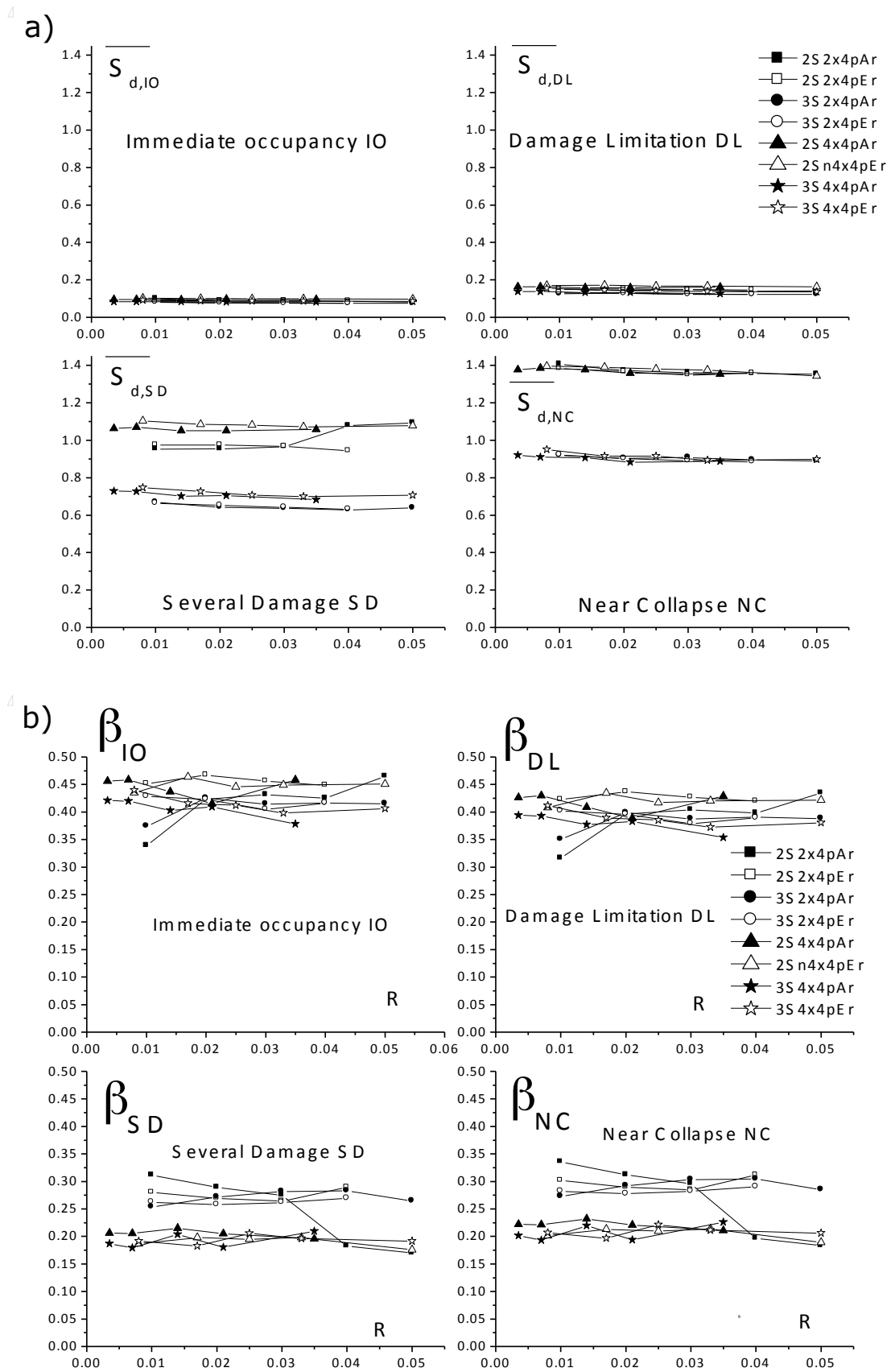


Figure 5.6: a) Variation of S_d as R increases. b) Variation of β as R increases.

Damage limit	N ^o Stories	\bar{S}_{d,DS_i} (%)
<i>IO</i>	2	0.09
	3	
<i>DL</i>	2	0.15
	3	
<i>SD</i>	2	1.05
	3	0.65
<i>NC</i>	2	1.35
	3	0.90

Table 5.5: Proposed values for \bar{S}_{d,DS_i}

Damage limit	N ^o Stories	β_{DS}
<i>IO</i>	2x4	0.43
	4x4	
<i>DL</i>	2x4	0.40
	4x4	
<i>SD</i>	2x4	0.27
	4x4	0.20
<i>NC</i>	2x4	0.3
	4x4	0.21

Table 5.6: Proposed values for β_{DS} .

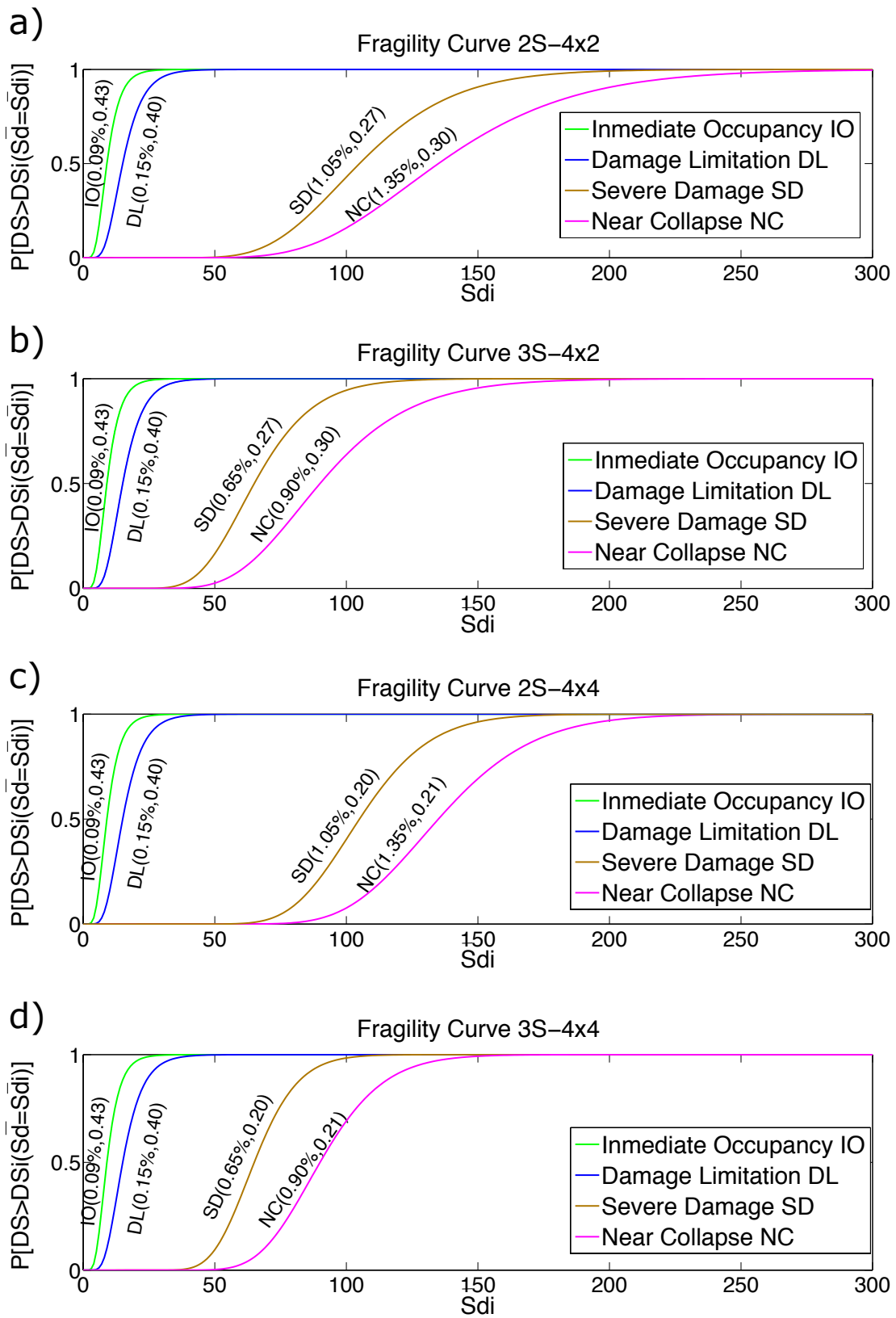


Figure 5.7: Proposed fragility curves: a) 2 story and 2x4 spans; b) 3 story and 2x4 spans; c) 2 story and 4x4 spans; d) 3 story and 4x4 spans.

5.9 The priority index [Hassan and Sozen, 1997]

Shiga et al. (1968) [4] proposed a simple methodology for rapid assessment and ranking of vulnerability for low-rise RC buildings. The two principal variables to define a building as vulnerable or not vulnerable are (1) the amount of area of the structural elements that could resist lateral loads in plan and (2) their nominal shear stress. This method is presented to evaluate a post-earthquake scenario. The 1968 Tokachi-Oki earthquake was used to calibrate it, finding that slight and no damage was produced when buildings had a wall-area index higher than $30\text{cm}^2/\text{m}^2$ and shear stress lower than $12\text{kgf}/\text{cm}^2$ [Shiga et al. 1968]. The information needed to evaluate this index is obtained through visual inspection with no need of technical training. The effectiveness of this method is restricted to low-rise buildings as it was demonstrated after applying it to the data from the 1985 Chile earthquake [Riddell et al. 1987]. Hassan and Sözen (1997) proposed a modification on this methodology for buildings with the next properties:

1. Low-rise buildings.
2. Small areas of reinforced concrete walls.
3. Masonry infill walls.
4. Poor reinforcement detailing.

Defining the “Priority Index” (PI) as:

$$PI = \frac{\sum A_{RCWalls} + 1/2 \sum A_{columns} + 1/10 A_{MIWalls}}{\sum A_{floor}} \quad (5.8)$$

$\sum A_{RCwalls}$ = sum of the cross-sectional areas of RC walls in the direction with smallest wall area at ground story.

$\sum A_{columns}$ = sum of the cross-sectional areas of columns at ground story.

$\sum A_{MIWalls}$ = sum of the cross-sectional areas of masonry infill walls.

$\sum A_{floor}$ = total floor area above ground level.

The Priority Index was first tested in 1999 after the earthquakes in Turkey by *Dörmöz and Pujo* (2005) concluding that a building whose PI is less than 0.4% is vulnerable to earthquakes.

In the last years, the priority index has been extended and used in different scenarios. It was tested by Gur and his associates in 2009 [Gur et al. 2009]. In Istanbul the priority index was used to estimate quantitatively the damage that a future earthquake could provoke [Ozcebe et al. 2004, Griffiths et al. 2007]. It was also used to classify hundreds of school structures and thousands of residential buildings in Bogotá [Ramírez 2000] [10] and Anguilla as part of the Caribbean Disaster Mitigation Project [Gibbs 1998] [11].

The application of the PI in Haiti [O’Brien 2011] confirmed that a value of $PI = 0.4\%$ defines the threshold to evaluate the vulnerability of a building. The level of damage in a non vulnerable building after an earthquake will be “light damage” or “non damage”, while in a vulnerable building the level of damage will rank from “severe damage” to “collapse”, the lower the PI , the higher level of damage after an earthquake in the building. This study also included information about:

1. Data from damage state of buildings.
2. It allowed to deep in some variables (proximity to the fault, construction practices, presence of captive columns).
3. It related the PI to the probability of suffering severe damage in masonry infill walls, P_{SDIW} :
 - a) for $PI \in (0.0\%-0.09\%)$, $P_{SDIW} = 77\%$.
 - b) for $PI \in (0.10\%-0.19\%)$, $P_{SDIW} = 65\%$.

Another useful conclusion from the studies mentioned above [*Dönmez and Pujol (2005)* and *O'Brien (2011)*], is that PI also proportionate a guide to prioritize the retrofitting necessities for low-rise buildings that have been constructed with poorly detailing. *O'Brien (2011)* proposed to screen the structures in a two-tiers way:

1st Classification of buildings from the lowest PI to the highest.

2nd Presence of captive columns among the buildings with lowest PI . Start strengthening efforts in these buildings. Technicians are encouraged to study these buildings in detail by means of complex procedures to detect particular types of failures or clarify the retrofitting measures.

The Priority Index was also tested in 116 buildings after the earthquake occurred in 2008 in *Wenchuan (Zhou 2013)*. This study confirms that the increase in the level of damage attained by the building is directly related to the decrease in PI . Secondly, this study offers a number of subgroups that help to determine how sharp is this relation in presence of other variables as, for example, the presence of non symmetrical frames, the exclusion of buildings with masonry infill panels, etc.

The PI has been used to evaluate the vulnerability of both bare frame prototypes and for each configuration of seismic upgrading with infill walls described in section 5.5. The results are presented in Tables 5.7 and 5.8.

		2 Levels							
		4x2 Spans				4x4 Spans			
		Perpendicular to joists		Parallel to joists		Perpendicular to joists		Parallel to joists	
		R	$PI(\%)$	R	$PI(\%)$	R	$PI(\%)$	R	$PI(\%)$
Prototype	0.00		0.1687	0.00	0.1687	0.00	0.1674	0.00	0.1674
	0.01		0.2187	0.01	0.2187	0.008	0.2091	0.0035	0.1853
	0.02		0.2688	0.02	0.2688	0.017	0.2507	0.007	0.2031
	0.03		0.3188	0.03	0.3188	0.025	0.2924	0.014	0.2388
	0.04		0.3687	0.04	0.3687	0.033	0.3341	0.021	0.2746
					0.05	0.4188	0.050	0.4174	0.035

Table 5.7: Priority Index for 2-levels prototypes as a function of R .

Conforming to the conclusions from *O'Brien [O'Brien 2011]* the buildings studied are vulnerable if no measures are taken. According to the post-earthquake scenario evidences described before, a PI higher than 0.4% is related to “light damage” or “non damage” in the building after an earthquake. Also, the damage on these buildings concentrates first on the captive columns and masonry infill walls. Captive columns are the first elements to repair, as short columns

		3 Levels							
		4x2 Spans				4x4 Spans			
		Perpendicular to joists		Parallel to joists		Perpendicular to joists		Parallel to joists	
		R	$PI(\%)$	R	$PI(\%)$	R	$PI(\%)$	R	$PI(\%)$
Prototype	0.00	0.1125	0.00	0.1125	0.00	0.1116	0.00	0.1116	
	0.01	0.1458	0.01	0.1458	0.008	0.1394	0.0035	0.1235	
	0.02	0.1792	0.02	0.1792	0.017	0.1672	0.007	0.1354	
	0.03	0.2125	0.03	0.2125	0.025	0.1949	0.014	0.1592	
	0.04	0.2458	0.04	0.2458	0.033	0.2227	0.021	0.1830	
			0.05	0.2792	0.050	0.2783	0.035	0.2307	

Table 5.8: Priority Index for 3-levels prototypes as a function of R .

effects are unpredictable and consequently, unacceptable. Masonry infill panels are conceived in this Thesis as retrofitting elements that, after an earthquake, can be demolished and rebuilt, consequently any level of damage in masonry infill walls is acceptable. Nevertheless, “severe damage” in masonry infill walls, whose probability of occurrence is 35% when $PI = 0.19\%$ and decreases as PI increases, is avoided in order to minimize the damage in the rest of structural elements. For this reason, the ratio of masonry walls recommended for these buildings will rank as a function of PI : $R(PI\%) \in \{R(0.19\%) \leq R(PI\%) \leq R(0.4\%)\}$. Figures 5.8 and 5.9 show the relationship between the ratio of masonry infill panels, R , and the Priority Index, PI , for 2- and 3-levels buildings respectively. It is worth noting that these relationships are hardly dependent of the geometry of the building, and consequently, can be formulated as:

$$PI(\%) = 0.16 + 5.2R \quad 2 - N \quad (5.9)$$

$$PI(\%) = 0.10 + 7.6R \quad 3 - N \quad (5.10)$$

where N is the number of stories.

Fig 5.8 and 5.9 or equations 5.9 and 5.10 are used below to recommend a value of R that is related with a likely level of damage on the structure:

- For 2-levels buildings it is recommended (Figure 5.8):
 - A value of $R=0.015$ ($PI=0.24\%$), in red in fig. 5.8, to minimize the probability of several damage on masonry infill walls.
 - A value of $R=0.025$ ($PI=0.29\%$), in blue in fig. 5.8, to minimize the reparation works.
 - A value of $R=0.046$, in magenta in fig. 5.8, to ensure that the level of damage in the building is minimal and close to zero.
- For 3-levels buildings it is recommended (Figure 5.9):
 - A value of $R = 0.035$ ($PI=0.23\%$), in red in fig. 5.9, to minimize the probability of several damage on masonry infill walls.

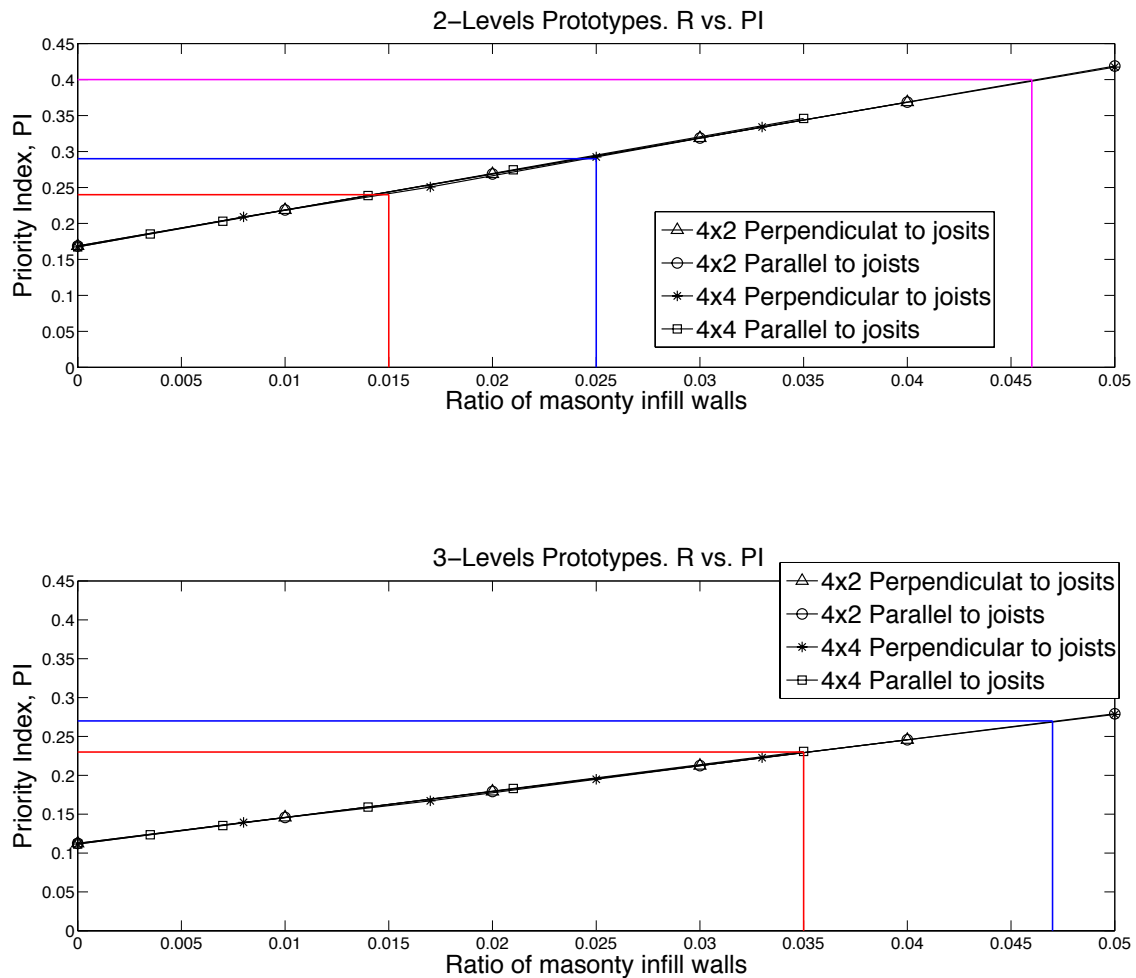


Figure 5.9: 3-Levels prototypes. R vs PI

5.10 Proposed approach to evaluate the seismic risk of RC frames seismic upgraded with infill walls

The priority index PI proposed by Hassan and Sozen has the advantages of simplicity and the robustness of having been calibrated with observed damage that conclude that PI must be larger than 0.4% to consider the buildings not vulnerable. Also, the study of the post-earthquake information related to this PI available allows knowing the influence of the PI values, not only on the stability of the building, but also on the probability of failure of a given structural element. The bare RC frames investigated in this thesis are found to be very vulnerable according to this criterion because PI was far below 0.4%. Previous results propose different values of R for each building to minimize a given damage level on the structural elements or at the building.

The disadvantage of the priority index PI proposed by Hassan and Sozen is that it cannot be used in seismic risk studies because it does not provide information on the vulnerability (or fragility) of the buildings retrofitted with infill walls. To overcome this, the fragility curves proposed in section 5.9 can be used.

In this Thesis it is proposed to use the Hassan and Sozen PI index in combination with the fragility curves proposed in section 5.9 to evaluate quantitatively the seismic risk of RC frames seismic upgraded with infill walls. The procedure would be as follows. First calculate the PI index and determine if the existing RC frame is vulnerable or not. If the answer is affirmative, reinforce the building by adding infill walls in an amount controlled by the ratio R . Second, obtain the capacity curve of the RC frame with infill walls (using for the walls the polygonal lateral force-displacement curves proposed in previous chapter) and by using non-linear static methods (i.e. the N2 method or the Capacity-Spectrum method) obtain the target displacement S_d for a given level of seismic hazard. Finally, plotting in the fragility curves proposed in section 5.9 this value of S_d would provide the probability of exceeding a given level of damage. Performing this process for different levels of seismic hazard allows evaluating the seismic risk of an existing RC frame seismic upgraded with an amount of infill walls controlled by R .

Methodology for seismic retrofitting of reinforced concrete frames using masonry infill panels

6.1 General considerations and scope of application of the proposed solution

This Chapter proposes a simple method to assess and retrofit low-rise buildings (2-3 levels) that have been previously damaged by an earthquake. It is applicable to low-rise reinforced concrete frame buildings. The proposed methodology reduces the vulnerability of the structure and allows attaining higher levels of safety in the building through the implementation of masonry infill panels. The construction of the clay brick units and the preparation of the mortar is assumed to be done following the experience of local masons and constructors, and the recommendations of the authority designed by the government (if any). The proposed seismic upgrading strategy requires that the new masonry infill walls fill the entire clear span of the frame defined by two neighboring columns and the upper and lower beams.

The benefits of the retrofitting measures proposed in this guide are assumed to be independent of the initial damage state of the building. For this reason, it is not necessary to detail the level of damage of each structural element of the existing RC frame but to ensure that a maximum level of damage has not been exceeded.

This guide intends to be used by local constructors or people with similar level of technical knowledge, which normally do not have a technical training but can differentiate structural elements and understand the requirements in assessing the level of damage. Before defining the steps to accomplish, it is important to remark some concepts and aspects that anticipate to different situations to face during the visual inspection.

1. The methodology and proposed seismic retrofit solution is intended to be applied to low-rise building (2-3 levels) typically used in Haiti for schools whose main load bearing system is composed of reinforced concrete frames.

2. It is recommended preparing a layout or grid paper for the story sketch and the structural elements and approximate dimensions. This plan also contains the wind rose to note the estimated orientation of the building.
3. Especial concepts:
 - (a) A building is considered irregular along its height when the stiffness of each frame defined by two neighboring columns changes from one level to another. The irregularities in plan can be studied easily from the story sketch when all the structural elements have been noted. Irregularities in the vertical dimensions, especially due to the presence of masonry infill panels, need to be noted.
 - (b) Captive columns normally develop in the presence of an opening, a window or a door. The opening is surrounded by a masonry wall. If there is not a gap or element structurally separating the wall and the surrounding frame, the movement of the column is (i) free in the region of the opening and (ii) restricted in the rest. The shear demand in the columns is higher than the shear design. This effect can provoke the collapse of the column or even a soft story mechanism (Fig. 6.1).
4. The location of elements other than RC frame should be noted, more precisely:
 - (a) Masonry infill panels.
 - (b) Captive columns.

In school buildings in Haiti, stairs are present normally in the outer façade of the building, for this reason its level of damage does not affect the integrity of the school building itself. The use of the stairs is characterized by short times with high demand of people, corresponding to changes of activity in the school. Although this analysis is out of the scope of the present retrofitting scheme, it is recommended to check the structure of the stairs after an earthquake to ensure they are still useful and the absence of risk for children and teachers.

6.2 Assessment of the damaged structure and limits of the application of the masonry infill panel retrofitting strategy

6.2.1 Maximum level of damage of the existing structure

There is a maximum level of damage that can be accepted on the RC frame structure to apply the proposed seismic upgrading solution with additional infill walls. This minimum strength come from the need that a truss mechanism develops in the masonry infill wall and that the RC frame elements do not fail under low lateral loads. The following levels of damage are not acceptable for beams and or columns:

1. Spalling or crushing on the concrete, especially found at the extremes of the element, which reduces the effective section and confinement of bars. Fig 6.2 (a) and (b).
2. Buckling of the longitudinal rebars. Special attention must be paid to the extreme of the elements where plastic hinges tend to develop. Fig 6.2 (c) and (d).



Figure 6.1: a) Irregularities in the vertical dimension triggers soft story effect (photo Chungwook Sim et al.). b) Captive columns. Short-column effect. (photo Rebekah Green. EERI Special Earthquake Report-May 2010).

3. Diagonal or horizontal cracks along the whole width of the element. Neither any other crack whose width is equal or higher than 1 mm in beams or 0.3mm in columns. Fig 6.2 (e) and (f).
4. Diagonal cracks in the joints from 0.1mm to 0.3 mm.
5. Lost of concrete on the structural element.

If any of the damage grades mentioned above is exceeded in any column or beam, the proposed retrofitting scheme cannot be implemented without previously repairing the element.

The reparation of the columns depends on the extension of the damaged zone. We can distinguish two cases. The first case is when the extension is, in length, smaller or equal to the depth of the column. In this case the reparation is limited to this area of the column. The second case is when it is larger, in this case the column needs to be demolished and rebuild. The reparation process is carried out as follows (Fig 6.3 and Fig 6.4):

1. Remove the damaged concrete.
2. Straight the bars in the interior of the column.
3. If the damage is superficial and limited to a region:
 - a) Clean with air-blower the remaining concrete and moisten it.
 - b) Add an additional mesh of rebars around the concrete.
 - c) Cast concrete the surface.
4. If the column needs to be rebuilt

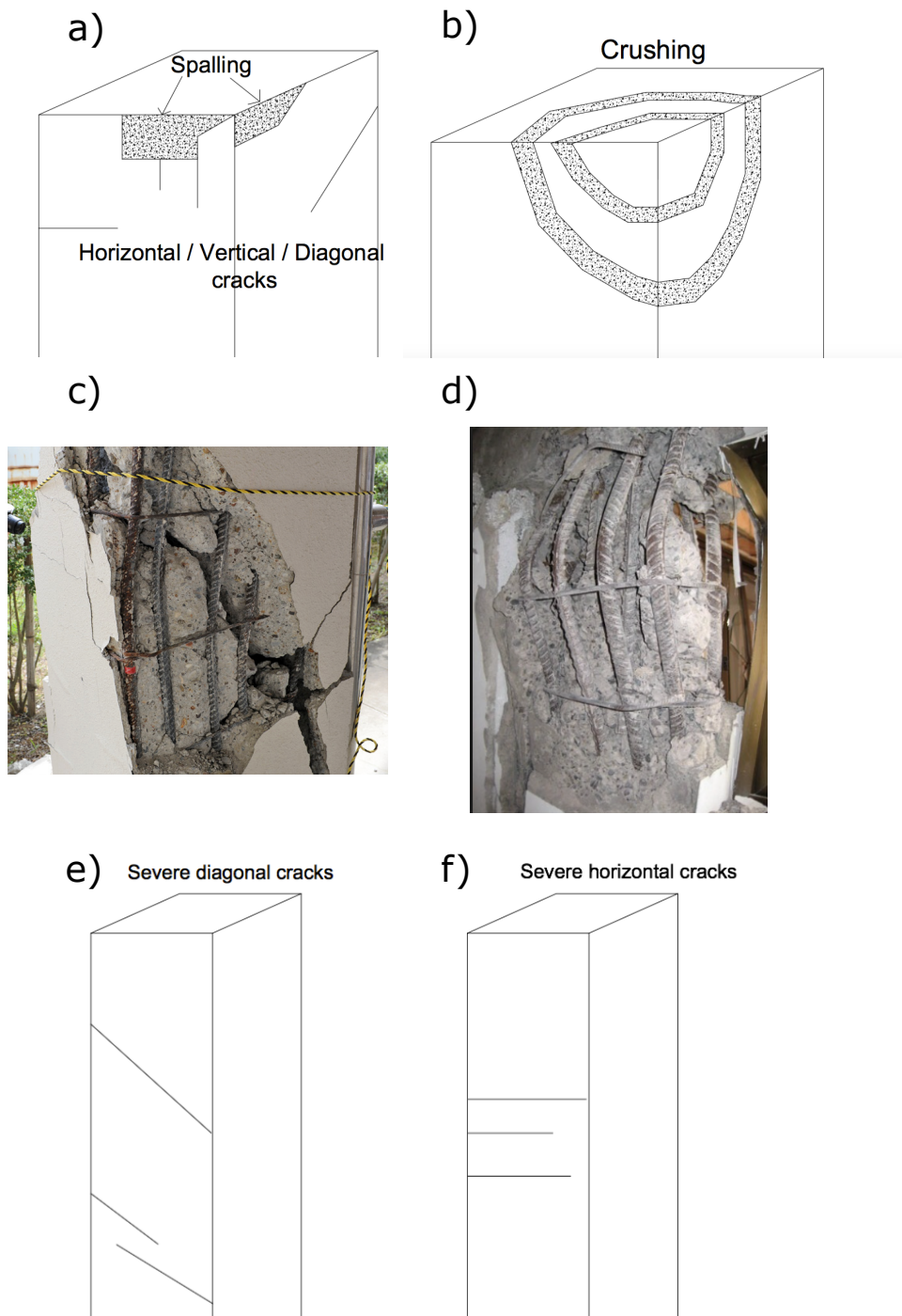


Figure 6.2: a) Spalling in concrete. b) Crushing in concrete. c) and d) Bucking of rebar. e) and f) Severe diagonal/horizontal cracks

- a) Add additional longitudinal rebars with the same or higher diameter than the original ones. Add 7.5cm-separated stirrups along the column height.
- b) Build the formwork around the column
- c) Cast concrete the column from a hole made on the upper slab
- d) Apply the plaster two weeks later

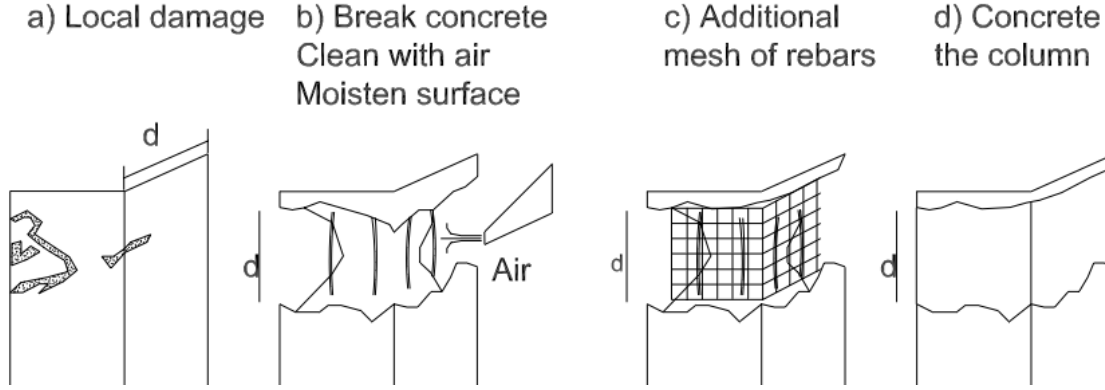


Figure 6.3: Repairation of local damage in column.

6.2.2 Minimum required dimensions of the columns of the existing RC frame

Following the formulation proposed by *Zarnic (2001)* the maximum lateral load attained in the masonry infill walls is

$$Q_{w,max} = 0.818 \frac{L_w t_w f_{tp}}{1.925 L_w / h_w} \left(1 + \sqrt{(1.925 L_w / h_w)^2 + 1} \right) \quad (6.1)$$

where L_w , h_w , t_w are the length, height and width of the infill; f_{tp} is the cracking strength of the masonry that can be assumed to value 0.25 MPa. The squat panels that have been considered for this work have an aspect ratio $0.7 \leq h_w / L_w \leq 2$. Consequently, $Q_{w,max}$ is in the range of $5.75 L_w \leq Q_{w,max} \leq 10 L_w$.

The shear strength of the column is computed by the equations proposed by Priestly and his associates [*Priestly et al. 1994*] and is given by eq.

$$V_n = V_c + V_p + V_s \quad (6.2)$$

where, V_c is the concrete component given by

$$V_c = k \sqrt{f'_c} A_e \quad (6.3)$$

k depends on the ductility of the column and varies between 0.085 and 0.25. A_e is the effective shear area and is taken as $A_e = 0.8 A_{gross}$. Considering $f'_c = 25 \text{ MPa}$, V_c varies in the range of $(0.34 - 1) A_{gross}$. To be on the safety side, we consider $k = 0.085$.

V_p is the axial load component

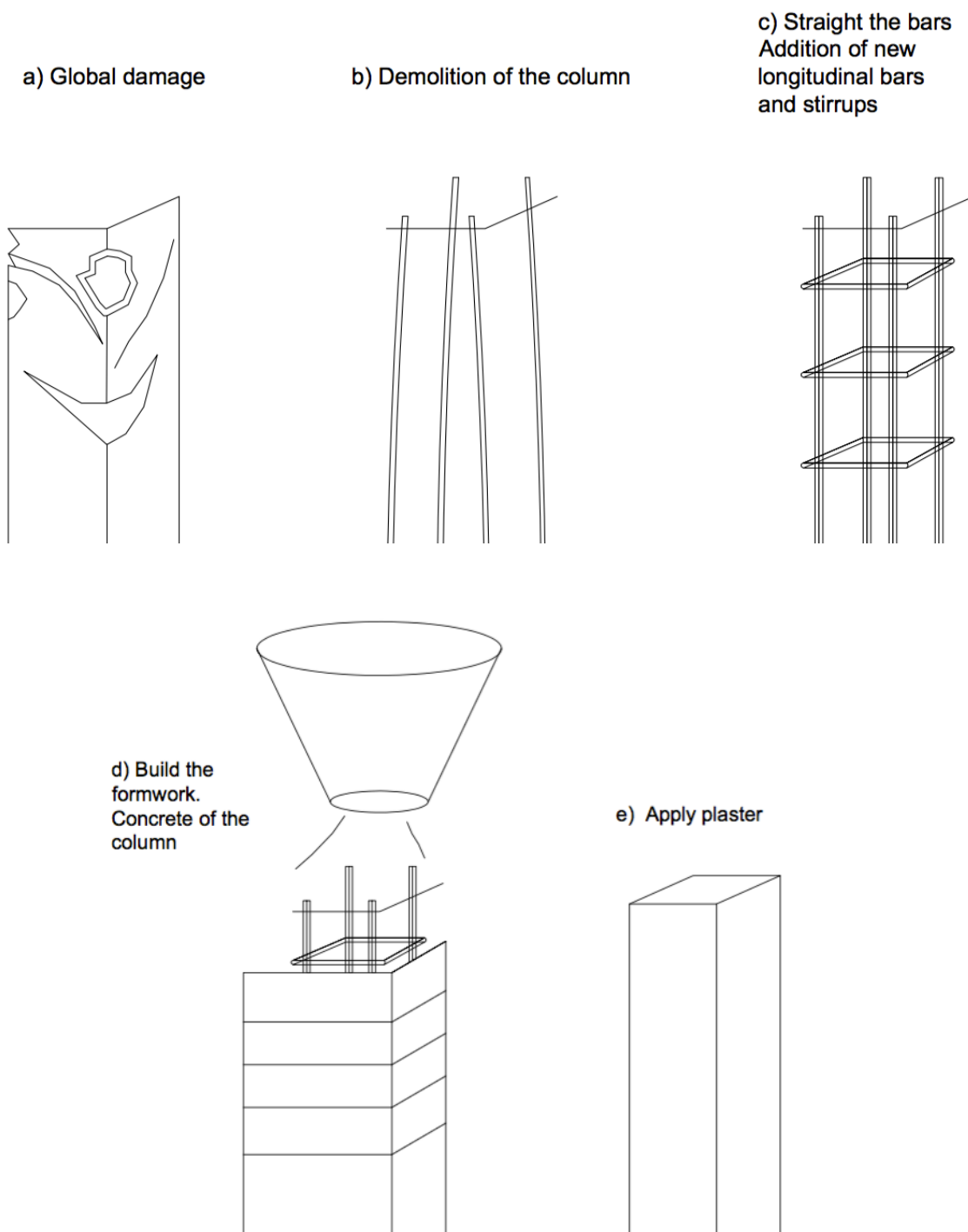


Figure 6.4: Reparation of global damage in column.

$$V_p = P \tan \alpha = \frac{D - c}{2a} P = \frac{0.8d}{L/2} P \quad (6.4)$$

where D is the overall section depth and c the depth of the compression zone, $a = L/2$ for a column in reversed bending. For squat columns this term is influential while for slender columns this contribution is minimal. Taken advantage of this conclusion we will ignore the contribution of axial loads in this study

V_s is the truss mechanism component, measures the contribution from shear reinforcement and is given by

$$V_s = \frac{A_v f_{yd} D'}{S} \cot 35^\circ \quad (6.5)$$

where A_v is the area of shear reinforcement, f_{yd} the strength of steel reinforcement, D' is the distance between centers of the more external hoop and can be assumed to be $0.9d$, where d is the depth of the square column, and S the separation between stirrups. There is a lack of information in general and also about shear reinforcement. The photo in fig 6.5 shows a building in construction just after the 2010 January earthquake (*DesRoches et al. 2011*). The authors reported some information about the reinforcement: the longitudinal bars are $\phi = 4$ mm while the reinforcement bars were minimal $\phi=2$ mm spaced a distance approximate to the column depth. The strength of the steel recommended by the local government (*MTPTC and MICT 2010*) is 400 MPa. Thus an approximation of V_s is

$$V_s = \frac{\frac{2^2\pi}{4} \cdot 400 \cdot 0.9d}{d} \cot 35^\circ \approx 1.6kN \quad (6.6)$$

Finally, an approximation of the shear strength of the column is given by:

$$V_n = \frac{0.34d^2}{1000} + 1.6[kN] \quad (6.7)$$

By imposing,

$$Q_{w,max} \leq V_n \quad (6.8)$$

We can differentiate two cases: for the case of squat walls (i), $Q_{w,max} \cong 5.75L_w$, and for slender walls (ii) $Q_{w,max} \cong 10L_w$. Imposing eq. 6.8 yields a value for d :

$$\begin{aligned} (i) \quad d &\geq 4\sqrt{L_w - 278} \\ (ii) \quad d &\geq 5.4\sqrt{L_w - 160} \end{aligned} \quad (6.9)$$

d and L_w are in mm, by interpreting the order of magnitude of the quantities in the root square, we can simplify by:

$$\begin{aligned} (i) \quad d &\geq 4\sqrt{0.9L_w} \\ (ii) \quad d &\geq 5.4\sqrt{0.9L_w} \end{aligned} \quad (6.10)$$

that finally gives:

$$\begin{aligned}
 (i) \quad d &\geq 3.8\sqrt{L_w} && \text{for squat walls} && (h_w/L_w \leq 1.35) \\
 (ii) \quad d &\geq 5\sqrt{L_w} && \text{for slender walls} && (h_w/L_w \geq 1.35)
 \end{aligned}
 \tag{6.11}$$



Figure 6.5: Building under construction in Haiti. Source DesRoches et al. 2011.

6.2.3 Consideration of existing masonry walls

The existing masonry panels in the building can also present structural damage caused by previous earthquakes. These masonry walls can be part of the retrofitting scheme if they are able to develop the truss mechanism and do not provoke drastic changes on the stiffness of the building. Next, the different possibilities that can arise and the decision to take are presented:

1. Separation from the RC frame. There are no cracks on the mortar or brick units. In this case, the masonry wall can be maintained in the scheme Figure 6.6 (a).
2. The masonry wall has some horizontal and/or stepped cracks on the mortar and/or the brick units (Figure 6.6 (b)). A complete diagonal or horizontal crack is not defined. It is necessary to study the case with regard the whole building. We can differentiate two cases:
 - a) The amount of the cracks is the same in almost all the panels (80-90%). We can conclude that the initial stiffness will correspond to the secant stiffness of the panel, and that the masonry infill wall will reach almost 100% of its maximum lateral strength. The masonry infill walls can be maintained in the scheme.

- b) The amount of cracks varies from one panel to the other. In this case, maintaining the panels will risk the building suffering torsion effects. For this reason the infill panels are not acceptable for the scheme and need to be rebuilt. In some cases, the panels with slight damage can be maintained if the amount of cracks is low.
3. The masonry has a horizontal or diagonal crack, whose length is higher than $0.4L$, where L is the horizontal length of the wall for the horizontal crack, and the length of the diagonal for the diagonal crack. In this case the wall needs to be demolished. Figure 6.6 (c).

6.3 Guidelines for seismic retrofitting of reinforced concrete frames with masonry infill walls. Criteria to follow and checks required

The practical application of the proposed seismic retrofitting strategy of reinforced concrete frames with masonry infill walls requires two types of actions: visual inspection and checkups.

- Visual inspection.
 1. Sketch the floor plan and sketch each story.
 2. Determine the use of the building.
 3. Determine if there are vertical irregularities.
 4. Identify the structural elements.
 5. Determine the dimensions (approximate) of structural elements and the geometry of each story.
 6. Determine the level of damage in beams and columns and define if it is acceptable or non acceptable.
 - a) Spalling of concrete. Non acceptable.
 - b) Crushing of concrete Non acceptable.
 - c) Buckling of rebars Non acceptable.
 - d) Excessive diagonal/horizontal cracks Non acceptable.
 - e) Lost of concrete material inside the rebars Not acceptable.
 7. Determine the level of damage in masonry infill panels and decide if it is acceptable or non acceptable.
 - a) Wall separated from frame. Acceptable.
 - b) Non-totally defined failure mode. Damage in walls is homogeneous in most of the walls. Acceptable.
 - c) Non-totally defined failure mode. Damage in walls differs from one wall to the other. Non acceptable.
 - d) Totally defined failure mode. Cracks with length higher than $0.6L$, where L is the total length in the direction of the crack (horizontal/diagonal) Non acceptable.
 8. Identify the presence of captive columns.

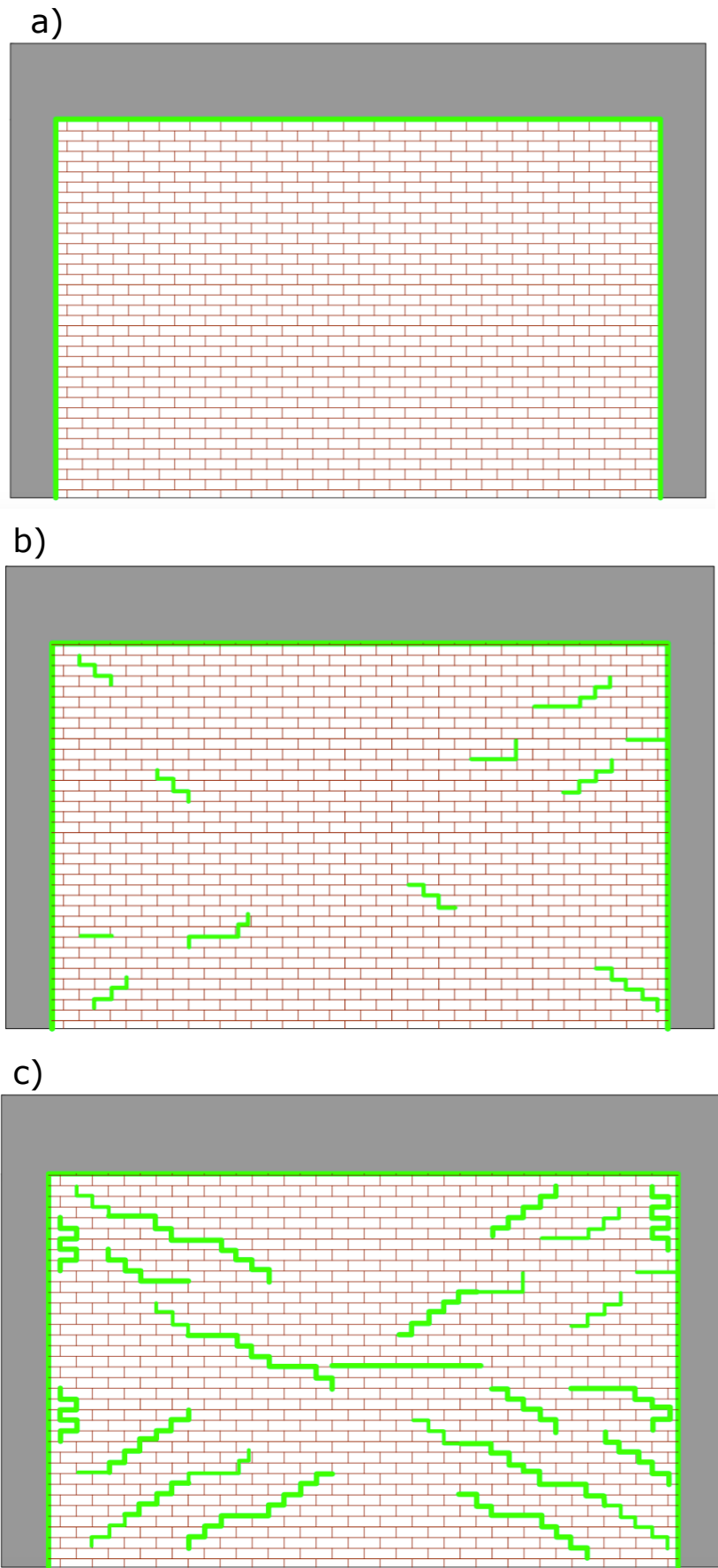


Figure 6.6: Types of damage in masonry infill walls. a) Separation of the wall. b) Slight damage on the wall. c) Severe damage on the wall.

- a) Check the presence of a gap between masonry and column. If it does not exist, demolish partially or completely the wall and rebuild it with the gap.
 - b) Check any level of damage in the columns. Same requirements than for columns and beams are needed to be fulfilled. The retrofitting scheme is conditioned to the reparation of the captive columns.
 - c) In the case of windows, it is much preferable a new design of the opening that could be to place a masonry infill panel in a frame and leave the consecutive one completely open.
9. Irregularities in plan and/or vertical dimension are absolutely restricted. In the retrofitting scheme, new walls will be placed symmetrically to the ones installed or if they are not necessary, they will be demolished.

- Checkups.

1. Calculate the relationship between dimensions of the wall L_w and the width of the column d given by eq. 6.11. This requires:

$$\begin{aligned}
 (i) \quad d &\geq 3.8\sqrt{L_w} && \text{for squat walls} && (h_w/L_w \leq 1.35) \\
 (ii) \quad d &\geq 5\sqrt{L_w} && \text{for slender walls} && (h_w/L_w \geq 1.35)
 \end{aligned} \tag{6.12}$$

2. Compute the Priority Index (PI, *Hassan*) defined by eq. 6.13 and determine if it is higher than 0.4. *PI* is computed with the information of structural elements of the first floor and has three terms: RC_{walls} index + Column index + Masonry index:

$$PI = \frac{\sum A_{RCWalls} + 1/2 \sum A_{columns} + 1/10 A_{MIWalls}}{\sum A_{floor}} \tag{6.13}$$

where

$\sum A_{RCwalls}$ = sum of the cross-sectional areas of RC walls in the direction with smallest wall area at ground story.

$\sum A_{columns}$ = sum of the cross-sectional areas of columns at ground story.

$\sum A_{MIWalls}$ = sum of the cross-sectional areas of masonry infill walls.

$\sum A_{floor}$ = total floor area above ground level.

The PI index can also be expressed as the sum of three indexes, this is

$$PI = [RC_wI + CI + M_{IW}I] \tag{6.14}$$

where

$RC_wI = \frac{\sum A_{RCwalls}}{\sum A_{floor}}$ is the “reinforced concrete walls index”.

$CI = \frac{1}{2} \frac{\sum A_{col}}{\sum A_{floor}}$ is the “column index”.

$M_{IW}I = \frac{1}{10} \frac{\sum A_{MIW}}{\sum A_{floor}}$ is the “masonry infill wall index”.

As explained in Chapter 5, if the Hassan index is higher than 0.4, the building is not vulnerable. Otherwise, if $PI < 0.4$ the building needs to be seismically upgraded to reduce its vulnerability.

6.4 Determine the required ratio $\sum A_{MasonryWall}/\sum A_{floor}$ for different seismic scenarios

If after the visual inspection it is concluded that the building needs to be seismically upgraded, it is necessary to determine the retrofitting scheme. The conclusions from Chapter 5 together with the PI (*Hasan and Sozen*) are used to define the measures to take.

The level of retrofit is characterized by the value of the ratio of $\sum A_{MasonryWall}/\sum A_{floor}$. The required ratio $\sum A_{MasonryWall}/\sum A_{floor}$ for ensuring that the IP of the building is $IP \geq 0.4$ can be determined solving $A_{MIWalls}$ in Eq. 6.13. The larger $\sum A_{MasonryWall}/\sum A_{floor}$ is the smaller is the expected displacement under a given ground motion and the smaller the level of damage. The level of damage for a given spectral displacement is characterized by the fragility curves determined as explained in Chapter 5.

This ratio is the same for all different levels of the building. The position of the walls must be symmetrical with regard both axes in plan, and continuous in vertical (same column lines define a wall at different levels). If the building contains masonry infill walls previous to applying the retrofitting scheme, the damage state of the panels will be checked following the prescriptions given in section 6.1. Later, it is necessary to determine if the walls are maintained, demolished or demolished and rebuild.

6.5 Comparison with field data

Next, one of the buildings from the database used in this Thesis (*Chungwook Sim et al*) is studied in deep.

The sketch of the building is shown in Fig. 6.7 and more information can be found in the mentioned database for the building case ID A001.

The building corresponds to a school structure, 2 levels, with 8 spans in one of the axes directions (\sim North-South, D1) and 1 in the orthogonal direction (\sim East-West, D2). The structure is composed of RC frames with wide beams. The clear span in both directions measures 7,6 m.

Spans in D2 are filled with masonry panels made of blocks of concrete. The total area of concrete masonry panels is 9.49 m², this is a “masonry wall index” in *IP* eq. 6.14 of 0.05.

In D1 the spans contains openings, both windows and doors (Figure 6.8). There are no walls filling the complete frame. The “masonry wall index” in this direction is 0 and consequently the wall index for the building is 0 (direction with lowest area of masonry is D1).

The column index for the building is computed as $(\sum A_{columns}/\sum A_{floor} = 0.17$. Finally, the PI index (Eq. 6.14) computed as the sum of the column index and the masonry wall index values 0.17. Following O’Brien [*O’Brien et al 2011*] conclusions, this building is vulnerable (severe damage or collapse after earthquake).

The visual inspection reported several damage for structural elements and for masonry. The presence of captive columns in D1 leaded several damage on columns, with cases of spalling (Figure 6.8) shear cracks on the columns and buckling of the rebars (Fig 6.9). Also, the columns surrounding the walls in D2 are exposed to a lateral force that acts all along their axis in one face while the other faces are free. This force leads the appearance of a shear crack-plan along

the longitudinal axis of the column (Fig. 6.9). The confinement of the column by placing walls around it creating profiles in *T* or *L* is in some cases helpfully in order to avoid these types of cracks. The building cannot be retrofitted without repairing the damage on columns and joints.

Some characteristics aggravated the damage on these building as: the presence of captive columns and the presence of masonry walls in only one direction.

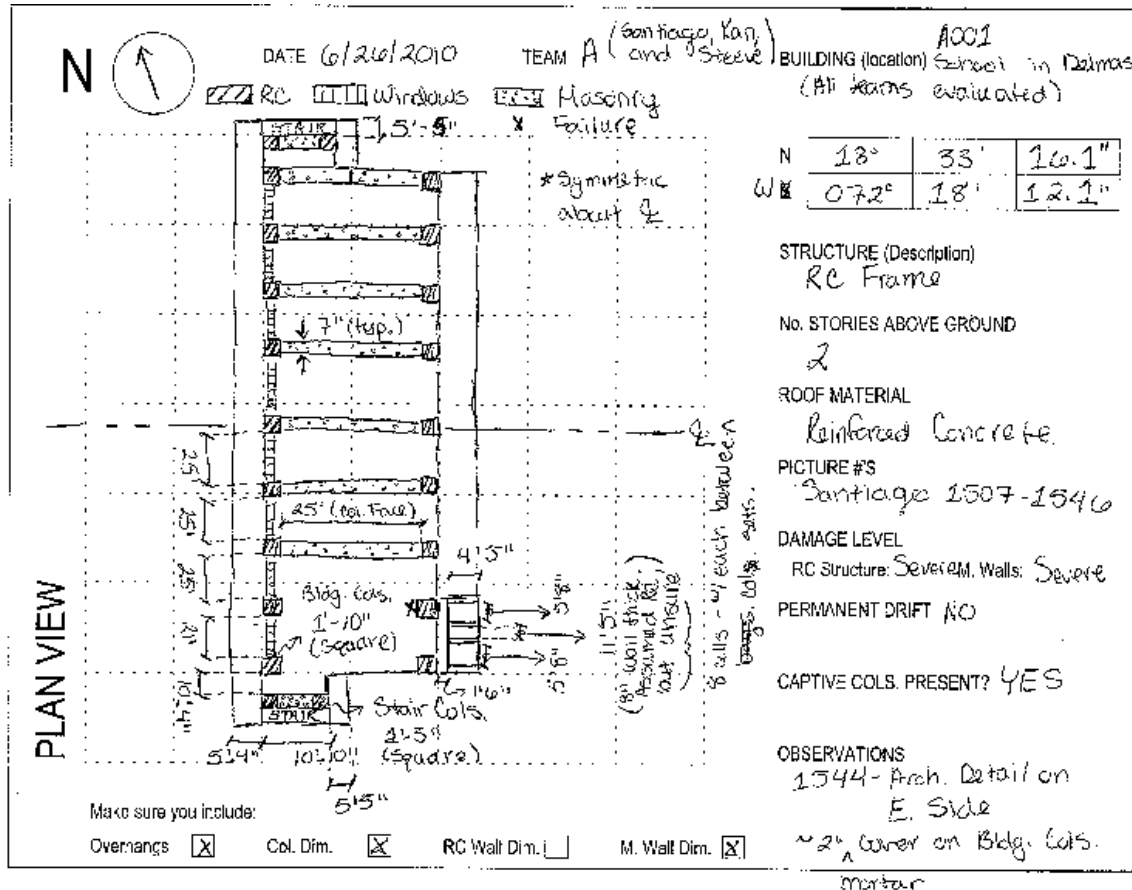


Figure 6.7: Sketch of the plant.

The retrofitting strategy for this building is presented hereafter:

1. First all the effort should be destined to repair the columns and joints following instructions in section 6.1.
2. Captive columns caused by the presence of openings have to be avoided. Partial walls placed on windows and doors need reparation. There are two options in order to avoid captive columns effects in a future earthquake:
 - a) Include a gap between the column and the wall.
 - b) Re-allocate the windows and doors in a new schema.
3. The concrete masonry walls should be demolished because (i) in the retrofitting scheme clay walls are used and (ii) the damage state of the walls is severe.

4. Computation of the minimal masonry wall needed to ensure that the building would not collapse or suffer severe damage in a new earthquake. The “masonry infill wall index”, M_{IWI} , is computed from the difference between the minimal threshold PI index that is fixed at 0.4 [O’Brien et al 2011] and the “column index”, CI , that in this case values 0.17:

$$\begin{aligned} M_{IWI} &= PI_{min} - CI \\ M_{IWI} &= 0.4 - 0.17 = 0.23 \end{aligned} \tag{6.15}$$

This yields an area of masonry wall of 4.13 m², and a lineal amount of masonry of 20.7 m. As each clear span measures 7.6m (in both orthogonal directions) only three walls are needed to ensure the safety in the building.

5. Check that columns do not fail under shear forces. In this case, the ratio $h_w/L_w = 3/7.6 = 0.4$, the walls are considered as squat walls and the minimal depth of the column is given by eq. 6.11(i):

$$\begin{aligned} (i) \quad d &\geq 3.8\sqrt{L_w} = 331mm \\ d &= 560mm > 331mm \end{aligned} \tag{6.16}$$

The column will not fail under shear forces and its depth is conservatively larger than the minimal needed.

6. Figure 6.10 presents some examples of retrofitting of this building. First the columns and beams diagram of the building are represented. The retrofitting scheme can be faced from different points of view in this case three different alternatives are exposed. Clay-brick masonry infill panels’ allocation is displayed in green. The first option is the simplest one: the walls are distributed evenly along both axes ensuring the minimal area. The second option incorporates profiles in T on the kernel of the building. Finally, the third configuration is probably the best option as it combines the double L profile with the separation of spaces and a homogeneous distribution of openings. This third distribution was proposed by Prof. Pujol (January 2010, New York Times, “Building Safer Schools in Poor, Shaky Places”) Figure 6.11 after the 2010 January earthquake on Haiti and it is applicable for the case of study.

The walls must fulfill the total clear span of the frame. Doors and windows can be allocated in the free spans. Also, non-structural elements can be used if needed to separate classrooms such as sliding doors or plaster panels whose link to the frame ensures free movement in case of earthquake.

7. Finally, figure 6.12 shows the fragility curve proposed in Chapter 5 for this retrofitted building.



Figure 6.8: Frames in D1. Windows in one span and openings in the other span (photo Chungwook Sim et al).



Figure 6.9: Buckling of rebars. Shear crack on the longitudinal axis of the column.

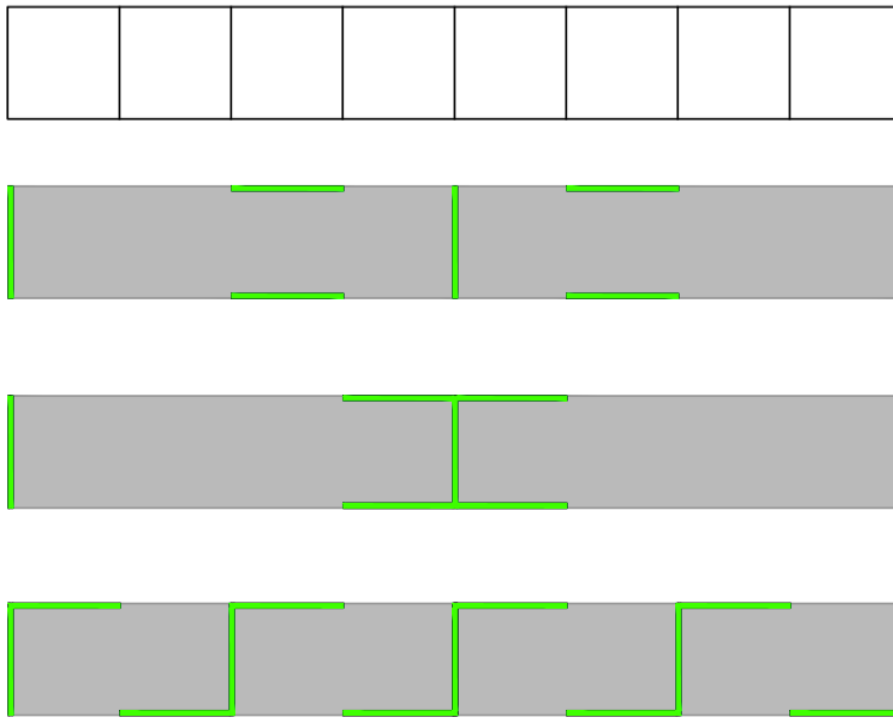


Figure 6.10: Glass masonry walls configuration

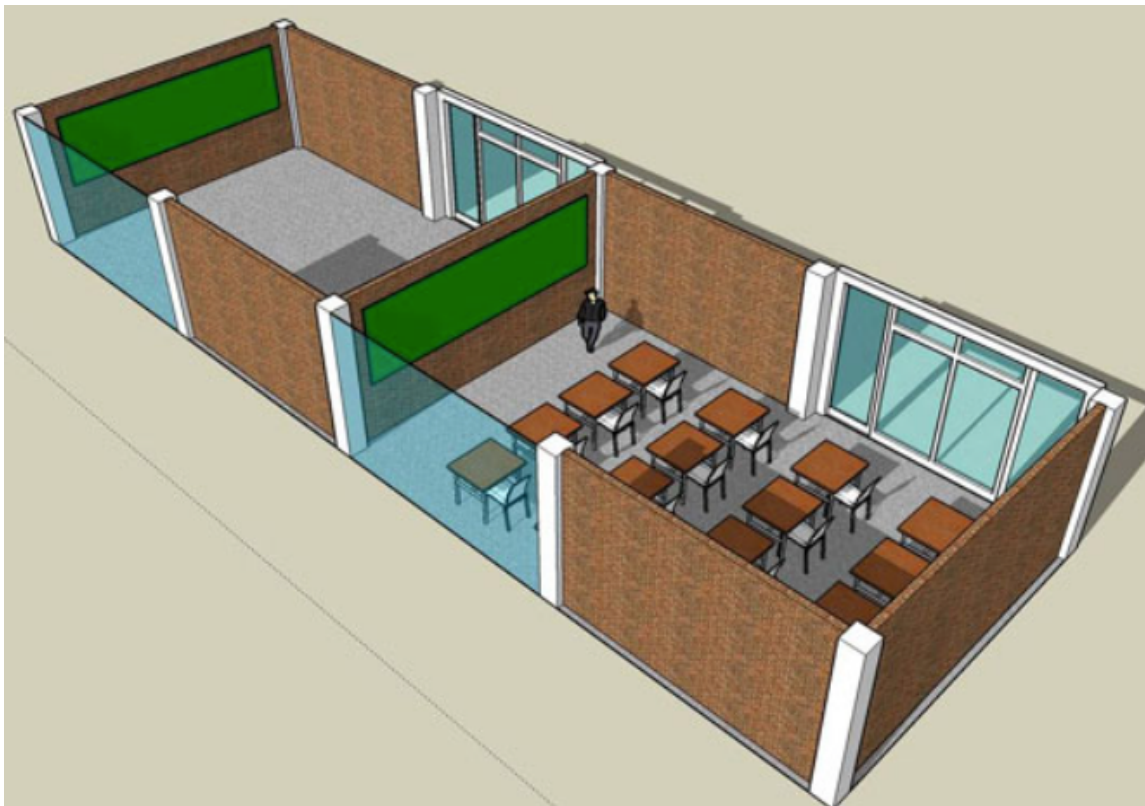
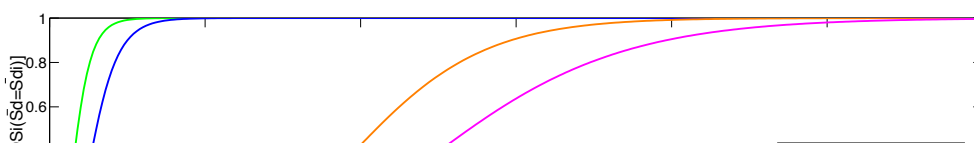


Figure 6.11: 3D representation of a retrofitting configuration (Prof. Pujol, The New York Times 2010).



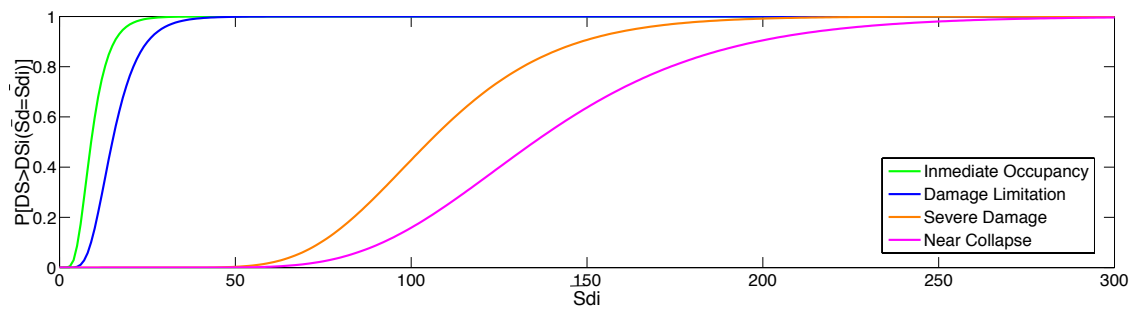


Figure 6.12: Fragility curve for the retrofitted building.

Conclusions

1. The influence of the masonry infill panels in buildings has first been studied in this Thesis by comparing the behavior of two buildings in Lorca. Originally, the buildings had masonry infill panels used as partition elements and assumed as non-structural elements in the design of the structure. The analysis consisted in (1) comparing the expected response according to the Spanish code with the observations in the post earthquake scenario in terms of earthquake hazard and ductility of buildings; and (2) comparing the seismic behavior and the vulnerability of each of the buildings with and without masonry infill panels. The main conclusion of the study can be summarized as follows. First, it was found that the ductility reduction factor adopted by the Spanish code is similar to the ductility exhibited by the structure through pushover analyses. Secondly, the energy input demand during the Lorca earthquake exceeded by about four times the energy input demand implicit in the Spanish seismic code NCSE-02. Thirdly, the infill walls played a significant and determinant role in the response of the structure; the larger amount of infill walls in the upper stories in comparison to the first floor caused a concentration of damage in the later and the subsequent collapse of the structure. Fourthly, it is of paramount importance to control the distribution of lateral strength between stories and to include in the calculation of the strength of each storey the contribution of the infill walls. If this strength distribution is controlled (avoiding the formation of soft stories) the presence of infill walls can improve the response of the overall structure and increase its resistance against earthquakes.
2. This Thesis has proposed and investigated a seismic retrofitting solution for developing countries that can be implemented in mass, and that is based on optimizing the use and distribution of clay masonry infill panels. Several reasons support the use of masonry infill walls for retrofitting existing structures in developing countries: (1) the clay bricks and mortar that are employed in the construction of masonry infill panels are used worldwide with homogeneous properties regardless of the economical or social level of the country; (2) the unreinforced panel can fill the complete frame, (3) the presence of masonry infill panels increases the strength and stiffness of the building. However, three principal problems have been identified in the literature in relation with the use of masonry infill walls: (1)

- the geometry of the panel is related to failure modes of the masonry wall that cause abrupt decay of the lateral strength, and consequently, weak and catastrophic failure of the building; (2) irregularities in plan and in vertical of the masonry panel distribution can trigger catastrophic failure modes in the building and very often collapse; and (3) the shear failure of the surrounding frame needs to be avoided.
3. In this Thesis, Haiti has been adopted as a real scenario for developing and producing the proposed solution, in the context of the damage caused by the recent 2010 earthquake. Different earthquake scenarios for Haiti have been defined after the study of recent geological and seismic reports. Since there are not any acceleration records of the earthquake which occurred in Haiti in 2010 an attempt was made to represent this seismic motion with an historical ground motion recorded in the past and having a similar magnitude (7). It was decided to use the NS component of the Campano-Lucano ground motion recorded at Calitri which encloses a large number of frequencies and corresponds to a moment-magnitude of 6.9. The properties of the soil and the amplification effects in combination with different return periods have been used to define a frequent earthquake scenario ($T_R = 200$ years, $PGA = 0.25g$ for the main shock and $T_R = 100$ years, $PGA = 0.18g$ for aftershocks), and a very rare earthquake scenario ($T_R = 1500$ years, $PGA = 0.57$ and $T_R = 5000$ years $PGA = 0.93$).
 4. An extensive experimental campaign consisting in static tests at the material level were conducted with the aim of obtaining the mechanical properties of the clay-bricks, mortar and masonry materials. The results of the tests were compared with the values proposed by FEMA 356 and served to make numerical predictions. It was concluded that the values proposed by FEMA are conservative (from 20-30% lower than the ones measured in the experimental tests) in terms of compressive strength and elastic modulus of the clay-bricks, mortar and masonry, while they are very accurate when measuring the bed-slide shear strength. Nevertheless, using the values proposed by FEMA is justified by the fact that the construction practices of the walls in situ are subjected to uncertainties that can lead to dispersions in the strength of elastic modulus larger than 20-30% of the nominal value.
 5. An additional campaign consisting in dynamic shake-table tests was conducted on a 2/5 specimen consisting in an RC frame (previously damaged) with infill walls. The results of the tests showed that the presence of masonry infill panels in a damaged reinforced concrete frame permits the structure to sustain new earthquake motions. The proposed earthquake scenarios allowed us to study the behavior of the retrofitted structure in case of a main-shock followed by an aftershock, whose $PGAs$ were 0.25g and 0.18g respectively and represented a frequent earthquake scenario. The structure did not exhibit any decrease in strength between both simulations. The maximum lateral drift in these simulations was 1%. The system remained elastic up to an interstory drift of 0.07% and reached the maximum lateral strength at a lateral drift of 0.5%. The second important conclusion from these tests is related to the behavior of the structure under very demanding ground motions that induced large lateral drifts. The two earthquake scenarios investigated corresponded to very rare earthquakes (PGA 0.56g and 0.93g). Under these extreme ground motions the system maintained a lateral strength of about 80% up to a lateral drift of 1.7% and the maximum lateral drift achieved a value of 5% without suffering any abrupt drop in strength or stiffness. For drift ratios between 1.7-5% the system described stable force-deformation relationship with some pinching effect and a gradual decay of stiffness. The final failure mode of the infill within the RC frame was a typical diagonal tension failure mode.

6. The aspect ratio of the masonry infill panel (height/length) was 0.7 and the properties of the panel relative to the surrounded frame can be categorized as “weak frame with strong infill”. The results of the tests also showed that this aspect ratio for the masonry wall in conjunction with a “weak frame with strong infill” lead to a diagonal tension failure mode. This is one of the four “failure modes” defined in the literature for masonry infill panels subjected to lateral loads. In fact, this failure mode is not considered a “real” failure mode as the structure itself does not collapse, but the large lateral drifts associated with this behavior can trigger significant non-structural damage.
7. Based on the results of the shake-table tests and the extensive study of the formulation proposed in the bibliography to determine the maximum lateral strength capacity of the infill, this Thesis proposes a new model to characterize the lateral capacity curve of the panel subjected to lateral monotonic loading. The maximum lateral drift attainable by the RC frame with infills is much larger than that proposed in previous studies.
8. The Thesis adopts the Bouc-Wen model for characterizing the dynamic behavior of the masonry infill panels and proposes values for the parameters that govern the behavior of this numerical model. The parameters that define the hysteretic behavior of the panel were calibrated to replicate numerically the experimental behavior observed during the shake-table tests by matching: (1) the maximum lateral strength (2) the maximum lateral drift and (3) the energy dissipated for the seismic simulation corresponding to the first maximum earthquake scenario.
9. The influence of the area of masonry infill wall per floor area, R , in the vulnerability of RC frame structures was studied in this Thesis applying the following two different approaches.
 - a) The application of a pushover-based methodology to compute the fragility curves of the buildings retrofitted with masonry infill panels. In this approach it is assumed that the fragility curves follow a lognormal standard distribution defined by the spectral displacement on the top of the building, $\bar{S}_{d_{DS_i}}$, and the natural logarithm of the spectral displacement β_{DS_i} . A parametric study was performed to determine the relationship between R and $\bar{S}_{d_{DS_i}}$, β_{DS_i} and this allowed us to propose fragility curves for buildings in terms of the geometry in plan of the building and the number of stories.
 - b) The experimental vulnerability index PI . In this approach an index proposed by Hassan and Sozen and tested in post earthquake scenarios was used. The values of this index are linked to different levels of damage in the structural elements of the building and to its overall stability. This vulnerability index was computed by dividing the area of each structural element on the ground floor multiplied by a weighting factor that depends on the structural typology over the total floor area. It was concluded that for the retrofitted buildings studied in this Thesis, the value of PI depends linearly on the value of R and the number of stories of the building. Two simple equations are proposed that relate R and PI and that are useful to determine the area of masonry infill walls to guarantee a maximum level of damage on the building or the masonry infill panels.
10. This Thesis proposes a guide for seismic retrofitting RC frames in developing countries by means of masonry infill walls. First, the guide describes the structural elements and the different levels of damage that they can present after an earthquake. Secondly, the guide determines when the level of damage on the structural element is acceptable for the retrofitting strategy or when they need reparation. Thirdly the guide proposes a reparation

scheme for the structural elements in case they need it. Fourthly the guide describes the retrofitting strategy for low-rise buildings in developing countries, which consists primarily in:

- a) Giving a simple formulation to obtain the amount of masonry needed in plan for a likely level of damage after an earthquake.
- b) Giving a simple formulation, based on geometric lengths, to check if the columns that surround the wall can fail under shear.
- c) Giving advice about the disposition of the masonry walls in plan and in elevation.

This Thesis ends with the application of the retrofitting strategy to a two-level school building in Haiti that suffered severe damage after the January 2010 earthquake.

- ACI Committee (2008) Building code requirements for structural concrete (ACI 318–08) and commentary. American Concrete Institute Edition, 318–08
- Akiyama H (1985) Earthquake resistant limit-state for buildings. University of Tokyo Press, Tokyo
- Aiken, I. D., Nims, D. K., and Kelly, J. M., 1992. Comparative study of four passive energy dissipation systems, *Bull. N. Z. Natl. Soc. Earthquake Eng.* 25 (3), 175–192.
- Asteris, P. G. (2003). “Lateral stiffness of brick masonry infilled plane frames.” *J. Struct. Eng.*, 129(8), 1071–1079.
- Asteris, P. G. (2005). “Closure to ‘Lateral stiffness of brick masonry infilled plane frames’ by P. G. Asteris.” *J. Struct. Eng.*, 131(3), 523–524.
- Asteris, P. G. (2008). “Finite element micro-modeling of infilled frames.” *Electron. J. Struct. Eng.*, 8, 1–11.
- Asteris PG, Antoniou ST, Sophianopoulos DS, Chrysostomou CZ. Mathematical macromodelling of infilled frames: State of the art. *J. Struct. Eng.*, 2011, 137(12): 1508-1517
- Asteris PG, Repapis CC, Cavaleri L, Sarhosis V, Athanasopoulou A. On the fundamental period of infilled RC frame buildings. *Structural Engineering and Mechanics*, Vol 54 N^o6 (2015) 1175-1200, DOI:<http://dx.doi.org/10.12989/sem.2015.54.6.1175>
- ATC-40. (1996). Seismic evaluation and retrofit of concrete buildings (No. SSC 96-01). Redwood City, CA: Applied Technology Council.
- Baber, T. T., and Noori, M. N. (1985). “Random vibration of degrading, pinching systems.” *J.*

- Engrg. Mech., ASCE, 111(8), 1010–1026.
- Balendra, T., and Huang, X. (2003). “Overstrength and ductility factors for steel frames designed according to BS 5950.” *J. Struct. Eng.*, 129(8), 1019–1035
- Benavent-Climent A, Pujades LG, Lopez-Almansa F (2002) Design energy input spectra for moderate- seismicity regions. *Earthquake Engineering and Structural Dynamics* 31:1151–1172
- Benavent-Climent A (2007) “Seismic Behavior of RC Wide Beam-Column Connections Under Dynamic Loading”. *Journal of Earthquake Engineering* 11(4):493-511.
DOI: 10.1080/13632460601064814
- Benavent-Climent A, Cahís X, Vico JM (2009a): “Interior wide beam-column connections in existing RC frames subjected to lateral earthquake loading,” Springer Science Business Media, B.V.
- Benavent-Climent A, Cahís X, Zahran R (2009b): “Exterior wide beam column connections in existing RC frames subjected to lateral earthquake loads,” *Engineering Structures*, 31 141-1424.
- Benavent-Climent, A., Morillas, L., and Vico, J. M. (2011). A study on using wide-flange section web under out-of-plane flexure for passive energy dissipation. *Earthquake Engineering & Structural Dynamics*, 40(5), 473–490. doi:10.1002/eqe.1031
- Benavent-Climent A, Escobedo A, Donaire-Avila J, Oliver-Saiz E, Ramírez-Márquez AL (2013). Assessment of expected damage on buildings subjected to Lorca earthquake through an energy-based seismic index method and nonlinear dynamic response analyses. *Bull Earthquake Engineering* 12(5) 2049-2073. doi:10.1007/s10518-013-9513-9
- Benavent-Climent, A., Morillas, L., and Escolano-Margarit, D. (2014). Seismic performance and damage evaluation of a reinforced concrete frame with hysteretic dampers through shake-table tests. *Earthquake Engineering & Structural Dynamics*, 43(15), 2399–2417.
doi:10.1002/eqe.2459
- Benavent-Climent, A., Oliver-Saiz, E., and Donaire-Avila, J. (2015). New connection between reinforced concrete building frames and concentric braces: Shaking table tests. *Engineering Structures*, 96, 7-21. doi:10.1016/j.engstruct.2015.03.023
- Bentz EC, Collins MP (2000) Response-2000. "Reinforced Concrete Sectional Analysis using the Modified Compression Field Theory." University of Toronto, Toronto
- Billman, R. 2010 Lessons from the Haitian Earthquake. *Nature* 463(7283):878-79.
<http://www.nature.com/nature/journal/v463/n7283/full/463878a.html>.
- Borzi B, Pinho R, Crowley H (2008) "Simplified pushover-based vulnerability analysis for large-scale assessment of RC buildings." *Engineering of Structures* 30:804–820
- Bouc, R. (1967). “Forced vibration of mechanical systems with hysteresis.” *Proc.*, 4th Conf.

on Non-linear Oscillations.

- Bracci, J.M., Kunnath, S.K. and Reihorn, A.M., 1997. "Seismic performance and retrofit evaluation of reinforced concrete structures," *ASCE Journal of Structural Engineering*, Vol. 123(1), pp. 3-10.
- Buonopane, S. G., and White, R. N. (1999). "Pseudodynamic Testing of Masonry Infilled Reinforced Concrete Frame." *J. Struct. Eng.*, 125(6), 578–589.
- Bush, T.D. Jr., Talton, C.R. and Jirsa, J.O., 1990. "Behavior of a structure strengthened using reinforced concrete piers," *ACI Structural Journal*, Vol. 87(5), pp. 557-563.
- Calvi GM (1999) "A displacement-based approach for vulnerability evaluation of classes of buildings". *Journal of Earthquake Engineering* 3(3):411–438.
- Calvi GM, Pinho R, Magenes G, Bommer JJ, Restrepo-Velez LF, Crowley H (2006) "Development of seismic vulnerability assessment methodologies over the past 30 years." *ISET Journal of Earthquake Technology* 43(3):75–104.
- Casciati, F. (1989). "Stochastic dynamics of hysteretic media." *Struct. Safety*, Amsterdam, 6, 259–269.
- Celarec D, Ricci P, Dolšek M. The sensitivity of seismic response parameters to the uncertain modelling variables of masonry-infilled reinforced concrete frames. *Engineering Structures* 2012;35:165–177.
- Chaker A, Cherifati A. "Influence of masonry infill panels on the vibration and stiffness characteristics of R/C frame buildings". *Earthquake Engineering and Structural Dynamics* 28, 1061-1065 (1999)
- Chrysostomou CZ, Asteris PG (2012) On the in-plane properties and capacities of infilled frames. *Engineering Structures* 41 (2012) 385-402
- Chopra, A. K. (2001). "Dynamics of Structures: Theory and Applications to Earthquake Engineering." Prentice Hall, Upper Saddle River, NJ.
- Choudhuri, D., Mander, J.B. and Reihorn, A.M., 1992. "Evaluation of seismic retrofit of reinforced concrete frame structures: Part 1 – experimental performance of retrofitted sub-assemblages," National Center for Earthquake Engineering Research, Report No. NCEER-92- 0030, State University of New York at Buffalo, 136p.
- Chungwook Sim; Cheng Song; Nick Skok; Ayhan Irfanoglu; Santiago Pujol; Mete Sozen (2015), "Database of low-rise reinforced concrete buildings with earthquake damage", <https://datacenterhub.org/resources/123>. Filter Haiti
- CIA (Central Intelligence Agency). 2011. World Factbook. <https://www.cia.gov/library/publications/the-world-factbook/geos/ha.html>.

- Comité Euro-International du Béton (CEB). (1996). "RC frames under earthquake loading." State of the Art Rep., CEB, Paris.
- Constaninou MC and Adnane MA (1987) Dynamics of soil base isolated structure systems: evaluation of two models for yielding systems. Report to NSAF. Department of Civil Engineering, Drexel University, Philadelphia, PA
- Cosenza E, Manfredi G, Polese M, Verderame GM (2005) A multi-level approach to the capacity assessment of existing RC buildings. *Journal of Earthquake Engineering* 9(1):1–22
- Crisafulli FJ. Seismic behaviour of reinforced concrete structures with masonry infills, PhD dissertation, University of Canterbury, 1997.
- CTE. Código Técnico de la Edificación. Documento Básico. Seguridad Estructural. SE1 y SE2. Ministerio de Fomento. Gobierno de España.
- Daniell, J. 2011. Damaging Earthquakes Database 2010 – The Year in Review. <http://earthquake-report.com/damaging-earthquakes-2010/>.
- Decanini, L. D., and Fantin, G. E. (1987). "Modelos simplificados de la mampostería incluida en porticos. Características de rigidez y resistencia lateral en estado límite." *Jornadas Argentinas de Ingeniería Estructural III*, Vol. 2, Asociacion de Ingenieros Estructurales, Buenos Aires, Argentina, 817–836 (in Spanish).
- Decanini LD, Mollaoli F, Oliveto G (1995) Observations and lessons learned from the earthquake of the 12th December 1990 in south-east Sicily. In: *Proceedings of the 10th European Conference on Earthquake Engineering and Structural Dynamics*, Vienna
- Decanini, L.D., Mollaioli F. (1998) "Formulation of elastic earthquake input energy spectra". *Earthquake Engineering and Structural Dynamics* 27(12):1503–1522
- DesRoches R, Comerio M, Eberhard M, Mooney W, Rixx GJ. " Overview of the 2010 Haiti earthquake". *Earthquake Spectra* 27, No. S1, pages S1-S21, October 2011, Earthquake Engineering Research Institute.
- Dhanasekar, M., and Page, A. W. (1986). "Influence of brick masonry infill properties on the behaviour of infilled frames." *ICE Proc.*, 81(4), 593–605.
- Dolšek M, Fajfar P. The effect of masonry infills on the seismic response of a four-storey reinforced concrete frame—a deterministic assessment. *Eng Struct* 2008;30(7):1991–2001.
- Dönmez, C., and Pujol, S., 2005. Spatial distribution of damage caused by the 1999 Earthquakes in Turkey, *Earthquake Spectra* 21 , 53–69.
- El-Dakhkhni, W. W. (2002). "Experimental and analytical seismic evaluation of concrete masonry-infilled steel frames retrofitted using GFRP laminates." Ph.D. thesis, Drexel Univ., Philadelphia

-
- El-Dakhakhni, W. W., Elgaaly, M., and Hamid, A. A. (2003). "Three-strut model for concrete masonry-infilled frames." *J. Struct. Eng.*, 129(2), 177–185.
- El-Dakhakhni, W. W., Hamid, A. A., Hakam, Z. H. R., and Elgaaly, M. (2006). "Hazard mitigation and strengthening of unreinforced masonry walls using composites." *Compos. Struct.*, 73(4), 458–477.
- EN 1998-1 (2004) (English): Eurocode 8: Design of structures for earthquake resistance – Part 1: General rules, seismic actions and rules for buildings
- Fajfar P, Gaspersic P (1996) "The N2 method for the seismic damage analysis of RC buildings." *Earthquake Engineering and Structural Dynamics* 25:31–46
- Fardis, M. N., and Calvi, O. M. (1994). "Effects of infills on the global response of reinforced concrete frames." *Proc., 10th European Conf. on Earthquake Engineering, European Association for Earthquake Engineering (EAEE), Istanbul, Turkey, 2331–2336.*
- Fardis, M. N., and Panagiotakos, T. B. (1997). "Seismic design and response of bare and masonry-infilled reinforced concrete buildings. Part II: Infilled structures." *J. Earthquake Eng.*, 1(3), 475–503.
- Fardis MN. Seismic design issues for masonry-infilled RC frames. In: *Proceedings of the 1st European Conference on Earthquake Engineering and Seismology, Geneva, 2006.*
- Fardis, M. N. (2009). *Seismic design, assessment and retrofitting of concrete buildings: based on EN-Eurocode 8 (Vol. 8).* In A. Ansal (Series Ed.), *Geotechnical, Geological and Earthquake Engineering.* Dordrecht: Springer Netherlands. doi:10.1007/978-1-4020-9842-0
- FEMA (1997) "NEHRP Guidelines for the seismic rehabilitation of buildings (FEMA Publication 273). FEMA-273, Washington, DC
- FEMA. (1997). "NEHRP commentary on the guidelines for the seismic rehabilitation of buildings." FEMA-274, Washington, DC.
- FEMA. (1998). "Evaluation of earthquake damaged concrete and masonry wall buildings: Basic procedures manual." FEMA-306, Washington, DC.
- FEMA (2000) "Prestandard and commentary for the seismic rehabilitation of buildings". FEMA 356, Washington DC
- Fiorato E., Sozen M.A., Gamble W.L. An investigation of the interaction of reinforced concrete frames with masonry filler infills. *Civ. Eng. Stud. Struct. Res. Ser.; No. 370.* Univ. of Illinois. Urbana, Illinois, 1970.
- Flanagan RD, Bennett RM. In-plane behavior of structural clay tile infilled frames. *J Struct Eng* 1999; Volume 12, Issue 6, pp 590-9
- Frankel A, Harmsen S, Mueller C, Calais E, Haase J (2011). *Seismic hazard maps for Haiti.*

- Earthquake Spectra, Volumen 27, No S1, pages S23-S41. October 2011, Earthquake Engineering Research Institute
- Gesualdo, A., Monaco, M. (2015). Constitutive behaviour of quasi-brittle materials with anisotropic friction. *Latin American Journal of Solids and Structures* 12: 695-710.
- Ghosh, A. K., and Amde, A. M. (2002). "Finite element analysis of infilled frames." *J. Struct. Eng.*, 128(7), 881–889.
- Government of the Republic of Haiti (GOH), 2010. Action Plan for National Recovery and Development of Haiti, Port-au-Prince.
- Griffiths JHP, Irfanoglu A, Pujol S. Istanbul at the threshold: An Evaluation of the Seismic Risk in Istanbul. *Earthquake Spectra*, Volume 23, No. 1, pages 63–75,
- Grigorian, C. E., Tsong-Shuoh, Y., and Popov, E. P., 1992. Slotted bolted connection energy dissipators, Report UCB/EERC-92/10, University of California, Berkeley.
- Gur, T., Pay, A. C., Ramirez, J. A., Sözen, M. A., Johnson, A. M., Irfanoglu A., and Bobet, A., 2009. Performance of school buildings in Turkey during the 1999 Düzce and 2003 Bingol earthquakes, *Earthquake Spectra* 25 , 239–256.
- Hassan, A. F., and Sozen, M. A., 1997. Seismic vulnerability assessment of low-rise buildings in regions with infrequent earthquakes, *ACI Structural Journal* 94 , 31–39.
- Holmes, M. (1961). "Steel frames with brickwork and concrete infilling." *ICE Proc.*, 19(4), 473–478.
- Hou L, Shi P (2010) Haiti earthquake-How to explain such huge losses? *Int. J. Disaster Risk Sci.* 2011, 2 (1): 25–33 doi:10.1007/s13753-011-0003-x
- Kappos AJ, "Seismic design and performance assessment of masonry infilled RC frames". Proc., 12th World Conference on Earthquake Engineering, International Association of Earthquake Engineering (IAEE), Tokyo
- Kent DC, Park R (1971) "Flexural members with confined concrete" *Journal of the Structural Division, ASCE* Vol 97, NoST7, pp. 1969-1990
- Klingner, R. E., and Bertero, V. V. (1978). "Earthquake resistance of infilled frames." *J. Struct. Div.*, 104(ST6), 973–989.
- Kodur, V. K. R., Erki, M. A., and Quenneville, J. H. P. (1995). "Seismic design and analysis of masonry-infilled frames." *Can. J. Civ. Eng.*, 22(3), 576–587
- Kodur, V. K. R., Erki, M. A., and Quenneville, J. H. P. (1998). "Seismic analysis of infilled frames." *J. Struct. Eng.*, 25(2), 95–102.
- Kunnath SK, Reinhorn A M and Abel JF (1992a) "A computational tool for seismic performance

- of reinforced concrete buildings". *Computers and Structures*, PERgamon Press, Vol 41, No. 1, 157-173
- López-Comino JA, Mancilla FL, Morales J, Stich D. "Rupture directivity of the 2011, Mw 5.2 Lorca earthquake (Spain). *Geophysical Research Letters*, vol. 39, L03301, doi:10.1029/2011GL050498, 2012
- Liauw, T. C., and Kwan, K. H. (1984). "Nonlinear behaviour of non- integral infilled frames." *Computers and Structures*, 18, 551–560.
- Liu, Y., Dawe, J.L. (2003). Analytical modeling of masonry load-bearing walls, *Canadian Journal of Civil Engineering* 30: 795 – 806.
- Mainstone, R. J. (1971). "On the stiffnesses and strengths of infilled frames." *Proc., ICE Suppl.*, Vol. 4, Building Research Station, Garston, UK, 57–90.
- Mainstone, R. J. (1974). Supplementary note on the stiffness and strengths of infilled frames, Building Research Station, Garston, UK.
- Mainstone RJ (1974b). Supplementary note on the stiffnesses and strengths of infilled frames. Building Research Establishment, Building Research Station, 1974.
- Mainstone, R. J., and Weeks, G. A. (1970). "The influence of bounding frame on the racking stiffness and strength of brick walls." *Proc., 2nd Int. Brick Masonry Conf.*, Building Research Establishment, Watford, England, 165–171.
- Ma F., Zhang H., Bockstedte A, FOLiente GC and Paevere P (2004). Parameter analysis of the differential model of hysteresis. *Journals of applied mechanics ASME*, 71, pp 342-349
- Martínez-Rueda JE (2002) On the Evolution of Energy Dissipation Devices for Seismic Design. *Earthquake Spectra*: May 2002, Vol. 18, No. 2, pp. 309-346.
- Mehrabi, A. B., Shing, P. B., Schuller, M., and Noland, J. (1996). "Experimental evaluation of masonry-infilled RC frames." *J. Struct. Eng.*, 122(3), 228–237.
- Mehrabi, A. B., and Shing, P. B. (1997). "Finite element modeling of masonry-infilled RC frames." *J. Struct. Eng.*, 123(5), 604–613.
- Mettupalayam V Sivaselvan; Andrei M Reinhorn. (2000) "Hysteretic models for deteriorating inelastic structures". *Journal of Engineering Mechanics*. Vol 126, N^o6, June 2000; Paper n^o 21348
- Milutinovic ZV, Trendafiloski GS (2003) WP04 Vulnerability of current buildings RISK-UE project of the EC: an advanced approach to earthquake risk scenarios with applications to different European towns
- Ministerio de Obras Publicas y Transportes (1991) Instruccion para el proyecto y la ejecucion de obras de hormigon en masa o armado (EH-91). Cent de Publicaciones Minist Obras Publicas

- y Transp, Madrid
- Ministerio de Obras, Publicas, T y M A (1995) "Norma de Construccion Sismorresistente, Parte General y de Edificacion (NCSE-94)." Servicio de Publico del Ministerio de Obras Publicas, T y M A, Madrid
- Moghaddam, H. A. (2004). "Lateral load behavior of masonry infilled steel frames with repair and retrofit." *J. Struct. Eng.*, 130(1), 56–63.
- Nazir S. Studies on the failure of unreinforced masonry shear walls. PhD School of Civil Engineering and Build Environment. Science and Engineering Faculty. Queensland University of Technology, Australia 2015.
- NCSE-02. (2002). Norma de Construcción Sismorresistente: parte general y edificación (RD 997/2002 de 27 de Septiembre). Madrid: Ministerio de Fomento.
- Negro, P., and Colombo, A. (1997). "Irregularities induced by non- structural masonry panels in framed buildings." *Eng. Struct.*, 19(7), 576–585.
- Noy, I. 2009. The Macroeconomic Consequences of Disasters. *Journal of Development Economics* 88 (2): 221–31.
- Obrien P, Eberhard M, Haraldsson O, Irfanoglu A, Lattanzi D, Lauer S, Pujol S. Measures of the seismic vulnerability of reinforced concrete buildings in Haiti. *Earthquake Spectra* Volume 27, No. S1, pages S373-S386. October 2011.
- Ozcebe, G., Yucemen, M. S., and Aydogan, V., 2004. Statistical seismic vulnerability assessment of existing reinforced concrete buildings in Turkey on a regional scale, *Journal of Earthquake Engineering* 8 , 749–773.
- Page, A.W. (1978). Finite element model for masonry. *Journal of the Structural Division – ASCE* 104: 1267-1285.
- Page, A.W. (1981). The biaxial compressive strength of brick masonry. *Proceedings of the Institution of Civil Engineers* 71: 893-906.
- Page, A.W. (1983). The strength of brick masonry under biaxial compression –tension. *International journal of masonry construction* 3: 26-31.
- Page, A. W., Kleeman, P. W., and Dhanasekar, M. (1985). "An in-plane finite element model for brick masonry." *Proc., Structures Congress, ASCE, Reston, VA*, 1–18.
- Pall A, Masrh C. Response of friction damped braced frames. *Journal of the Structural Division* 108(6) June 1982
- Park, Y., and Ang, A. (1985). Mechanistic seismic damage model for reinforced concrete. *Journal of Structural Engineering*, 111(4), 722–739. doi:10.1061/(ASCE)0733-9445(1985)111:4(722)
- Paulay T, Priestley MJN. Seismic design of reinforced concrete and masonry buildings. New

York: John Wiley & Sons; 1992

PEER 2007/100. Seismic evaluation of reinforced concrete buildings including effects of masonry infill walls. Alidad Hashemi and Khalid M. Mosalam. July 2007.

Polyakov, S. V. (1960). "On the interaction between masonry filler walls and enclosing frame when loading in the plane of the wall." Translation in earthquake engineering, Earthquake Engineering Research Institute (EERI), San Francisco, 36–42.

Pravin S, Waghmare B. Materials and jacketing technique for retrofitting of structures. International Journal of Advanced Engineering Research and Studies. Vol1. Issue I. October-December 2011, 15-19

Priestly MJN, Verma R, Xiao Y. "Seismic shear strength of reinforced concrete columns". Journal of Structural Engineering. Vol 120 Issue 8, pp 2310-2329

Pujades LG, Vargas-Alzate YF, Barbat AH, Gonzalez-Drigo JR (2015) Parametric model for capacity curves. Bulletin of Earthquake Engineering (2015) 13:1347-1376

Pujol S, Benavent A, Rodriguez ME, Smith-Pardo JP. Masonry infill walls: An effective alternative for seismic strengthening of low-rise reinforced concrete building structures. The 14th World Conference on Earthquake Engineering. October 12-17, 2008, Beijing, China

Reinhorn, A. M., Madan, A., Valles, R. E., Reichmann, Y., and Mander, J. B. (1995). "Modeling of masonry infill panels for structural analysis." Tech. Rep. NCEER-95-0018, State University of New York at Buffalo, Buffalo, N.Y.

Reinhorn A M, and Valles R E (1995) "Damage Evaluation in Inelastic Response of Structures: A Deterministic Approach", Report n^o NCEER-95-xxxx, National Center of Earthquake Engineering Research, State University of New York at Buffalo

Reinhorn A, Roh H, Sivaselvan M, Kunnath S, Valles RE, Madan A, Li C, Lobo R, Park YJ. (2009) IDARC 2D Version 7.0: A Program for the Inelastic Damage Analysis of Structures. MCEER-09-0006, Affiliation: University at Buffalo – the State University of New York. DOI: 10.13140/RG.2.1.2518.8724

Riddell, R., Wood, S. L., de la Llera, J. C., 1987. The 1985 Chile Earthquake: Structural Characteristics and Damage Statistics for the Building Inventory in Viña del Mar , Structural Research Series No. 534, University of Illinois, Urbana-Champaign, 265 pp

Rodriguez, M. and Park, R., 1994. "Seismic load tests of reinforced concrete columns strengthened by jacketing," ACI Structural Journal, Vol. 91(2), pp. 150-159.

Saneinejad, A., and Hobbs, B. (1995). "Inelastic design of infilled frames." J. Struct. Eng., 121(4), 634–650.

Santhi, M. H., Knight, G. M. S., and Muthumani, K. (2005a). "Evaluation of seismic performance of gravity load designed reinforced concrete frames." J. Perform. Constr. Facil., 19(4),

277–282.

Santhi, M. H., Knight, G. M. S., and Muthumani, K. (2005b). “Evaluation of seismic response of soft-storey infilled frames.” *Comput. Concr.*, 2(6), 423–437.

Sayed-Ahmed, E.Y., Shrive, N.G. (1996). Nonlinear finite-element model of hollow masonry. *Journal of Structural Engineering* 122: 683 - 690

Scales WGM (1998) European macroseismic scale. GeoForschungsZentrum, Postdam

Sezen H, Moehle P (2006) "Seismic tests of concrete columns with light transverse reinforcement." *Am Concr Inst* 103(6):842–849

Shiga, T., Shibata, A., and Takahashi, T., 1968. Earthquake damage and wall index of reinforced concrete buildings, in *Proceedings, 1968 Tobuku District Symposium (in Japanese)*, Architectural Institute of Japan, Tokyo, Japan, 29–32.

Smith, B. S. (1966). “Behavior of square infilled frames.” *J. Struct.*, 92(1), 381–403.

Smith, B. S. (1967). “Methods for predicting the lateral stiffness and strength of multi-storey infilled frames.” *Build. Sci.*, 2(3), 247–257.

Smith, B. S., and Carter, C. (1969). “A method of analysis for infilled frames.” *ICE Proc.*, 44(1), 31–48.

Song J; Kiureghian AD. (2006) Generalized Bouc-Wen model for highly asymmetric hysteresis. University of California Postprints. Year 2006. Paper 2030

Sobaih, M., and Abdin, M. M. (1988). “Seismic analysis of infilled reinforced concrete frames.” *Comput. Struct.*, 30(3), 457–464.

Stafford Smith B, Carter C (1969). A method of analysis for infilled frames. *Proc Inst Civil Eng (Lond)*, Volume 44, Issue 1, pp 31-48.

Sucuoglu H, Nurtug A (1995) "Earthquake ground motions characteristics and seismic energy dissipation." *Earthquake Engineering and Structural Dynamics* 24(9):1195–1213

UNE-EN 772-1:2011. Methods of test for masonry units - Part 1: Determination of compressive strength

UNE-EN 998-1:2010. Specification for mortar for masonry - Part 1: Rendering and plastering mortar

UNE-EN 998-2:2004. Specification for mortar for masonry - Part 2: Masonry mortar

UNE-EN 1015-11:2000/A1:2007. Methods of test for mortar for masonry - Part 11: Determination of flexural and compressive strength of hardened mortar

-
- UNE-EN 1052-3:2003/A1:2008. Methods of test for masonry - Part 3: Determination of initial shear strength
- Vamvatsikos D, Cornell A (2002) Incremental dynamic analysis. *Eathq Eng Struct Dyn* 31:491–514
- Wen, Y. K. (1976). "Method for random vibration of hysteretic systems". *Journal of Engineering Mechanics*. American Society of Civil Engineers.102 (2): 249–263.
- Wood RH (1978). Plasticity, composite action and collapse design of unreinforced shear wall panels in frames. *Proc Inst Civil Eng (Lond)*; Volume 65, Issue 2, pp 381-411.
- Zarnic R, Gosti S, Crewe AJ, Taylor CA. (2001) Shaking Table Tests of 1:4 Reduced-Scale Models of Masonry Infilled Reinforced Concrete Frame Buildings. *Earthquake Engineering and Structural Dynamics*; 30(6):819–834.
- Zhuge, Y, Thambiratnam, D, Corderoy, J. (1998). Nonlinear dynamic analysis of unreinforced masonry. *Journal of Structural Engineering* 124: 270-277.
- Zia, P., White, R. N., and Vanhorn, D. A. (1970). Principles of model analysis. In R. N. White (Ed.), *Models of concrete structures* (pp. 19–40), ACI Special Publication, SP-24-02, American Concrete Institute. doi:10.14359/17583
- Zucchini, A., Lourenço, P.B. (2002). A micro-mechanical model for the homogenisation of masonry. *International Journal of Solids and Structures* 39: 3233- 3255.

Appendices

Appendix A

DEFINITION OF PROTOTYPES

Appendix B

PUSHOVER CURVES OF PROPTOTYPES

Appendix A

Definition of Prototypes

A.1 2-STORY 4x2 PARALLEL TO JOISTS.....	126
A.2 2-STORY 4x2 PERPENDICULAR TO JOISTS.....	128
A.3 3-STORY 4x2 PARALLEL TO JOISTS.....	130
A.4 3-STORY 4x2 PERPENDICULAR TO JOISTS.....	132
A.5 2-STORY 4x4 PARALLEL TO JOISTS.....	134
A.6 2-STORY 4x4 PERPENDICULAR TO JOISTS.....	136
A.7 3-STORY 4x4 PARALLEL TO JOISTS.....	138
A.8 3-STORY 4x4 PERPENDICULAR TO JOISTS.....	141

Three tables are defined for each prototype:

- Table 1: Loads definition
- Table 2: Beams reinforcement details
- Table 3 Columns axial loads and reinforcement details

A1 2 STORY 4x2 PARALLEL TO JOISTS

Table 1: Loads definition

Analysis: Parallel to joists		Level:	Ground Floor-Intermediate Floor	Top Floor
Uniformly loaded beams [kN/m]	Parallel to joists	outer	3,68	3,68
		interior	3,68	3,68
	Perpendicular to joists	outer	10,35	10
		interior	28,9	25,9
Nodal weights [kN]	Frame 1	corner	35,075	34,2
		central 1	90,65	83,15
	Frame 2	corner	60,95	59,2
		central 1	162,9	147,9
Axial loads [kN]	Frame 1	corner	69,275	34,2
		central 1	173,8	83,15
	Frame 2	corner	120,15	59,2
		central 1	310,8	147,9

Table 2: Beams reinforcement details

BEAMS DEFINITION. REINFORCEMENT AREA IN THE SECTION mm2																	
height	305cm	Type	Frame 1			Type	Frame 2			Type	Frame 3						
			left bottom	left top	right bottom		right top	left bottom	left top		right bottom	right top	left bottom	left top	right bottom	right top	
beam 1	1	1	678,58	678,58	678,58	678,58	678,58	678,58	678,58	1	678,58	678,58	678,58	678,58	678,58	678,58	678,58
beam 2	1	1	678,58	678,58	678,58	678,58	678,58	678,58	678,58	1	678,58	678,58	678,58	678,58	678,58	678,58	678,58
height	610cm	Type	Frame 1			Type	Frame 2			Type	Frame 3						
beam 1	2	1	791,68	791,68	791,68		791,68	791,68	791,68		791,68	1	678,58	678,58	678,58	678,58	678,58
beam 2	2	1	791,68	791,68	791,68	791,68	791,68	791,68	791,68	1	678,58	678,58	678,58	678,58	678,58	678,58	678,58

Table 3: Columns axial loads and reinforcement details

COLUMNS DEFINITION. REINFORCEMENT AREA IN ONE FACE OF THE SECTION mm2													
height	0cm	Type	Frame 1			Type	Frame 2			Type	Frame 3		
			Axial load	area in one face	area in one face		Axial load	area in one face	area in one face		Axial load	area in one face	area in one face
col 1	1	3	69,275	226,19	226,19	3	120,15	226,19	226,19	3	120,15	226,19	226,19
col 2	2	4	173,8	226,19	226,19	4	310,8	226,19	226,19	4	310,8	226,19	226,19
col 3	1	3	69,275	226,19	226,19	3	120,15	226,19	226,19	3	120,15	226,19	226,19
height	305cm	Type	Frame 1			Type	Frame 2			Type	Frame 3		
col 1	5	7	34,2	226,19	226,19		7	59,2	226,19		226,19	7	59,2
col 2	6	8	83,15	226,19	226,19	8	147,9	226,19	226,19	8	147,9	226,195	226,195
col 3	5	7	34,2	226,19	226,19	7	59,2	226,19	226,19	7	59,2	226,195	226,195

A2 2 STORY 4x2 PERPENDICULAR TO JOISTS

Table 1: Loads definition

Analysis: Perpendicular to joists		Level:	Ground Floor-Intermediate Floor	Top Floor
Uniformly loaded beams [kN/m]	Parallel to joists	outer	3,68	3,68
	Perpendicular to joists	interior	3,68	3,68
Nodal weights [kN]		outer	10,35	10
	interior	28,9	25,9	
Axial loads [kN]	Frame 1	corner	35,075	34,2
		central 1	60,95	59,2
	Frame 2	corner	90,65	83,15
		central 1	162,9	147,9
Axial loads [kN]	Frame 1	corner	69,275	34,2
		central 1	120,15	59,2
	Frame 2	corner	173,8	83,15
		central 1	310,8	147,9

Table 2: Beams reinforcement details

BEAMS DEFINITION. REINFORCEMENT AREA IN THE SECTION mm ²																						
height 305cm	Type	frame 1				Type	frame 2				Type	frame 3 = frame 1										
beam 1	1	left botto	left top	right bott	right top	2	left bott	left top	right bott	right top	3	left bott	left top	right bott	right top	1	left bott	left top	right bott	right top		
beam 2		678,58	678,58	678,58	678,58		791,68	678,58	791,68	1130,97		1130,97	791,68	678,58	791,68		1130,97	1130,97	678,58	678,58	678,58	678,58
beam 3		678,58	678,58	678,58	678,58		791,68	1130,97	791,68	1017,88		1017,88	791,68	678,58	791,68		1130,97	1130,97	678,58	678,58	678,58	678,58
beam 4		678,58	678,58	678,58	678,58		791,68	1130,97	791,68	1017,88		1017,88	791,68	678,58	791,68		1130,97	1130,97	678,58	678,58	678,58	678,58
height 610cm	Type	frame 1				Type	frame 2				Type	frame 3 = frame 1										
beam 1	1	left botto	left top	right bott	right top	2	left bott	left top	right bott	right top	3	left bott	left top	right bott	right top	1	left bott	left top	right bott	right top		
beam 2		678,58	678,58	678,58	678,58		791,68	678,58	791,68	1130,97		1130,97	791,68	678,58	791,68		1130,97	1130,97	678,58	678,58	678,58	678,58
beam 3		678,58	678,58	678,58	678,58		791,68	1130,97	791,68	1017,88		1017,88	791,68	678,58	791,68		1130,97	1130,97	678,58	678,58	678,58	678,58
beam 4		678,58	678,58	678,58	678,58		791,68	1130,97	791,68	1017,88		1017,88	791,68	678,58	791,68		1130,97	1130,97	678,58	678,58	678,58	678,58

Table 3: Columns axial loads and reinforcement details

COLUMNS DEFINITION. REINFORCEMENT AREA IN ONE FACE OF THE SECTION mm2						
height 0cm	Type	frame 1 Axial load area in one face	Type	frame 2 Axial load area in one face	Type	frame3 = frame 1 Axial load area in one face
col 1	1	69,275	3	173,8	1	69,275
col 2	2	120,15	4	310,8	2	120,15
col 3	2	120,15	5	310,8	2	120,15
col 4	2	120,15	4	310,8	2	120,15
col 5	1	69,275	3	173,8	1	69,275
height 305cm	Type	frame 1 Axial load area in one face	Type	frame 2 Axial load area in one face	Type	frame3 = frame 1 Axial load area in one face
col 1	6	34,2	9	83,15	6	34,2
col2	7	59,2	10	147,9	7	59,2
col 3	8	59,2	11	147,9	8	59,2
col 4	7	59,2	10	147,9	7	59,2
col 5	6	34,2	9	83,15	6	34,2

A3 3 STORY 4x2 PARALLEL TO JOISTS

Table 1: Loads definition

Analysis: Parallel to joists		Level:	Ground Floor-Intermediate Floor	Top Floor
Uniformly loaded beams [kN/m]	Parallel to joists	outer	3,68	3,68
	Perpendicular to joists	interior	3,68	3,68
Nodal weights [kN]		Frame 1	outer	10,35
	interior		28,9	25,9
	Frame 2	corner	35,075	34,2
		central 1	90,65	83,15
	Frame 1	corner	60,95	59,2
		central 1	162,9	147,9
Axial loads [kN]	Frame 1	corner	104,35	34,2
		central 1	264,45	83,15
	Frame 2	corner	181,1	59,2
		central 1	473,7	147,9

Table 2: Beams reinforcement details

BEAMS DEFINITION. REINFORCEMENT AREA IN THE SECTION mm2												
height	Type	frame 1		Type	frame 2		Type	frame 3		Type	frame 3	
height 305cm	1	left bottom	right bottom	1	left bottom	right bottom	1	left bottom	right bottom	1	left bottom	right bottom
beam 1		678,58	678,58		678,58	678,58		678,58	678,58		678,58	678,58
beam 2		678,58	678,58		678,58	678,58		678,58	678,58		678,58	678,58
height 610cm	Type	frame 1		Type	frame 2		Type	frame 3		Type	frame 3	
beam 1	1	left bottom	right bottom	1	left bottom	right bottom	1	left bottom	right bottom	1	left bottom	right bottom
beam 2		678,58	678,58		678,58	678,58		678,58	678,58		678,58	678,58
height 915cm	Type	frame 1		Type	frame 2		Type	frame 3		Type	frame 3	
beam 1	2	left bottom	right bottom	1	left bottom	right bottom	1	left bottom	right bottom	1	left bottom	right bottom
beam 2		791,681	791,681		791,681	791,681		791,681	791,681		791,681	791,681

Table 3: Columns axial loads and reinforcement details

COLUMNS DEFINITION. REINFORCEMENT AREA IN ONE FACE OF THE SECTION mm2						
height 0cm	Type	frame 1 Axial load area in one face	Type	frame 2 Axial load area in one face	Type	frame 3 Axial load area in one face
col 1	1	104,35 226,19	3	181,1 226,19	3	181,1 226,19
col 2	2	264,45 226,19	4	473,7 981,75	6	473,7 804,25
col 3	1	104,35 226,19	3	181,1 226,19	3	181,1 226,19
height 305cm	Type	frame 1 Axial load area in one face	Type	frame 2 Axial load area in one face	Type	frame 3 Axial load area in one face
col 1	7	69,275 226,19	9	120,15 226,19	9	120,15 226,19
col 2	8	173,8 402,12	10	310,8 226,19	10	310,8 226,19
col 3	7	69,275 226,19	9	120,15 226,19	9	120,15 226,19
height 610cm	Type	portico 1 Axial load area in one face	Type	portico 2 Axial load area in one face	Type	portico 3 Axial load area in one face
col 1	11	34,2 226,19	13	59,2 226,19	13	59,2 226,19
col 2	12	83,15 226,19	14	147,9 226,19	14	147,9 226,19
col 3	11	34,2 226,19	13	59,2 226,19	13	59,2 226,19

A4 3 STORY 4x2 PERPENDICULAR TO JOISTS

Table 1: Loads definition

Analysis: Perpendicular to joists		Level:	Ground Floor-Intermediate Floor	Top Floor
Uniformly loaded beams [kN/m]	Parallel to joists	outer	3,68	3,68
	Perpendicular to joists	interior	3,68	3,68
Nodal weights [kN]		Frame 1	outer	10,35
	interior		28,9	25,9
	Frame 2	corner	35,075	34,2
		central 1	60,95	59,2
Axial loads [kN]	Frame 1	corner	90,65	83,15
		central 1	162,9	147,9
	Frame 2	corner	104,35	34,2
		central 1	181,1	59,2
	Frame 2	corner	264,45	83,15
		central 1	473,7	147,9

Table 2: Beams reinforcement details

BEAMS DEFINITION. REINFORCEMENT AREA IN THE SECTION mm ²											
height 305cm	Type	frame 1		Type	frame 2		Type	frame 3 = frame 1			
beam 1	1	left bottom	right bott right top	left botto left top	right bottom	right top	left bottom	right bottom	right top		
beam 2		678,58	678,58	678,58	1017,88	678,58	1130,97	678,58	678,58	678,58	
beam 3		678,58	678,58	678,58	1017,88	1130,97	1017,88	678,58	678,58	678,58	
beam 4		678,58	678,58	678,58	1017,88	1017,88	1130,97	678,58	678,58	678,58	
height 610cm	Type	frame 1		Type	frame 2		Type	frame 3 = frame 1			
beam 1	1	left bottom	right bott right top	left botto left top	right bottom	right top	left bottom	right bottom	right top		
beam 2		678,58	678,58	678,58	1017,88	678,58	1130,97	678,58	678,58		
beam 3		678,58	678,58	678,58	1017,88	1130,97	1017,88	678,58	678,58		
beam 4		678,58	678,58	678,58	1017,88	1017,88	1130,97	678,58	678,58		
height 915cm	Type	frame 1		Type	frame 2		Type	frame 3 = frame 1			
beam 1	1	left bottom	right bott right top	left botto left top	right bottom	right top	left bottom	right bottom	right top		
beam 2		678,58	678,58	678,58	1017,88	678,58	1017,88	678,58	678,58		
beam 3		678,58	678,58	678,58	791,68	1017,88	791,68	678,58	678,58		
beam 4		678,58	678,58	678,58	791,68	791,68	1017,88	678,58	678,58		

Table 3: Columns axial loads and reinforcement details

COLUMNS DEFINITION. REINFORCEMENT AREA IN ONE FACE OF THE SECTION mm2									
height 0cm	Type	frame 1 Axial load area in one face	Type	frame 2 Axial load area in one face	Type	frame 3 = frame 1 Axial load area in one face			
col 1	1	104,35 226,19	3	264,45 226,19	1	104,35 226,19			
col 2	2	181,1 226,19	4	473,7 981,75	2	181,1 226,19			
col 3	2	181,1 226,19	5	473,7 804,25	2	181,1 226,19			
col 4	2	181,1 226,19	4	473,7 981,75	2	181,1 226,19			
col 5	1	104,35 226,19	3	264,45 226,19	1	104,35 226,19			
height 305cm	Type	portico 1 Axial load area in one face	Type	portico 2 Axial load area in one face	Type	portico 3 = portico 1 Axial load area in one face			
col 1	6	69,275 226,19	9	173,8 402,12	6	69,275 226,19			
col 2	7	120,15 226,19	10	310,8 226,19	7	120,15 226,19			
col 3	8	120,15 226,19	11	310,8 226,19	8	120,15 226,19			
col 4	7	120,15 226,19	10	310,8 226,19	7	120,15 226,19			
col 5	6	69,275 226,19	9	173,8 402,12	6	69,275 226,19			
height 610cm	Type	portico 1 Axial load area in one face	Type	portico 2 Axial load area in one face	Type	portico 3 = portico 1 Axial load area in one face			
col 1	12	34,2 226,19	15	83,15 226,19	12	34,2 226,19			
col 2	13	59,2 226,19	16	147,9 226,19	13	59,2 226,19			
col 3	14	59,2 226,19	16	147,9 226,19	14	59,2 226,19			
col 4	13	59,2 226,19	16	147,9 226,19	13	59,2 226,19			
col 5	12	34,2 226,19	15	83,15 226,19	12	34,2 226,19			

A5 2 STORY 4x4 PARALLEL TO JOISTS

Table 1: Loads definition

Analysis: Parallel to joists		Level:	Ground Floor-Intermediate Floor	Top Floor
Uniformly loaded beams [kN/m]	Parallel to joists	outer	3,68	3,68
		interior	3,68	3,68
Nodal weights [kN]	Perpendicular to joists	outer	7,7	7,7
		interior	15,87	15,38
	central	15,38	13,18	
	Frame 1	corner	33,065	32,47
		central 1	66,585	64,87
		central 2	64,87	57,17
Axial loads [kN]	Frame 2	corner	60,61	59,42
		central 1	122,13	118,7
		central 2	118,7	103,3
	Frame 3	corner	60,61	59,42
		central 1	122,13	118,7
		central 2	118,7	103,3
Axial loads [kN]	Frame 1	corner	65,535	32,47
		central 1	131,455	64,87
		central 2	122,04	57,17
	Frame 2	corner	120,03	59,42
		central 1	240,83	118,7
		central 2	222	103,3
	Frame 3	corner	120,03	59,42
		central 1	240,83	118,7
		central 2	222	103,3

Table 2: Beams reinforcement details

BEAMS DEFINITION. REINFORCEMENT AREA IN THE SECTION mm2																				
height 305cm	Type	frame 1			Type	frame 2			Type	frame 3										
		left bottom	left top	right bottom		right top	left bottom	left top		right bottom	right top	left bottom	left top	right bottom	right top					
beam 1	1	791,68	791,68	791,68	791,68	678,58	678,58	678,58	678,58	2	678,58	678,58	678,58	678,58	339,29	339,29	678,58	678,58	339,29	339,29
beam 2		791,68	791,68	791,68	791,68	678,58	678,58	678,58	678,58	3	678,58	678,58	678,58	678,58	339,29	339,29	678,58	678,58	339,29	339,29
beam 3		791,68	791,68	791,68	791,68	678,58	678,58	678,58	678,58	2	678,58	678,58	678,58	678,58	339,29	339,29	678,58	678,58	339,29	339,29
beam 4		791,68	791,68	791,68	791,68	678,58	678,58	678,58	678,58	3	678,58	678,58	678,58	678,58	339,29	339,29	678,58	678,58	339,29	339,29
height 610cm	Type	frame 1			Type	frame 2			Type	frame 3										
beam 1	678,58	678,58	678,58	678,58		left bottom	left top	right bottom		right top	left bottom	left top	right bottom	right top	left bottom	left top	right bottom	right top		
beam 2	4	678,58	678,58	678,58	678,58	791,68	791,68	791,68	791,68	5	791,68	791,68	791,68	791,68	339,29	339,29	791,68	791,68	339,29	339,29
beam 3		678,58	678,58	678,58	678,58	791,68	791,68	791,68	791,68	6	791,68	791,68	791,68	791,68	339,29	339,29	791,68	791,68	339,29	339,29
beam 3		678,58	678,58	678,58	678,58	791,68	791,68	791,68	791,68	5	791,68	791,68	791,68	791,68	339,29	339,29	791,68	791,68	339,29	339,29
beam 4		678,58	678,58	678,58	678,58	791,68	791,68	791,68	791,68	6	791,68	791,68	791,68	791,68	339,29	339,29	791,68	791,68	339,29	339,29

Table 3: Columns axial loads and reinforcement details

COLUMNS DEFINITION. REINFORCEMENT AREA IN ONE FACE OF THE SECTION mm2												
height 0cm	Type	frame 1			Type	frame 2			Type	frame 3		
		Axial load	area in one face	Area in one face		Axial load	area in one face	Area in one face		Axial load	area in one face	Area in one face
col 1	1	65,54	226,19	226,19	4	120,03	226,19	226,19	4	120,03	226,19	226,19
col 2	2	131,46	402,12	402,12	5	240,83	226,19	226,19	5	240,83	226,19	226,19
col 3	3	122,04	402,12	402,12	6	222	226,19	226,19	6	222,00	226,19	226,19
col 4	2	131,46	402,12	402,12	5	240,83	226,19	226,19	5	240,83	226,19	226,19
col 5	1	65,54	226,19	226,19	4	120,03	226,19	226,19	4	120,03	226,19	226,19
height 305cm	Type	frame 1			Type	frame 2			Type	frame 3		
col 1	7	Axial load	area in one face	Area in one face		Axial load	area in one face	Area in one face		Axial load	area in one face	Area in one face
col 1	7	32,47	402,12	402,12	10	59,42	226,19	226,19	10	59,42	226,19	226,19
col 2		64,87	628,32	628,32	11	118,7	226,19	226,19	11	118,70	226,19	226,19
col 3		222,00	452,39	452,39	12	103,3	226,19	226,19	12	222,00	226,19	226,19
col 4		64,87	628,32	628,32	11	118,7	226,19	226,19	11	118,70	226,19	226,19
col 5		32,47	402,12	402,12	10	59,42	226,19	226,19	10	59,42	226,19	226,19

A6 2 STORY 4x4 PERPENDICULAR TO JOISTS

Table 1: Loads definition

Analysis: Perpendicular to joists		Level	Ground Floor-Intermediate	Top Floor
Uniformly loaded beams [kN/m]	Parallel to joists	outer	3,68	3,68
		interior	3,68	3,68
Nodal weights [kN]	Perpendicular to joists	outer	7,87	7,7
		interior	15,87	15,38
		central	15,38	13,18
Axial loads [kN]	Frame 1	corner	33,065	32,47
		central 1	60,61	64,94
	Frame 2	corner	66,585	64,87
		central 1	122,13	118,7
	Frame 3	corner	64,87	57,17
		central 1	118,7	103,3
	Frame 1	corner	65,535	32,47
		central 1	125,55	64,94
	Frame 2	corner	131,455	64,87
	central 1	240,83	118,7	
Frame 3	corner	122,04	57,17	
	central 1	222	103,3	

Table 2: Beams reinforcement details

BEAMS DEFINITION. REINFORCEMENT AREA IN THE SECTION mm ²															
height 305cm	Type	frame 1				frame 2				frame 3					
		left bottom	left top	right bot	right top	left botto	left top	right bottom	right top	left bottom	left top	right botto	right top		
beam 1	1	678,58	678,58	678,58	678,58	678,58	678,58	1017,88	1470,27	1017,88	1470,27	678,58	678,58	791,68	1130,97
beam 2		678,58	678,58	678,58	678,58	1017,88	1470,27	1017,88	1130,97	1017,88	1470,27	1130,97	1130,97	791,68	1017,88
beam 3		678,58	678,58	678,58	678,58	1017,88	1130,97	1017,88	1470,27	1017,88	1470,27	1470,27	1470,27	791,68	1130,97
beam 4		678,58	678,58	678,58	678,58	1017,88	1470,27	1017,88	678,58	678,58	678,58	678,58	1244,07	791,68	678,58
height 610cm		Type	frame 1				frame 2				frame 3				
beam 1	1	left bottom	left top	right bot	right top	left botto	left top	right bottom	right top	left bottom	left top	right botto	right top	1017,88	678,58
beam 2		678,58	678,58	678,58	678,58	1545,66	1357,17	1545,66	678,58	1017,88	678,58	1017,88	678,58	791,68	1017,88
beam 3		678,58	678,58	678,58	678,58	1143,54	1130,97	1143,54	1130,97	1357,17	1357,17	1357,17	1357,17	791,68	1017,88
beam 4		678,58	678,58	678,58	678,58	1545,66	1357,17	1545,66	678,58	1017,88	678,58	1017,88	678,58	791,68	1017,88

Table 3: Columns axial loads and reinforcement details

COLUMNS DEFINITION. REINFORCEMENT AREA IN ONE FACE OF THE SECTION mm ²									
height 0cm	Type	frame 1		Type	frame 2		Type	frame 3	
		Axial load	area in one face		Axial load	area in one face		Axial load	area in one face
col 1	1	65,54	226,19	3	131,46	402,12	5	122,04	402,12
col 2	2	125,55	226,19	4	240,83	226,19	6	222,00	226,19
col 3	2	125,55	226,19	4	240,83	226,19	6	222,00	226,19
col 4	2	125,55	226,19	4	240,83	226,19	6	222,00	226,19
col 5	1	65,54	226,19	3	131,46	628,32	5	122,04	402,12
height 305cm	Type	frame 1		Type	frame 2		Type	frame 3	
		Axial load	area in one face		Axial load	area in one face		Axial load	area in one face
col 1	7	32,47	402,12	9	64,87	1256,64	11	57,17	452,39
col 2	8	64,94	226,19	10	118,70	226,19	12	103,30	226,19
col 3	8	64,94	226,19	10	118,70	226,19	12	103,30	226,19
col 4	8	64,94	226,19	10	118,70	226,19	12	103,30	226,19
col 5	7	32,47	402,12	9	64,87	1256,64	11	57,17	452,39

A7 3 STORY 4x4 PARALLEL TO JOISTS

Table 1: Loads definition

Analysis: Parallel to joists		Level	Ground Floor-Intermediate Floor	Top Floor
Uniformly loaded beams [kN/m]	Parallel to joists	outer	3,68	3,68
		interior	3,68	3,68
	Perpendicular to joists	outer	7,87	7,7
interior		15,87	15,38	
central		15,38	13,18	
Nodal weights [kN]	Frame 1	corner	33,065	32,47
		central 1	66,585	64,87
		central 2	64,87	57,17
	Frame 2	corner	60,61	59,42
		central 1	122,13	118,7
		central 2	118,7	103,3
	Frame 3	corner	60,61	59,42
		central 1	122,13	118,7
		central 2	118,7	103,3
Axial loads [kN]	Frame 1	corner	98,6	32,47
		central 1	198,04	64,87
		central 2	122,04	57,17
	Frame 2	corner	180,64	59,42
		central 1	362,96	118,7
		central 2	340,7	103,3
	Frame 3	corner	180,64	59,42
		central 1	362,96	118,7
		central 2	340,7	103,3

Table 2: Beams reinforcement details

BEAMS DEFINITION. REINFORCEMENT AREA IN THE SECTION mm2											
height	Type	frame 1		Type	frame 2		Type	frame 3			
		left	right		left	right		left	right		
305cm	1	791,68	791,68	2	678,58	678,58	2	678,58	678,58		
beam 1		791,68	791,68		678,58	678,58		678,58	678,58		
beam 2		791,68	791,68		678,58	678,58		678,58	678,58		
beam 3		791,68	791,68		678,58	678,58		678,58	678,58		
beam 4		791,68	791,68		678,58	678,58		678,58	678,58		
610cm	3	791,68	791,68	7	678,58	678,58	7	678,58	678,58		
beam 1		791,68	791,68		678,58	678,58		678,58	678,58		
beam 2		339,29	339,29	8	339,29	339,29	8	339,29	339,29		
beam 3		678,58	678,58	7	678,58	678,58	7	678,58	678,58		
beam 4		339,29	339,29	8	339,29	339,29	8	339,29	339,29		
915cm	7	678,58	678,58	3	791,68	791,68	7	678,58	678,58		
beam 1		678,58	678,58		791,68	791,68		678,58	678,58		
beam 2		339,29	339,29	4	339,29	339,29	8	339,29	339,29		
beam 3		678,58	678,58	5	678,58	678,58	7	678,58	678,58		
beam 4		339,29	339,29	6	339,29	339,29	8	339,29	339,29		

A7 3 STORY 4x4 PARALLEL TO JOISTS

Table 3: Columns axial loads and reinforcement details

COLUMNS DEFINITION. REINFORCEMENT AREA IN ONE FACE OF THE SECTION mm ²									
height 0cm	Type	frame 1 Axial load	frame 1 area in one face	Type	frame 2 Axial load	frame 2 area in one face	Type	frame 3 Axial load	frame 3 area in one face
col 1	1	98,6	226,19	4	180,64	226,19	4	180,64	226,19
col 2	2	198,04	628,32	5	362,96	226,19	5	362,96	226,19
col 3	3	122,04	402,12	6	340,7	226,19	6	340,7	226,19
col 4	2	198,04	628,32	5	362,96	226,19	5	362,96	226,19
col 5	1	98,6	226,19	4	180,64	226,19	4	180,64	226,19
height 305cm	Type	frame 1 Axial load	frame 1 area in one face	Type	frame 2 Axial load	frame 2 area in one face	Type	frame 3 Axial load	frame 3 area in one face
col 1	7	65,535	402,12	10	120,03	226,19	10	120,03	226,19
col 2	8	131,455	804,25	11	240,83	226,19	11	240,83	226,19
col 3	9	122,04	628,32	12	222	226,19	12	222	226,19
col 4	8	131,455	804,25	11	240,83	226,19	11	240,83	226,19
col 5	7	65,535	402,12	10	120,03	226,19	10	120,03	226,19
height 610cm	Type	frame 1 Axial load	frame 1 area in one face	Type	frame 2 Axial load	frame 2 area in one face	Type	frame 3 Axial load	frame 3 area in one face
col 1	13	32,47	402,12	16	59,42	226,19	16	59,42	226,19
col 2	14	64,87	452,39	17	118,7	226,19	17	118,7	226,19
col 3	15	340,7	402,12	18	103,3	226,19	18	222	226,19
col 4	14	64,87	452,39	17	118,7	226,19	17	118,7	226,19
col 5	13	32,47	402,12	16	59,42	226,19	16	59,42	226,19

Table 1: Loads definition

Analysis: Perpendicular to joists		Level	Ground Floor-Intermediate Floor	Top Floor	
Uniformly loaded beams [kN/m]	Parallel to joists	outer	3,68	3,68	
		interior	3,68	3,68	
	Perpendicular to joists	outer	7,87	7,7	
		interior	15,87	15,38	
		central	15,38	13,18	
Nodal weights [kN]	Frame 1	corner	33,065	32,47	
		central 1	60,61	64,94	
		corner	66,585	64,87	
	Frame 2	central 1	122,13	118,7	
		corner	64,87	57,17	
	Frame 3	central 1	118,7	103,3	
		corner	98,6	32,47	
	Axial loads [kN]	Frame 1	central 1	186,16	64,94
			corner	198,04	64,87
central 1			362,96	118,7	
Frame 2		corner	186,91	57,17	
		central 1	340,7	103,3	
		corner			
Frame 3		central 1			
		corner			
		central 1			

A8 3 STORY 4x4 PERPENDICULAR TO JOISTS

Table 2: Beams reinforcement details

BEAMS DEFINITION. REINFORCEMENT AREA IN THE SECTION mm2														
height	305cm	Type	frame 1		Type	frame 2		Type	frame 3					
			left	right		left	right		left	right				
beam 1			678,58	678,58	2	1545,66	791,68	1545,66	1470,27	6	1017,88	678,58	1017,88	1244,07
beam 2		1	678,58	678,58	3	1143,54	1470,27	1143,54	1244,07	7	1017,88	1244,07	1017,88	1017,88
beam 3			678,58	678,58	4	1143,54	1244,07	1143,54	1470,27	8	1017,88	1017,88	1017,88	1244,07
beam 4			678,58	678,58	5	1545,66	1470,27	1545,66	791,68	9	1017,88	1244,07	1017,88	678,58
height	610cm	Type	frame 1		Type	frame 2		Type	frame 3					
beam 1			678,58	678,58		10	1545,66		791,68	1545,66	1357,17	14	1017,88	678,58
beam 2		1	678,58	678,58	11	1143,54	1357,17	1143,54	1130,97	15	1017,88	1130,97	1017,88	1017,88
beam 3			678,58	678,58	12	1143,54	1130,97	1143,54	1357,17	16	1017,88	1017,88	1017,88	1130,97
beam 4			678,58	678,58	13	1545,66	1357,17	1545,66	791,68	17	1017,88	1130,97	1017,88	678,58
height	915cm	Type	frame 1		Type	frame 2		Type	frame 3					
beam 1			678,58	678,58		18	1545,66		678,58	1545,66	678,58	22	1244,07	678,58
beam 2			678,58	678,58	19	1143,54	678,58	1143,54	1130,97	23	904,78	678,58	904,78	1017,88
beam 3		1	678,58	678,58	20	1143,54	1130,97	1143,54	678,58	24	904,78	1017,88	904,78	678,58
beam 4			678,58	678,58	21	1545,66	678,58	1545,66	678,58	25	1244,07	678,58	1244,07	678,58

Table 3: Columns axial loads and reinforcement details

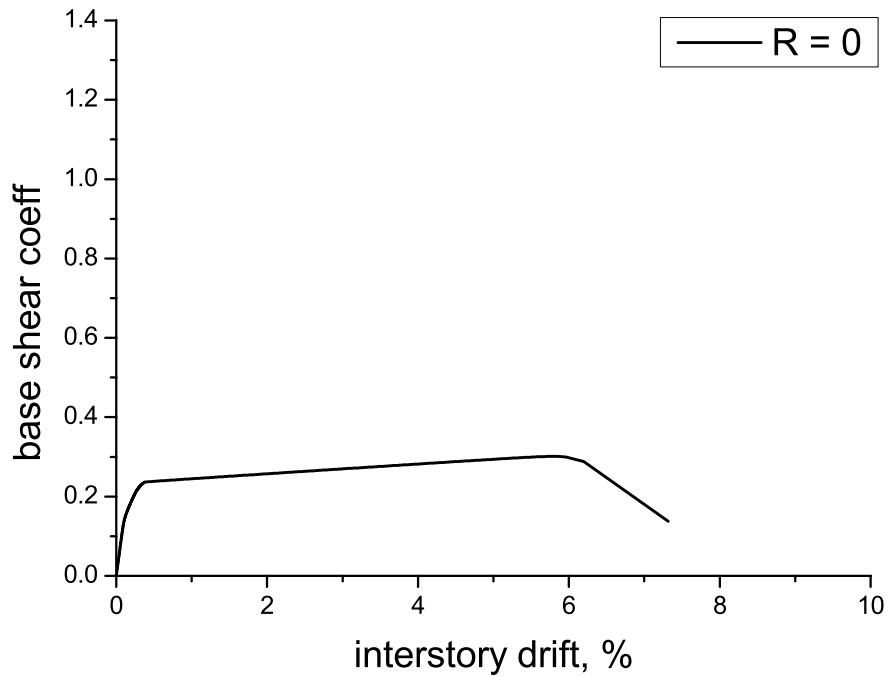
COLUMNS DEFINITION. REINFORCEMENT AREA IN ONE FACE OF THE SECTION mm ²							
height 0cm	Type	frame 1 Axial load area in one face	Type	frame 2 Axial load area in one face	Type	frame 3 Axial load area in one face	
col 1	1	98,6 226,19	3	198,04 628,32	5	186,91 402,12	
col 2	2	186,16 226,19	4	362,96 226,19	6	340,7 226,19	
col 3	2	186,16 226,19	4	362,96 226,19	6	340,7 226,19	
col 4	2	186,16 226,19	4	362,96 226,19	6	340,7 226,19	
col 5	1	98,6 226,19	3	198,04 628,32	5	186,91 402,12	
height 305cm	Type	frame 1 Axial load area in one face	Type	frame 2 Axial load area in one face	Type	frame 3 Axial load area in one face	
col 1	7	65,535 402,12	9	131,46 804,25	11	122,04 628,32	
col 2	8	125,55 226,19	10	240,83 226,19	12	222 226,19	
col 3	8	125,55 226,19	10	240,83 226,19	12	222 226,19	
col 4	8	125,55 226,19	10	240,83 226,19	12	222 226,19	
col 5	7	65,535 402,12	9	131,46 804,25	11	122,04 628,32	
height 610cm	Type	frame 1 Axial load area in one face	Type	frame 2 Axial load area in one face	Type	frame 3 Axial load area in one face	
col 1	13	32,47 402,12	15	64,87 452,39	17	57,17 402,12	
col 2	14	64,94 226,19	16	118,7 226,19	18	103,3 226,19	
col 3	14	64,94 226,19	16	118,7 226,19	18	103,3 226,19	
col 4	14	64,94 226,19	16	118,7 226,19	18	103,3 226,19	
col 5	13	32,47 402,12	15	64,87 452,39	17	57,17 402,12	

Appendix B

Pushover curves of prototypes

B.1 2-STORY 4x2 PARALLEL TO JOISTS.....	146
B.2 2-STORY 4x2 PERPENDICULAR TO JOISTS.....	149
B.3 3-STORY 4x2 PARALLEL TO JOISTS.....	152
B.4 3-STORY 4x2 PERPENDICULAR TO JOISTS.....	155
B.5 2-STORY 4x4 PARALLEL TO JOISTS.....	158
B.6 2-STORY 4x4 PERPENDICULAR TO JOISTS.....	162
B.7 3-STORY 4x4 PARALLEL TO JOISTS.....	165
B.8 3-STORY 4x4 PERPENDICULAR TO JOISTS.....	169

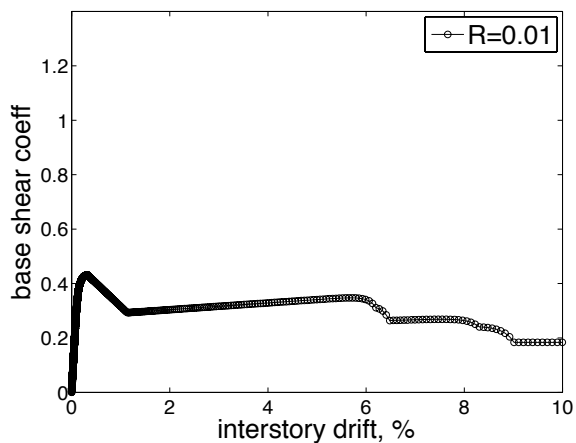
B1 2 STORY 4x2 PARALLEL TO JOISTS



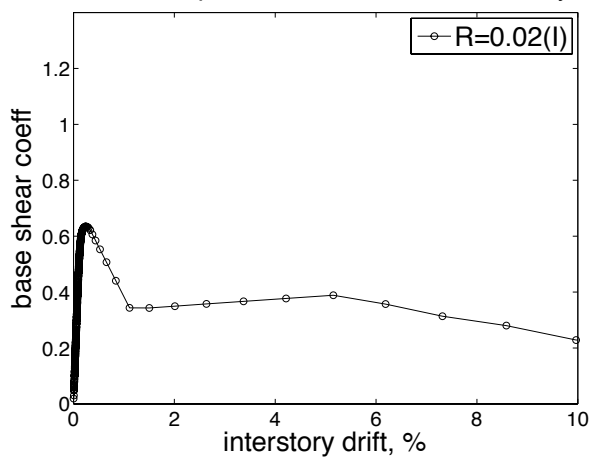
Prototype 4x2 spans						
Ratio	0.05	0.04	0.03	0.02	0.01	Y
Wall configuration Parallel to joists						I

B1 2 STORY 4x2 PARALLEL TO JOISTS

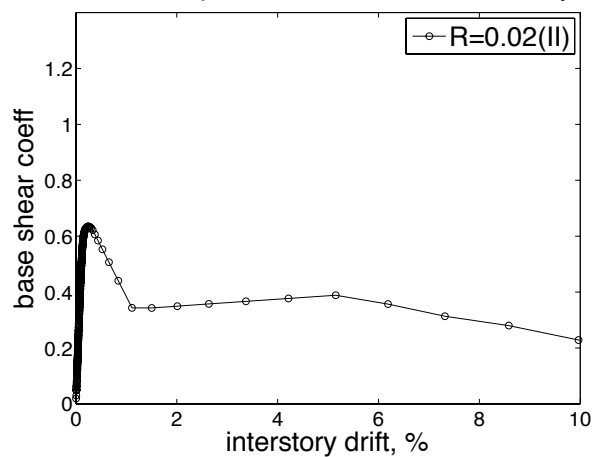
2 stories 4x2spans Parallel to unidirectional joists



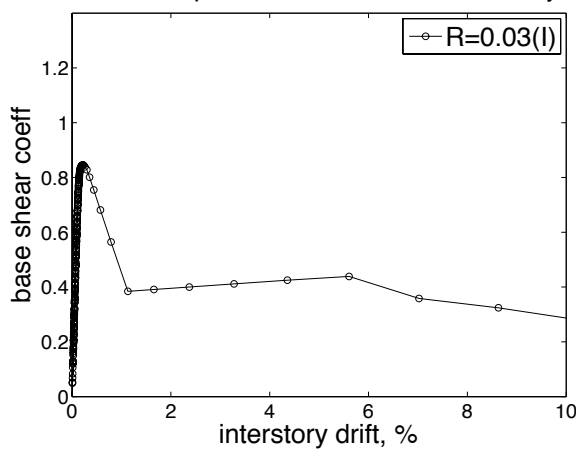
2 stories 4x2spans Parallel to unidirectional joists



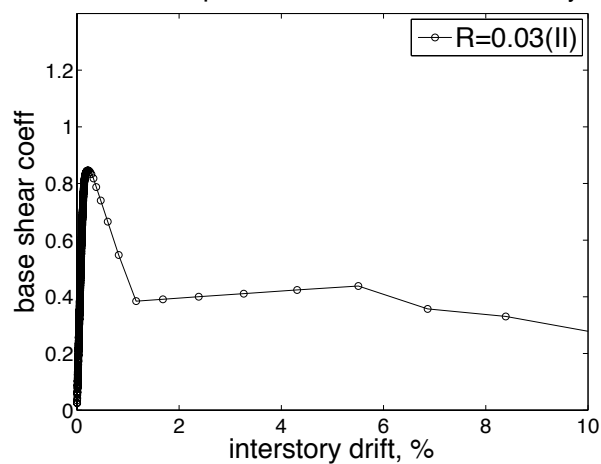
2 stories 4x2spans Parallel to unidirectional joists



2 stories 4x2spans Parallel to unidirectional joists

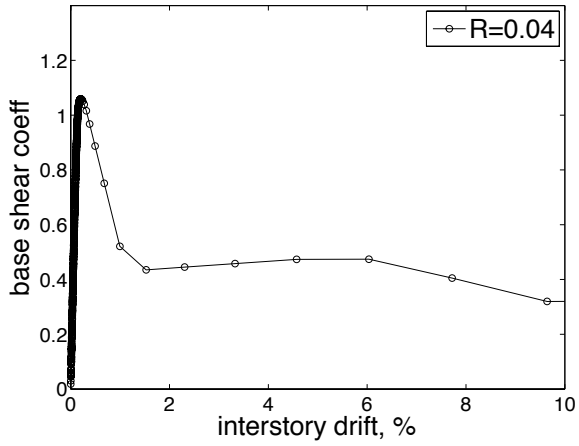


2 stories 4x2spans Parallel to unidirectional joists

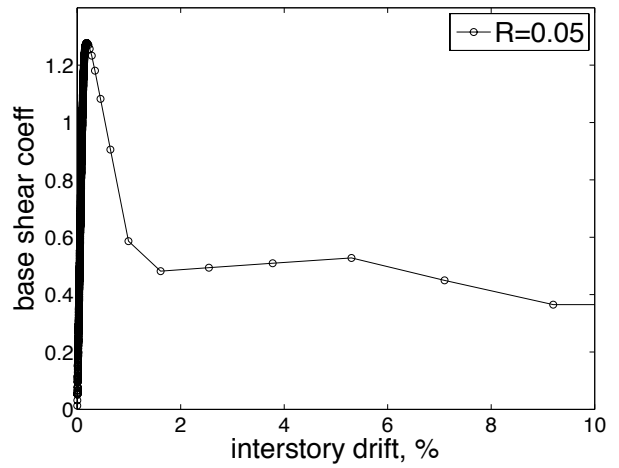


B1 2 STORY 4x2 PARALLEL TO JOISTS

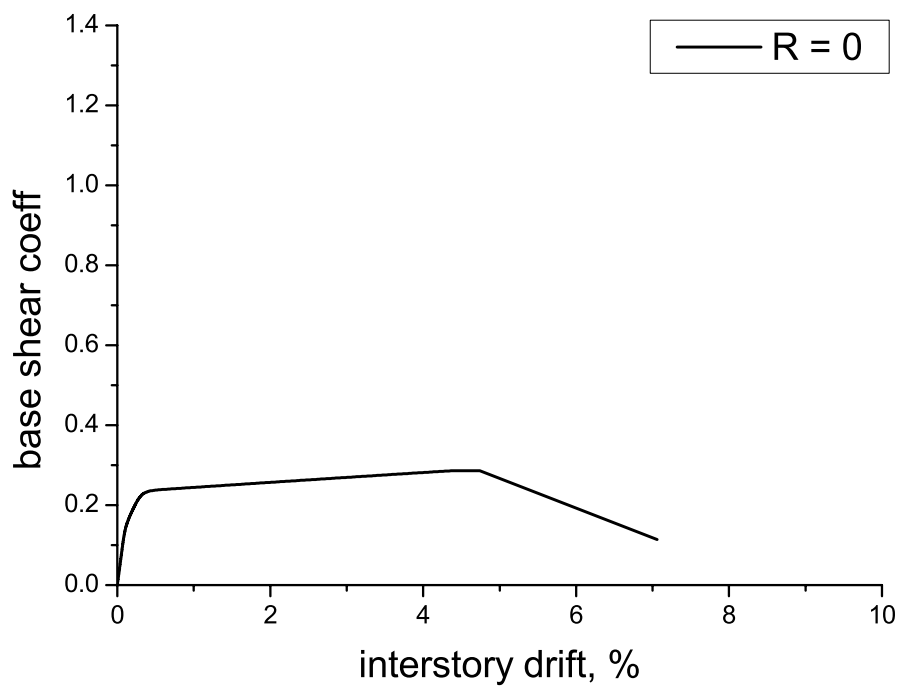
2 stories 4x2spans Parallel to unidirectional joists



2 stories 4x2spans Parallel to unidirectional joists



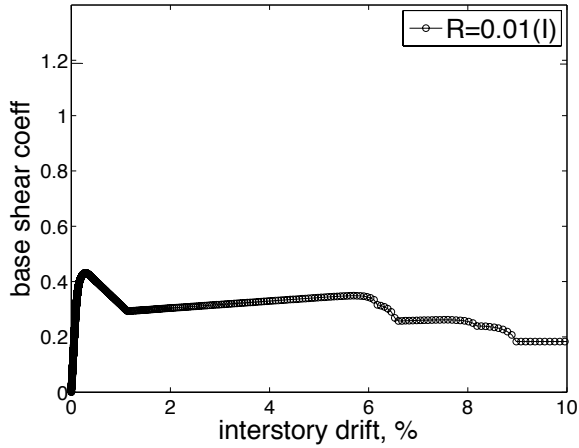
B2 2 STORY 4x2 PERPENDICULAR TO JOISTS



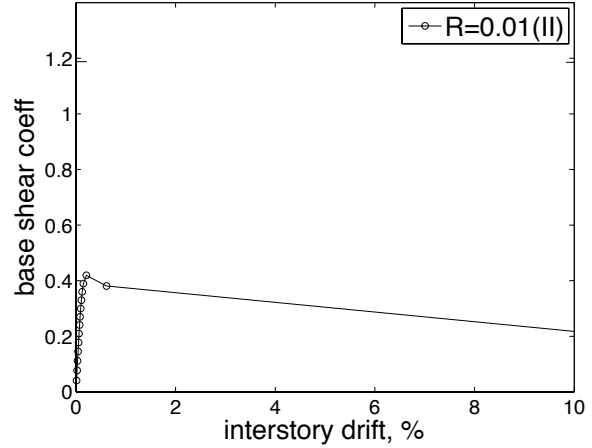
Prototype 4x2 spans					
Ratio	0.04	0.03	0.02	0.01	X
Wall configuration Perpendicular to joists					I
					II
					III

B2 2 STORY 4x2 PERPENDICULAR TO JOISTS

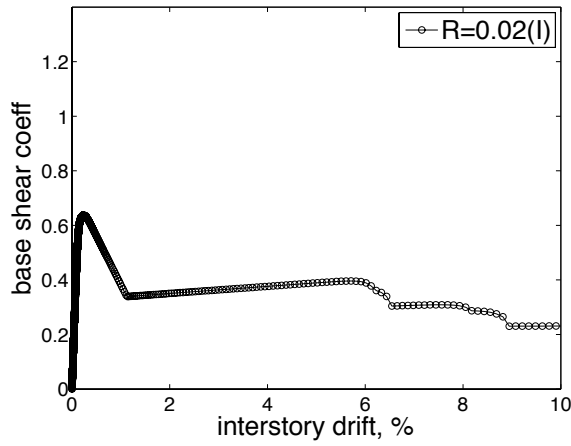
2 stories 4x2spans Perpendicular to unidirectional joists



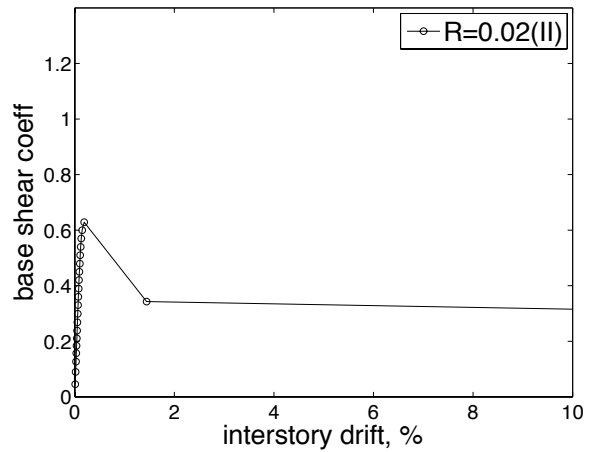
2 stories 4x2spans Perpendicular to unidirectional joists



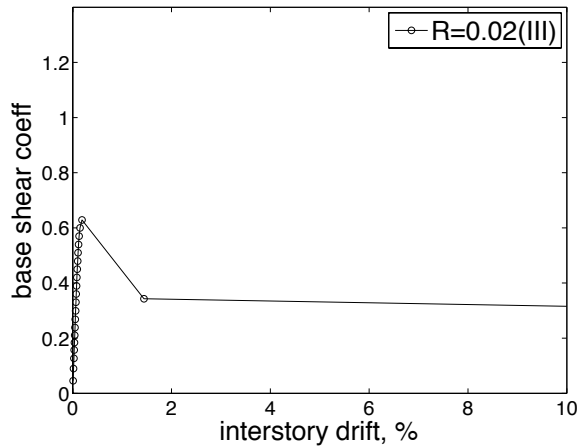
2stories 4x2spans Perpendicular to unidirectional joists



2stories 4x2spans Perpendicular to unidirectional joists

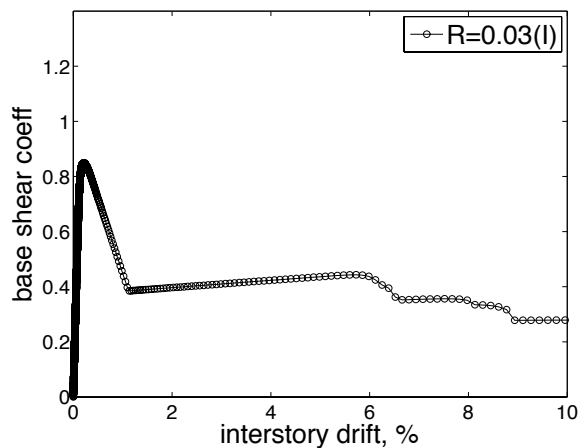


2stories 4x2spans Perpendicular to unidirectional joists

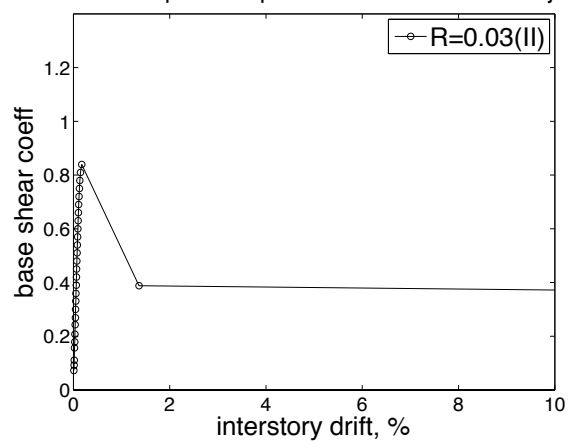


B2 2 STORY 4x2 PERPENDICULAR TO JOISTS

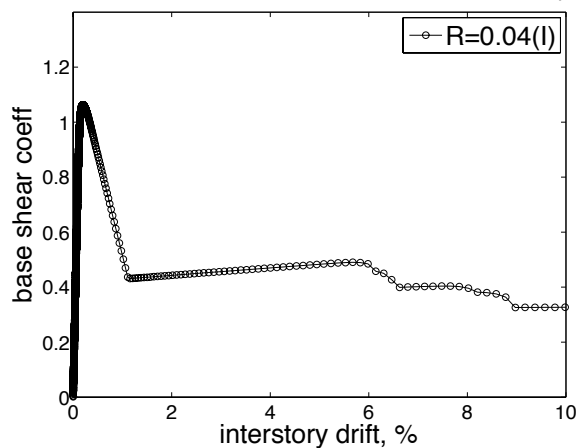
2stories 4x2spans Perpendicular to unidirectional joists



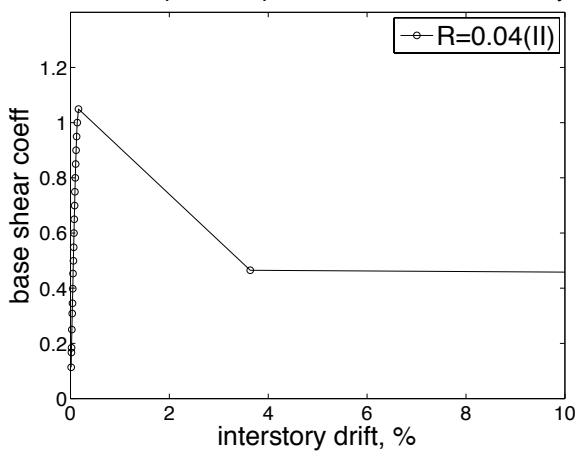
2stories 4x2spans Perpendicular to unidirectional joists



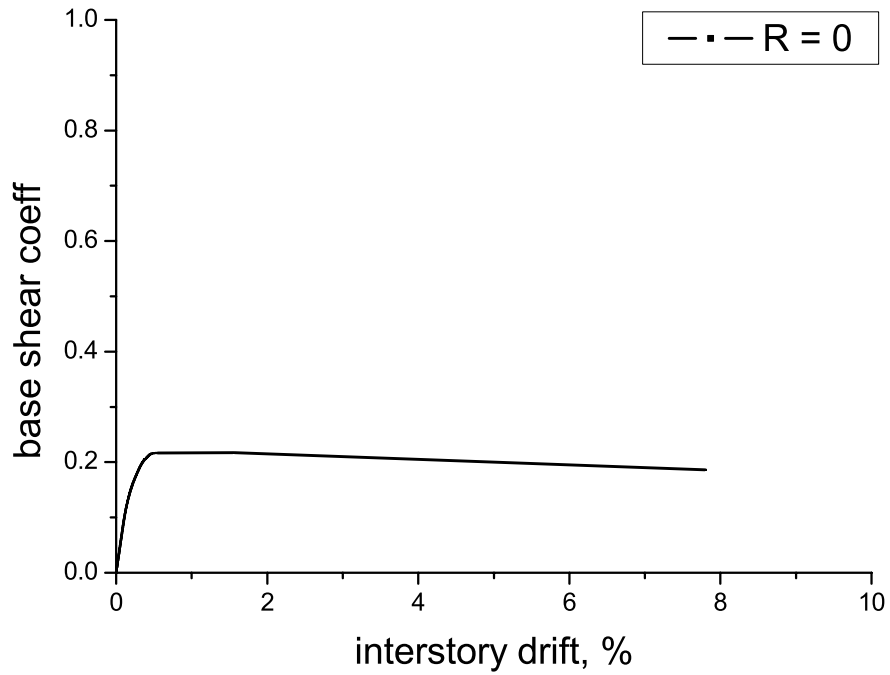
2stories 4x2spans Perpendicular to unidirectional joists



2stories 4x2spans Perpendicular to unidirectional joists



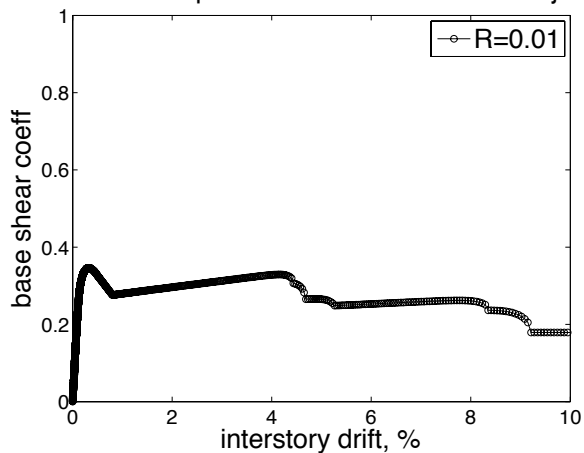
B3 3 STORY 4x2 PARALLEL TO JOISTS



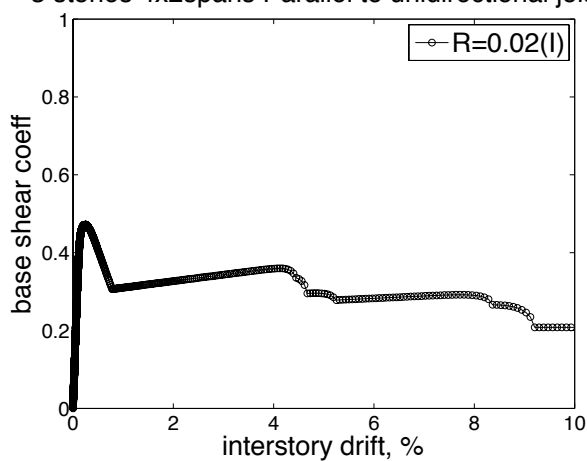
Prototype 4x2 spans						
Ratio	0.05	0.04	0.03	0.02	0.01	Y
Wall configuration Parallel to joists						I

B3 3 STORY 4x2 PARALLEL TO JOISTS

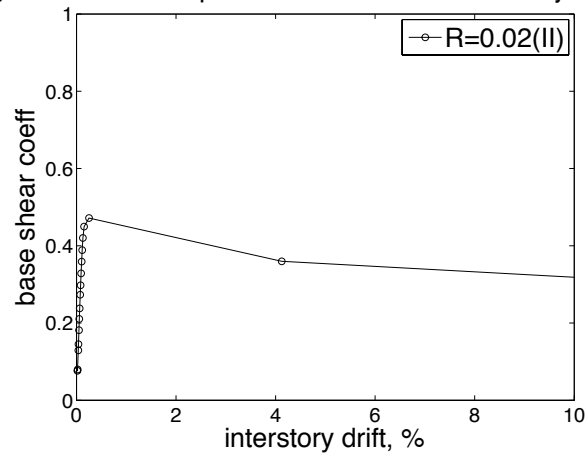
3 stories 4x2spans Parallel to unidirectional joists



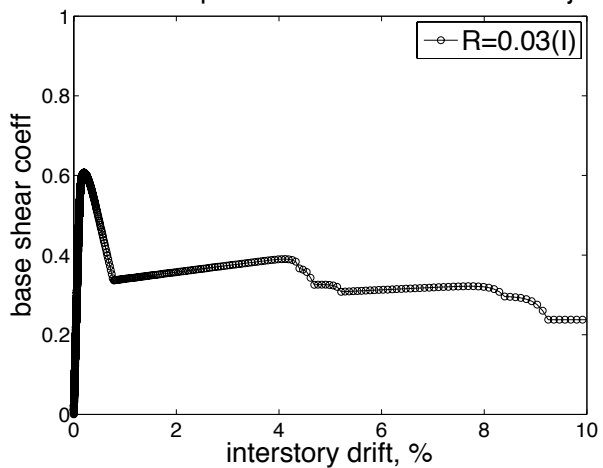
3 stories 4x2spans Parallel to unidirectional joists



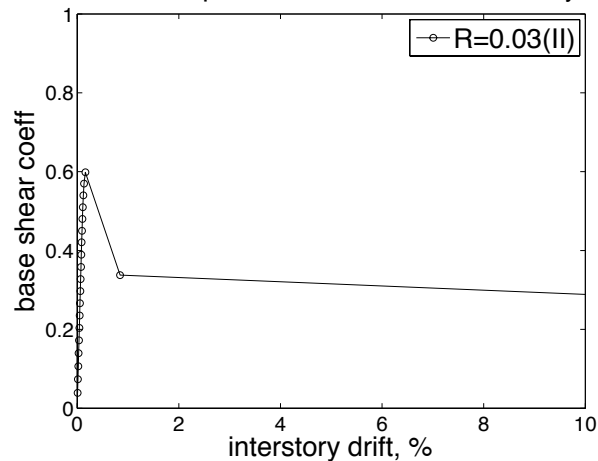
3 stories 4x2spans Parallel to unidirectional joists



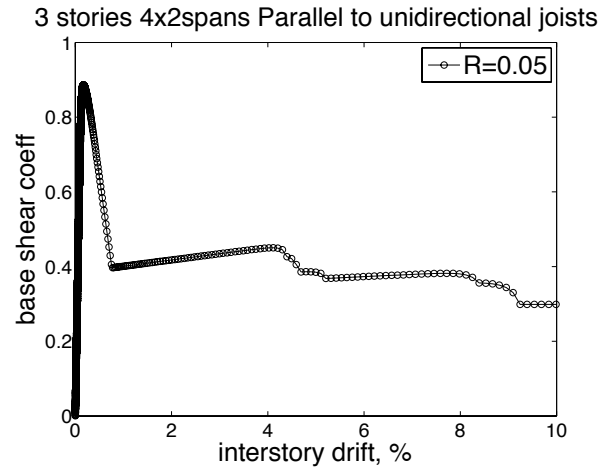
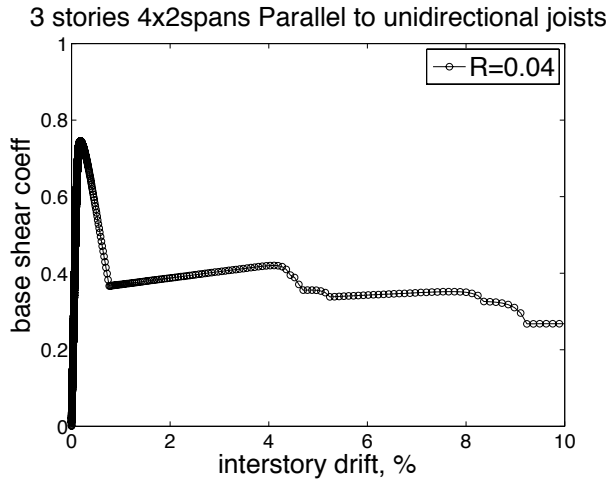
3 stories 4x2spans Parallel to unidirectional joists



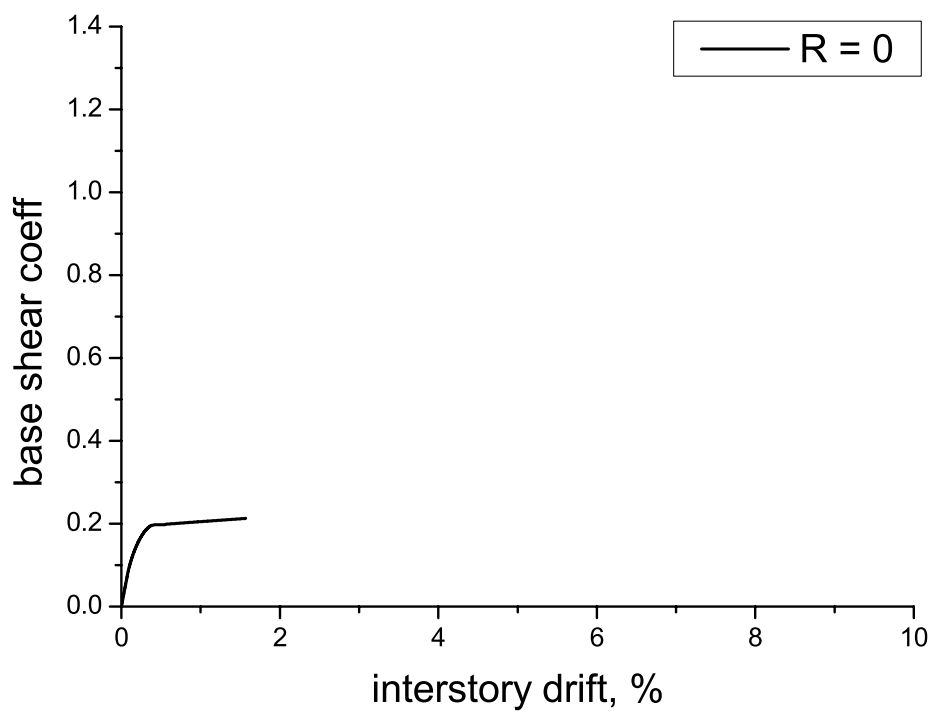
3 stories 4x2spans Parallel to unidirectional joists



B3 3 STORY 4x2 PARALLEL TO JOISTS



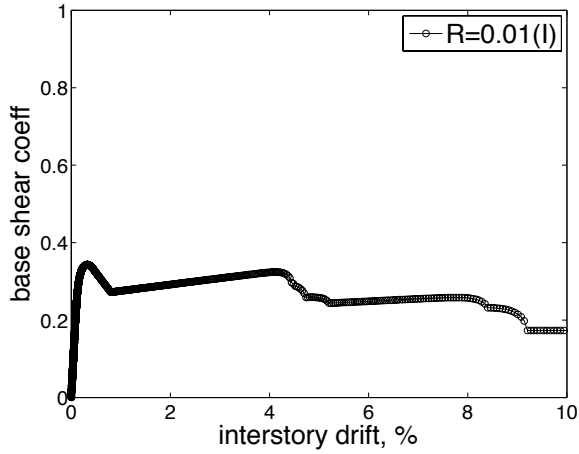
B4 3 STORY 4x2 PERPENDICULAR TO JOISTS



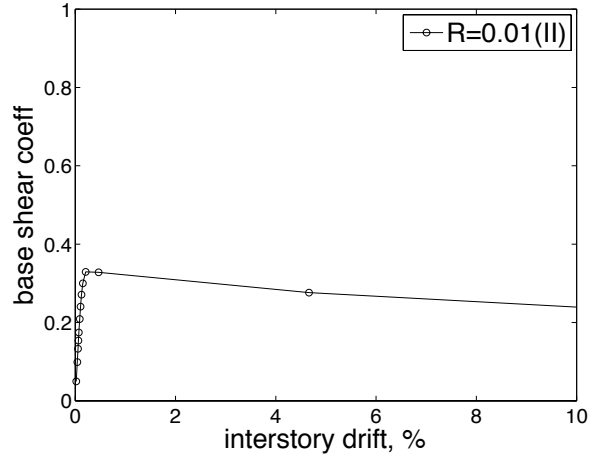
Prototype 4x2 spans					
Ratio	0.04	0.03	0.02	0.01	X
Wall configuration Perpendicular to joists					I
					II
					III

B4 3 STORY 4x2 PERPENDICULAR TO JOISTS

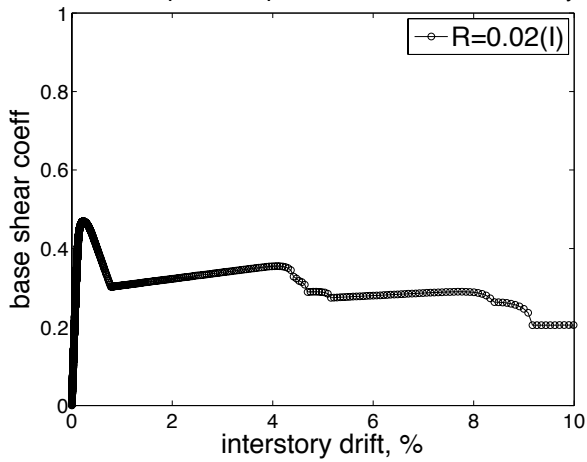
3stories 4x2spans Perpendicular to unidirectional joists



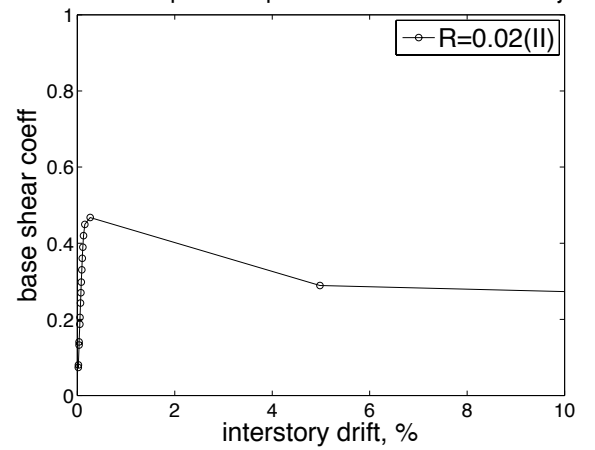
3stories 4x2spans Perpendicular to unidirectional joists



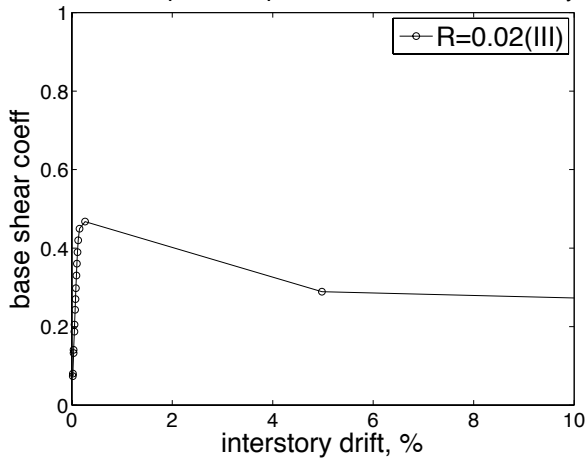
3stories 4x2spans Perpendicular to unidirectional joists



3stories 4x2spans Perpendicular to unidirectional joists

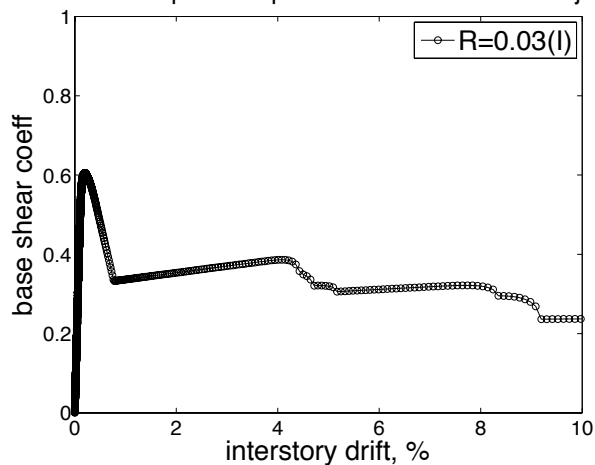


3stories 4x2spans Perpendicular to unidirectional joists

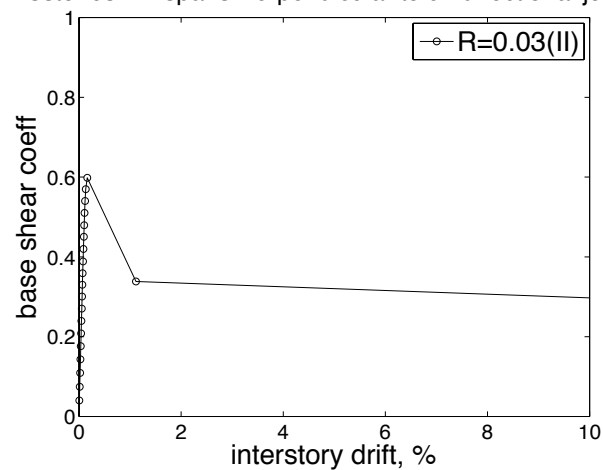


B4 3 STORY 4x2 PERPENDICULAR TO JOISTS

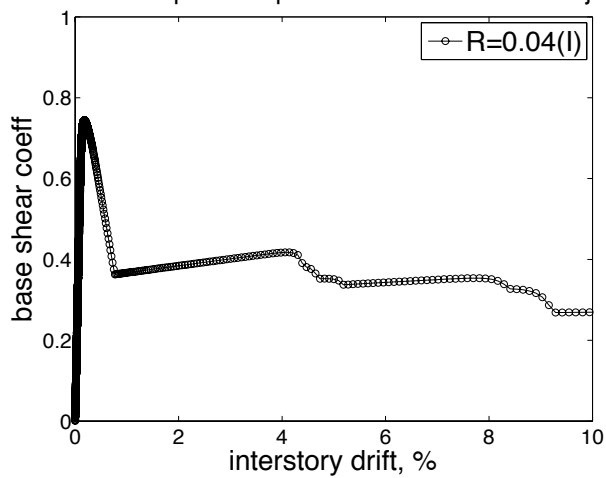
3stories 4x2spans Perpendicular to unidirectional joists



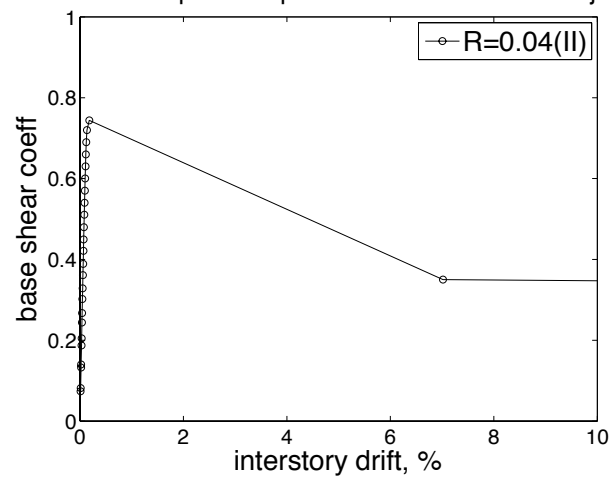
3stories 4x2spans Perpendicular to unidirectional joists



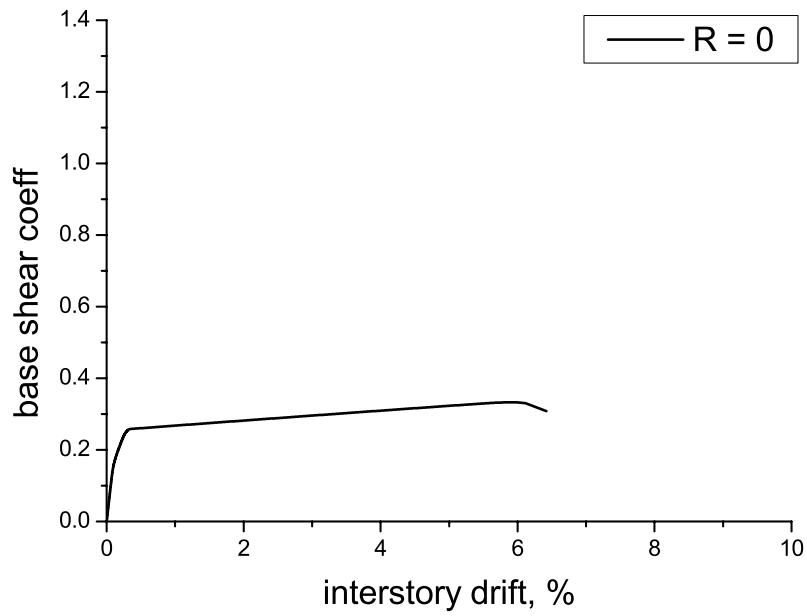
3stories 4x2spans Perpendicular to unidirectional joists



3stories 4x2spans Perpendicular to unidirectional joists



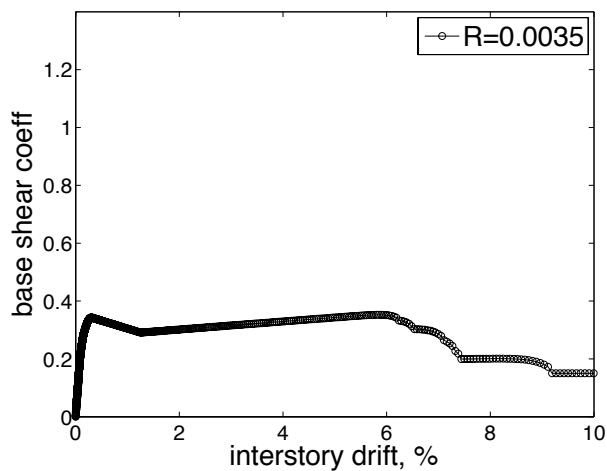
B5 2 STORY 4x4 PARALLEL TO JOISTS



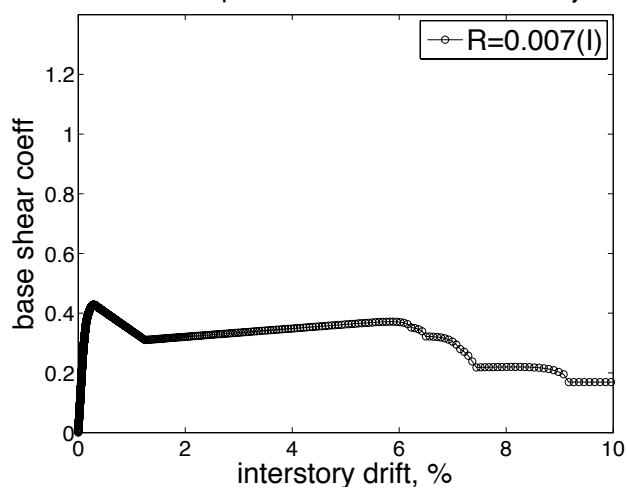
Prototype 4x4 spans						
Ratio	0.035	0.021	0.014	0.007	0.0035	Y
Wall configuration Parallel to joists						I
						II
						III
						IV
						V

B5 2 STORY 4x4 PARALLEL TO JOISTS

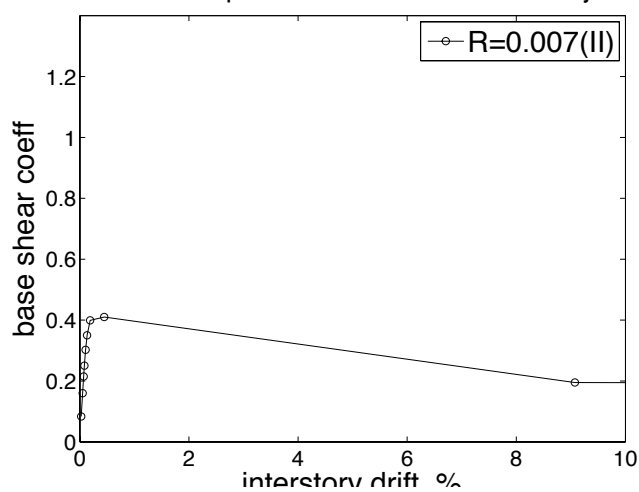
2 stories 4x4spans Parallel to unidirectional joists



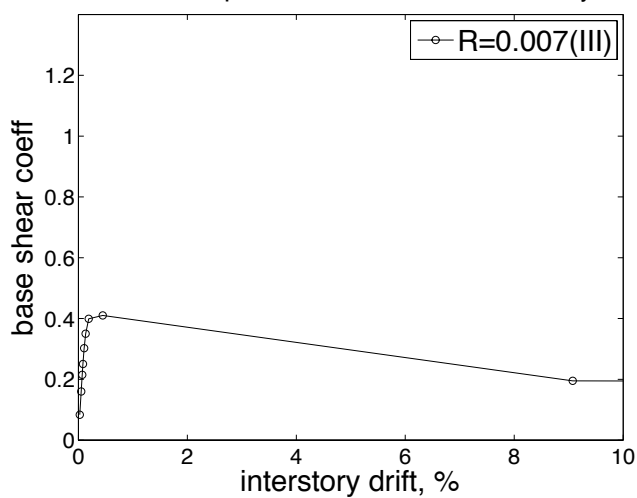
2 stories 4x4spans Parallel to unidirectional joists



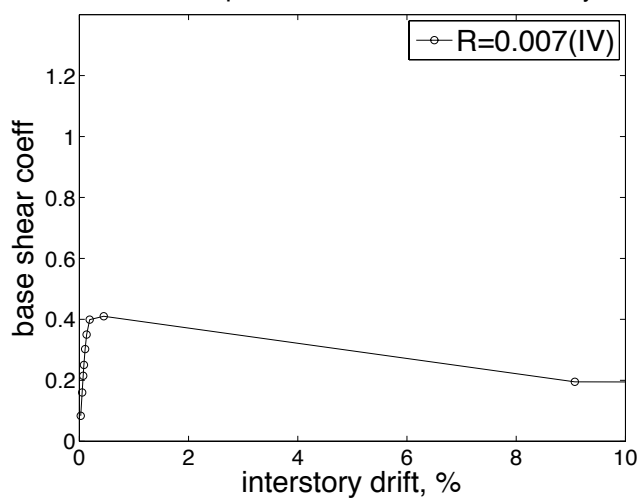
2 stories 4x4spans Parallel to unidirectional joists



2 stories 4x4spans Parallel to unidirectional joists

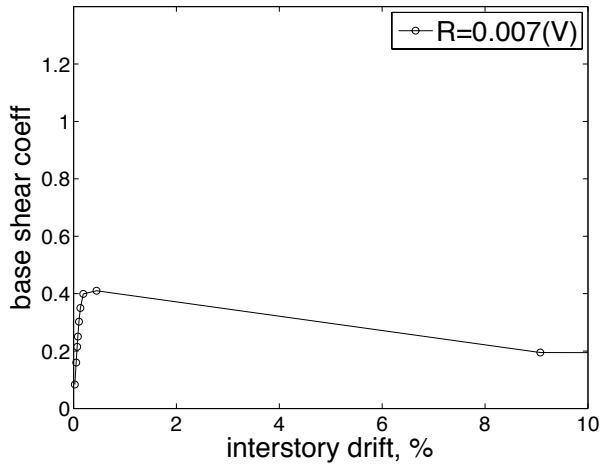


2 stories 4x4spans Parallel to unidirectional joists

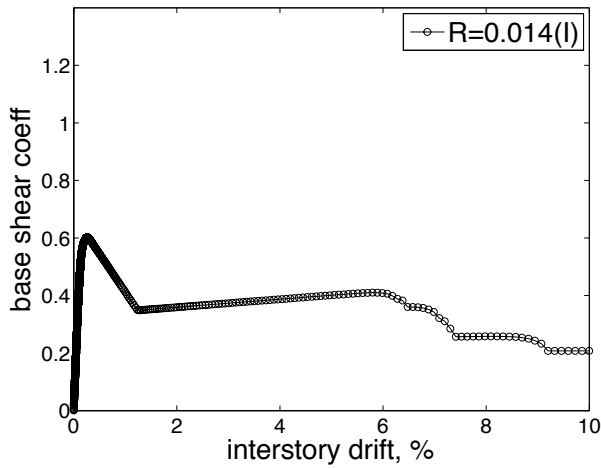


B5 2 STORY 4x4 PARALLEL TO JOISTS

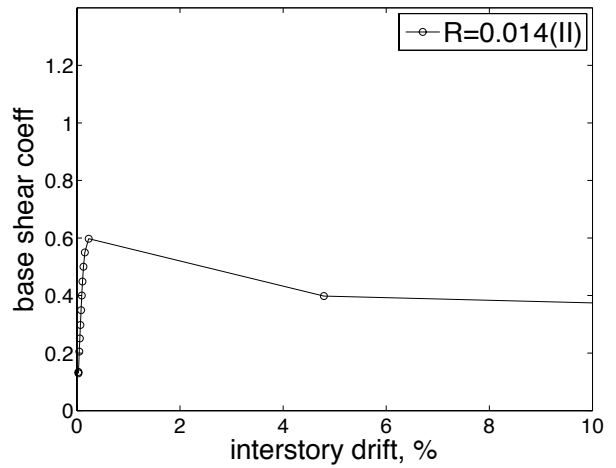
2 stories 4x4spans Parallel to unidirectional joists



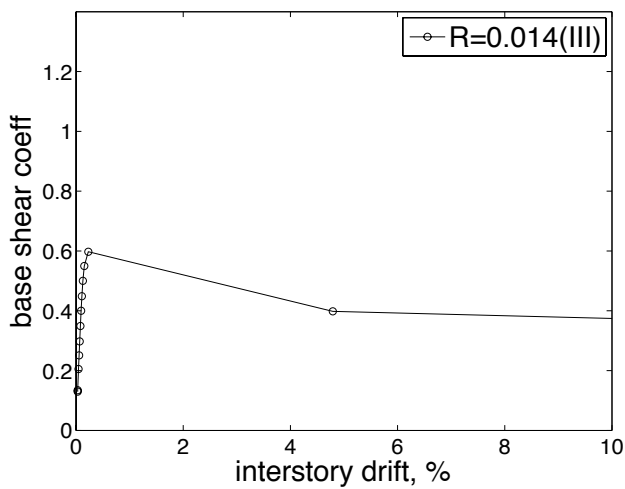
2 stories 4x4spans Parallel to unidirectional joists



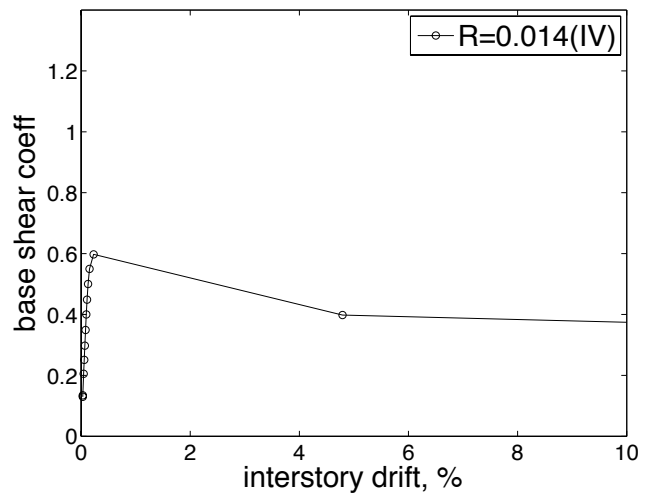
2 stories 4x4spans Parallel to unidirectional joists

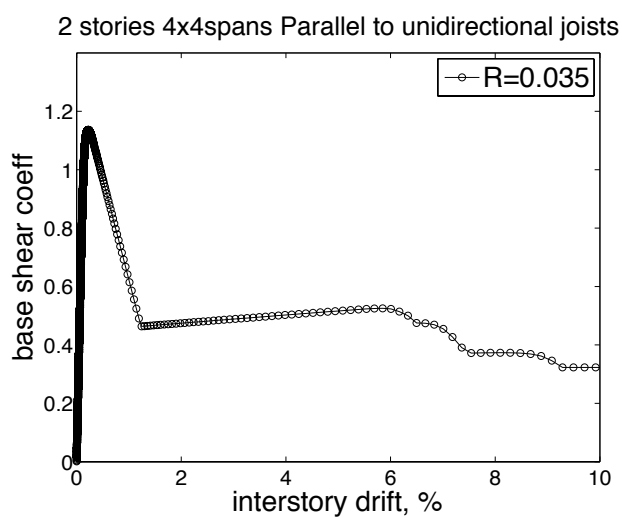
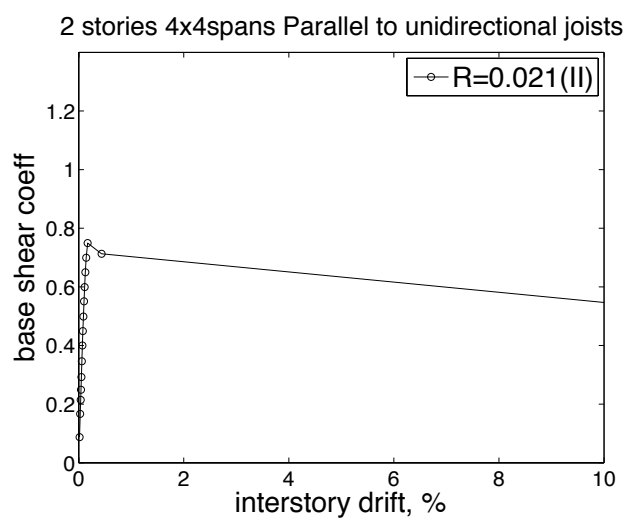
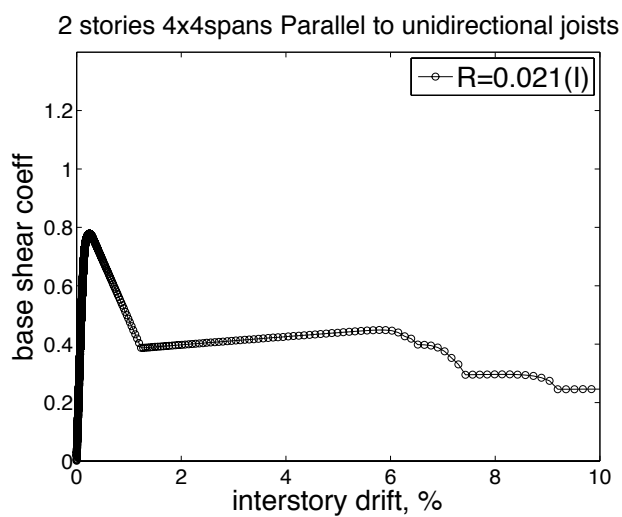


2 stories 4x4spans Parallel to unidirectional joists

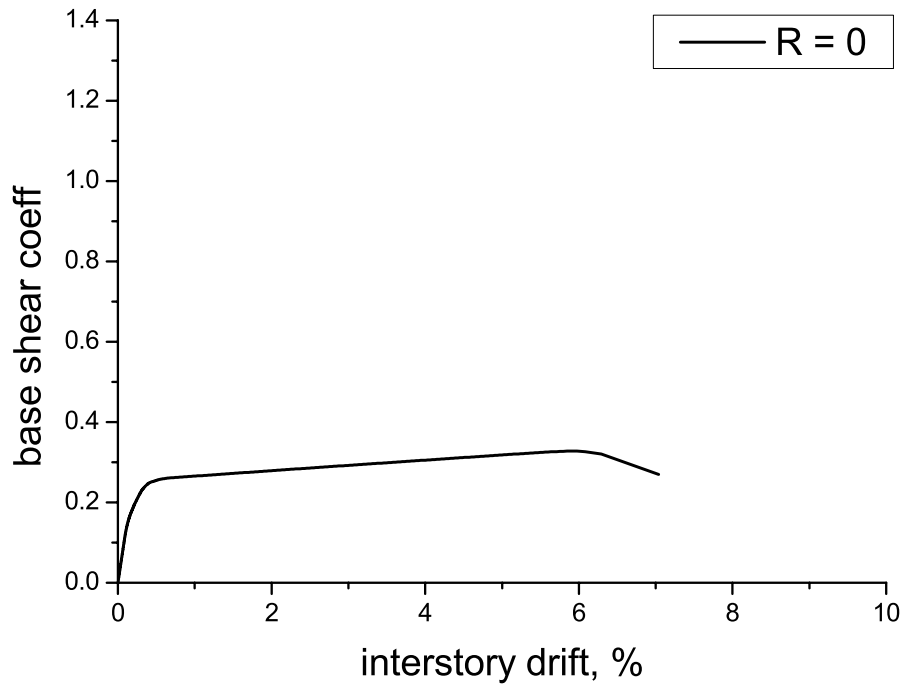


2 stories 4x4spans Parallel to unidirectional joists



B5 2 STORY 4x4 PARALLEL TO JOISTS

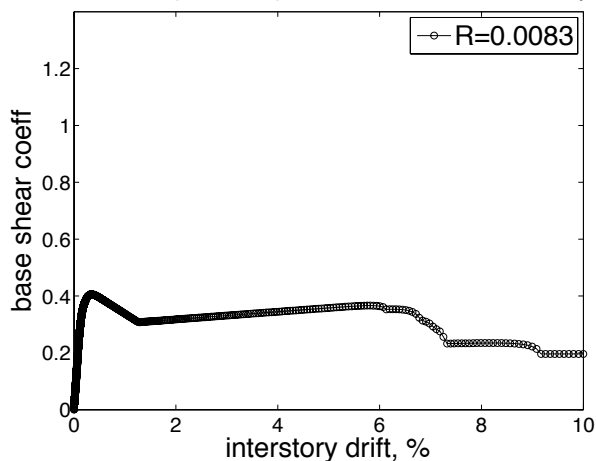
B6 2 STORY 4x4 PERPENDICULAR TO JOISTS



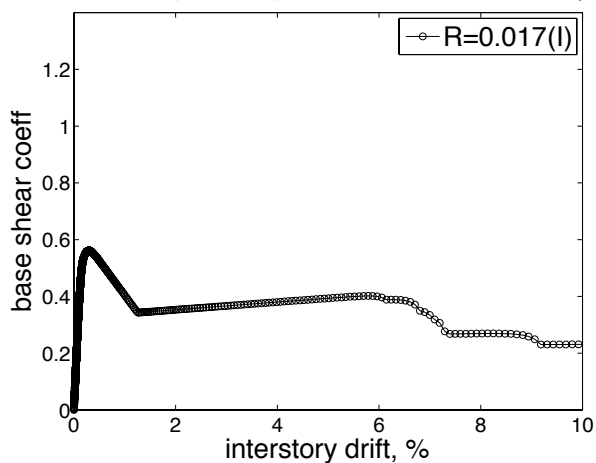
Prototype 4x4 spans						
Ratio	0.05	0.033	0.025	0.017	0.0083	X
Wall configuration Perpendicular to joists						I
						II
						III

B6 2 STORY 4x4 PERPENDICULAR TO JOISTS

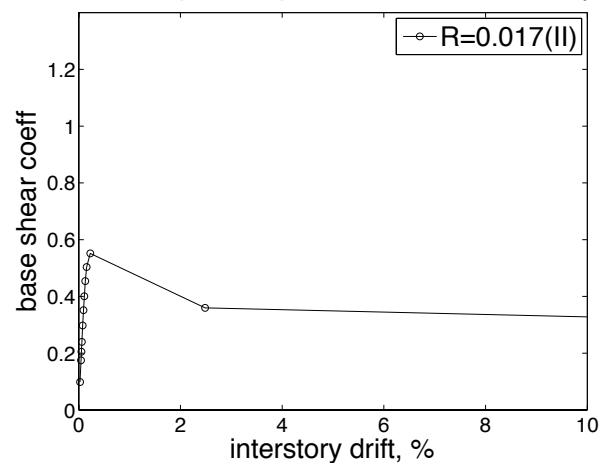
2 stories 4x4spans Perpendicular to unidirectional joists



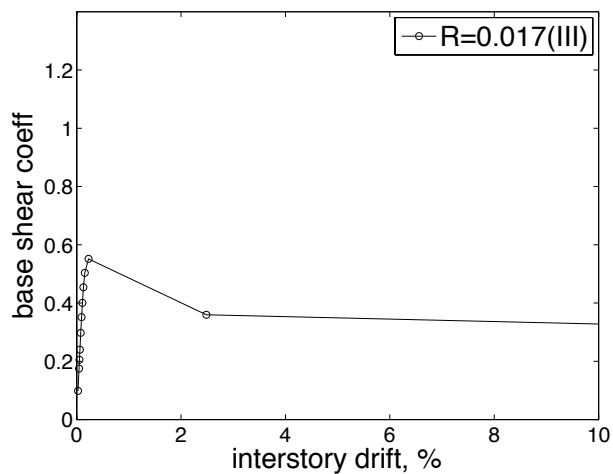
2 stories 4x4spans Perpendicular to unidirectional joists



2 stories 4x4spans Perpendicular to unidirectional joists

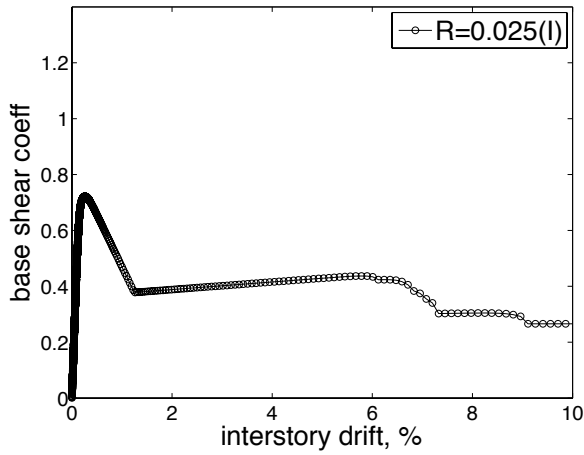


2 stories 4x4spans Perpendicular to unidirectional joists

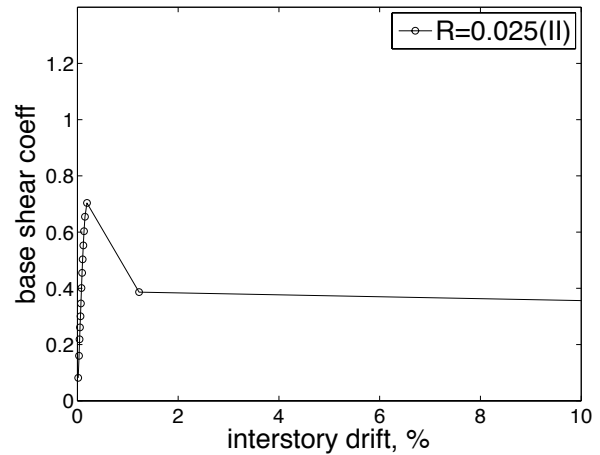


B6 2 STORY 4x4 PERPENDICULAR TO JOISTS

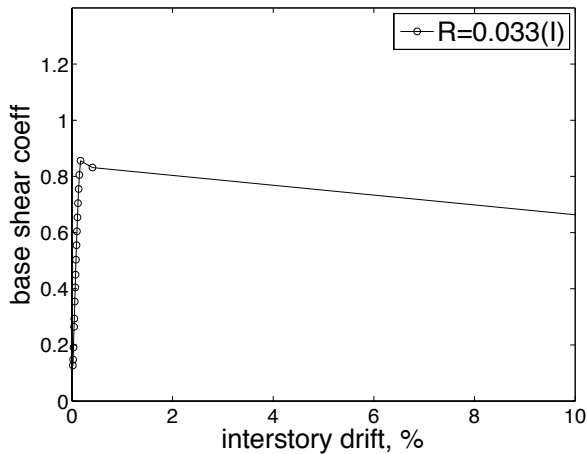
2 stories 4x4spans Perpendicular to unidirectional joists



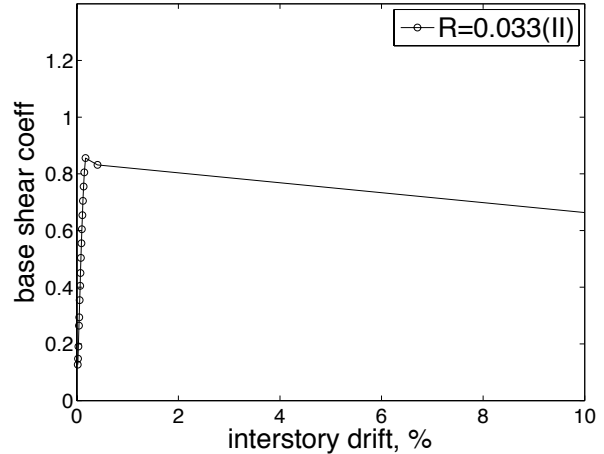
2 stories 4x4spans Perpendicular to unidirectional joists



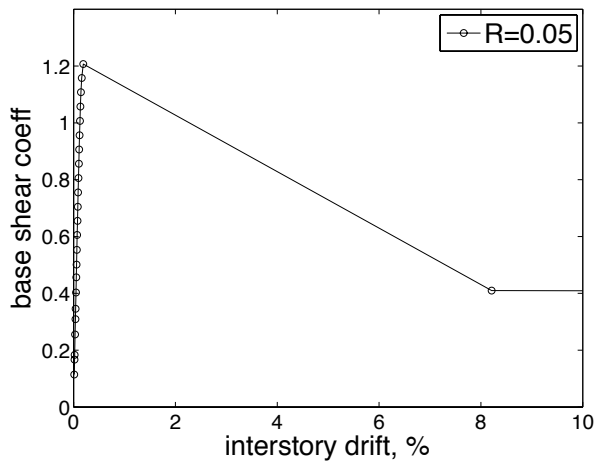
2 stories 4x4spans Perpendicular to unidirectional joists



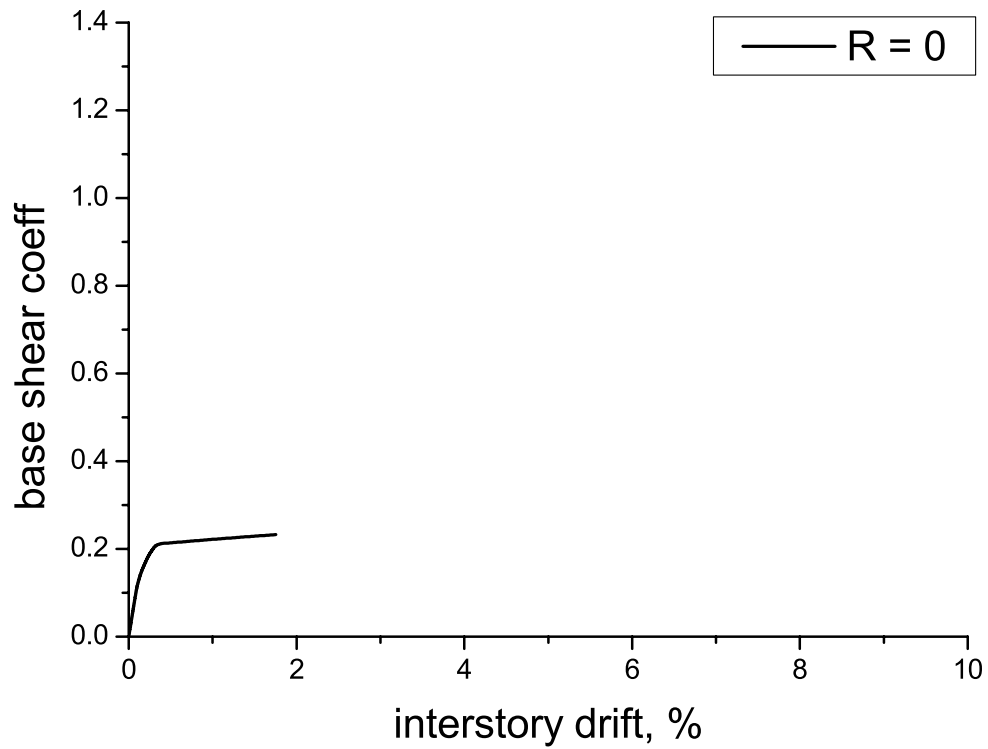
2 stories 4x4spans Perpendicular to unidirectional joists



2 stories 4x4spans Perpendicular to unidirectional joists

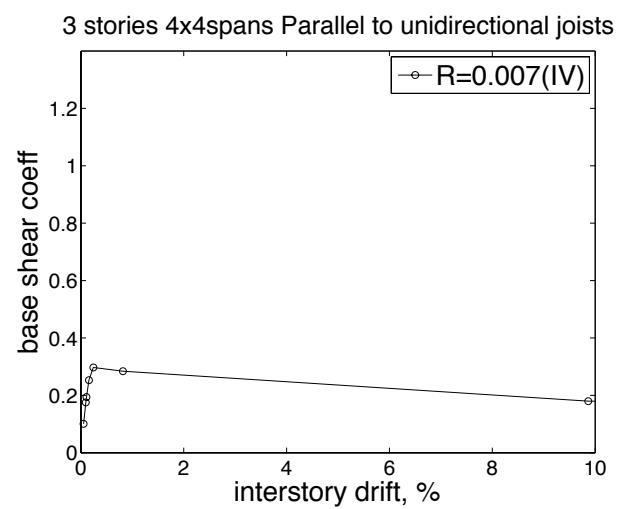
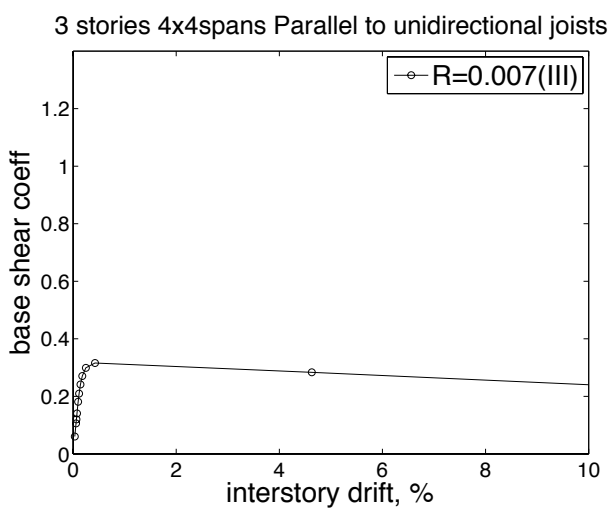
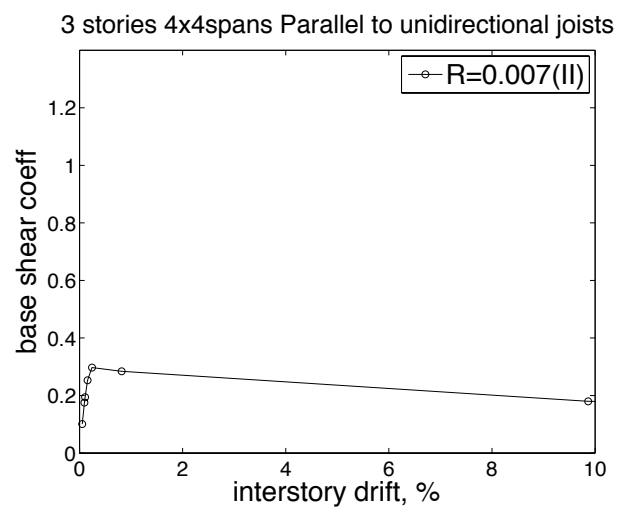
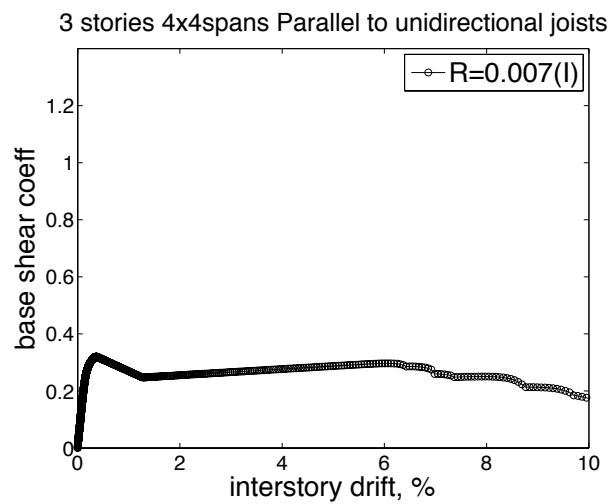
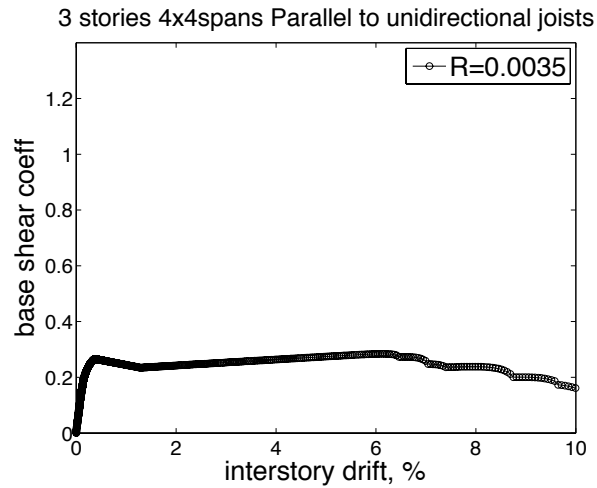


B7 3 STORY 4x4 PARALLEL TO JOISTS

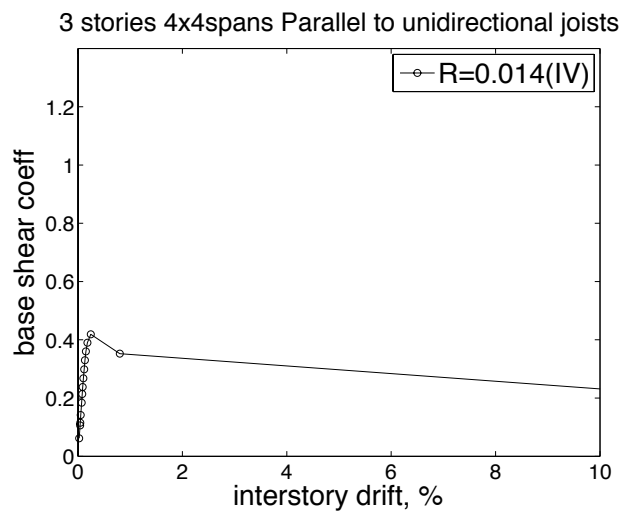
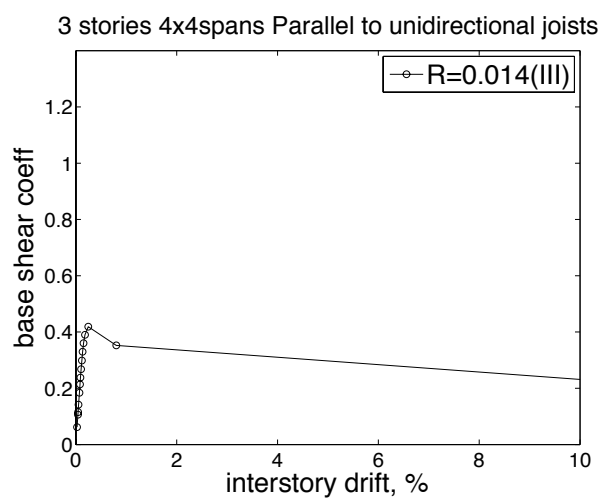
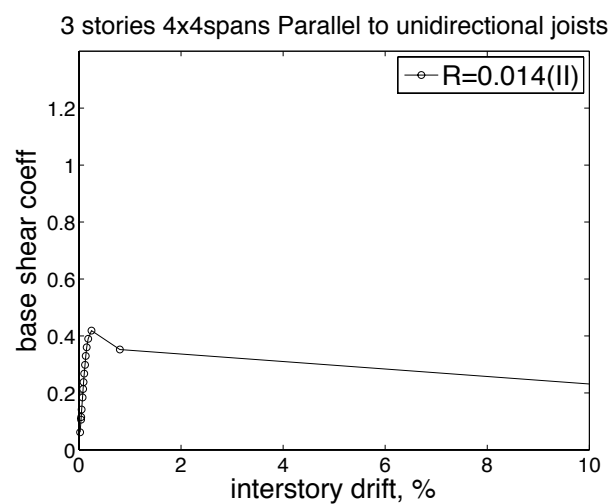
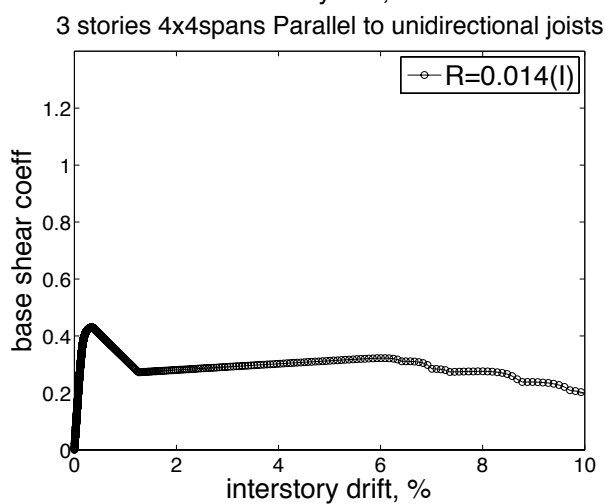
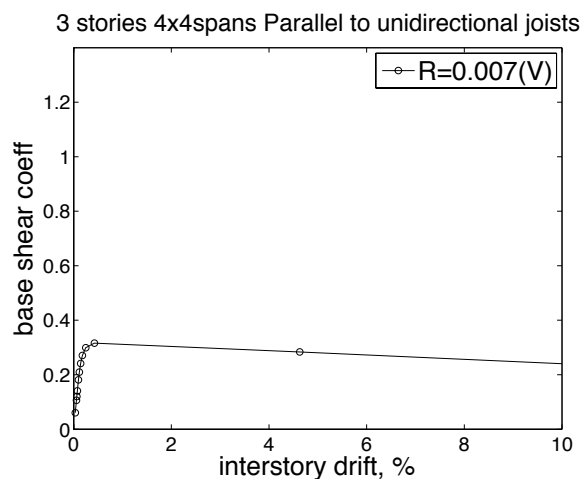


Prototype 4x4 spans						
Ratio	0.035	0.021	0.014	0.007	0.0035	Y
Wall configuration Parallel to joists						I
						II
						III
						IV
						V

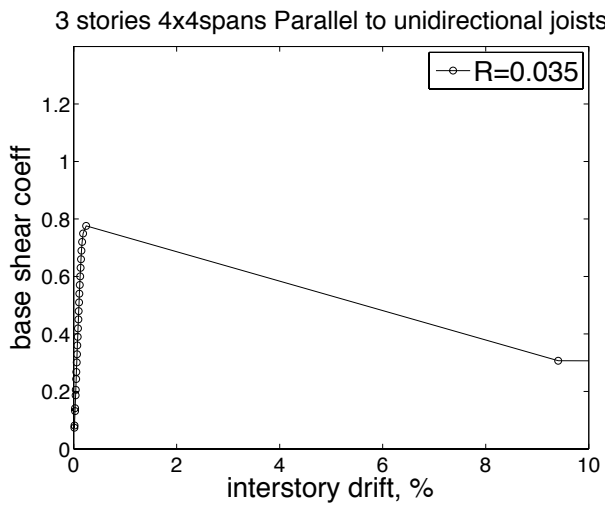
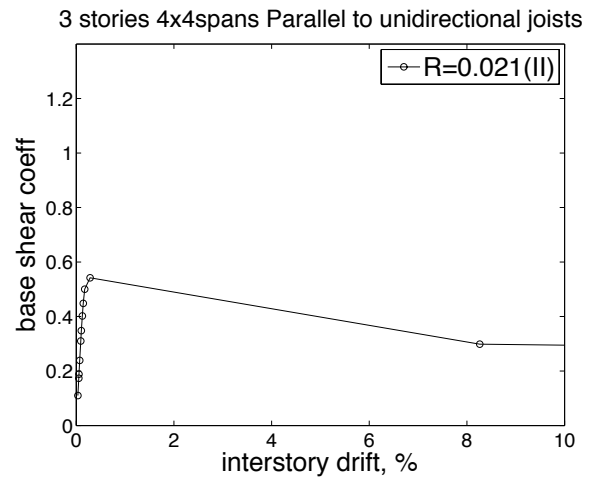
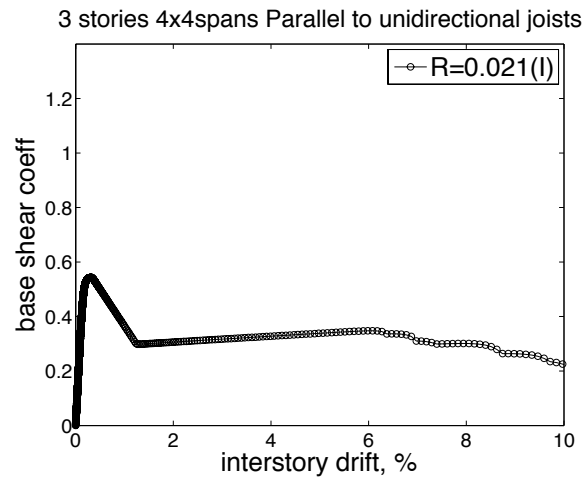
B7 3 STORY 4x4 PARALLEL TO JOISTS



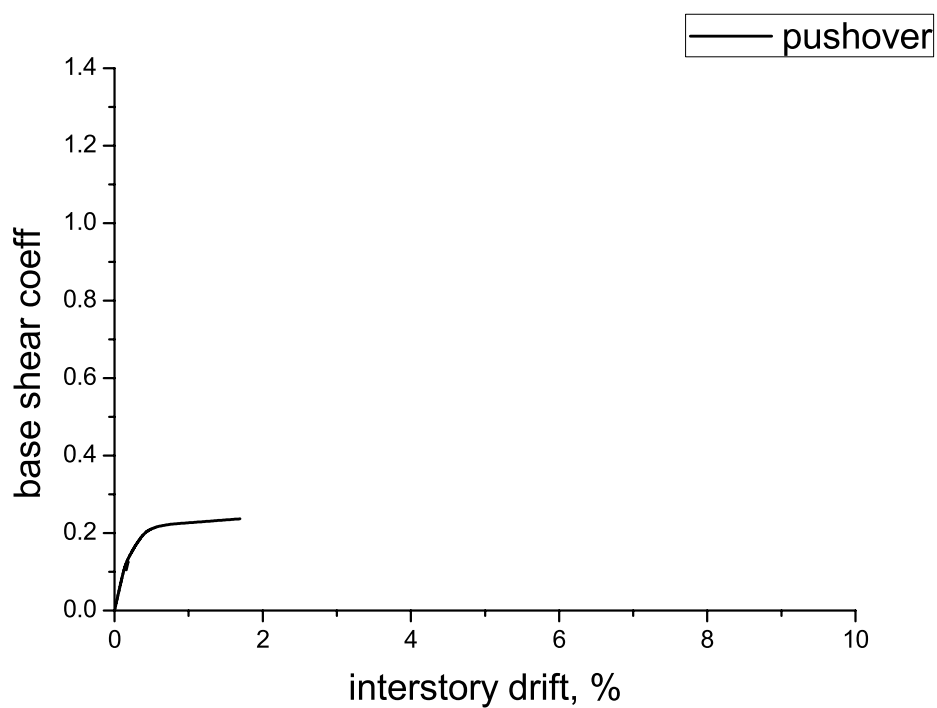
B7 3 STORY 4x4 PARALLEL TO JOISTS












B7 3 STORY 4x4 PARALLEL TO JOISTS



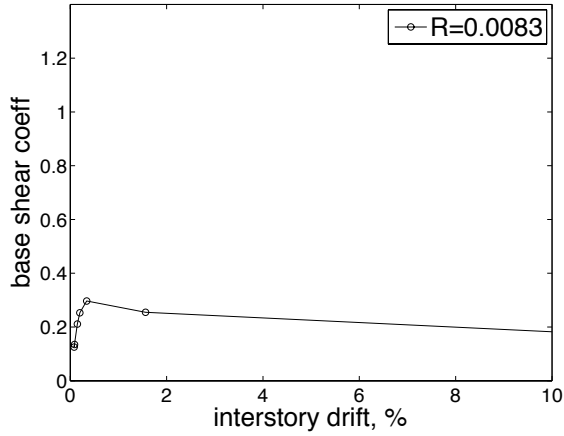
B8 3 STORY 4x4 PERPENDICULAR TO JOISTS



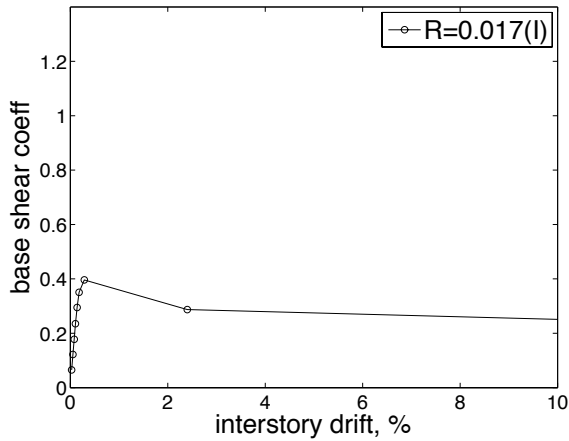
Prototype 4x4 spans						
Ratio	0.05	0.033	0.025	0.017	0.0083	X
Wall configuration Perpendicular to joists						I
						II
						III

B8 3 STORY 4x4 PERPENDICULAR TO JOISTS

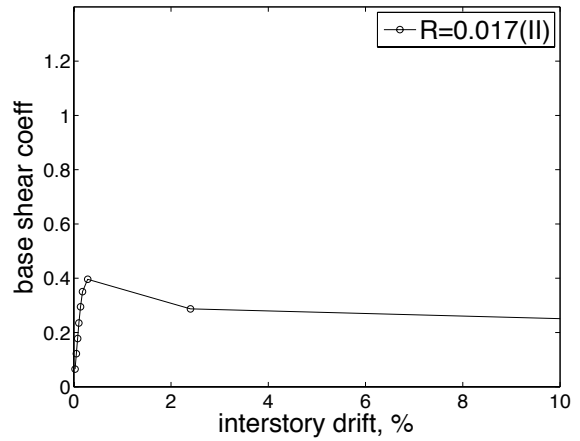
3 stories 4x4spans Perpendicular to unidirectional joists



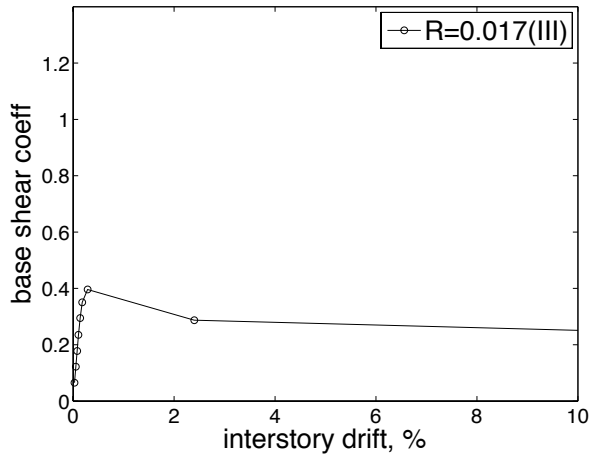
3 stories 4x4spans Perpendicular to unidirectional joists



3 stories 4x4spans Perpendicular to unidirectional joists

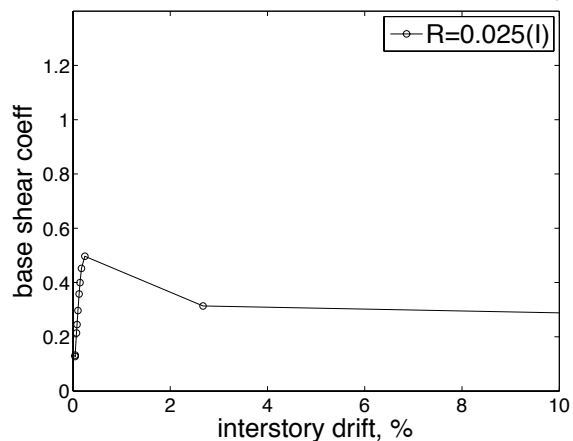


3 stories 4x4spans Perpendicular to unidirectional joists

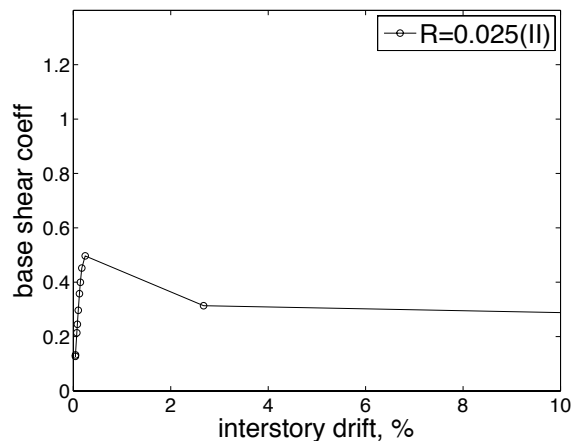


B8 3 STORY 4x4 PERPENDICULAR TO JOISTS

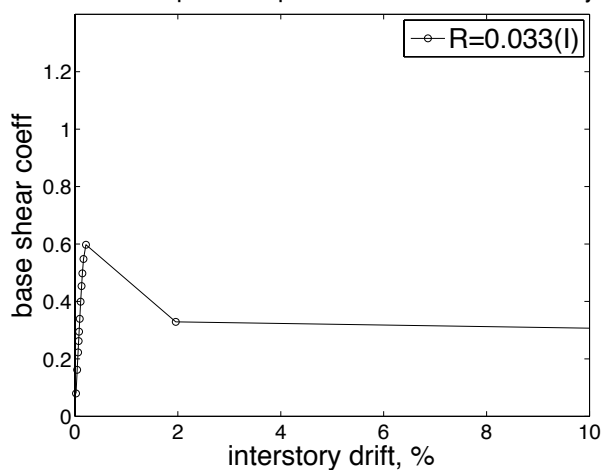
3 stories 4x4spans Perpendicular to unidirectional joists



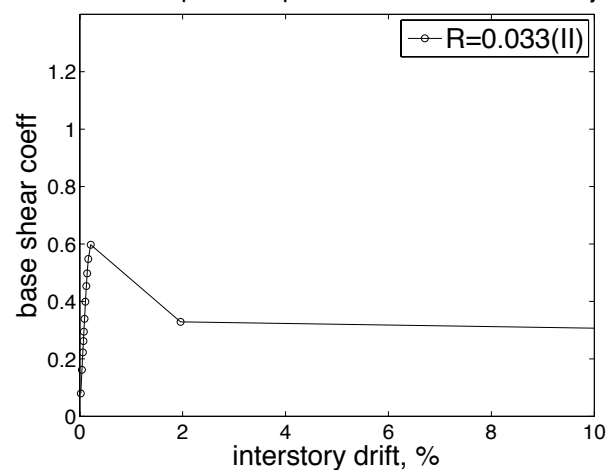
3 stories 4x4spans Perpendicular to unidirectional joists



3 stories 4x4spans Perpendicular to unidirectional joist



3 stories 4x4spans Perpendicular to unidirectional joists



3 stories 4x4spans Perpendicular to unidirectional joists

